

MASTER

Electromagnetic slurry density measurements

van Eeten, M.J.C.

Award date:
2005

[Link to publication](#)

Disclaimer

This document contains a student thesis (bachelor's or master's), as authored by a student at Eindhoven University of Technology. Student theses are made available in the TU/e repository upon obtaining the required degree. The grade received is not published on the document as presented in the repository. The required complexity or quality of research of student theses may vary by program, and the required minimum study period may vary in duration.

General rights

Copyright and moral rights for the publications made accessible in the public portal are retained by the authors and/or other copyright owners and it is a condition of accessing publications that users recognise and abide by the legal requirements associated with these rights.

- Users may download and print one copy of any publication from the public portal for the purpose of private study or research.
- You may not further distribute the material or use it for any profit-making activity or commercial gain

Electromagnetic Slurry Density Measurement

M.J.C. van Eeten

March 29, 2005

AQT 05-03

A graduation project performed at
IHC Systems B.V., Sliedrecht

Graduation tutor: prof. dr. H.C.W. Beijerinck

Abstract

This report is the result of an experimental research project on an innovative technique for slurry density measurements. Contrary to current density measurement techniques which use a radioactive source, this technique is based on electromagnetic transmission. The difference in the so-called permittivity of sand and water (which is a material property) causes a phase shift in the transmitted signal that depends on the amount of sand in the slurry, in other words, the density. In saline water there is also a measurable change in the signal attenuation.

In order to verify the applicability of electromagnetic transmission for density measurements, a static experimental setup has been designed and built. Using multiple sand packs in a –fresh and slightly saline– water filled setup, the effects of sand on the signal transmission have been measured. The measured data have been compared to a two-phase mixing model and a semi-empirical model.

This page intentionally contains only this sentence.

Contents

1	Introduction	1
1.1	IHC Systems	2
1.2	Motivation	2
1.3	Overview	4
1.4	Design goals	5
1.5	Project outline	6
2	Dielectrics and conductivity	9
2.1	Definitions	10
2.2	Pure water	10
2.3	Saline water	12
2.4	Soil	15
2.5	Other materials	16
3	Antenna design	17
3.1	Introduction	18
3.2	Electromagnetic wave equation	18
3.3	The dipole antenna	21
3.4	Near and far field	22
3.5	Insulated Antenna	23
3.6	Feeding the antenna	26
3.7	Antenna near conducting surface	33
4	Measuring density	37
4.1	Introduction	38
4.2	Propagation time and attenuation	39
4.3	Permittivity and conductivity	41
4.4	Mixing models	42
4.5	Volume to density	44
5	Experimental setup	47
5.1	Introduction	48
5.2	The pipe	49
5.3	Electrical setup	51
5.4	Antenna	53
5.5	Sand packs	56
6	Pure water measurements	61
6.1	First sand pack	62
6.2	Three sand packs	63
6.3	Improved sand packs	63
6.4	Goodwill oscilloscope	63
6.5	Painted pipe	63

6.6	Third antenna	65
6.7	Agilent oscilloscope	66
6.8	Probe measurements	67
6.9	Conclusions	69
7	River water measurements	71
7.1	Introduction	72
7.2	Varying conductivity	72
7.3	Combined measurements	77
7.4	Probe Measurements	80
7.5	Pack rotation	81
7.6	Conclusions	86
8	High salinity measurements	87
8.1	Varying conductivity	88
8.2	Probe Measurement	91
8.3	Shields effect	92
8.4	Inner pipe effect	94
8.5	Crosstalk	96
8.6	Conclusions	96
9	Concluding remarks	97
	Appendices	101
A	Permittivity in detail	103
B	Temperature Density Salinity	105
C	Water models	107
D	Transmission line model	109
E	Measurements to permittivity	117
F	Construction drawings	119
G	Transmission line transformer	131
H	Pickup coil	133
I	Low pass filter	135
J	Measurement in detail	137
K	Model selection	139
L	The Maxwell equations	145
M	Constants & Identities	147
N	Measurement data	149
	Bibliography	199

Dankwoord

(in Dutch)

Bij dezen wil ik de mensen die een bijdrage hebben geleverd aan mijn afstudeerproject bedanken. Allereerst mijn begeleider van de Technische Universiteit Eindhoven, Herman Beijerinck. Zijn grote toewijding, ongebreideld enthousiasme en constructieve kritiek zijn voor mij van grote waarde geweest. Ik denk niet dat ik een betere begeleider had kunnen treffen! Daarnaast mijn begeleider van IHC Systems, Cees de Keizer, voor de geboden gelegenheid tot afstuderen en zijn praktische kijk op het geheel.

Dan mijn projectgenoten Remco Fischbuch en Christiaan Huizer. De samenwerking met Remco en zijn enthousiasme heb ik als bijzonder prettig ervaren, en zijn welhaast grenzeloze parate elektronica kennis heeft mij keer op keer verrast. Christiaan heeft mij voortreffelijk geholpen met de bestellingen en heeft, in samenwerking met Peter van der Waal, de technische tekeningen keurig verzorgd. Ook wil ik Robert van Leuveren bedanken, voor een perfecte assemblage van de meetopstelling, maar zeker ook voor de gezellige samenwerking en de vriendschappelijke band.

Tenslotte, dank aan de collega's op de afdeling producten, alle anderen die een grotere of kleinere bijdrage hebben geleverd, en een ieder die ik onbedoeld nog vergeten ben. De sfeer in het bedrijf heeft me vanaf het begin af aan positief verrast, en ik zie er naar uit om het komend jaar voor IHC Systems aan de slag te gaan, nu als een echte collega!

Martijn van Eeten

This page intentionally contains only this sentence.

Chapter 1

Introduction

Contents

1.1	IHC Systems	2
1.2	Motivation	2
1.3	Overview	4
1.4	Design goals	5
1.5	Project outline	6

1.1 IHC Systems

IHC Systems is a business unit owned by Imtech Marine & Offshore, turnkey contractor in marine technology, and IHC Holland, leading supplier to the dredging world. Dredging used to be a purely mechanical process using buckets, but nowadays most dredging vessels use a hydraulic process for the transport of soils (though the excavation may still be mechanical). These hydraulic vessels all operate according to the same principle, which is outlined in figure 1.1. The central process in a hydraulic system is the so-called “slurrification”: the mixing of the soil with water to create a fluid mixture. The creation of this mixture, called “slurry”, enables soil transport from the sea or river bed using one or more pumps.

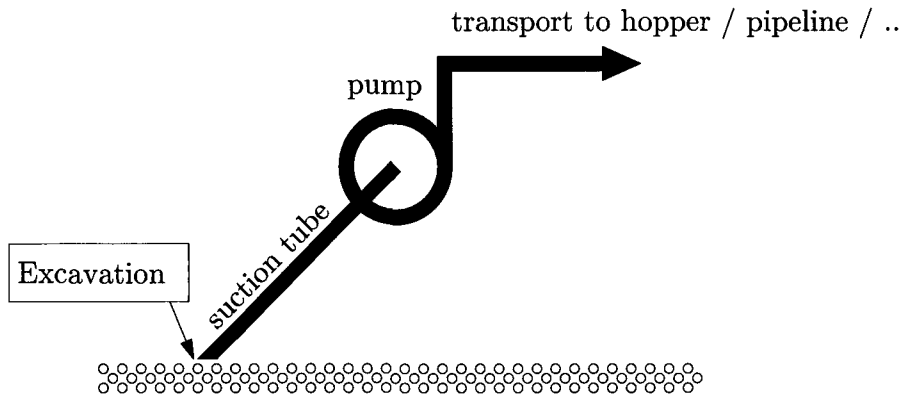


Figure 1.1: Hydraulic transport of slurry. The soil can be excavated using a variety of tools, such as the draghead, cutterhead and cutterwheel. Then, the excavated soil is mixed with water to create a fluid mixture, which is transported by the central process: the hydraulic system.

IHC Systems is dedicated to *efficient dredging*. Whether efficient means the largest production “with the least amount of energy” or “in the shortest amount of time”, both energy and time cost money so *knowing* the production is very important. For this purpose, IHC Systems has developed a range of instruments and automatic controllers. These provide the information necessary for a smooth, efficient dredging process, relieving the dredging master of repetitive, low-intelligence duties (his role becoming one of supervision) and achieving maximum operational efficiency of the vessel and its crew.

The term *production* is defined as the quantity of soil moved per unit of time (ton/s) and is calculated from the simultaneous measurement of density (ton/m^3) and flow rate (m^3/s) and is usually presented to the dredge master as shown in figure 1.2. The flow rate is the product of velocity and pipe diameter. The density during production is generally between 1.2 ton/m^3 and 1.8 ton/m^3 and the velocity varies between 3 and 10 m/s . Note that the measured production is not the pure soil but a mixture of water and solids.

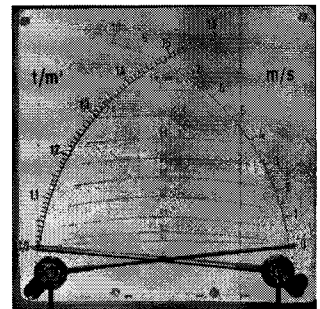


Figure 1.2: Cross needle indicator, which shows the momentaneous production.

1.2 Motivation

The focus of this research is on the *density* measurement, which is currently based on gamma ray absorption: a beam of gamma particles is sent through the pipe and detected by a Geiger-Müller tube or a scintillation probe. The higher the density, the higher the absorption of radiation by the slurry. Since the year 1960 IHC Systems delivered just over one thousand of these nuclear density

transmitters. The disadvantages of these radioactive density meters, which all arise from the use of a radioactive source, include:

- The use of radioactive sources is a sensitive issue.
- Certified personnel is required to operate radioactive devices.
- Transport and handling of devices containing radioactive material is more difficult and costly due to governmental regulations.

Of course, the radioactive density meter also has some strengths:

- Reliable technology: the “golden standard” in the industry
- Accurate (see section 1.4).
- Acceptable cost for larger dredgers.
- Physics of the measurement is straightforward.

Considering the growing public concern for the possible harmful effects of radioactive devices, IHC Systems has been trying to find an alternative for many years. A second reason to search for an alternative is that many smaller dredgers (e.g. the “Beaver” series) aren’t equipped with production monitors at all because of the high cost and the need for personnel that is trained to operate with radioactive devices. At the moment, the market of density meters for smaller dredging vessels shows more opportunities for IHC Systems than of jumbo dredgers. As a consequence, a low-cost, small-diameter density meter would be a great addition to the IHC Systems product portfolio.

A preliminary research of various measurement concepts by J. Barros [3] was finished in December 2003. Of the initial set of 14 ideas -which will not be repeated here- the pump-model, and the electromagnetic wave transmission turned out to be the most promising. According to Barros, the pump model can be a low-cost simple-design system with, however, a limited accuracy. The development of an electromagnetic system is expected to require considerable investment in time and resources - the expected accuracy is not mentioned. However, including the consideration that the new measurement technology should be patentable, in order to maintain an advantage on competitors, leaves the electromagnetic wave transmission as the only viable alternative.

During this research, it was reported by the “Nederlandsch Octrooibureau” (Dutch Patent Office) that (several aspects of) electromagnetic measurement systems were actually patented in the United States and Japan, see [26, 43, 44].

1.3 Overview

The operation principle of the experimental setup that has been used to assess the feasibility of an electromagnetic measurement system is shown in figure 1.3, without going into details yet.

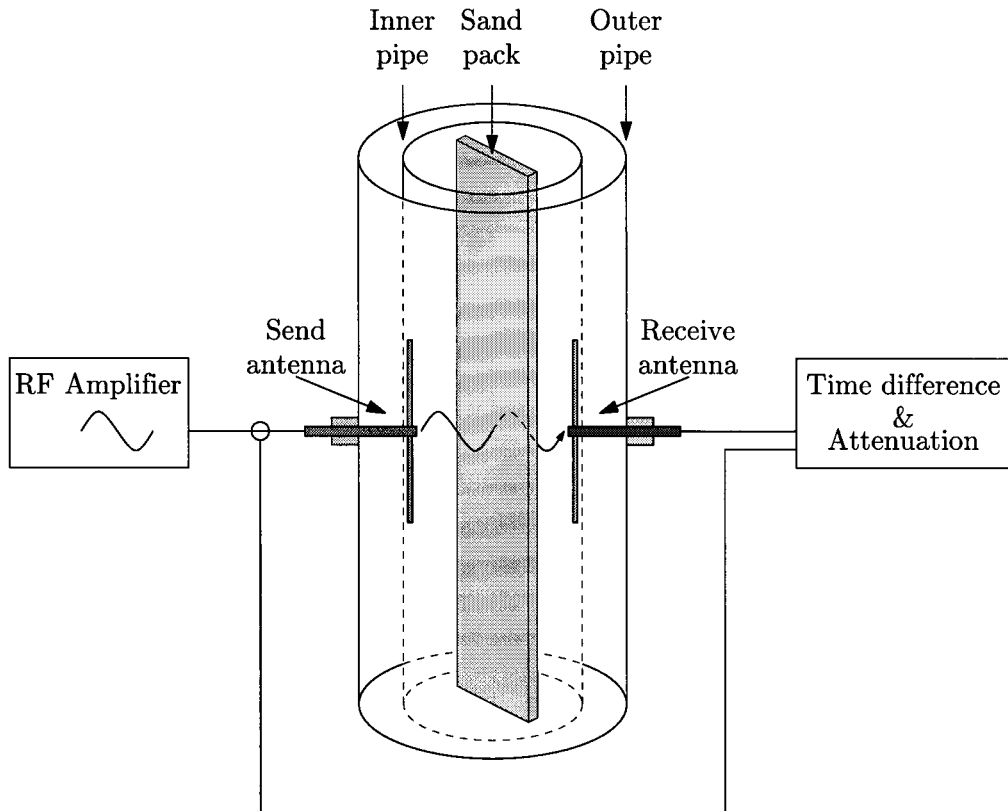


Figure 1.3: Overview of the experimental setup. The slurry is modeled by placing sand packs in the water in the inner pipe. The space between the two pipes is filled with water.

The density measurement is based on the differences in permittivity and or conductivity of water and sand. Slightly simplified, the permittivity of a medium determines the propagation velocity of electromagnetic waves and the conductivity attenuates the signal.

In the setup, a high-powered radio-frequency (RF) signal is fed to the transmitter antenna. The radiated electromagnetic waves propagate through the slurry, which has been modeled by placing one or more sand packs in a pipe filled with water, and will be delayed and/or attenuated depending on the permittivity and the conductivity of the slurry. The modified signal is picked up by the receiver antenna and compared to the original signal to detect the delay and the attenuation. The primary function of the outer pipe is to keep the electromagnetic waves within the measurement device.

The most important aspects of the experimental setup will be discussed in detail in the next chapters. In chapter 2 the terms permittivity and conductivity are defined and determined for water, sand and some other relevant materials. Chapter 3 deals with the most important aspects of the design of the used antennas. Chapter 4 describes how the slurry density can be determined from the measured delay and attenuation. The construction of the experimental setup is described in chapter 5. The results of the measurements are presented in chapters 6, 7 and 8. Finally chapter 9 contains some concluding remarks and suggestions for a follow-up of this project.

1.4 Design goals

The design of a density meter, based on electromagnetic transmission will be a trade-off between three factors:

1. Applicability
2. Accuracy
3. Cost

Applicability

The main limitation on the applicability of an electromagnetic meter is the signal attenuation in a conductive medium. The limit is the point where the signal is lost in the noise. In short, its applicability depends on its performance under the following operational conditions:

1. Salinity: the salinity of the water translates to conductivity. The typical conductivity ranges from 0.65 for river water to 4.0 S/m for sea water. A higher conductivity means more signal attenuation, so it is expected that measurements at low conductivities are easier to achieve.
2. Density: the density range of interest is 1.0 to 1.8 ton/m³. A higher density corresponds to a lower conductivity, because the soil is non-conductive. So if a signal is received at a density of 1.0, then certainly at higher densities.
3. Pipe diameter: ranges from 0.3 to 1.2 m. The larger the diameter the more attenuation, so small pipe diameters have an advantage.
4. Transport velocity: ranges up to 10 m/s. Considering the time period of the electromagnetic wave, which will generally be shorter than 100 ns, it is expected that the slurry can be regarded as stationary. However, a turbulent slurry flow containing air bubbles will affect density measurements - any density measurement, not just this one.
5. Harsh environment: the operating environment on dredgers can be quite rough. There's generally a lot of noise and vibrations, temperatures may vary from 5 °C to 45 °C and it will also be very moist. It is expected that the influence of noise and vibrations will be minimal, but temperature compensation *may* be necessary, as the conductivity is temperature dependent.
6. Soil type: different soil types (sand, rock, clay,...) may have different relevant properties. The permittivity of the soil should be known within some limits to make accurate electromagnetic measurements.
7. Homogeneity: when the density is measured in a subsection of the pipe, it should be accurately represent the density in the whole cross-section. In general, a homogeneous mixture gives more accurate results.

Accuracy

The *accuracy* of the electromagnetic density meter should be targeted against the performance of the radioactive density meter, which is determined by:

- $\Delta\rho = \pm 1\%$ full scale
- Time constant $\tau = 5$ s

The accuracy of an electromagnetic density meter is affected in (at least) three ways:

- (+) Because the electromagnetic density meter measures density over a larger cross-section than a radioactive density meter, the measured density represents more the average of a large volume instead of only the small section that the radioactive ray crosses.
- (−) The electromagnetic density measurement is only valid if the permittivity of the soils is known.
- (−) Electromagnetic transmission and accurate permittivity measurements are aggravated in saline solutions.

Cost

The *cost* of the electromagnetic density meter compared to the radioactive density meter is also important:

- If it costs significantly more, it should perform significantly better, i.e. more accurate and applicable under all conditions.
- If it costs significantly less, it may be less flexible and/or less accurate
- If it is to replace the radioactive density meter, it should be at least just as accurate and applicable under all conditions.

Expectations

Beforehand, some (possibly premature) conclusions were drawn based on the statements above. It was decided to initially focus on a static small diameter (500 mm) density meter for application in river water. This configuration would probably be the easiest to get up and running, without requiring too much amplifier power and depending too much on the performance of the antennas. If that configuration would work as desired, tests in more saline water were to be performed.

1.5 Project outline

Project result

The result of this project will be:

- An experimental setup
- Measurements performed on this experimental setup, in sweet and saline water.
- A theoretical discussion of the results
- Suggestions for improvement (if any)
- If the measurement systems works as desired: a project plan to make it the final product

Delimitation

The following items will specifically *not* be part of the project:

- Development of an optimized antenna.
- Development of a flowing setup.
- Measurements in a flowing setup.
- Development of a prototype.
- Development of a usable end product.

Internal contacts

This graduation project has been realized in association with the Stan Ackermans Institute (SAI). The Stan Ackermans Institute offers Technological Designer programs and because of this, it has many contacts with the industry from which the preliminary research project by Barros [3] already arose. The following people from SAI and IHC Systems were directly involved in this research:

C. de Keizer: manager Research & Development at IHC Systems, supervisor of this project on half of IHC Systems.

prof. dr. H.C.W. Beijerinck, chairman department “Design and Technology Instrumentation” at SAI, full professor of the section “Experimental Atomic Physics and Quantum Electronics” of the department of Applied Physics, supervisor of this project on behalf of Eindhoven University of Technology / SAI.

R. Fischbuch: co-worker Research & Development at IHC Systems, assisting in electrotechnical aspects of the project.

C. Huizer: CAD drafter / Constructor at IHC Systems, assisting in mechanical and construction aspects.

External contacts

In order to exchange ideas and gain more insight in specific aspects of electromagnetic devices, the following people from Eindhoven University of Technology were contacted:

prof. dr. ir. K. Kopinga: full professor of the section “Transport in Permeable Media” of the department of Applied Physics. Several discussions on the subject of dielectrics measurements, shielding of radiofrequency and microwave signals, enhancing signal-to-noise ratio, amplifiers, etc. His experience with microwave (NMR) systems has been of great value for the design of the experimental setup.

prof. dr. A.G. Tjihuis: full professor of the section “Electromagnetics” of the department of Electrical Engineering. Discussion on the development of antennas and on the use of electromagnetic waves for dielectrics measurements. Based on these discussions, it was decided to choose the dipole antenna type because of its relative simplicity and predictability.

S.H. Ypma: coordinator for the SAI / ICT of the section “Signal Processing Systems” of the department of Electrical Engineering. Discussion on antenna impedance matching. As an active radio amateur, he has many practical insights in the use of antennas.

This page intentionally contains only this sentence.

Chapter 2

Dielectrics and conductivity

Contents

2.1	Definitions	10
2.2	Pure water	10
2.3	Saline water	12
2.4	Soil	15
2.5	Other materials	16

2.1 Definitions

Water molecules are *polar*: the positive and negative charges do not completely overlap, which gives the molecules a dipole moment. In an applied electric field, polar molecules tend to align themselves parallel to this field and thus produce an electric field in the opposite direction. The degree to which a substance does this is called the dielectric constant or *permittivity*. Besides being a polar molecule, water has a strong hydrogen-bonding network which causes a long range correlation of molecular orientation and is reason for the high permittivity of water. The complex permittivity of a material is given by¹:

$$\varepsilon^* = \varepsilon_r^* \varepsilon_0 \quad (2.1)$$

where ε_0 is the permittivity in vacuum (M.3) and ε_r^* is the relative complex permittivity. The permittivity is in general a complex constant which can be expressed for a (lossy) dielectric material as [28]:

$$\varepsilon^* = \varepsilon' - j \left(\varepsilon'' + \frac{\sigma}{\omega} \right) \quad (2.2)$$

where ε' represents the refractive properties, ε'' and absorptive properties due to polarization of the dielectric material and σ the ‘zero frequency’ or DC conductivity. The conductivity is assumed to be real-valued. The ε' and ε'' terms are frequency dependent, as shown for water in the next section. A derivation of equation (2.2) can be found in appendix A.

The imaginary part of the permittivity and the DC conductivity can be combined in the real-valued *effective* conductivity σ_e . Assuming that the conductivity σ is real-valued, the definition of the effective conductivity (A.4b) can be written as:

$$\sigma_e = \sigma + \omega \varepsilon''. \quad (2.3)$$

The remaining real part of the permittivity is represented by the real-valued *effective* permittivity (A.4a) which is given by:

$$\varepsilon_e = \varepsilon', \quad (2.4)$$

again assuming that the conductivity σ is real-valued. Thus, the complex permittivity can be written in terms of the real-valued effective permittivity and the real-valued effective conductivity:

$$\varepsilon^* = \varepsilon_e - j \frac{\sigma_e}{\omega}. \quad (2.5)$$

2.2 Pure water

As described in section 2.1, polar molecules align themselves parallel to an applied electric field. The speed of this alignment is determined by the so-called “relaxation time” τ (see equation (C.2a) in appendix C). As a consequence, the dielectric behaviour of polar molecules in a varying electric field depends on the frequency ω in comparison with this relaxation time:

$$\varepsilon_r^* = \begin{cases} \varepsilon_r^\infty, & \text{the (real) infinite relative dielectric constant, } \omega\tau \gg 1 \\ \varepsilon_r^{\text{stat}}, & \text{the (real) static relative dielectric constant, } \omega\tau \ll 1. \end{cases} \quad (2.6)$$

Note that in both extremes, the complex permittivity is *real*-valued. Several models exist for the permittivity in between these extremes.

¹The superscript asterisk (*) denotes a complex value, the subscript *r* a relative value.

The two most essential models for the permittivity of water are:

The Debye equation:
$$\epsilon_r^*(\omega) = \epsilon_r^\infty + \frac{\epsilon_r^{\text{stat}} - \epsilon_r^\infty}{1 + j\omega\tau}. \quad (2.7a)$$

The Cole-Cole equation:
$$\epsilon_r^*(\omega) = \epsilon_r^\infty + \frac{\epsilon_r^{\text{stat}} - \epsilon_r^\infty}{1 + (j\omega\tau)^{1-\gamma}}, \quad (2.7b)$$

where the parameter $0 < \gamma \leq 1$ (typical 0.03) increases with internal degrees of freedom and decreases with temperature [4]. According to [23] the standard Debye model ($\gamma = 0$) is sufficiently accurate at the lower microwave frequencies. The infinite permittivity ϵ_r^∞ does not seem to depend on temperature (or salinity) and is assumed a constant value of 4.9 [23, 38]. The static permittivity ϵ_r^{stat} does depend on temperature (and salinity) and typical values lie between 70 and 85. Plots of the (relative) permittivity of water as a function of the frequency have been calculated (figure 2.1) using the Debye model (2.7a) and the following assumed (typical) values:

- $\epsilon_r^\infty = 4.9$
- $\epsilon_r^{\text{stat}} = 80$
- $\tau = 9 \times 10^{-12}$ s.

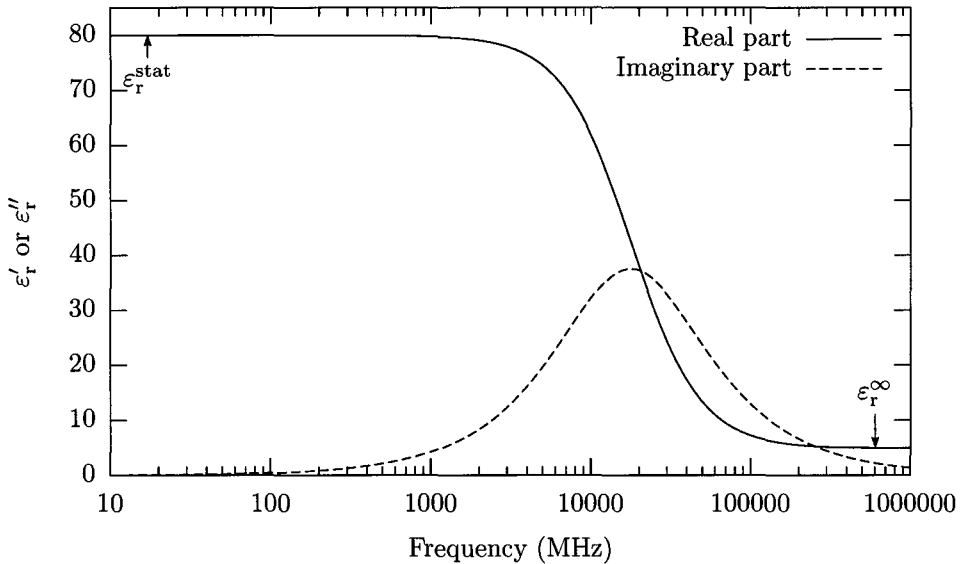


Figure 2.1: Plots of the real part (solid) and the imaginary part (dashed) of the relative permittivity of water as a function of the frequency, according to the Debye model.

From looking at these plots, it becomes quite clear that for the frequency range of interest ($f < 100$ MHz) the real part of the relative permittivity can be considered frequency independent and approximately equal to the static permittivity ϵ_r^{stat} . The imaginary part is almost zero. Thus, all lossy behaviour can be attributed to conductivity, which is also zero. This leads to the following approximations for pure water:

$$\epsilon_{er} \approx \epsilon_r^{\text{stat}} \quad (2.8a)$$

$$\sigma_e \approx 0. \quad (2.8b)$$

2.3 Saline water

Salinity

The principle salt in sea water is NaCl, and sea water can be reasonably approximated by an aqueous NaCl solution (see equation (C.4) in appendix C). The introduction of salt in water makes it conductive. The total dissolved salt concentration of water is called the salinity. Salinity is normally expressed in “parts per thousand” (ppt), i.e. grams of salt per 1000 grams of water, or in “practical salinity units” (psu) which is (numerically) approximately the same. The amount of salt in water is not the same everywhere: a map which depicts the average salinity of the oceans is shown in figure 2.2.

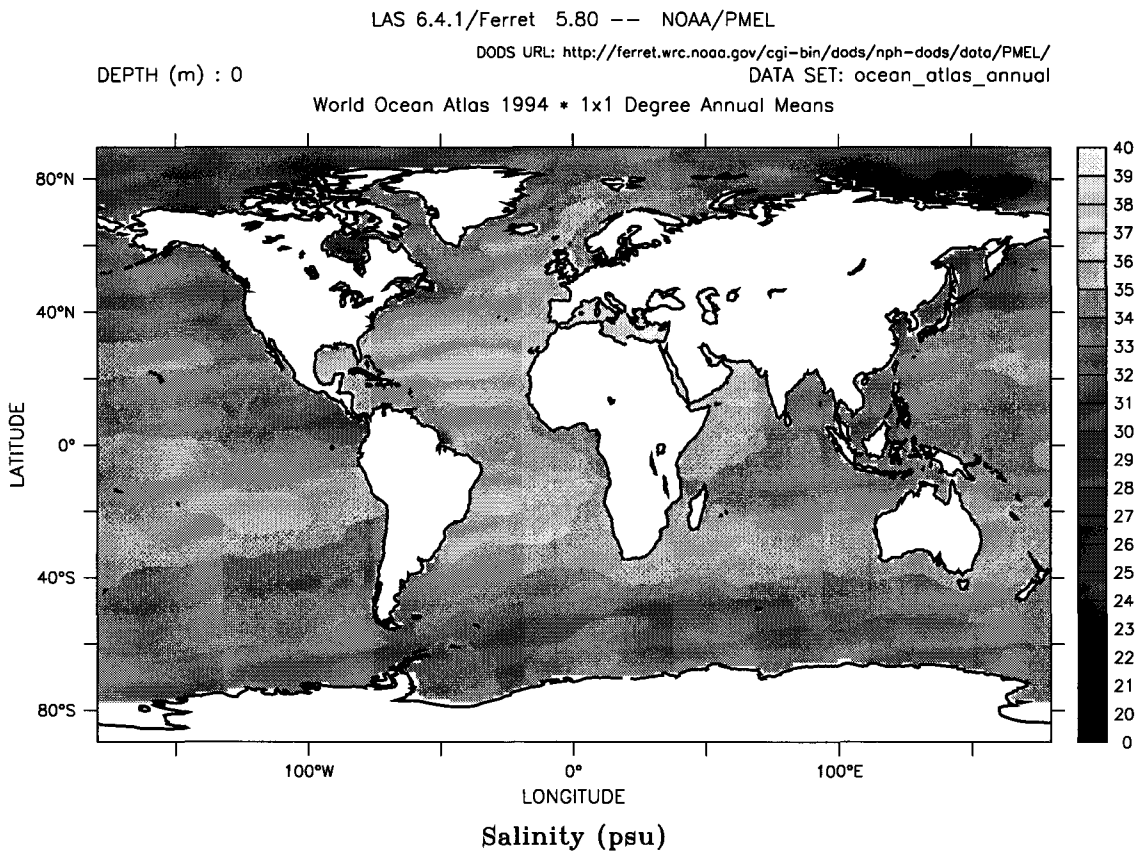


Figure 2.2: Plot of annual salinity of the oceans in 1994 as provided by the National Oceanic and Atmospheric Administration (NOAA). The unit “psu” is the *practical salinity unit*, which is quite close to parts per thousand (ppt).

Looking at the colour distribution in the map, the conductivity of sea water roughly varies between 30 and 40 ppt. By definition², “saline” water has a salt concentration greater than 18 ppt. River water has a much lower salinity: it may be as low as 0.5 ppt (fresh water). Water with a salinity between 5 and 18 ppt is called brackish and is usually found in estuaries where seawater mixes with fresh water. Another figure that is frequently used to characterize saline water is the density, which roughly varies between 1020 and 1030 kg/m³ for sea water. A conversion chart relating salinity, density and temperature can be found in appendix B.

²from European Environment Agency

For our purposes not the salinity, but the corresponding conductivity is of main interest. A numerical model for the conductivity of sea water as a function of salinity and temperature is given by [38] and is reproduced in appendix C. A plot of the conductivity as a function of the salinity and the temperature according to this model is shown in figure 2.3(a) for the range of salinities and temperatures that are found in the oceans. Because this model is not valid for lower salinities, the model from [37] has been used for the plot for salinities between 0 and 5 ppt in figure 2.3(b).

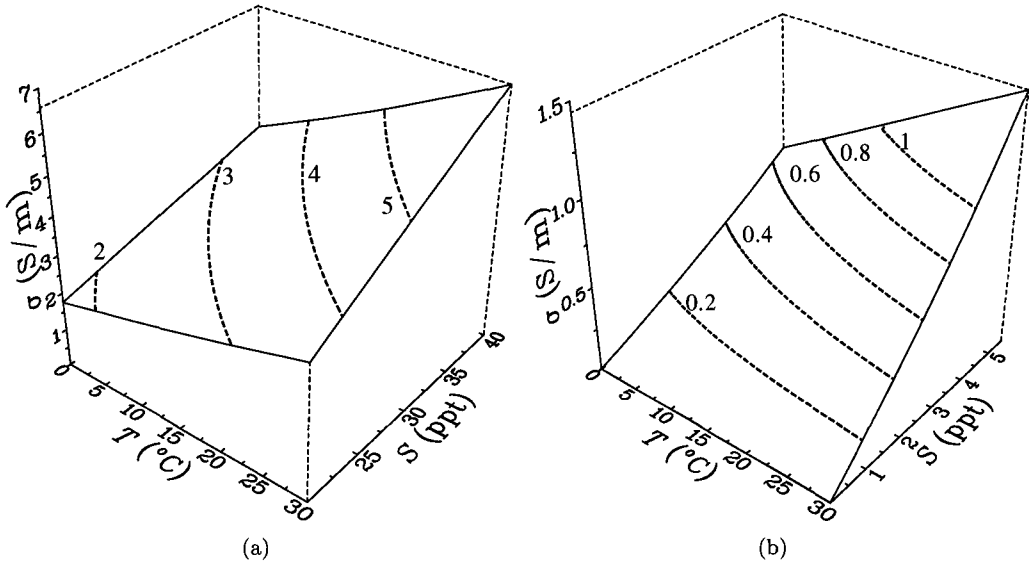


Figure 2.3: Plots of the conductivity of sea water (a) and river water (b) as a function of salinity and temperature. Contour lines for $\sigma = \{2.0, \dots, 5.0\}$ S/m and $\sigma = \{0.2, \dots, 1.0\}$ S/m are indicated.

Because of this wide range of possible conductivities (1.75 – 6.5 S/m at sea and generally below 1.5 S/m in rivers - except estuaries), it is convenient to use some characteristic values. The values that have been used in this research project are:

$$\sigma_{\text{river}} = 0.65 \text{ S/m}, \quad \text{corresponding to 4.5 ppt at a temperature of 15 } ^\circ\text{C} \quad (2.9a)$$

$$\sigma_{\text{sea}} = 4.0 \text{ S/m}, \quad \text{corresponding to 32.4 ppt at a temperature of 15 } ^\circ\text{C}. \quad (2.9b)$$

Permittivity & conductivity

For the frequency range used in the experiments ($f < 100$ MHz), the effective permittivity of saline water is still approximately equal to the static permittivity ϵ_r^{stat} .

To estimate the effective *conductivity* of saline water in this frequency range, plots of the conductivity of saline water as a function of the frequency for “river” and “sea” water are shown in figure 2.4. As the plot shows, the influence of the imaginary part of the permittivity on the effective conductivity is only visible at frequencies $f \gg 100$ MHz. So for our purposes the imaginary part of the permittivity is negligible. In other words, the following approximations apply for saline water:

$$\epsilon_{\text{er}} \approx \epsilon_r^{\text{stat}} \quad (2.10a)$$

$$\sigma_e \approx \sigma. \quad (2.10b)$$

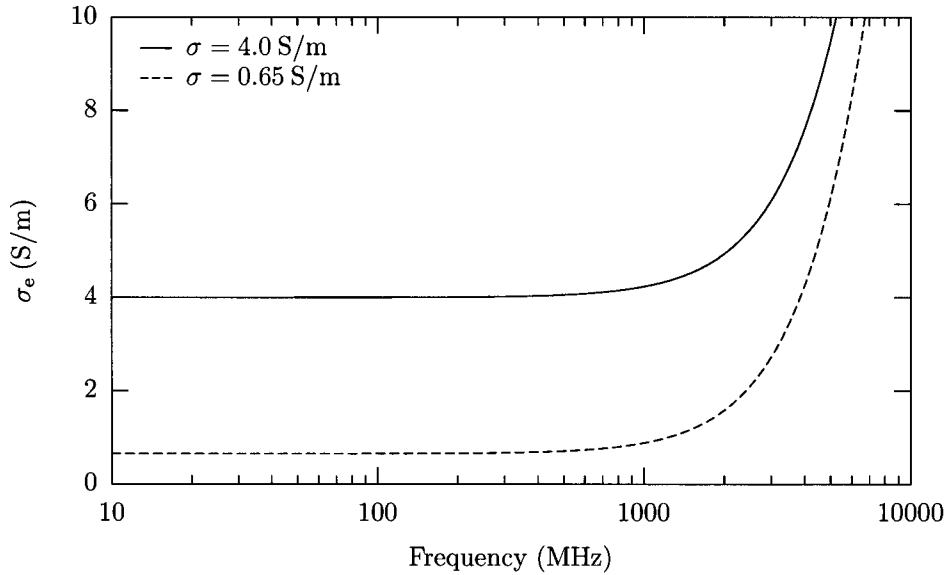


Figure 2.4: Plots of the conductivity of saline water as a function of the frequency, at a conductivity of 4 S/m (solid) and 0.65 S/m (dashed).

This does not mean that the permittivity does not depend on the conductivity of the water at all, because the static relative permittivity ϵ_r^{stat} has a conductivity dependence: it decreases with increasing salinity because the Na^+ and Cl^- ions attract water molecules, which form a hydrate sheet around each ion. These water molecules cannot reorient to an applied electrical field, thus the permittivity is reduced [12]. Plots of the relative static permittivity of saline water as a function of salinity and temperature, based on the numerical model found in [23], are shown in figure 2.5. This model is more accurate at lower frequencies than the model from [37, 38].

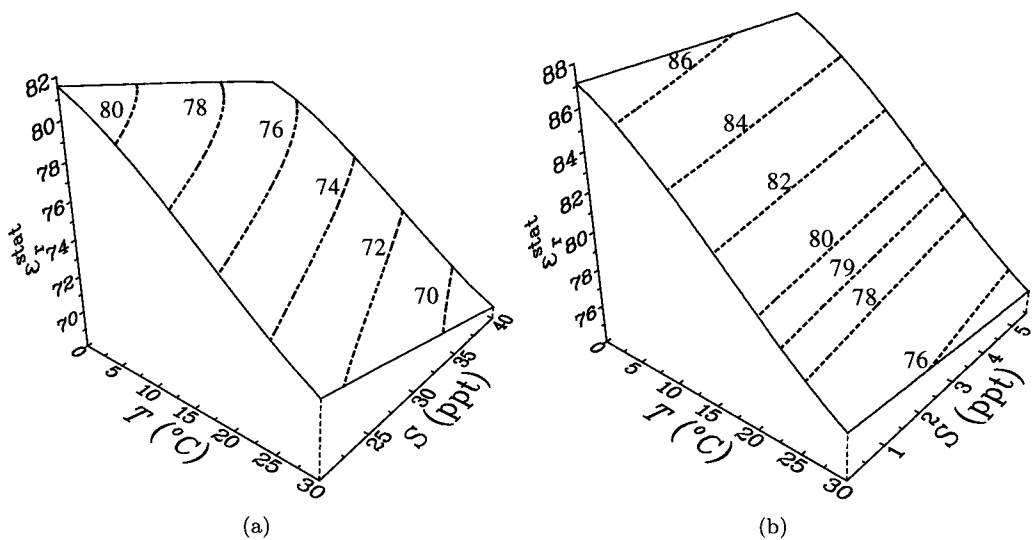


Figure 2.5: Plots of the relative static permittivity of sea water (a) and river water (b) as a function of salinity and temperature. Contour lines for $\epsilon_r^{\text{stat}} = \{70, \dots, 80\}$ and $\epsilon_r^{\text{stat}} = \{76, \dots, 86\}$ are indicated.

In this report, the temperature and salinity dependence of the static permittivity has *not* been taken into account. During the density measurements in saline water, the temperature variation during the experiments is at most 1.5 °C, and the salinity range was approximately 0 – 7 ppt so it is reasonable to use a constant static permittivity. For all density calculations, a value of 79.0 has been used. If at a later stage the accuracy appears to be deficient, corrections like this can still be incorporated. Note that the salinity and the corresponding conductivity *is* taken into account in the effective permittivity *measurements*, as described in chapter 4.

2.4 Soil

The permittivity of soil depends on the soil type (sand, clay, loam,...). Relative permittivities for soils are in the range 4 – 6. It is this (huge) difference between the permittivity of sand and the permittivity of water that makes density measurements possible.

The mentioned relative permittivities refer to *dry* soils. Literature values for *moist* soils are much higher: in the range 10 – 40. Approximate permittivities of various (dry and wet) soil constituents can be found in [6, 25]. In fact, the permittivity of moist soils strongly depends on the volumetric moisture content. Other parameters include porosity and salinity. In this research project, the porosity is not included in the calculations. The permittivity is not corrected for the influence of the salinity either, as described in the previous section.

Multiple mainly semi-empirical models describing the permittivity of moist soils exist, such as [7, 29, 30, 40]. These models are all based on the assumption that the *soil* is by far the dominating component. In the case of slurry however, *water* is the dominating component. The practical range of slurry densities varies between 1.0, pure water, and 1.8 ton/m³, a safe limit above which hydraulic transport becomes problematic. In this density range the sand volume fraction varies between 0 and approximately 0.5. More suitable models for the permittivity of a two-component mixture are described in chapter 4.

Example 1:

The relative permittivity of a mixture of sand with $\epsilon_{er} = 4$ and pure water with $\epsilon_{er} = 79$ will most likely be somewhere between those two values. One of the possible models is simple linear interpolation, as shown in figure 2.6.

As indicated, the density of an arbitrary sand-water mixture may vary between 1.0 and 2.65 ton/m³. In practice, the density range is limited to 1.8 ton/m³, just below the density of saturated water which has a density of approximately 2.0 ton/m³. So the range of relative permittivities that will be encountered is also limited - for this simple model between 40 and 79.

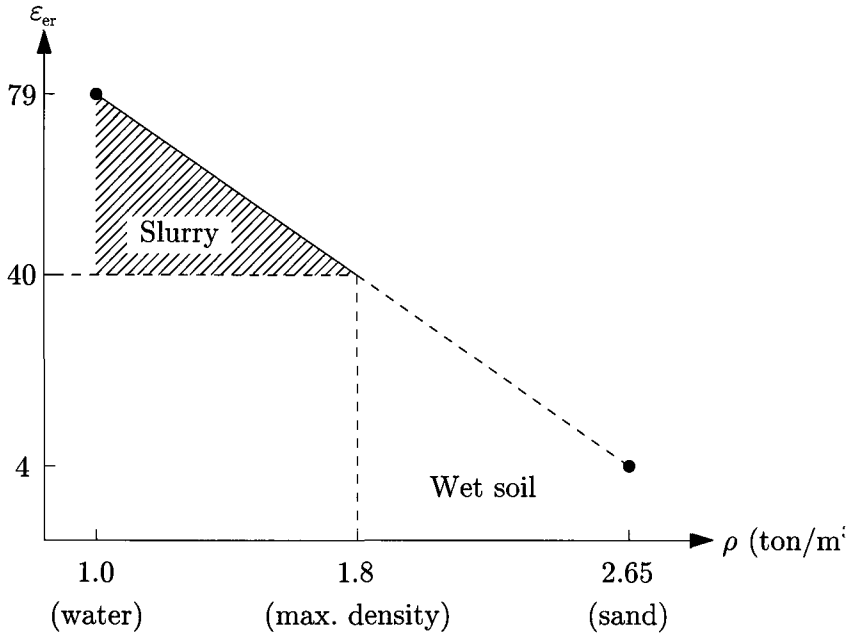


Figure 2.6: Abstract representation of the relative effective permittivity of a sand-water mixture, calculated using a simple linear interpolation. Typical slurry densities are in the range 1.0 – 1.8 ton/m³.

2.5 Other materials

The approximate relative permittivities of some materials that may be relevant for this research project are summarized in table 2.1 below:

Table 2.1: Relative effective permittivities of some relevant materials

Material	ϵ_{er}	Remarks
Water	70 – 85	
Soil	4 – 6	
Teflon / PTFE	2.1	
PVC	4.55	
Alumina (Al_2O_3)	10	
Nylon-6,6	6.6	$f = 1000 \text{ Hz}, T = 22 \text{ }^\circ\text{C}$
	> 20	Wet
Glass fiber laminates	3.5 – 4.0	Depends on resin

Chapter 3

Antenna design

Contents

3.1	Introduction	18
3.2	Electromagnetic wave equation	18
3.3	The dipole antenna	21
3.4	Near and far field	22
3.5	Insulated Antenna	23
3.6	Feeding the antenna	26
3.7	Antenna near conducting surface	33

3.1 Introduction

The antenna is the interface between the measurement system and the medium to be probed. The (dielectric) properties of this medium greatly affect the performance of the antenna. While for most antenna applications the medium is just air, for our purpose the antenna has to perform in water, with a widely varying conductivity, with and without sand.

In order to design an antenna that performs reasonably well in all these different environments, it is important to know how the antenna interacts with the medium and how its performance can be optimized. There are several parameters that affect an antenna's performance and can be adjusted during the design. The most common are:

- Resonance frequency / length
- Bandwidth
- Driving point impedance
- Gain
- Efficiency

For our purpose, a simple omnidirectional dipole antenna ($Gain = 1$) with a narrow *bandwidth* satisfies. This leaves the *resonance frequency* (or the corresponding *resonance length*) and the *driving point impedance* as the most important tuning parameters to make an antenna with a high *efficiency*, which is the ratio of power put into the antenna to power actually radiated. Both parameters depend, among others, on the physical length of the antenna and the propagation medium. However, the influence of the propagation medium on the antenna performance can be diminished by insulation of the antenna. The intricate properties of an insulated antenna are described in detail in section 3.5. First, the required electromagnetic theory is summarized in the sections below.

3.2 Electromagnetic wave equation

An antenna transmits or receives electromagnetic radiation, which is a combination of oscillating electric and magnetic fields moving through a medium. The electric and magnetic fields are linked by Maxwell's equations. An antenna couples to either the electric component (straight wire antenna) or the magnetic component (coil or looped wire antenna). Because the dipole antenna belongs to the first kind, it is more straightforward to describe the electromagnetic field by its electric component. The electromagnetic wave equation for the electric field follows directly from the Maxwell equations (appendix L) and is given by

$$\nabla^2 \mathbf{E} - \mu \varepsilon_e \frac{\partial^2 \mathbf{E}}{\partial t^2} - \mu \sigma_e \frac{\partial \mathbf{E}}{\partial t} = \frac{1}{\varepsilon_e} \nabla \rho \quad (3.1)$$

where μ , ε_e and σ_e are the permeability, effective permittivity and effective conductivity of the propagation medium and ρ is the space charge. Assuming a harmonic time dependence for the electric field $\mathbf{E}(\mathbf{r}, t) = \mathbf{E}(\mathbf{r}) \exp(-j\omega t)$ and no charge ($\rho = 0$) the wave equation can be simplified to

$$\nabla^2 \mathbf{E}(\mathbf{r}) + [\mu \varepsilon_e \omega^2 + j \mu \omega \sigma_e] \mathbf{E}(\mathbf{r}) = 0. \quad (3.2)$$

This leads to the definition¹ of the complex wavenumber k

$$k^2 = \mu \varepsilon_e \omega^2 + j \mu \omega \sigma_e \quad (3.3)$$

¹This definition assumes a time-dependence $\exp(+j\omega t)$. Other sources may use a $\exp(-j\omega t)$ dependence, in which case the plus sign becomes a minus. Derived quantities may change likewise.

and the wavevector in the propagation direction \mathbf{n} :

$$\mathbf{k} = k\mathbf{n}. \quad (3.4)$$

Assuming uniform plane waves propagating along a fixed direction, the solution of (3.2) is a superposition of a forward and a backward traveling wave

$$\mathbf{E}(\mathbf{r}, t) = \mathbf{E}_0^+(\mathbf{r}) \exp[j(\mathbf{k} \cdot \mathbf{r} - \omega t)] + \mathbf{E}_0^-(\mathbf{r}) \exp[-j(\mathbf{k} \cdot \mathbf{r} + \omega t)]. \quad (3.5)$$

The complex wavenumber can be split into a real and an imaginary component:

$$k = \beta + j\alpha. \quad (3.6)$$

Substitution in the plane wave solution (3.5) and dropping the time dependence yields

$$\mathbf{E}(r) = \mathbf{E}_0^+(r) \exp(j\beta r) \exp(-\alpha r) + \mathbf{E}_0^-(r) \exp(-j\beta r) \exp(\alpha r). \quad (3.7)$$

Considering the forward traveling wave, its behaviour is determined by the factor $\exp(j\beta r) \exp(-\alpha r)$. This behaviour is shown in figure 3.1.

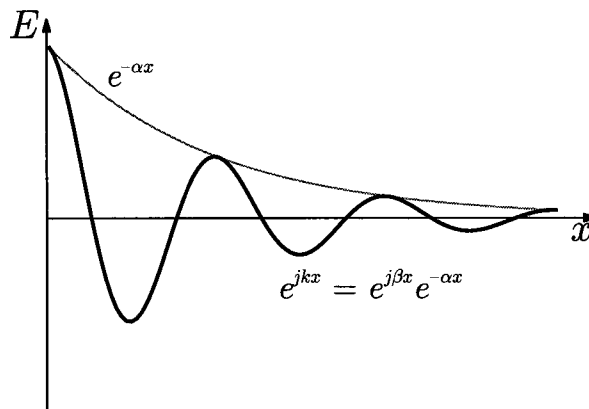


Figure 3.1: An electromagnetic wave with complex (non-real) wavenumber k shows exponential attenuation.

The graph shows that the constant β determines the phase and the constant α causes exponential attenuation of the forward moving wave $\mathbf{E}_0^+(\mathbf{r}) \exp(j\mathbf{k} \cdot \mathbf{r})$ (and of the backward moving wave $\mathbf{E}_0^-(\mathbf{r}) \exp(-j\mathbf{k} \cdot \mathbf{r})$ for decreasing r). The constants α and β can be derived by combining (3.3) with (3.6) squared:

$$\alpha = \beta_0 \sqrt{1/2} \sqrt{\sqrt{1 + \left(\frac{\sigma_e}{\epsilon_e \omega}\right)^2} - 1} \quad (3.8a)$$

$$\beta = \beta_0 \sqrt{1/2} \sqrt{\sqrt{1 + \left(\frac{\sigma_e}{\epsilon_e \omega}\right)^2} + 1} \quad (3.8b)$$

where β_0 is the real wavenumber at zero conductivity, given by:

$$\beta_0 = \frac{\omega}{c_0} \sqrt{\epsilon_{er}} \quad (3.8c)$$

with c_0 the speed of light in vacuum as defined by (M.1). Both the real wavenumber and the attenuation constant depend on the conductivity of the water. This dependence is plotted in figure 3.2 for a frequency of 62.5 MHz, which is used in most of the experiments.

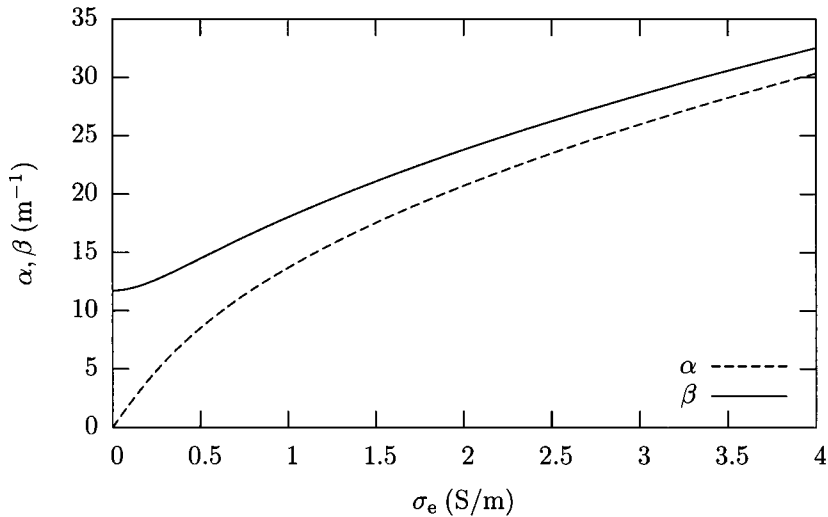


Figure 3.2: Plots of the real part β (solid) and imaginary part α (dashed) of the wavenumber k of electromagnetic waves in saline water at a frequency of 62.5 MHz as a function of the conductivity.

A plot of the wavelength $\lambda = 2\pi/\beta$ at a frequency of 62.5 MHz as a function of the conductivity is shown in figure 3.3. As the plot shows, the conductivity not only causes attenuation, but also changes the wavelength considerably.

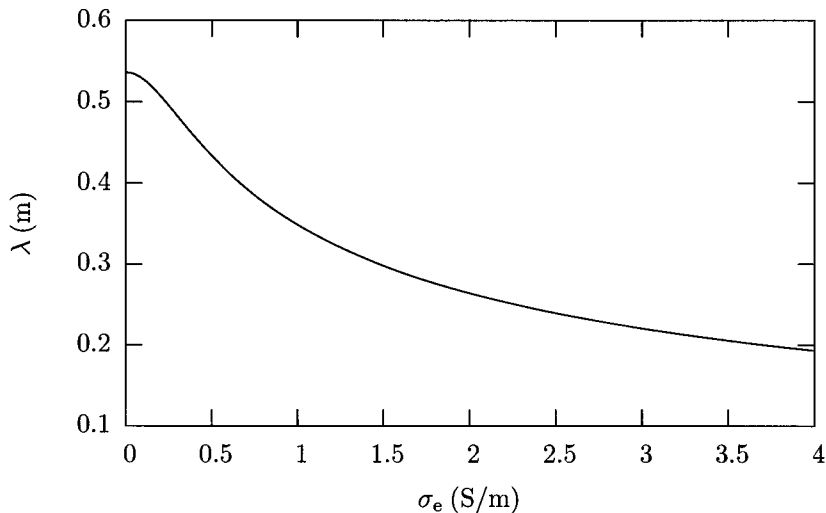


Figure 3.3: Plot of the wavelength of electromagnetic waves in saline water at a frequency of 62.5 MHz as a function of the conductivity.

The assumption of no charge ($\rho = 0$) is easily validated for a conducting medium. Taking the divergence of equation (L.2a) and substituting (L.2c) a first order differential equation is obtained

for the charge density ρ

$$\begin{aligned} 0 &= \sigma_e \nabla \cdot \mathbf{E} + \varepsilon_e \frac{\partial}{\partial t} \nabla \cdot \mathbf{E} \\ &= \frac{\sigma_e}{\varepsilon_e} \rho + \frac{\partial}{\partial t} \rho. \end{aligned} \quad (3.9)$$

Defining the relaxation time $\tau = \varepsilon_e / \sigma_e$, the solution of this differential equation can be written as

$$\rho(\mathbf{r}, t) = \rho(\mathbf{r}, 0) \exp(-t/\tau). \quad (3.10)$$

This means that in a conducting medium, the charge density decays to zero with a characteristic time on the order of τ . This time constant is much shorter than the timescale of the used electromagnetic frequencies, so the charge density will effectively be zero.

3.3 The dipole antenna

Conceptually the simplest antenna design is the half-wave dipole, which -as its name implies- has a length of $\lambda/2$, and consists of two separate wires of length $\lambda/4$ which are placed in line and connected to the source at the center. The two elements are fed the same signal 180 degrees out of phase.

Dipole antennas have a toroidal radiation pattern where the axis of the toroid centers about the dipole, see figure 3.4. Single antenna elements have wide radiation patterns. If necessary, the directionality can be increased by using arrays of antenna elements or by increasing the antenna length.

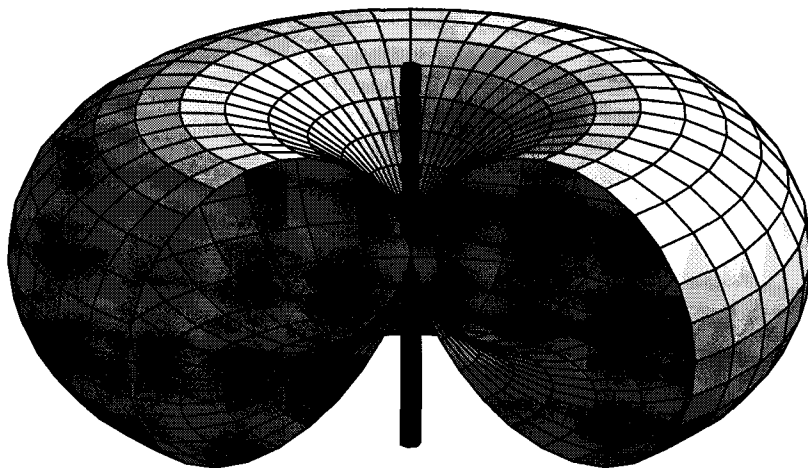


Figure 3.4: Cut-out view of the omnidirectional radiation pattern of a half-wave dipole

Ideally, the current distribution on a dipole antenna, placed at $\mathbf{r} = 0$ and pointed along the z axis, is sinusoidal:

$$\mathbf{I}(x', y', z') = I_0 \cos(z') \hat{\mathbf{z}}. \quad (3.11)$$

3.4 Near and far field

The electromagnetic field produced by an antenna (see figure 3.5) can be split in three separate regions depending on the nature of the field:

1. Reactive near field or evanescent field, varying as $E_\theta \sim 1/r^3$ and $E_r \sim 1/r^3$.
This is the field at distances that are small compared to the wavelength and for which the reactive field dominates over the radiative field. No power is radiated in this region: the energy circulates between the field and the antenna.
2. Radiating near field or Fresnel field, a transition region.
This is the field between the reactive near field and the far field. The radiation fields predominate but the angular field distribution is still dependent on the distance from the antenna.
3. Radiating far field or Fraunhofer field, varying as $E_\theta \sim 1/r$ and $E_r \approx 0$.
In this region only the radiating field components are significant. The radiation pattern is independent of distance from the transmitting antenna.

In the far field, the electromagnetic fields of an ‘electric’ antenna and a ‘magnetic’ antenna are indistinguishable. In the near field however, the electromagnetic fields are very different: an antenna which couples to the electric field will give a larger electric component and an antenna which couples to the magnetic field will give a larger magnetic component. As a guideline, the extents of the three regions can be approximated for a normal half-wave dipole antenna by:

$$\text{Reactive near field:} \quad r_{\text{nf}} < 0.62 \sqrt{\frac{D^3}{\lambda}} \quad (3.12a)$$

$$\text{Radiating far field:} \quad r_{\text{ff}} > \frac{2D^2}{\lambda} \quad (3.12b)$$

$$\text{Radiating near field:} \quad r_{\text{nf}} < r < r_{\text{ff}} \quad (3.12c)$$

where D is the largest dimension of the antenna and λ is the wavelength in the propagation medium. The dimension D is $\lambda/2$ for a normal half-wave dipole but can be much longer for an insulated antenna, which is discussed in the next section.

In the experimental setup the propagation medium is water of various salinities. Using the approximate wavelengths for pure, river and sea water from figure 3.3 the approximate distances for a bare $\lambda/2$ and an 48 cm insulated 62.5 MHz dipole antenna are shown in table 3.1.

Table 3.1: Approximate near and far field regions for a 25 cm and a 48 cm half-wave dipole antenna in pure, river and sea water.

Antenna		Pure	River	Sea
$D = 0.25$ m	$r_{\text{nf}} =$	0.11 m	0.12 m	0.17 m
	$r_{\text{ff}} =$	0.25 m	0.31 m	0.63 m
$D = 0.48$ m	$r_{\text{nf}} =$	0.29 m	0.33 m	0.46 m
	$r_{\text{ff}} =$	0.92 m	1.15 m	2.3 m

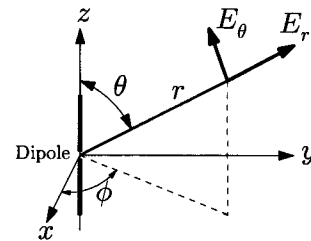


Figure 3.5: The electric field of a dipole is composed of a longitudinal component E_r and a transverse component E_θ .

Considering that the outer diameter of the metal pipe of the experimental setup is 0.75 m, it can be concluded that a large part of the measurements place in the reactive and radiating near fields. This is an exceptional range, which is rarely dealt with in literature.

3.5 Insulated Antenna

An interesting question is whether a dipole antenna in a lossy (conducting) medium should be insulated or not. According to [17] the measurable properties of an antenna are sensitive primarily to the electrical properties of the medium in *direct contact* with its surfaces. This means that the electrical properties of an antenna with insulation depend more on the properties of the insulating layer and change less when the propagation medium changes. Measurements by Iizuka [13] show that the resonance lengths of antennas with thicker insulation change less with varying water conductivity than the resonance length of a bare antenna.

Thus, the efficiency of an antenna which is to be operated in both lossy and loss free media will be better when it is insulated. On the other hand, the insulating layer should not be as too thick, because it absorbs some of the radiated energy and thus decreases the sensitivity. In other words: a careful selection of the insulating layer thickness is necessary.

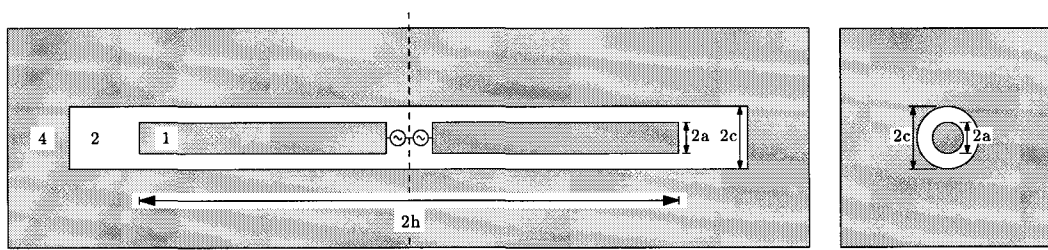


Figure 3.6: Schematic representation (side view and top view) of a dipole antenna (1) with two insulating layers (2) and (3) in medium (4).

In order to model the behaviour of the insulated antenna in a conducting medium, it can be represented by a *coaxial transmission line*, as shown in figure 3.6. Employing the same numbering convention as used by [17, 20, 21, 24, 42], the inner conductor (antenna) is assigned number 1, two insulating layers are numbered 2 and 3 and the ambient medium (water), which takes the role of outer conductor, is assigned number 4 - even in absence of insulating layer 3.

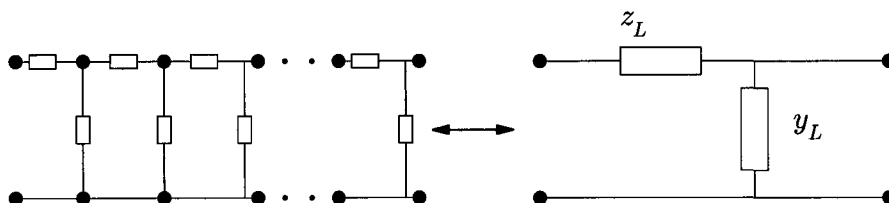


Figure 3.7: Electronic representation of a coaxial transmission line. The series impedance z_L and shunt admittance y_L of a coaxial transmission line are distributed parameters.

An electronic representation of a coaxial transmission line is shown in figure 3.7. In general, the series impedance (per unit length) consists of a resistance and an inductance ($z_L = R + j\omega L$) and the shunt admittance (per unit length) consists of a conductance and a capacitance ($y_L = G + j\omega C$). Both z_L and y_L are *distributed* parameters: impedance and admittance are spread out over the entire length of the transmission line and not confined to a single *lumped* element.

Transmission line parameters

To be able to calculate the important antenna parameters *resonance length* and *driving point impedance* using the coaxial transmission line model, the derivation of the transmission line parameters *characteristic impedance* Z_0 (which is independent of the line length) and *complex wavenumber* k_L is needed.

The complex wavenumber k_L of the transmission line can be derived from the propagation constant:

$$k_L = -j\gamma = \sqrt{-1}\gamma \quad (3.13)$$

and both the propagation constant γ and the characteristic impedance Z_0 can be derived from the distributed parameters z_L and y_L :

$$Z_0 = \sqrt{\frac{R + j\omega L}{G + j\omega C}} = \sqrt{\frac{z_L}{y_L}} \quad (3.14)$$

$$\gamma = \sqrt{(R + j\omega L)(G + j\omega C)} = \sqrt{z_L y_L}. \quad (3.15)$$

The derivation of the shunt admittance y_L and the series impedance z_L of the transmission line which represents the insulated antenna can be found in appendix D. This derivation results in equations for Z_0 and k_L for an antenna with a single insulating layer (no layer 3, see figure 3.6):

$$Z_0 = \frac{\eta_2 k_L}{2\pi k_2} \ln\left(\frac{c}{a}\right) \quad (3.16)$$

$$k_L = k_2 \sqrt{1 + \frac{H_0^{(1)}(k_4 c)}{k_4 c H_1^{(1)}(k_4 c) \ln(c/a)}} \quad (3.17)$$

where

$$\begin{aligned} \eta_2 &= \omega\mu/k_2, \text{ the complex characteristic impedance of medium 2,} \\ k_2 &= \omega/c_0 \cdot \sqrt{\epsilon_{r,2}}, \text{ the wavenumber of medium 2,} \\ k_4 &= \sqrt{\omega^2 \mu(\epsilon_{r,4}\epsilon_0 + j\sigma_4/\omega)}, \text{ the wavenumber of medium 4 and} \\ a, c &= \text{the dimensions as indicated in figure 3.6.} \end{aligned} \quad (3.18)$$

The speed of light in vacuum c_0 is defined by (M.1). The complex characteristic impedance of a propagation medium is related to the characteristic impedance of free space by $\eta = \eta_0/\sqrt{\epsilon^*}$, where ϵ^* is the complex permittivity of the propagation medium. The characteristic impedance of free space is given by $\eta_0 \equiv \sqrt{\mu_0/\epsilon_0} \approx 376.7 \Omega$. The permeability in vacuum μ_0 is defined by (M.2).

Antenna parameters

Finally the driving point impedance Z_{ant} of an insulated dipole antenna of half-length h can be calculated:

$$Z_{\text{ant}} = 2jZ_0 \cot k_L h. \quad (3.19)$$

At the resonance length, the imaginary component of the driving point impedance, the ‘reactance’, is zero. As explained in the next section, a completely real-valued (‘resistive’) driving point impedance results in the highest antenna efficiency. This length can be calculated by splitting equation (3.19) into its real and imaginary parts using identity (M.6) where the complex wavenumber k_L has been split into its real and imaginary parts using $k_L = \beta_L + j\alpha_L$. Thus, the real (resistance R_{ant}) and imaginary (reactance X_{ant}) parts of Z_{ant} are given by:

$$R_{\text{ant}} = \frac{\eta_2}{\pi k_2} \ln\left(\frac{c}{a}\right) \frac{\beta_L \sinh(2\alpha_L h) - \alpha_L \sin(2\beta_L h)}{\cosh(2\alpha_L h) + \cos(2\beta_L h)} \quad (3.20)$$

$$X_{\text{ant}} = \frac{\eta_2}{\pi k_2} \ln\left(\frac{c}{a}\right) \frac{\alpha_L \sinh(2\alpha_L h) + \beta_L \sin(2\beta_L h)}{\cosh(2\alpha_L h) + \cos(2\beta_L h)}. \quad (3.21)$$

Evaluating $X_{\text{ant}} = 0$ leads to the following resonance condition:

$$\alpha_L \sinh(2\alpha_L h) + \beta_L \sin(2\beta_L h) = 0 \quad (3.22)$$

which can be solved to determine the antenna resonance length h_{res} .

Example 1:

The resonance half-length of an insulated dipole antenna in water for a frequency of 60 MHz can be calculated using (3.22). For a plot of the resonance half-length versus the conductivity of the water, the following material properties are assumed:

- Medium 1: copper
 $\epsilon_{er,1} = 0$
 $\sigma_1 = 5.8 \times 10^7 \text{ S/m}$
- Medium 2: teflon
 $\epsilon_{er,2} = 2.1$
 $\sigma_2 = 0$
- Medium 4: water
 $\epsilon_{er,4} = 79$
 $\sigma_4 = \text{variable}$

The antenna dimensions (see figure 3.8) are assumed to be $2a = 10 \text{ mm}$ and $2c = 12 \text{ mm}$, so the insulation thickness is 1 mm. This leads to the plot shown in figure 3.9 below.

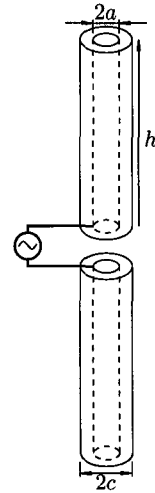


Figure 3.8:
An insulated dipole.

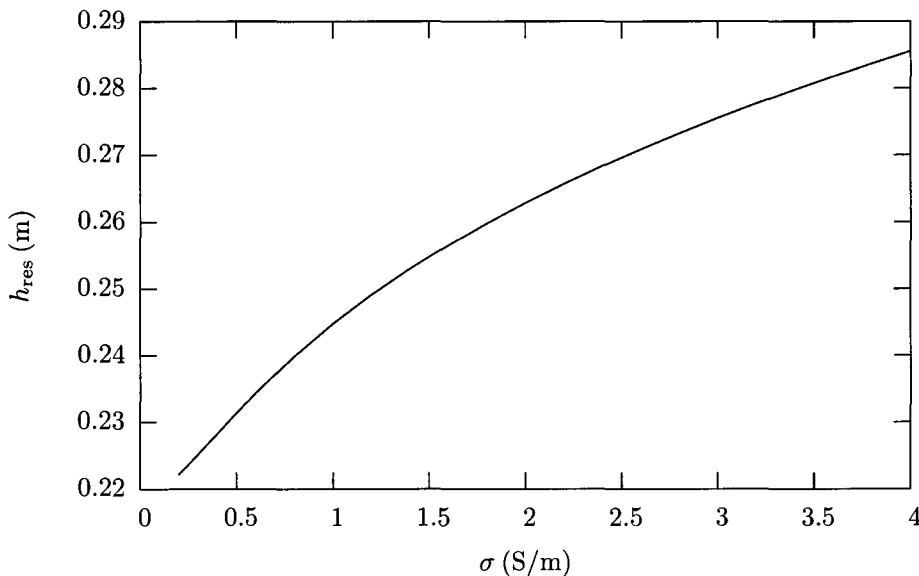


Figure 3.9: The resonance half-length of a 60 MHz insulated dipole antenna in water of varying conductivity.

So, depending on the conductivity, the resonance half-length should be somewhere between 22.5 and 28.5 cm, which corresponds to total dipole lengths between 45 cm and 57 cm. Note that this is considerably longer than a *bare* half-wave dipole antenna, which should be approximately 28 cm for pure water.

The driving point impedance of the antenna can be calculated once the half-length has been chosen. For three different half-lengths, the real and imaginary parts of Z_{ant} have

been plotted as a function of the conductivity of the water in figure 3.10 below:

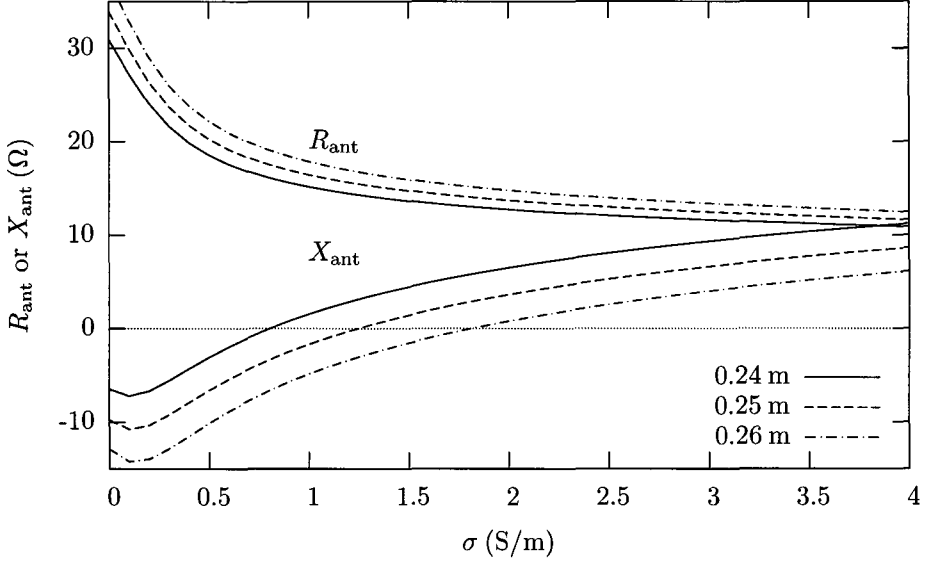


Figure 3.10: The resistance R_{ant} (upper curves) and reactance X_{ant} (lower curves) of a 60 MHz insulated dipole antenna in water of varying conductivity for three different antenna half-lengths h .

Recalling that an antenna is resonant when $X_{ant} = 0$, it can be concluded that each antenna length corresponds to a different optimum water conductivity. For river water with $\sigma = 0.65$ S/m the antenna with $h = 24$ cm would be nearly resonant, but for higher conductivities a longer antenna would be better. The corresponding (real) resistance R_{ant} of the insulated antenna varies between 15 and 17 Ω at resonance.

Practical deviations

According to [9] the characteristic impedance Z_0 of a cylindrically insulated antenna with $1.4 \leq c/a \leq 10$ approximates a planar geometry within 10%.

For very thin wires, the current distribution can be assumed to be sinusoidal. However, a practical antenna will have a certain thickness. The accuracy of the thin-wire approximation is usually limited to diameters $d < 0.05 \lambda$, see [2]. For a frequency of 100 MHz in water, this yields $d < 1.5$ cm.

3.6 Feeding the antenna

A transmission-line Thevenin equivalent [2] of an antenna with its feedline (transmission line) is shown in figure 3.11. The transmission line is represented by a line with characteristic impedance Z_{tl} and the antenna is represented by the antenna driving point impedance Z_{ant} , which can be split up in a real part (resistance) and an imaginary part (reactance):

$$Z_{ant} = R_{ant} + jX_{ant}. \quad (3.23)$$

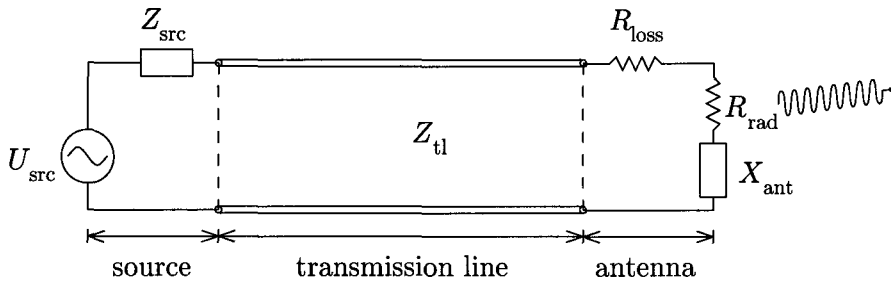


Figure 3.11: Transmission-line Thevenin equivalent of an antenna with its feedline in transmission mode. The total antenna impedance is $Z_{\text{ant}} = R_{\text{loss}} + R_{\text{rad}} + jX_{\text{ant}}$.

The antenna resistance R_{ant} consists of two components: the radiation resistance R_{rad} , which represents the radiation of power into the propagation medium, and the loss resistance R_{loss} , which represents both the conduction loss and the dielectric loss of the antenna.

$$R_{\text{ant}} = R_{\text{rad}} + R_{\text{loss}}. \quad (3.24)$$

The objective of an antenna system is to transfer most energy of the source to the radiation resistance R_{rad} . This is the case when the generator and the load are matched to the transmission line, so that $Z_{\text{src}} = Z_{\text{ant}} = Z_{\text{tl}}$. Now half of the generated power is delivered to the load and the other half is lost in the internal impedance. Thus at least half of the energy is always wasted. In a matched system, the radiated power is given by:

$$P_{\text{rad}} = \frac{1}{2} |I_0|^2 R_{\text{rad}} \quad (3.25)$$

which again indicates that half of the available power is radiated.

The match between an antenna and its transmission line is only proper and complete when the following two conditions are met:

1. The antenna *driving point impedance* is matched to the transmission line impedance.
2. The antenna (*un*)balance is matched to the feed line (*un*)balance.

The right way to do this, is to use a *matching network* between the transmission line and the antenna. These matching networks exist in many different forms.

Impedance matching

As a narrow-band match is sufficient for the application, a very simple quarter-wave match or Q-match can be used. It consists of a piece of transmission line of length $\lambda/4$ placed between the impedances that need to be matched. In order to match an impedance Z_1 to an impedance Z_2 , the impedance of this piece of transmission line should be chosen such that

$$Z_{\text{match}} = \sqrt{Z_1 \cdot Z_2}. \quad (3.26)$$

For the quarter-wave length the following equation can be used:

$$l = \lambda/4 = 1/4 \cdot \text{VF} \cdot c_0/f \quad (3.27)$$

where VF is the velocity factor, which is always specified for each type of transmission line and mainly depends on the dielectric used. For the commonly used RG-58 and RG-59 types, the dielectric is polyethylene and $\text{VF} = 0.66$.

Another, somewhat more complicated impedance matching circuit that has been tested is the transmission line transformer (TLT). This device is described in appendix G.

Voltage Standing Wave Ratio

Though a direct measurement of the impedance of the antenna is not possible, the correctness of the impedance matching used can be verified with a so-called Voltage Standing Wave Ratio (VSWR) meter. At each interface between two different impedances, a fraction of the wave's energy will reflect back to the source, forming a standing wave in the transmission line. This fraction is given by the reflection coefficient Γ :

$$\Gamma = \frac{Z_{\text{ant}} - Z_{\text{tl}}}{Z_{\text{ant}} + Z_{\text{tl}}} \quad (3.28)$$

where Z_{ant} is the driving point impedance of the antenna and Z_{tl} is the characteristic impedance of the transmission line. The Voltage Standing Wave Ratio is then given by:

$$\text{VSWR} = \frac{1 + |\Gamma|}{1 - |\Gamma|}. \quad (3.29)$$

In case of a perfect impedance match, the reflection coefficient is zero and the VSWR equals 1. In practice however, this is almost never achieved. A stylized representation of the electromagnetic waves on an antenna with feedline system in the ideal situation ($\text{VSWR} = 1$) and in reality ($\text{VSWR} > 1$) is shown in figure 3.12.

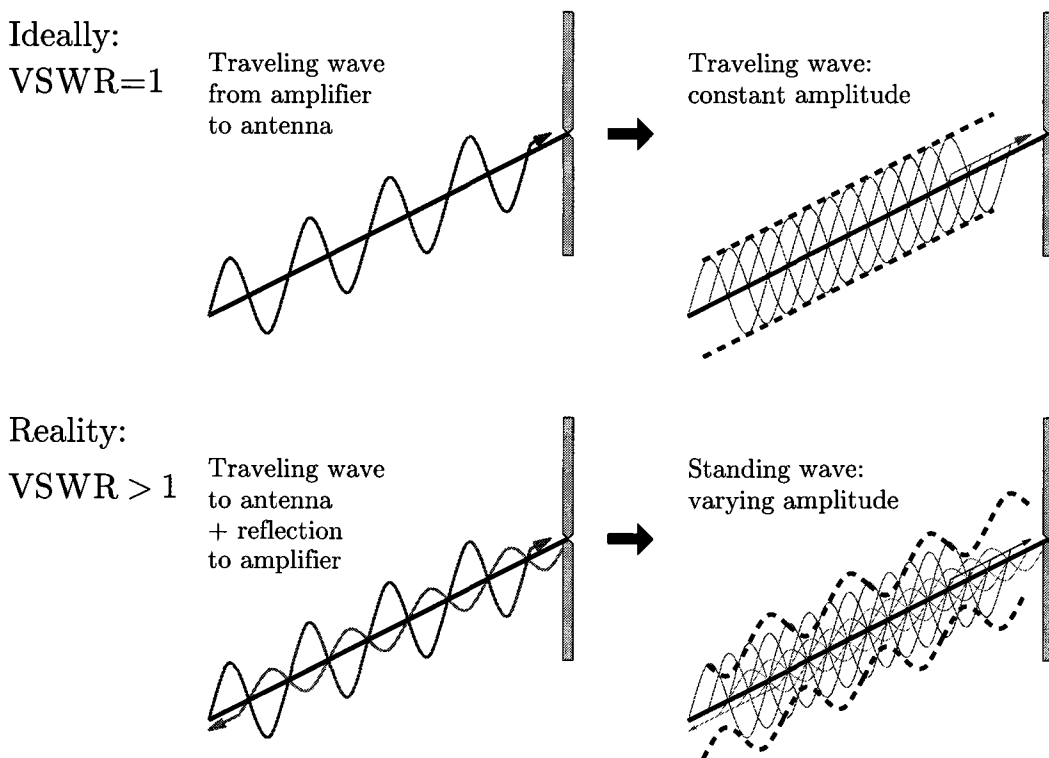


Figure 3.12: Upper: a traveling wave from the amplifier to the antenna causes a constant amplitude along the transmission line. Lower: an imperfect match causes a part of the signal to be reflected, back to the amplifier. The sum of the forward and backward traveling waves causes a standing wave on the transmission line.

Another approach to the VSWR, which shows that it is really a *voltage ratio*, is depicted in figure 3.13. For calculations however, (3.29) is usually more practical.

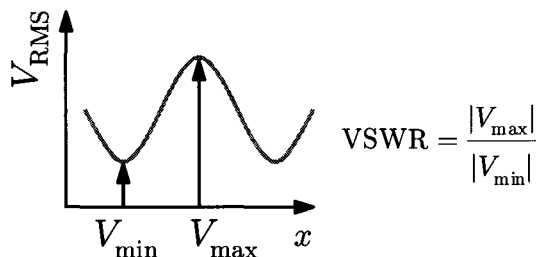


Figure 3.13: A schematic representation of the RMS voltage versus the position of standing wave along a transmission line. The VSWR corresponds to the proportion of the maximum to the minimum voltage of the standing wave.

The power loss due to an impedance mismatch between the antenna and the transmission line is given by [2]:

$$\frac{P_{\text{lost}}}{P_{\text{avail}}} = \left| \frac{Z_{\text{ant}} - Z_{\text{tl}}}{Z_{\text{ant}} + Z_{\text{tl}}} \right|^2 = |\Gamma|^2 \tag{3.30}$$

which gives a power loss of 1/9 or 0.5 dB for $\Gamma = 2$. The power that is lost when an antenna with driving point impedance Z_{ant} is fed by a coaxial transmission line depends on the impedance Z_{tl} of that transmission line, as shown in figure 3.14.

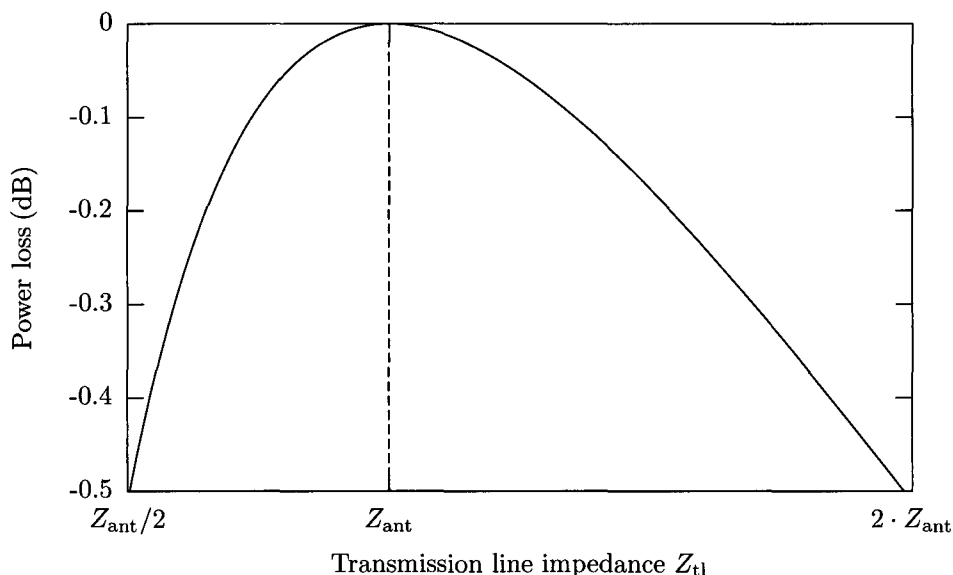


Figure 3.14: Power loss in an antenna - transmission line system due to a mismatch between the impedance of the antenna (Z_{ant}) and the impedance of the transmission line Z_{tl} .

The transmission line impedances $Z_{\text{tl}} = Z_{\text{ant}}/2$ and $Z_{\text{tl}} = 2Z_{\text{ant}}$ correspond to $\text{VSWR} = 2$. The power loss increases less for antenna impedances higher than the impedance of the coaxial transmission line than for lower impedances. While this power loss may not seem very much, in practice a VSWR of 2 is generally the upper limit if the amplifier is to operate at full power because most amplifiers are not very good at handling power that is sent back to its output.

Example 2:

The impedance of a signal generator and coaxial transmission line, which is generally 50Ω for both, has to be matched to the impedance of the antenna. For the setting introduced in example 1, the driving point impedance at resonance is somewhere between 15 and 17Ω , depending on the antenna length. The optimal antenna length, besides depending on the frequency, also depends on the conductivity of the water.

Focussing on a 60 MHz antenna for use in river water ($\sigma = 0.65 \text{ S/m}$), a contour plot which shows the VSWR as a function of the impedance of the transmission line and the antenna half-length is shown in figure 3.15.

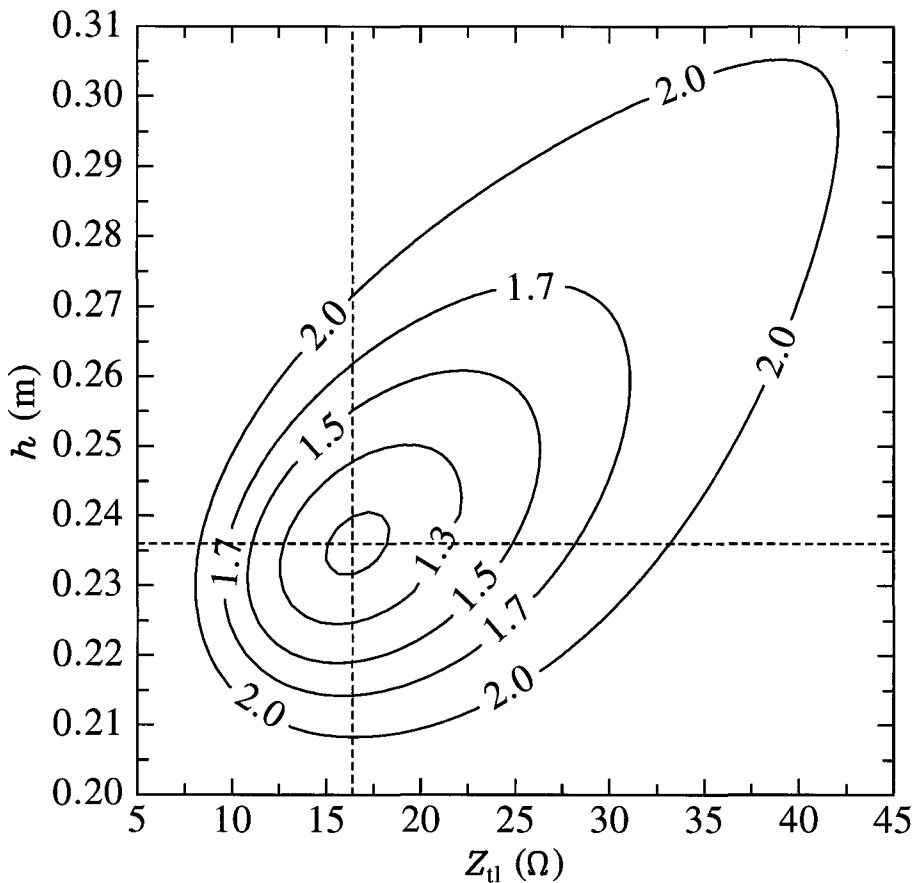


Figure 3.15: The VSWR of an insulated antenna in river water with transmission line is plotted as a function of the impedance of the transmission line (Z_{t1}) and the half-length (h) of the antenna. The plotted contours correspond to $\text{VSWR} = \{1.1, 1.3, 1.5, 1.7, 2.0\}$. The optimum setting ($\text{VSWR} = 1$) is indicated and corresponds to $h = 23.6 \text{ cm}$ and $Z_{t1} = 16.4 \Omega$.

This plot immediately shows that the optimal antenna for use in river water has a half-length of 23.6 cm and is fed by a transmission line of 16.4Ω .

Using (3.26) the desired impedance of the Q-match is calculated to be 28.6Ω . Because coaxial cables are not readily available in every thinkable impedance, a practical workaround is shown in figure 3.16 below.

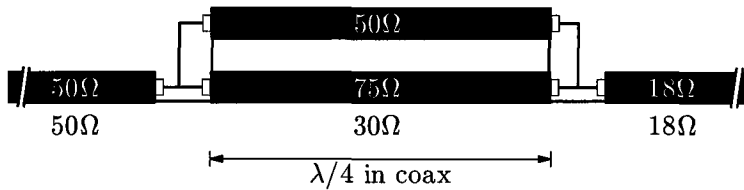


Figure 3.16: Parallel connection of two standard 50 and 75 Ω coaxial transmission lines yields a transmission line with an impedance of 30 Ω , which can be used as a Q-match between 50 and 18 Ω .

This matching circuit uses a parallel connection of two standard coaxial transmission lines to create a transmission line of 30 Ω and results in an impedance of 18 Ω at the feedpoint of the antenna. The power loss introduced by using this circuit as a Q-match is negligible. As figure 3.15 shows, the choice of a transmission line impedance isn't very critical. In practical situations, a VSWR of 1.1 is already considered to be very good.

For the assumed frequency of 60 MHz the length of the Q-match should be 82.4 cm. However, because of the parallel connection of two coaxial transmission lines, the optimum length may be a bit different in practice.

Balance-to-unbalance transformation

The dipole is inherently a *balanced* antenna, because of its symmetry. Ideally, a balanced antenna should be fed using a balanced feed line. However, on the amplifier side a (50 Ω) unbalanced impedance is expected. To connect an *unbalanced* coaxial transmission line to the dipole antenna a *balun* must be used, which adapts the *balanced* antenna to the *unbalanced* feed line.

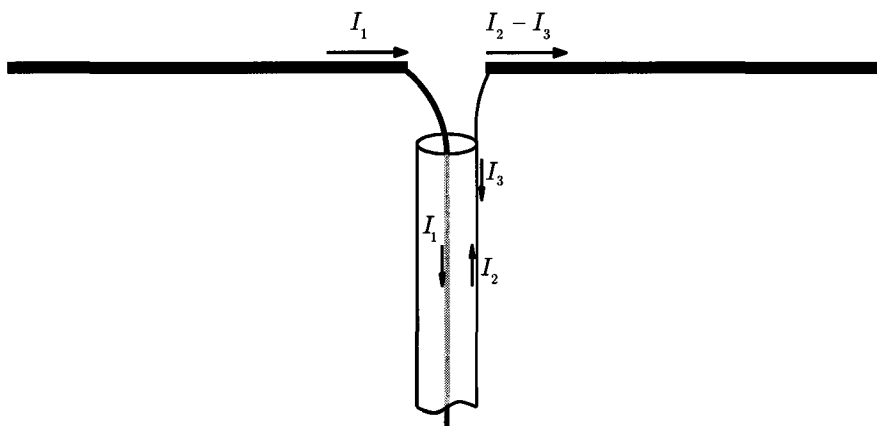


Figure 3.17: Dipole antenna with coaxial feed. Besides the intended antenna currents I_1 and I_2 there is a current I_3 on the outside of the outer conductor of the coaxial transmission line.

Without balance matching, a current I_3 (see figure 3.17) will flow on the outside of the outer conductor of the coaxial transmission line: the feed line becomes essentially one big radiating antenna, which is undesirable because it distorts the radiation pattern and power will be radiated in unwanted directions.

A simple balun design is the Pawsey stub, which is shown in figure 3.18.

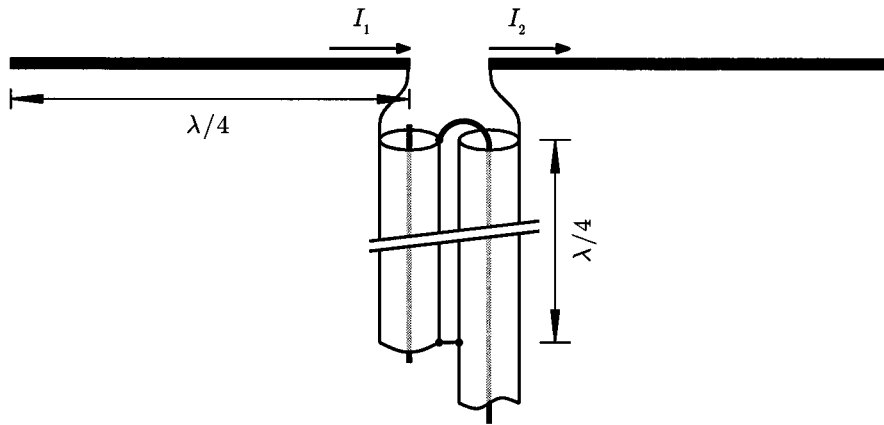


Figure 3.18: Dipole antenna with a Pawsey stub. The antenna currents I_1 and I_2 are balanced now: there is no current on the outside of the outer conductor of the coaxial transmission line.

This balun operates by using an additional coaxial transmission line parallel to the feedline. This second transmission line is short circuited to the feedline $\lambda/4$ away from the feed point. The quarter-wave transmission line will result in a very high (theoretically infinite) impedance at the frequency where it is quarter of a wave long and will choke the outer conductor current I_3 . Just like the Q-match, this is a narrow-band device.

Example 3:

Continuing with the antenna from examples 1 and 2, the circuit can now be completed. Combining the Q-match and the Pawsey stub leads to the circuit shown in figure 3.19.

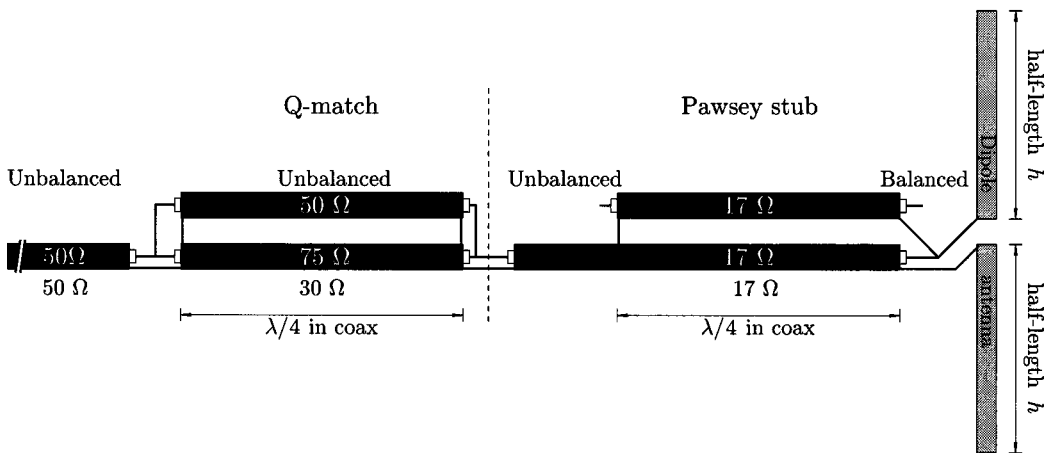


Figure 3.19: Impedance matching using a quarter wave match and unbalance to balance transformation using a Pawsey stub.

The transmission line on the left comes from the amplifier, and is 50 Ω unbalanced. First a transition is made to 18 Ω unbalanced by means of the Q-match. Then a transition from 18 Ω unbalanced to balanced is made using Pawsey stub. Having 18 Ω coaxial cables for this purpose would be ideal, but these cables are not commonly available. Using a similar

trick to obtain the $30\ \Omega$ transmission line for the Q-match, a $16.7\ \Omega$ transmission line can be constructed using three $50\ \Omega$ transmission lines in parallel. Strikingly, this impedance matches the antenna driving point impedance of $16.4\ \Omega$ even better. In practice, deviations due to imperfections in the antenna construction, cables and connections will surely occur.

3.7 Antenna near conducting surface

In the experimental setup, the antenna is placed near a metal wall (the pipe wall). A conducting surface reflects electromagnetic waves, and these reflected waves will interfere with the source waves. Depending on the phase difference this interference will be destructive or constructive. This means that the wall will attenuate or amplify the emitted waves, depending on the distance between the antenna and the wall.

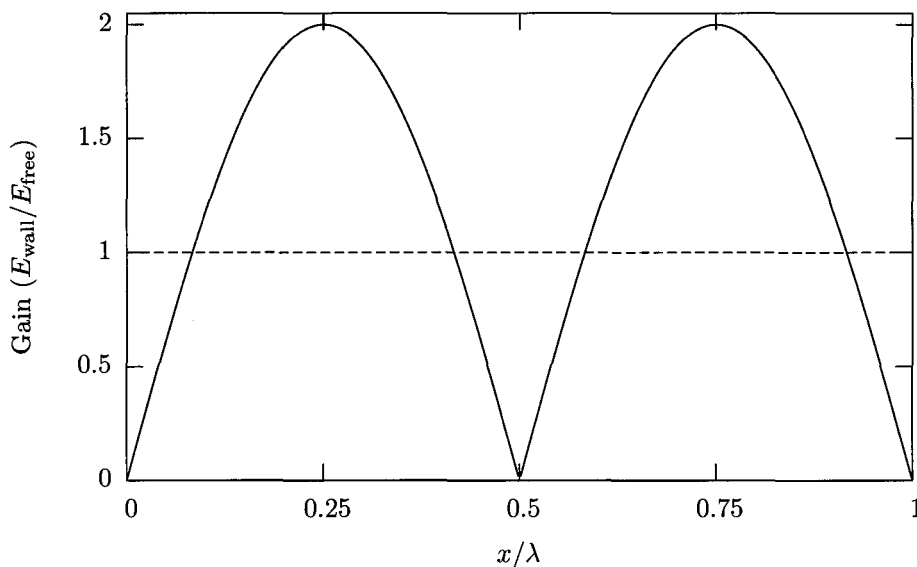


Figure 3.20: The gain in the electric field of an antenna at a distance x from a conducting surface compared to an antenna in free space. Naturally, a gain < 1 indicates a loss.

The gain in the electric component E of the electromagnetic field of an antenna near a conducting wall compared to a free antenna is shown in figure 3.20. This plot makes it clear that placing the antenna at a distance of $x = \lambda/4$ to the wall is a great advantage, for the electric field is doubled.

To mathematically describe an *insulated* antenna near a conducting surface, a *virtual* source is introduced to account for the reflections [2]. For a dipole, placed vertically at a distance $x = d/2$ to the right of a conducting wall, this virtual dipole is located at a distance $d/2$ at the left of this wall and has a reversed polarity, as shown in figure 3.21. So the antenna configuration can be mathematically described by two antennas at a distance d , without conducting wall.

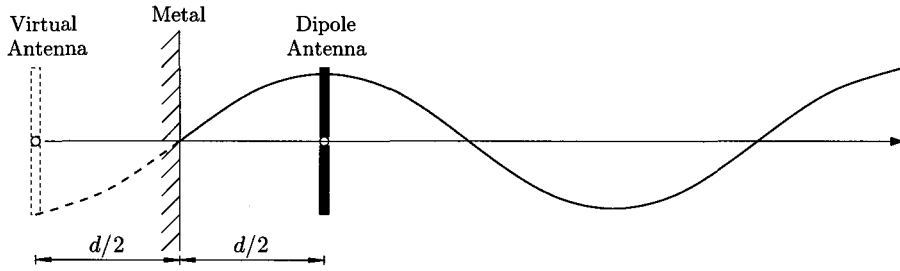


Figure 3.21: Antenna at a distance $d/2$ from a conducting surface behaves like two coupled antennas at a distance d .

The driving-point impedance of the dipole antenna (1) is changed by the presence of the virtual dipole (2). For antisymmetrical excitation, the driving point impedance is

$$Z_{\text{ant}} = Z_{11} + Z_{12} \quad (3.31)$$

where Z_{11} is the self-impedance of antenna 1 and $Z_{12} = Z_{21}$ is the mutual impedance of the two antennas (real and virtual). To apply the transmission line model, the following two assumptions are made [19]:

The antenna thickness is much smaller than the distance between the two antennas:

$$c \ll d \quad (3.32a)$$

the distance between the two antennas is smaller than the antenna half-length:

$$d < h. \quad (3.32b)$$

However, if the antenna half-length h is (substantially) smaller than d , which is the case in the experimental setup where $h = 0.24$ m and $d \approx 0.25$ m, agreement between theory and experiment should still be reasonable. Under these assumptions the antisymmetrical driving point impedance can be calculated using equation (3.19) with a modified wavenumber [10, 19, 22]:

$$\kappa_L = \kappa_2 \sqrt{1 + \frac{H_0^{(1)}(k_4 c) - H_0^{(1)}(k_4 d)}{k_4 c H_1^{(1)}(k_4 c) \ln(c/a)}}. \quad (3.33)$$

In the limit $d \rightarrow \infty$ the term $H_0^{(1)}(k_4 d) \rightarrow 0$ and equation (3.17) is obtained as expected.

Example 4:

An interesting parameter is the VSWR, because it indicates how well a specific antenna-feedline system works. Again using the antenna from example 1, specifically the antenna with half-length $h = 24$ cm, and the matching circuit of example 3 which feeds the antenna with an impedance $Z_{t1} = 17 \Omega$, the influence of the coupling between the antenna and the wall at a distance of $\lambda/4$ can be calculated. For pure water, this distance amounts to $x = 14$ cm for a frequency of 60 MHz.

The VSWR has been calculated for a free antenna and for an antenna near the wall using (3.19,3.28,3.29) and the corresponding wavenumbers (3.17) and (3.33). Plots of the VSWR versus the conductivity are shown in figure 3.22.

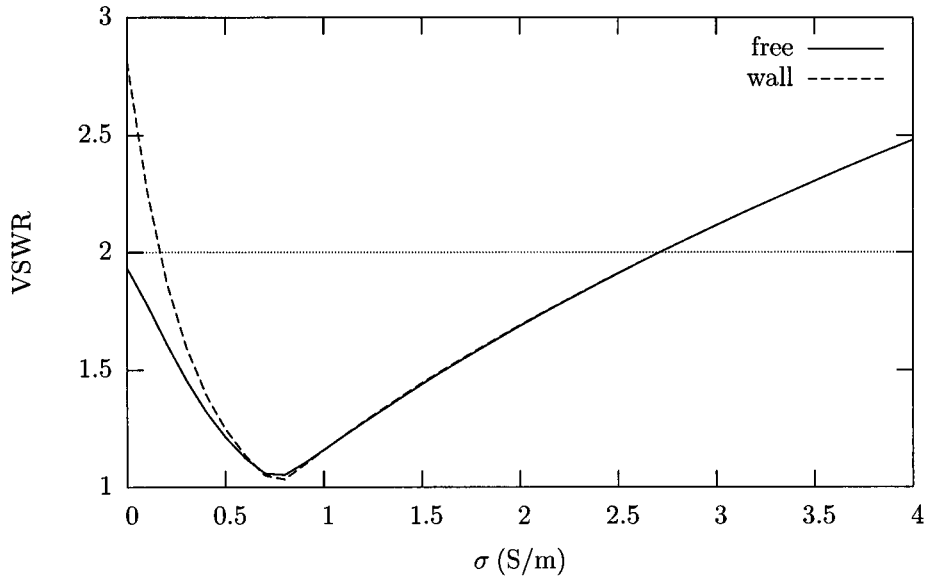


Figure 3.22: Plots of the VSWR of the example antenna in water at a distance of 14 cm to a conducting wall, and VSWR of the same antenna without wall (free), as a function of the conductivity of the water.

It can be concluded that the influence of coupling between the antenna and the wall at a distance of $\lambda/4$ can be neglected at the range of conductivities of interest (0.65 S/m to 4.0 S/m). In pure water however, a significantly higher VSWR should be expected.

Another interesting aspect is that the antenna, which is optimized for the conductivity of river water, can still be used for conductivities up to $\sigma \approx 2.8$ S/m as far as the limit $\text{VSWR} \leq 2$ is concerned, which is a real limitation in many amplifiers.

This page intentionally contains only this sentence.

Chapter 4

Measuring density

Contents

4.1	Introduction	38
4.2	Propagation time and attenuation	39
4.3	Permittivity and conductivity	41
4.4	Mixing models	42
4.5	Volume to density	44

4.1 Introduction

The objective of this chapter is to explain how slurry density can be measured using electromagnetic waves. The measurement method used is called *Time Domain Transmissometry*.

Time Domain Transmissometry measures the propagation time and amplitude attenuation of an electromagnetic wave over a predetermined distance. In contrast with Time Domain Reflectometry, where a signal travels back and forth from the same antenna, Time Domain Transmissometry uses (at least) *two* antennas, of which one is the transmitting antenna and the other the receiving antenna. The medium to be measured should be in between these antennas.

The conversion from the measured time difference between the source signal and the received signal (t_{meas}) and the voltage on the receiver antenna (V_{rec}) to the slurry density (ρ) consists of four steps, see figure 4.1.

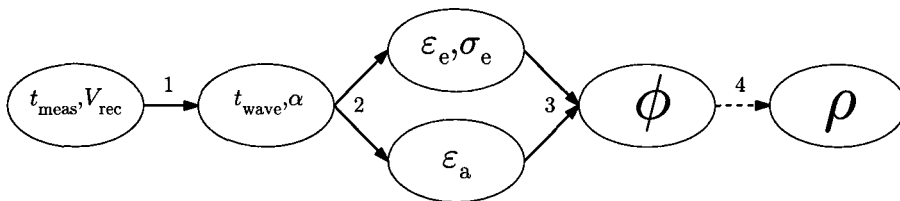


Figure 4.1: The transformation from $(t_{\text{meas}}, V_{\text{rec}})$ to ρ consists of four steps.

These steps are in short:

Step 1 ($t_{\text{meas}}, V_{\text{rec}} \rightarrow t_{\text{wave}}, \alpha$): In practice not the absolute propagation time t_{wave} but a time difference t_{meas} between the source signal and the received signal is measured. The attenuation constant α , which is defined by equation (3.8a), is also not measured directly: it is derived from the voltage on the receiver antenna V_{rec} .

Step 2 ($t_{\text{wave}}, \alpha \rightarrow \epsilon_e, \sigma_e$ or ϵ_a): the propagation time and the attenuation both depend on the effective permittivity and the effective conductivity of the propagation medium, so using the inverse relation the permittivity and the conductivity can be derived from the measured parameters. An alternative method just disregards the attenuation and calculates the so-called *apparent* permittivity using only the propagation time.

Step 3 (ϵ_e, σ_e or $\epsilon_a \rightarrow \phi$): In case of a two-phase mixture like water and soil, the soil volume fraction can be calculated using so-called mixing models. These models relate the effective or apparent permittivity and/or the conductivity of the mixture to the volume fractions of the components.

Step 4 ($\phi \rightarrow \rho$): The final step is a bit trivial: once the soil volume fraction and the density of the solid soil are known, the density of the soil-water mixture can be calculated.

In the next section, step 1 will be treated in more detail. The derivation of the equations for step 2 is rather laborious and can be found in appendix E. The results of this derivation are presented in section 4.3. In section 4.4 various “mixing models” for the permittivity of a sand-water mixture are described, which relate the volume fraction of soil in water. Finally the conversion to density is described in section 4.5.

4.2 Propagation time and attenuation

In practice not the absolute propagation time t_{wave} but a time difference $0 \leq t_{\text{meas}} \leq T$ between the source signal and the received signal is measured, $T = 1/f$ being the period of the signal. This time difference is proportional to the propagation time. Likewise not the attenuation constant itself but the voltage on the receiver antenna is measured. The absolute propagation time and the attenuation constant can be derived from the measured time difference and voltage.

Propagation time

The measured time difference is the sum of the propagation time of the wave and the propagation time (delay) in the wiring, modulo T :

$$t_{\text{meas}} = t_{\text{wave}} + t_{\text{wire}} \pmod{T}. \quad (4.1)$$

The fact that the time difference is determined modulo T poses no problem as long as the *range* of measured time differences is restricted to $\Delta t_{\text{meas}} < T$.

Under the assumption $0 \leq t_{\text{meas}} \leq T$ the absolute propagation time can be derived from t_{meas} by means of a calibration measurement without sand: having measured the conductivity σ_e and the time difference $t_{\text{meas}}|_{\sigma_e}$ and using an assumed value for the permittivity ϵ_e of the water, the corresponding propagation time $t_{\text{wave}}|_{\sigma_e}$ can be calculated using:

$$t_{\text{wave}}|_{\sigma_e} = t_{\text{wave}}|_0 \cdot \sqrt{1/2} \sqrt{\sqrt{1 + \left(\frac{\sigma_e}{\epsilon_e \omega}\right)^2} + 1} \quad (4.2)$$

where $t_{\text{wave}}|_0$ is the propagation time at zero conductivity, given by:

$$t_{\text{wave}}|_0 = \frac{d}{c_0} \sqrt{\epsilon_{\text{er}}} \quad (4.3)$$

where d is the distance the wave has traveled (the antenna separation) and ϵ_{er} the relative part of ϵ_e . The other propagation times can be calculated by observing the change in the measured times:

$$t_{\text{wave}} = t_{\text{meas}} + (t_{\text{wave}}|_{\sigma_e} - t_{\text{meas}}|_{\sigma_e}). \quad (4.4)$$

Example 1:

The propagation times in river and sea water, with density 1.0 (no sand) and 1.8 ton/m³ (almost saturated with sand) have been calculated, based on the following typical values:

- Frequency: 62.5 MHz
- Distance between antennas: 47 cm
- Relative effective permittivity of water: 79.0
- Relative effective permittivity of sand: 4.0
- Density of sand: 2.65 ton/m³

The calculated propagation times have been visualized in a plot using a single-period source signal, see figure 4.2.

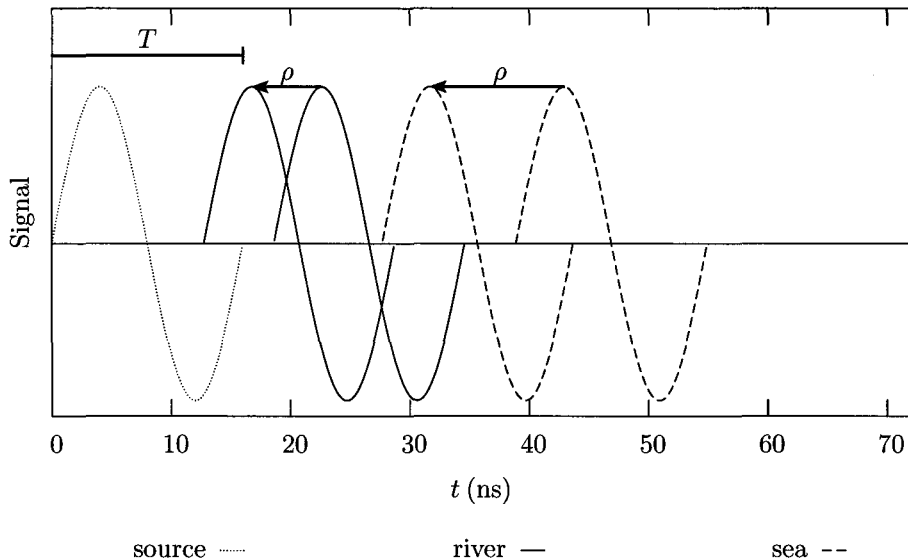


Figure 4.2: Stylized representation of the transmitted (source) and received electromagnetic waves in pure ($\rho = 1$) and almost saturated ($\rho = 1.8 \text{ ton/m}^3$) river ($\sigma_e = 0.65$) and sea ($\sigma_e = 4.0 \text{ S/m}$) water. The arrows indicate the change in propagation time as the density increases from 1.0 to 1.8. The time period T is also indicated. The signal attenuation is not shown because it would render the sea water signal invisible at the same scale.

From this plot, it can be concluded that $\Delta t_{\text{meas}} < T$ as long as the conductivity stays constant, or at least within certain limits. Only when the conductivity is allowed to change without an interim calibration of some sort, becomes the propagation time ambiguous and is an absolute propagation time measurement needed.

Attenuation

The voltage measured on the receiver antenna V_{rec} decays exponentially as the product of distance and attenuation constant increases:

$$V_{\text{rec}} = V_0 \exp(-\alpha d), \quad (4.5)$$

where the distance d is determined by the antenna separation and V_0 is a constant, so the only variable here is the attenuation constant α . The attenuation constant can be derived from the voltage on the receiver antenna using:

$$\alpha = -\frac{1}{d} \ln \left(\frac{V_{\text{rec}}}{V_0} \right). \quad (4.6)$$

The ‘zero conductivity’ voltage V_0 is to be found by a calibration measurement without sand: the effective conductivity σ_e and the voltage on the receiver antenna $V_{\text{rec}}|_{\sigma_e}$ have to be measured. Using these measured values and an assumed value for the permittivity ϵ_e of the water, the attenuation constant $\alpha|_{\sigma_e}$ can be calculated using (3.8a). The calibration voltage V_0 is then given by:

$$V_0 = V_{\text{rec}}|_{\sigma_e} \exp(+\alpha|_{\sigma_e} d). \quad (4.7)$$

In short, the conversions from t_{meas} and V_{rec} to t_{wave} and α are given by equations (4.4) and (4.6) respectively.

4.3 Permittivity and conductivity

The factor $\sqrt{\varepsilon_{\text{er}}}$ in equation (4.3) corresponds to the index of refraction at zero conductivity. As indicated by (4.2), this index of refraction increases when conductivity comes into play, as in saline water. As can easily be verified, the *apparent* index of refraction in conducting media is given by:

$$\sqrt{\varepsilon_{\text{ar}}} = \sqrt{\varepsilon_{\text{er}}} \cdot \sqrt{1/2} \sqrt{\sqrt{1 + \left(\frac{\sigma_e}{\varepsilon_e \omega}\right)^2} + 1} \quad (4.8)$$

where ε_{ar} is the relative *apparent* permittivity. Using this equation, the propagation time in saline water with effective conductivity σ_e takes the following simple form, analogous to (4.3):

$$t_{\text{wave}}|_{\sigma_e} = \frac{d}{c_0} \sqrt{\varepsilon_{\text{ar}}} \quad (4.9)$$

which leads to a simple equation which has been used in this project to obtain the apparent permittivity from propagation time measurements in chapter 7:

$$\varepsilon_{\text{ar}} = \left(\frac{c_0 t_{\text{wave}}|_{\sigma_e}}{d}\right)^2. \quad (4.10)$$

The *effective* permittivity can easily be derived from the apparent permittivity by taking the square on both sides of equation (4.8):

$$\varepsilon_{\text{er}} = \varepsilon_{\text{ar}} - \frac{\sigma_e^2}{4 \varepsilon_{\text{ar}} \varepsilon_0^2 \omega^2}. \quad (4.11)$$

Note that $\varepsilon_{\text{er}} \rightarrow \varepsilon_{\text{ar}}$ for $\sigma_e \rightarrow 0$. So for non-saline water, there is no difference between the apparent permittivity and the effective conductivity. This is shown in figure 4.3 for a relative effective permittivity of 79. Note that many literature sources on soil science just disregard this difference, because it is (implicitly) assumed that the soils are non-saline.

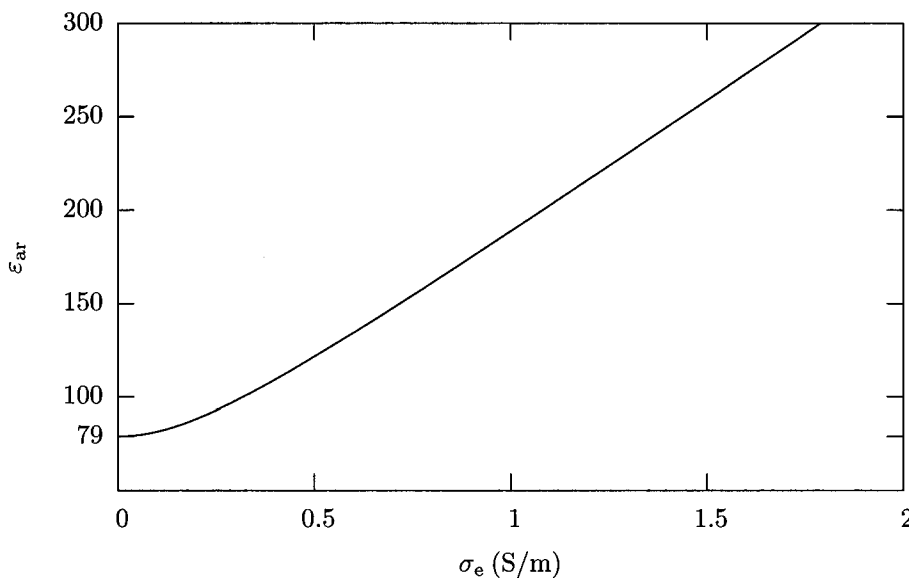


Figure 4.3: The relative apparent permittivity ε_{ar} of water as a function of the conductivity of the water, calculated for the typical relative effective permittivity $\varepsilon_{\text{er}} = 79$ and a frequency of 62.5 MHz.

As shown in appendix E, the relative effective permittivity and the effective conductivity can both be written as simple equations of t_{wave} and α :

$$\varepsilon_{\text{er}} = c_0^2 \left\{ \left(\frac{t_{\text{wave}}}{d} \right)^2 - \left(\frac{\alpha}{\omega} \right)^2 \right\} \quad (4.12a)$$

$$\sigma_{\text{e}} = \frac{2 \alpha t_{\text{wave}}}{\mu_0 d}, \quad (4.12b)$$

where both t_{wave} and α are to be measured at the same effective conductivity σ_{e} .

4.4 Mixing models

The relation between the permittivity of a mixture and the volume fractions of its constituents is governed by mixing models. For the permittivity of a two-phase mixture, various mixing models can be found in literature. These mixing models can be classified into four categories [25]:

1. Volumetric

- Method: Relates the bulk permittivity of a mixture to the permittivities of its constituents.
- Types: Lichtenecker-Rother model, Complex Refractive Index Model (CRIM), Arithmetic model.

2. (Semi-)Empirical

- Method: Mathematical relationship between the permittivity and other measurable properties
- Types: Logarithmic, polynomial fit.

3. Effective medium

- Method: Connects the effective dielectric function of a two-phase mixture with the (micro)geometry information about the composite and the dielectric functions of the two components.
- Types: Bruggeman-Hanai model.

4. Phenomenological

- Method: Involves calculating the field induced in a uniform ‘host’ material by a single spherical or ellipsoidal inclusion and a treatment of its distortion by the electrostatic interaction between the different inclusions.
- Types: Maxwell-Garnett model.

The first two models are most suitable for our purposes, because they require nothing more than the permittivities of the constituents. The other two require much more information such as microgeometry and microscopic electric field. The volumetric and the semi-empirical mixing models are described below.

Volumetric models

The most general form of the volumetric models, which give the effective permittivity ε_{e} as a function of the volumetric soil fraction ϕ in water is the Lichtenecker-Rother model [45]:

$$\varepsilon_{\text{e}}(\phi) = [\phi \cdot (\varepsilon_{\text{e}}^{\text{s}})^{\nu} + (1 - \phi) \cdot (\varepsilon_{\text{e}}^{\text{w}})^{\nu}]^{\frac{1}{\nu}}, \quad (4.13)$$

where ε_e^s is the effective permittivity of the soil, ε_e^w the effective permittivity of the water and $-1 \leq \nu \leq 1$ an empirical constant. For most mineral soils, $0.4 < \nu < 0.8$. The limits $\nu = 1$ and $\nu = -1$ are called the upper and lower “Wiener bounds”. The upper Wiener bound corresponds to the (artificial) situation where alternating flat layers of sand and water are placed parallel to the electromagnetic field and the lower Wiener bound corresponds to flat layers of sand and water normal to the electromagnetic field [27]. Two specific values for ν lead to the C.R.I.M. model and the Arithmetic model and are described below.

C.R.I.M. model: The particular case $\nu = 1/2$ gives the Complex Refractive Index Model [8, 11, 15] or Birchak formula [14], which supposedly gives a statistically better representation than other mixing models [8]:

$$\sqrt{\varepsilon_e(\phi)} = \phi\sqrt{\varepsilon_e^s} + (1 - \phi)\sqrt{\varepsilon_e^w} \quad (4.14)$$

and the inverse relation:

$$\phi(\varepsilon_e) = \frac{\sqrt{\varepsilon_e} - \sqrt{\varepsilon_e^w}}{\sqrt{\varepsilon_e^s} - \sqrt{\varepsilon_e^w}}. \quad (4.15)$$

The C.R.I.M. model is also valid for lossy (conducting) media, in which case *complex* permittivities instead of effective permittivities have to be used [8, 41]. So for conducting mixtures the actual notation should be:

$$\sqrt{\varepsilon^*(\phi)} = \phi\sqrt{(\varepsilon^s)^*} + (1 - \phi)\sqrt{(\varepsilon^w)^*}. \quad (4.16)$$

This complex permittivity includes both the effective permittivity and the effective conductivity, as given by (2.5). Though it would be possible to completely evaluate the complex permittivity from both the propagation time and the attenuation measurement, an alternative method is found in literature [8, 41], which ultimately needs *only* the propagation time measurement. By equating the real part of both sides of equation (4.16), the real part of every $\sqrt{\varepsilon^*}$ takes the form of equation (4.8):

$$\Re(\sqrt{\varepsilon^*}) = \sqrt{\varepsilon_e} \cdot \sqrt{1/2} \sqrt{\sqrt{1 + \left(\frac{\sigma_e}{\varepsilon_e \omega}\right)^2} + 1} = \sqrt{\varepsilon_a} \quad (4.17)$$

which results in the use of *apparent* permittivities instead of *effective* permittivities. Thus equation (4.16) becomes:

$$\sqrt{\varepsilon_a(\phi)} = \phi\sqrt{\varepsilon_a^s} + (1 - \phi)\sqrt{\varepsilon_a^w}. \quad (4.18)$$

So in this equation the *apparent* permittivities of the mixture and the water have to be used. These are the values that result directly from propagation time measurements (using equation (4.10)) in the mixture and in the water, without the need for an attenuation measurement. The inverse of this model, which is the model that has been used for density calculations in chapter 7, is given by:

$$\phi(\varepsilon_a) = \frac{\sqrt{\varepsilon_a} - \sqrt{\varepsilon_a^w}}{\sqrt{\varepsilon_a^s} - \sqrt{\varepsilon_a^w}}. \quad (4.19)$$

In this research project, it has been assumed that a conductive soil-water mixture is caused by the conductivity of the water, in other words the dry soil is assumed to have zero conductivity, which leads to:

$$\varepsilon_a^s = \varepsilon_e^s. \quad (4.20)$$

Recall that $\varepsilon_a \rightarrow \varepsilon_e$ for $\sigma_e \rightarrow 0$, so mixing model (4.19) can be used for both saline and non-saline water, and in both cases the apparent permittivity can be derived from measured data using (4.10).

Arithmetic model: With $\nu = 1$ the *arithmetic model* is obtained [31] (which corresponds to the upper Wiener bound):

$$\varepsilon_e(\phi) = \phi \varepsilon_e^s + (1 - \phi) \varepsilon_e^w \quad (4.21)$$

and the inverse relation:

$$\phi(\varepsilon_e) = \frac{\varepsilon_e - \varepsilon_e^w}{\varepsilon_e^s - \varepsilon_e^w}. \quad (4.22)$$

Because the arithmetic mixing model is not useable for complex permittivities, it is not used here.

(Semi-)Empirical

In case the volumetric model does not reliably reproduce the desired volumetric soil fraction, a polynomial (or logarithmic) fit can be used to obtain the desired relation. In fact, for the development of an electromagnetic density meter, compliance with physical models is not essential. An unambiguous and reproducible relation (within a given accuracy) between the slurry density and one or more measurable parameters is sufficient. This procedure has been carried out for the combined density measurements in river water (see section 7.3 and appendix K).

4.5 Volume to density

The relation between the volumetric soil fraction ϕ and the density of a soil-water mixture ρ is given by:

$$\rho = \phi \rho_s + (1 - \phi) \rho_w. \quad (4.23)$$

with ρ_s the density of the soil and ρ_w the density of the water. The reverse relation is:

$$\phi = \frac{\rho - \rho_w}{\rho_s - \rho_w} \quad (4.24)$$

Because this last step is a bit trivial, mainly depends on an *assumed* value (ρ_s) and consequently does not provide a lot more insight, this step is skipped for most of the density calculations. The density calculation is only performed for the final combined density measurements in section 7.3, to get an idea of the resulting uncertainty in the density measurement.

Example 2:

Realistic slurry densities vary between 1.0 (water) to 1.8 ton/m. The density of water ρ_w is assumed to be 1.0 ton/m³ and the density of soil ρ_s is assumed to be 2.65 ton/m³. To illustrate the C.R.I.M. model described above, plots of the density as a function of the effective permittivity are shown in figure 4.4 for river water and sea water. For the solid curves, the following values have been used:

- Permittivity soil: $\varepsilon_{er}^s = 5$
- Permittivity water: $\varepsilon_{er}^w = 79$
- Conductivity water: $\sigma_e = 0.65$ S/m (river), $\sigma_e = 4.0$ S/m (sea).

Note that the *complex* permittivity has been calculated in compliance with (4.16), from which the real part or *effective* permittivity (see section 2.1) has been plotted. It has been chosen not to use the *apparent* permittivity here, because those values bear no resemblance to the common notion of permittivity: they are generally not in the range 5 – 79, as shown in figure 4.3 for water ($\rho = 1.0$).

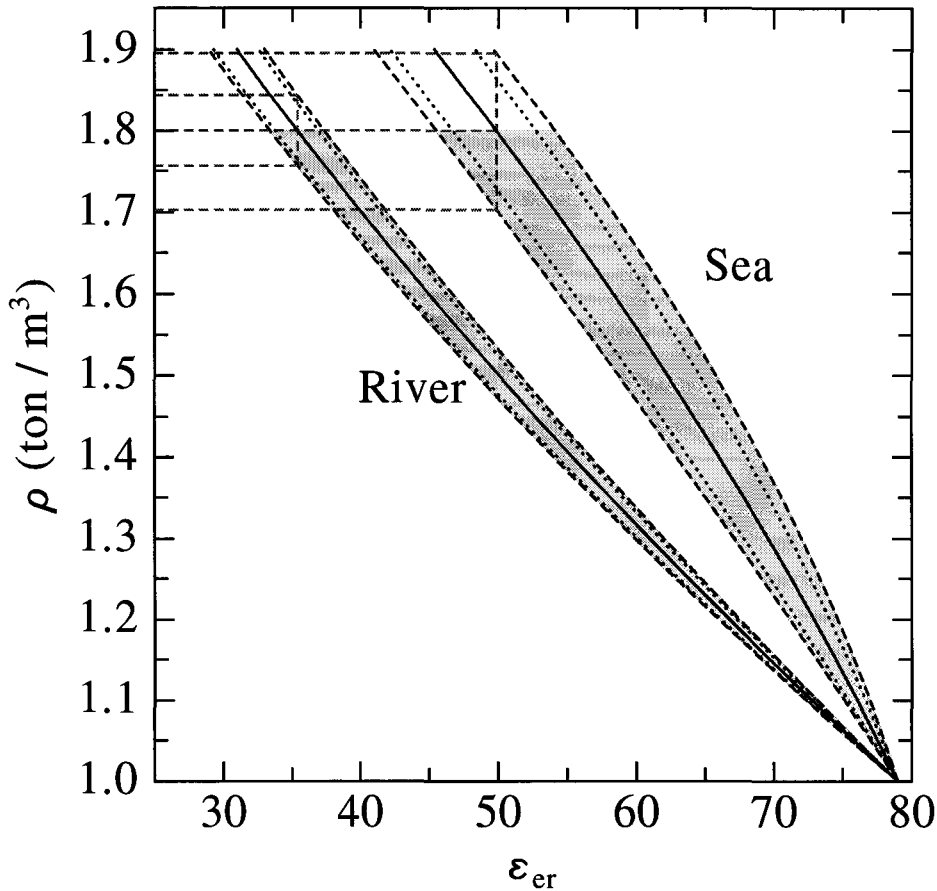


Figure 4.4: The C.R.I.M. volumetric mixing model for sand in river water and sea water. The solid curves represent $\epsilon_{er}^s = 5$ and $\sigma_e = 0.65$ S/m (river), $\sigma_e = 4.0$ S/m (sea). The dotted curves represent $\epsilon_{er}^s = 5 \pm 1$ and $\sigma_e = 0.65$ S/m (river), $\sigma_e = 4.0$ S/m (sea). The dashed curves and shaded area represent $\epsilon_{er}^s = 5 \pm 1$ and $\sigma_e = 0.65 \pm 10\%$ S/m (river), $\sigma_e = 4.0 \pm 10\%$ S/m (sea). The grey helper lines indicate the uncertainty in $\rho = 1.8$ ton/m³ for river and pure water.

The dotted curves indicate the uncertainty in the calculated density when the relative permittivity of the soil has an uncertainty: $\epsilon_{er}^s = 5 \pm 1$. This uncertainty is based on the typical range of soil permittivities as already indicated in section 2.4. The dashed curves and enclosed shaded area indicate the uncertainty in the density when $\epsilon_{er}^s = 5 \pm 1$ and the conductivity of the water is known within 10%: $\sigma_e = 0.65 \pm 10\%$ and $\sigma_e = 4.0 \pm 10\%$ respectively.

The plot also shows that the uncertainties in the permittivity of the soil and the conductivity of the water have the greatest influence on the density calculation for sea water. The calculated uncertainty for a density of 1.8 ton/m³ is approximately ± 0.04 for river water and ± 0.09 for sea water, both for the *assumed* uncertainties in the permittivity and the conductivity.

The uncertainty also depends on the mixing model. When the parameter ν in the volumetric mixing model (4.13), which is 0.5 in case of the C.R.I.M. model, is increased to 1 the uncertainty decreases to ± 0.01 for both river and sea water. Values $\nu < 0.5$ no longer result in a one-to-one model, and are therefore rejected.

This page intentionally contains only this sentence.

Chapter 5

Experimental setup

Contents

5.1	Introduction	48
5.2	The pipe	49
5.3	Electrical setup	51
5.4	Antenna	53
5.5	Sand packs	56

5.1 Introduction

The experimental setup globally consists of the following parts:

- A double-walled measurement pipe containing the ‘slurry’
- An electrical measurement circuit connected to:
 - two (or more) antennas
 - Rectangular sand packs to be placed in the measurement pipe

A computer generated impression of the measurement pipe with six antennas is shown in figure 5.1 below. The pipe is described in the next section. Details on the electrical equipment used can be found in section 5.3. The design and construction of the antennas is described in detail in section 5.4. Finally the sand packs are described in section 5.5.

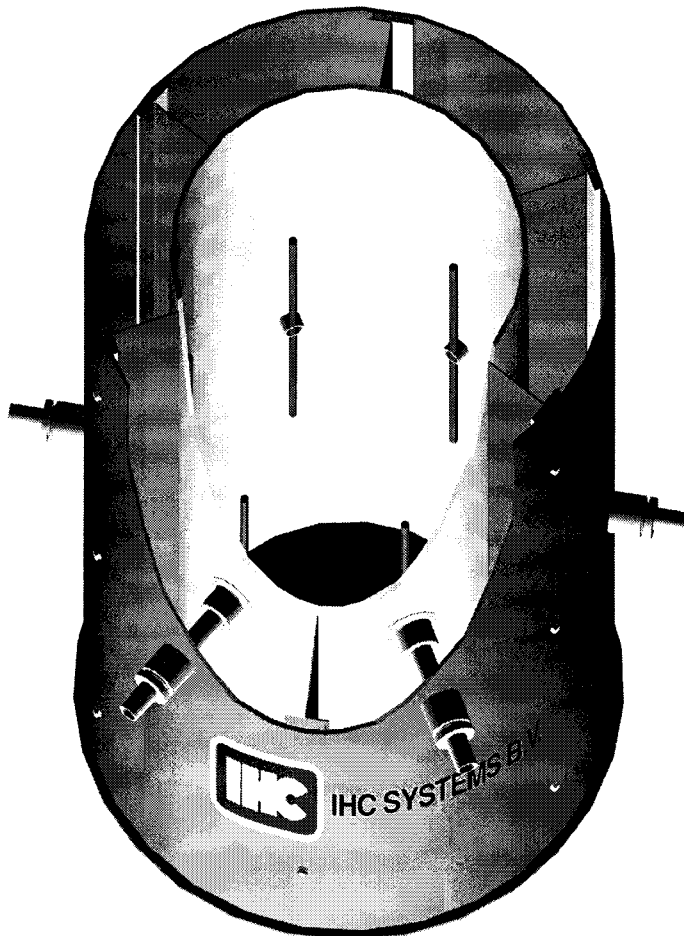


Figure 5.1: Computer generated cut-out view of the double-walled measurement pipe, containing six antennas mounted on PVC pipes, and six shields between the inner and the outer pipe.

5.2 The pipe

Dimensions

In establishing a sensible and flexible construction and determining the dimensions which yield the best chance at success, according to available knowledge, the following initial choices were made:

- A static setup, i.e. no flow. This simplifies the construction considerably while having no significant impact on the physical process, considering the huge difference in the timescale of the flow and the electromagnetic waves.
- The basic construction consists of two pipes, one plastic pipe containing the slurry, and a metal pipe around it as a shield for the electromagnetic waves. Both pipes are closed at the bottom.
- The inner pipe should be made of a non conducting plastic to keep it from absorbing power from the antennas. For this purpose glass fibre reinforced polymer (epoxy) was chosen because of its strength and thus its applicability in a real density meter.
- The antennas should be mounted inside the inner pipe, along the pipe wall. In the final product they can be protected and insulated by placing them inside the commonly used polymer layer or, in case Alumina tiles are desired along the inner pipe wall for enhanced protection, glued in the spacing between the tiles.
- The length of the pipe should be about $2\times$ larger than the diameter of the metal pipe, to reduce the influence of the bottom and top of the setup on the propagation of the electromagnetic waves.
- Diameter inner pipe: $D_{\text{inner}} = 0.5$ m. This relatively small size is chosen because it is expected that larger diameters are problematic and because the density meter is targeted at smaller dredgers.
- Diameter outer pipe: the selection of the (inner) diameter of the metal (outer) pipe needs a closer examination.

– A conducting wall enforces a node on an electromagnetic wave. As a lower frequency limit, it is demanded that at least half a wavelength is contained in the metal pipe. Otherwise it would much more resemble an oscillating electric field instead of an electromagnetic *wave* and a propagation time measurement would be questionable. So the pipe diameter poses the following limit on the diameter of the metal pipe:

$$* D_{\text{outer}} \geq \lambda/2$$

where λ is taken for pure water. Because the wavelength in saline water is shorter, the condition is sufficient for all salinities.

– The antenna performance is enhanced when the distance between the antenna and the metal pipe equals $\lambda/4$, as discussed in section 3.7. The corresponding frequency is given by $f = v/\lambda$ and thus depends on the propagation velocity of the water between the two pipes. To make sure that the optimal frequency remains constant the outer (metal) pipe is to be filled with ‘pure’ water, separate from the contents (slurry) in the inner (epoxy) pipe. For optimum antenna performance, the following condition is added:

$$* D_{\text{outer}} = D_{\text{inner}} + 2 \cdot \lambda/4 = 0.5 \text{ m} + \lambda/2$$

which generously satisfies the previous limiting condition.

In general, it is desirable to make the frequency as low as possible, because the lower the frequency the lower the signal attenuation. Thus the wavelength should be as large as possible. However, the outer dimensions of the measurement device should remain reasonable. Therefore, the following outer dimensions and resulting frequency were chosen:

- Diameter outer pipe: $D_{\text{outer}} = 0.75 \text{ m}$
- Frequency: $f = v_{\text{water}}/\lambda = c_0/\sqrt{79}\lambda \approx 67 \text{ MHz}$

Antennas

To be able to investigate various antenna configurations, such as straight across the pipe, at 120° or at 60° flanges were made on the inner and outer pipe for a total of 6 antennas, at 60° distance from each other. The unused flanges were plugged with short closed PVC pipes.

Shields

Because it is likely that the electromagnetic waves will not only propagate through the slurry in the inner pipe, six metal shields were designed for the space between the inner and the outer pipe, to impede the propagation of waves in that area. The shields were made removable and (limitedly) slidable along the metal pipe wall, to be able to investigate the influence of the shields. This leads to the schematic setup as shown in figure 5.2. CAD drawings of the final design can be found in appendix F.

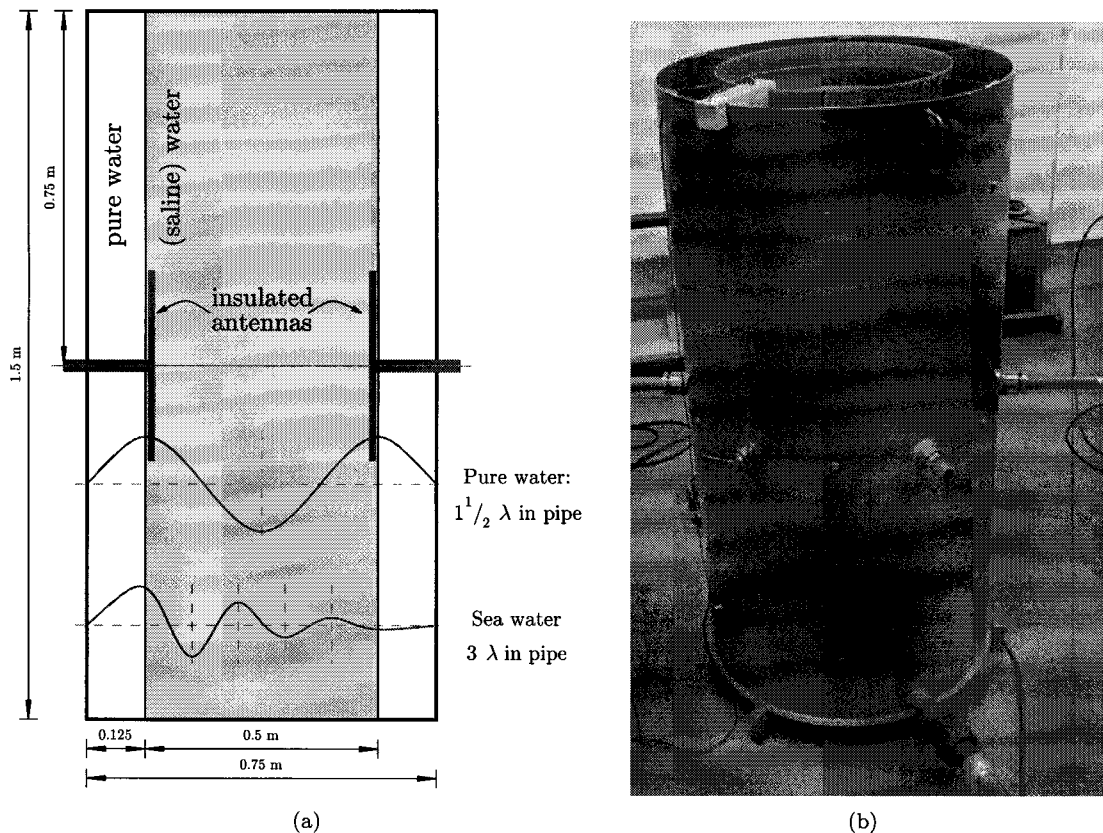


Figure 5.2: (a) Experimental setup for electromagnetic measurements, dimensioned for a frequency of 67 MHz. The wavelength of electromagnetic waves in the pipe has been indicated for river water and sea water. The depicted attenuation is only symbolic for it is much larger in reality. (b) Photo of the measurement pipe. The two wires along the left side of the pipe carry a low voltage DC current which serves as cathodic protection of the pipe wall.

After the first few measurements, the pipe and shields were sand blasted, primed with red lead and coated because the pipe showed too much oxidation even in non-saline water. Furthermore,

cathodic protection was installed in order to reduce the oxidation rate. This circuit was removed when salt was added to the outer pipe, because the required currents would be too high.

5.3 Electrical setup

In an electrical aspect, the measurement setup consists of the following components:

- At the *source* side:
 - A frequency generator, delivering a continuous wave signal. For the first few measurements a tuned oscillator was used. Higher harmonics were attenuated using a 75 MHz low pass filter. For subsequent measurements the oscillator was replaced by a Hewlett Packard 8647A frequency generator, which delivers a much more accurate and stable signal. For a few measurements at high conductivity, an Agilent 33250A arbitrary function generator was used to create short pulses instead of a continuous wave.
 - A broadband power amplifier, amplifying the signal to 0.5 W or more. The amplifier used is a R.F.P.A. RF001220-25, which delivers up to 25 Watt in the frequency range 10 kHz – 220 MHz. The measurements with the oscillator were performed without amplifier as the oscillator itself delivered enough power.
 - A VSWR meter, to observe the antenna performance: Diamond SX-1000.
 - A transmitter antenna.
- At the *receiver* side:
 - A receiver antenna.
 - A pre-amplifier (optional).

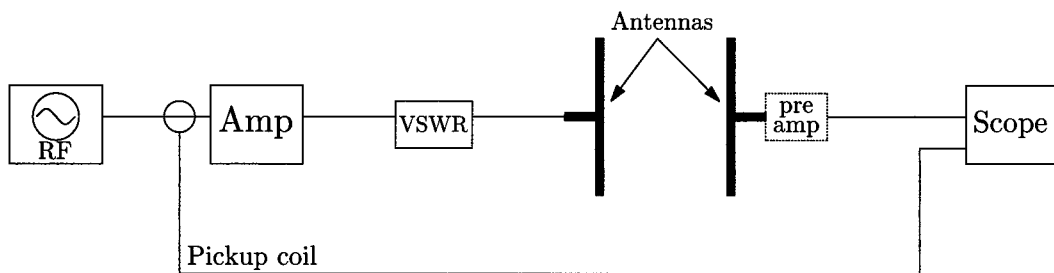


Figure 5.3: Electrical setup for electromagnetic measurements

The total setup is shown in figure 5.3. The radio-frequency (RF) low-level signal from the frequency generator is fed to a power amplifier. The high-level signal is fed through a VSWR meter to the transmitter antenna. The received signal is optionally amplified using a pre-amplifier and then fed directly to the oscilloscope. For time difference measurements a reference signal is needed. This signal is obtained by means of a pickup coil around the low-level source cable. The source signal is not coupled directly to the scope (e.g. using a tee adapter) to maintain as much separation between the transmitter and the receiver side as possible. Details on the pickup coil can be found in appendix H. The low pass filter, which has been placed between the frequency generator and the pickup coil to remove higher harmonics, is described in section I.

Amplifier

The required amplifier power depends on two factors:

1. The attenuation of the electromagnetic waves in the slurry.

2. The lowest measurable voltage.

The total power attenuation of the electromagnetic waves in dB is determined by the attenuation constant (3.8a) and the distance:

$$\text{Att [dB]} = 20^{10} \log \left(\frac{V_0}{V} \right) = 20^{10} \log (\exp(\alpha d)) \approx 8.7 \cdot \alpha d. \quad (5.1)$$

To still be able to measure the transmitted signal after propagation and attenuation in the measurement pipe, the transmitted signal should be sufficiently amplified and the received signal should be measured with a highly sensitive oscilloscope.

In other words: the dynamic range of the amplifier and the oscilloscope should at least equal the power attenuation. The dynamic range of the amplifier and the oscilloscope can be calculated as follows. The amplifier produces its power in a 50Ω load, so the maximum RMS output voltage is:

$$V_{\text{amp}}(P) = \sqrt{P \cdot 50 [\Omega]}. \quad (5.2)$$

and the dynamic range of the amplifier–oscilloscope combination is given by:

$$\text{Range [dB]} = 20^{10} \log \left(\frac{V_{\text{amp}}}{V_{\text{scope}}} \right), \quad (5.3)$$

where V_{scope} is the smallest the smallest RMS voltage that can be reliably measured on the oscilloscope. The smallest measurable voltage is assumed to be 10 mV, based on experience with the Agilent oscilloscopes.

In case a pre-amplifier is used, the amplification which is usually expressed in dB is to be added to the dynamic range. Calculated plots of the attenuation in a 50 cm pipe as a function of the slurry density for river water and sea water, combined with the dynamic range of the power amplifier, the oscilloscope and optionally a pre-amplifier are shown in figure 5.4.

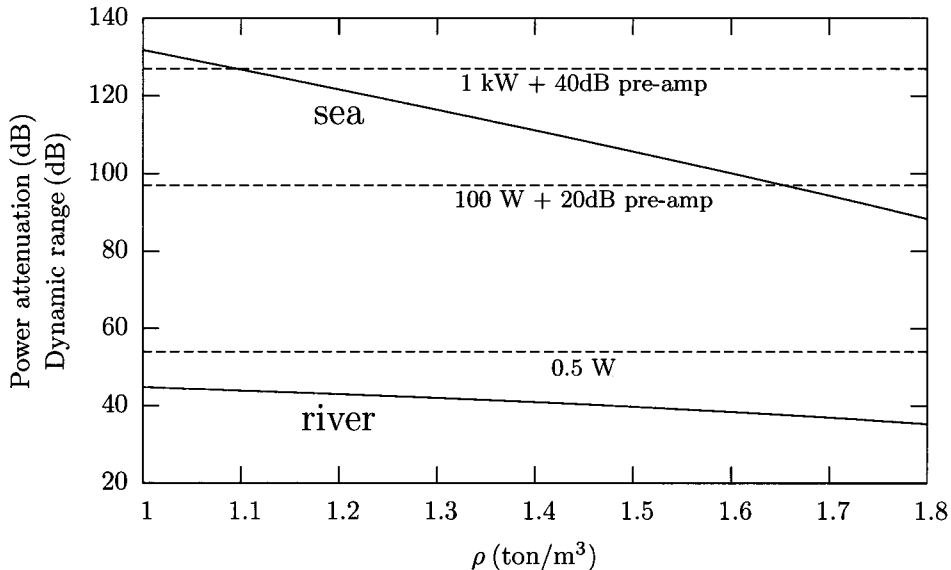


Figure 5.4: Plots of the power attenuation (solid) in slurry based on river water and sea water and the dynamic range (dashed) obtained by using different amplifier powers on the transmitter antenna, combined with different pre-amplifiers on the receiver antenna.

As the plot shows, for river water ($\sigma = 0.65 \text{ S/m}$) measurements, an amplifier power of 0.5 W easily serves our purposes. For sea water ($\sigma = 4.0 \text{ S/m}$), even a 1 kW amplifier with a 40 dB

pre-amplifier is not sufficient. It may be necessary to use short high-powered signal bursts here in order to save power.

Oscilloscope

Several different oscilloscopes were used, starting with a Fluke Combiscope PM3380B. Because the best time resolution of this scope is in the same order magnitude as the time difference to be measured, alternatives have been sought. First a low-cost Goodwill GDS-840S was tried, which was marginally better, and finally two Infiniium oscilloscopes from Agilent: a 54832D and a 54831D. The last two oscilloscopes are superior to the first two in every possible aspect – except transportability. A great advantage of the Agilent oscilloscopes is its capability to perform automatic time difference measurements and gather statistical data like average, minimum and maximum value. This enables the determination of a measurement error for each single measurement point instead of estimating the error from the smallest resolvable step.

5.4 Antenna

Design

The dipole antennas have been designed in accordance with the examples from chapter 3. Just the parameters have been tuned to match the boundary conditions of the experimental setup. In short, these parameters are:

- A half-wave dipole
- Optimized for river water, because that is selected as the primary test area
- Half length: $h = 24$ cm. This is a bit longer than needed for a frequency of exactly 67 MHz. This length was chosen to be on the safe side: it is easier to reduce the antenna length, in case it doesn't work as desired, than to increase it.
- Conducting legs: 8 mm outer, 4 mm inner diameter copper pipe. So parameter $a = 4$ mm. Copper is chosen because it is an excellent conductor and available at various diameters. The thickness of 8 mm is a trade-off between the ideal dipole, which is infinitesimally thin, and a certain mechanical robustness.
- Insulated with PTFE tube: 10 mm outer, 8 mm inner diameter. So parameter $c = 5$ mm. The choice for PTFE or Teflon has some advantages: its permittivity is well-defined and does not vary with frequency or moistness and it is smooth, so it's relatively easy to slide it over the copper pipe. A possible drawback is that nothing adheres to it, which may cause some leakage in the antenna

A detailed drawing of the antenna design is shown in figure 5.5 and a photo of the antenna near completion is shown in figure 5.6.

Construction

The antenna has been constructed as follows:

1. The two hollow antenna legs are made of 8 mm outer and 4 mm inner diameter copper pipe. They are connected with a 10.5 cm long, 4 mm diameter PVC spacer and kept electrically separate using a 5 mm long, 8 mm outer and 4 mm inner diameter FEP ring.
2. The PTFE tube is slid over the two legs and closed at both sides with a 5 cm long, 8 mm diameter FEP spacer, to maintain a constant permittivity near the antenna, and a 8.4 mm diameter rubber plug to keep the water out.

3. Near the middle of the antenna, two M3 bolts are screwed through the antenna legs to create electrical contacts.
4. A 10 cm wide slot is made in a 32 mm (outer diameter) PVC pipe.
5. The six coaxial cables are taped to a 16 mm PVC pipe and slid in the larger PVC pipe.
6. The coaxial cables are soldered to the bolts.
7. The PVC pipe is filled with 3M Cast Resin (No. 8).

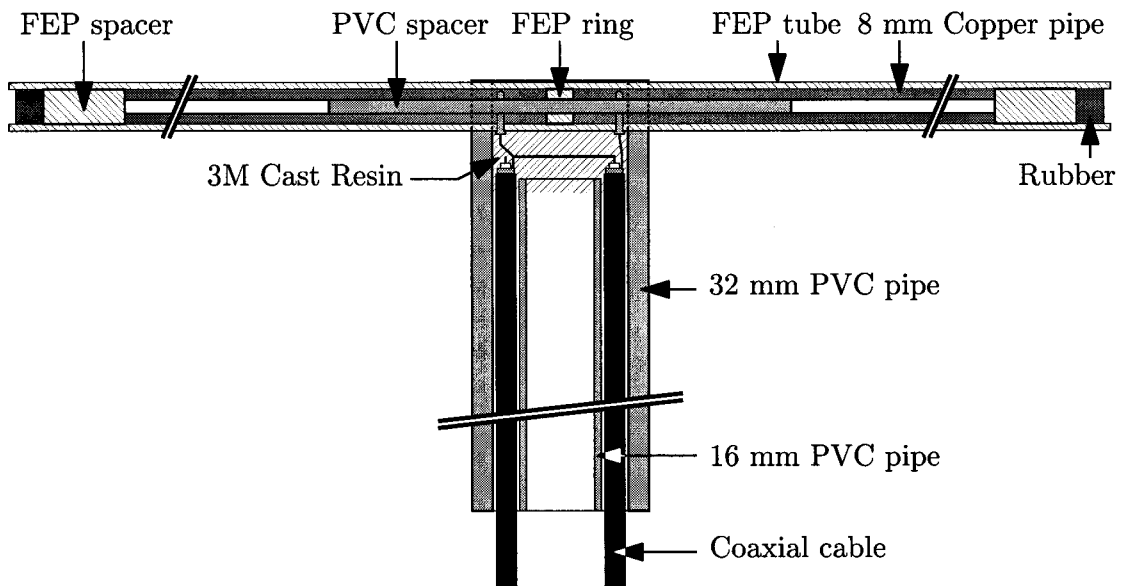


Figure 5.5: Schematic drawing of the antenna construction. The length of the two copper pipes, which corresponds to the half-length, is not indicated as it depends on the desired operating frequency.

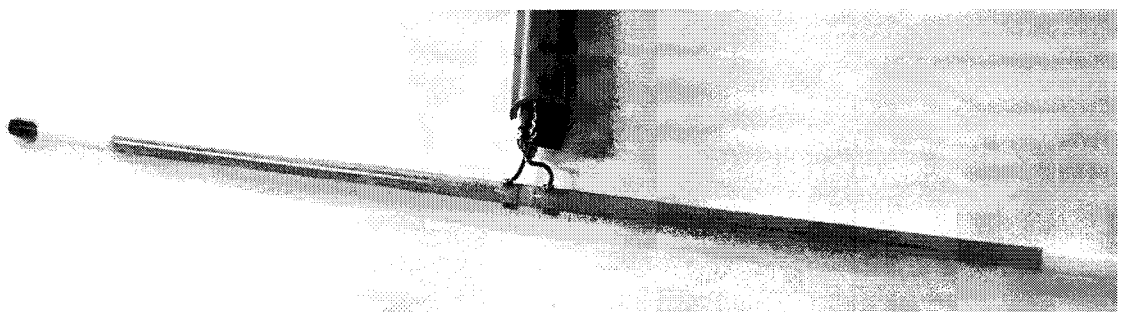


Figure 5.6: Photo of the antenna during construction. The antenna has a half-length of 24 cm and is thus optimized for application in river water. The antenna legs have yet to be placed in the PVC shaft and sealed with cast resin.

Matching

The antenna matching circuit was designed according to example 3 in chapter 3. The Q-match was verified using a simple oscillator connected using a $50\ \Omega$ coaxial cable on one side and 3 parallel termination resistors ($50\ \Omega$ each) which result in an impedance of $16.7\ \Omega$ on the other side. It appeared that the length of the Q-match had to be shortened from the theoretical 74 cm to 66.4 cm to obtain a $VSWR = 1.1$ at a frequency of approximately 64 MHz. This deviation is

probably caused by the parallel connection of a $50\ \Omega$ and a $75\ \Omega$ coaxial cable. It was not possible to test the Pawsey stub, so the original design using 2×3 coaxial cables of $50\ \Omega$ is assumed to be sufficiently correct.

Initial tests of the matching circuit connected to the antenna in water showed that a VSWR of 1.1 – 1.2 is achievable at 66 MHz, but that the VSWR also depends on the position of the antenna in the basin: it shouldn't be too close to the bottom or walls of the basin or near the surface. Both the antenna and the matching circuit were duplicated, and the second set showed nearly the same performance.

As soon as the construction of the pipes was finished, the performance of the antennas in the pipe was analyzed. The intention is to find the optimum operating frequency for the combination of transmitter antenna (#1), quarter wave match and measurement pipe. This is the frequency where the VSWR has a minimum. The measurements reveal that the optimum frequency (i.e. lowest VSWR) occurs between 60 and 63 MHz, see figure 5.7. The data can be found in appendix N.1.1.

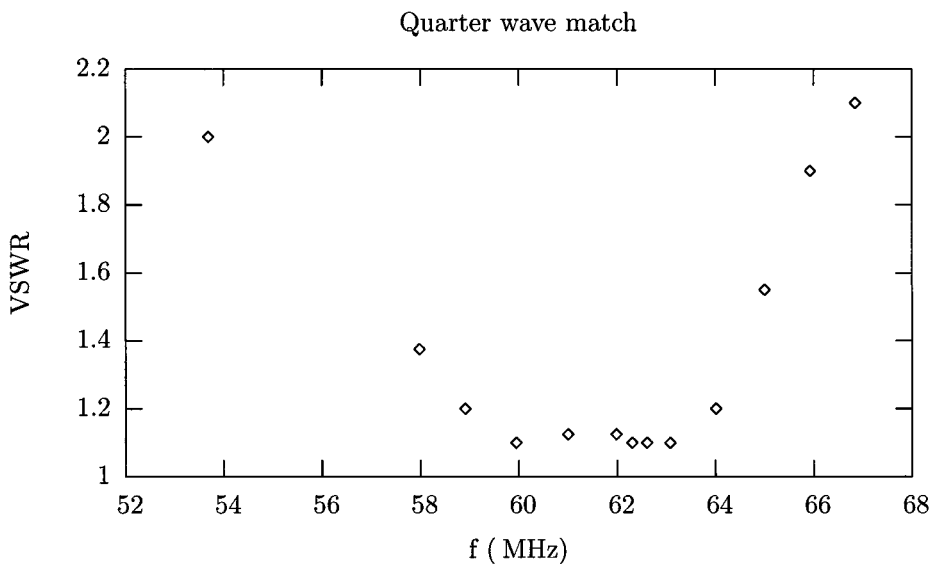


Figure 5.7: VSWR vs. frequency for the quarter wave match, used as transmitter antenna impedance match.

Transmission line transformer

An analogous frequency sweep was performed with a transmission-line transformer (TLT) as an impedance matching device instead of a quarter wave match. A transmission line transformer has the advantages that it can be very small and with a very large bandwidth. The disadvantages are that it can be quite complicated to build one properly and not every impedance ratio is feasible in practice. Details on the TLT can be found in appendix G.

The constructed TLT is actually a $50:22\ \Omega$ transformer. This design has been chosen over a $50:17\ \Omega$ design as it is much less complicated and should have a higher bandwidth [34]. As a result, the lowest VSWR will be a bit higher than the lowest VSWR using the quarter wave match. The measurements reveal that the bandwidth of the setup has not improved by the change in impedance matching device, contrary to expectations. However, its performance is still good enough to make useable. It is believed that a better performance can be obtained by a more careful selection of wire type and construction.

The TLT has *not* been used for the density measurements, because the Q-match delivers better performance and because it is easier to make two or more equivalent Q-matches than to

make two equally performing transmission line transformers. The data and plot of the bandwidth measurement can be found in appendix N.1.2.

Positioning

As a third test, the influence of the position of the receiving antenna was measured. The measurements show quite some interaction between the two antennas, as the source antenna voltage (measured using the pickup coil) changes with changing receiver antenna position. The propagation time measurement reveals that the inner and/or outer pipe walls also have a significant influence on the antenna performance: near the inner pipe wall the propagation time decreases where it would otherwise increase. The plots of these measurements can be found in appendix N.1.3.

Third antenna

Later a third antenna and matching circuit were built. The third antenna exhibits a slightly higher VSWR, typically 1.3 at an operating frequency of 62.5 MHz, which is still good enough. A probable cause for the decreased performance is that slightly longer (unshielded) wires were used for the connection between the coaxial cables and the bolts in the antenna.

5.5 Sand packs

Design & construction

For the calibration of the radioactive density meter, IHC Systems uses glass packs with a known thickness. These glass packs cannot be used for the electromagnetic density meter, because the glass is contained in a metal frame and because they are too small. Therefore sand packs were designed with the following considerations in mind:

- Flat rectangular frames of a non-conducting material, filled with (non-saline) sand
- The same height as the pipe
- As wide as the width of the pipe allows
- Four packs of approximately the same thickness and one pack of approximately half the thickness. This way, sand pack thicknesses ranging from 0 to 4.5 packs can be made in steps of 0.5
- As flat as possible, to maintain the same thickness over the entire sand pack
- Semi-permeable: water should be able to pass through, but the sand should stay inside
- As few metallic parts as possible.

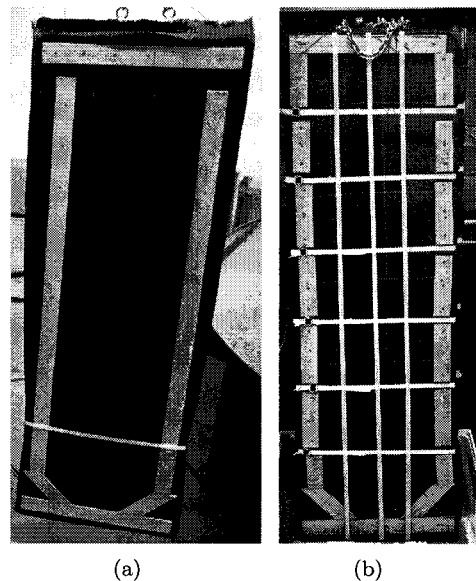


Figure 5.8: Sand pack, first version (a) and enhanced version (b).

This led to the construction of wooden frames, assembled using stainless steel screws and wood glue, and covered on both sides with anti-root foil. The frame was filled with washed river sand

(“play sand”). A finished sand pack is shown in figure 5.8(a). The approximate outer dimensions (thickness \times width \times length) and width of the sand in centimeters are shown in table 5.1:

The four ‘thick’ sand packs are not identical, because a sand pack in the middle of the pipe can be wider than the packs next to it. Packs #1 and #2 are the widest and should be placed in the middle of the pipe, while packs #4 and #5 are narrower to fit alongside the other packs. The idea has been, to keep the inner width (and height) and thus the amount of sand as constant as possible. For packs #4 and #5 this was not possible without jeopardizing the strength of the wooden frame.

After a few measurements, all these sand packs appeared to expand considerably: the thickness was no longer well-defined. To overcome this issue, the sand packs were flattened out and then reinforced with 9 Cordstrap[®] polyester strappings and stitched all the way through the sand pack at 18 points. This is shown in figure 5.8(b).

Table 5.1: sand pack dimensions

Pack #	t	w	l	w_{sand}
#1:	6	48	150	33.5
#2:	6	48	150	33.5
#3:	3	43	150	33.5
#4:	6	41	150	31.5
#5:	6	41	150	31.5

Calibration

To improve the accuracy of the density measurements, it was decided to calibrate the sand packs - at first using a radioactive density meter and later using the electromagnetic density meter and by measuring the drop in water level as a sand pack was removed from the pipe. The results of these calibration measurements are described below.

Radioactive

The “enhanced” sand packs (see section 5.5) were calibrated using a radioactive density meter (Number 584-422A-1131, 1000 mm diameter). This pipe had just been calibrated using the glass-packs. The results of this calibration are listed in table N.3 and shown in figure N.6.

The first sand pack was measured in the radioactive density meter at three positions: near the source, in the middle of the pipe and near the receiver (scintillation counter). These measurements reveal an increase in the number of radioactive counts when the sand pack is placed near the receiver. The measurements near the source and in the middle of the pipe do not differ much. This behaviour is known at IHC Systems, and as a rule calibrations are performed with the object near the source. This convention is followed in the subsequent sand pack calibration measurements.

The direct result of this calibration is the density ρ in table 5.2. Because the radioactive density meter actually only measures the thickness at the cross-section of the beam, this density value has to be corrected for the different sand pack widths. The heights of the sand packs are nearly the same and thus not taken into account. The sand volumes will be normalized on the volume of sand pack #2. The normalized volume of the sand packs is calculated as the product of the relative thickness d/d_2 and the relative width w/w_2 and is called the Sand Pack Equivalent (SPEQ).

The volumes have been normalized on sand pack #2 instead of the larger sand pack #1, because the latter pack is not used in the river water measurements. This makes the SPEQ numerically comparable to the norm used for the density measurements in river water (the $\langle \text{SPEQ} \rangle$, which is introduced below). The SPEQ values will be substituted in the measurements performed in the electromagnetic measurement setup.

After the calibration, a measurement series of increasing sand pack thickness was performed, to get an idea of the accuracy of the radioactive density measurement in comparison to the electromagnetic density measurements. The results of these measurements are shown in figure N.7. Note that the radioactive density measurements are not directly

Table 5.2: Sand pack calibration using radioactive density meter yields the SPEQ

#	ρ	d/d_2	w/w_2	SPEQ
1	1.04622	1.0314	1.00	1.031
2	1.04481	1.0000	1.00	1.000
3	1.02303	0.5139	1.00	0.514
4	1.04017	0.8964	0.94	0.843
5	1.03533	0.7884	0.94	0.741

comparable to electromagnetic measurements, because the radioactive measurement is restricted to the cross-section of the beam, whereas the electromagnetic measurement appears to have a much larger cross-section, integrating over a large section of the pipe.

Electromagnetic

Using the same method that is used for the electromagnetic density measurements in ‘river’ water, the sand packs were measured one at a time. This measurement series was performed twice. Only sand pack #1 was not measured, because it was decided to keep that sand pack fresh in case a measurement in non-saline water had to be repeated. The results of these measurements are listed in tables N.4 and N.5. Again the C.R.I.M. method was used to calculate the sand volume fractions.

Water displacement

During all density measurements in the radioactive density meter, the water level in the pipe was kept at a constant level by pumping (saline) water in or out. So the submerged part of the sand packs was kept constant too. This submerged volume corresponds to the drop in the water level when the sand pack is removed from the pipe: $V_{\text{sand}} = 1/4\pi d^2 \cdot \Delta h$. Again sand pack #1 was not measured. The measurement data can be found in table.

Average

The three calibration measurements for sand packs #2 to #5 can be compared, see the bar chart in figure 5.9. This chart provides a quick visual representation of the measured normalized volumes, the slight differences between the three different measurement methods and the average of these measurements, indicated by the stepped line.

For the averaging, the radioactive and volume measurements have been given weight 1 and the two electromagnetic measurements each have weight 0.5. This weighting is a bit arbitrary, but is still more objective than using any of the three methods alone.

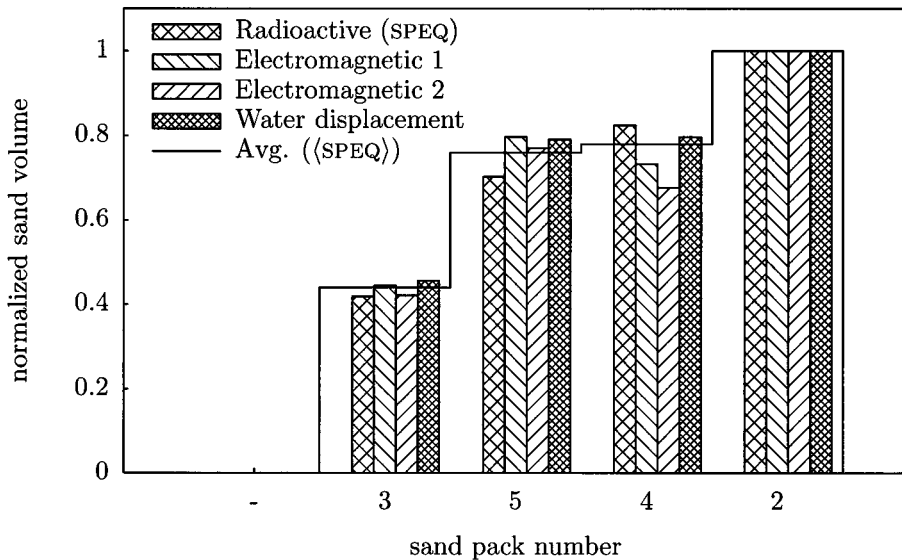


Figure 5.9: Calibration of the sand pack volumes using the radioactive method, the electromagnetic method (1 & 2) and the water displacement method, normalized on the volume of sand pack #2. The *average* normalized volume of each sand pack is indicated by the stepped line.

The bar chart shows that the three measurement methods yield somewhat different results. This is quite understandable, because the methods are entirely different:

- The radioactive method measures the thickness of a small cross-section of the sand packs;
- The electromagnetic method measures the effective permittivity of a large cross-section between the antennas;
- The volume method measures the total submerged volume.

For sand packs #2 – #5 the average normalized sand pack volume $\langle \text{SPEQ} \rangle$ is defined as the average sand volume fraction as indicated in figure 5.9. The $\langle \text{SPEQ} \rangle$ is not used for the density measurements in pure water, because there is no average value for sand pack #1 (for reasons mentioned above). Numerical values of the $\langle \text{SPEQ} \rangle$ are shown in table 5.3.

Table 5.3: Values of the $\langle \text{SPEQ} \rangle$, which is the average of the sand pack calibration measurements.

pack #	$\langle \text{SPEQ} \rangle$
3	0.44 ± 0.02
5	0.76 ± 0.05
4	0.78 ± 0.07
2	1.00 ± 0.05

This page intentionally contains only this sentence.

Chapter 6

Pure water measurements

Contents

6.1	First sand pack	62
6.2	Three sand packs	63
6.3	Improved sand packs	63
6.4	Goodwill oscilloscope	63
6.5	Painted pipe	63
6.6	Third antenna	65
6.7	Agilent oscilloscope	66
6.8	Probe measurements	67
6.9	Conclusions	69

6.1 First sand pack

The first density measurement in the pipe was performed when the first sand pack (#1) was ready. Measurements were performed with and without sand pack and when the pack was approximately 50% submerged. The water level in the inner pipe and in the outer pipe was kept at a reasonably constant (within 5 cm) level, a few centimeters below the brim. To improve the accuracy of the time difference measurement between the source signal and the received signal, the time interval was enlarged by one period.

To be able to calculate the permittivity of the mixture, some values had to be assumed for the permittivities of sand and water. These values are summarized in table 6.1.

Table 6.1: Assumed relative permittivities for density calculations

Material	ϵ_{er}
sand	4.0
water	79.0

The calculation of the permittivity of the mixture and the sand volume fraction can be found in detail in appendix J. Using the calculated permittivities and the C.R.I.M. model (4.15) the volume fraction occupied by the sand pack has been calculated and plotted in figure 6.1. The use of the *sand volume fraction* instead of *density* is intentional: the transformation from volume fraction to density is the same for all models. Moreover, it requires knowledge of the density of the sand pack. It would have been possible to assume a certain value for the density of the sand and the wooden frame but that would have been more suggestive than informative.

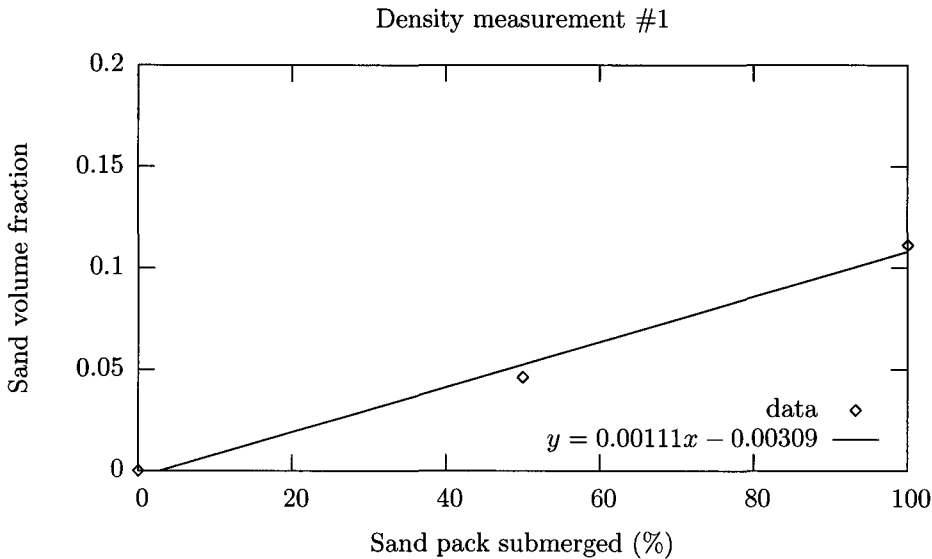


Figure 6.1: Measurement 1: Calculation of the sand volume fraction in the water using the C.R.I.M. model. A non-weighted fit using $y = ax + b$ yields $a = 0.00111 \pm 0.00011$ and $b = -0.00309 \pm 0.0069$.

The plot reveals a reasonably good linear correlation: a fit using $y = ax + b$ yields as squared correlation coefficient $r^2 = 0.991$ and a fit using $y = cx$ yields $r^2 = 0.989$. This is particularly interesting, as it means that the electromagnetic density measurement is not a point-to-point transmission, but measures the density over a larger volume. This is an advantage because it means that for a heterogenous density, which will certainly be the case in a flowing medium, an average density is measured. The data can be found in appendix N.2.1.

6.2 Three sand packs

The second measurement in the pipe was performed with the first two thick sand packs (#1 and #2) and the thin sand pack (#3). It is assumed that the two thick sand packs have an equal thickness and that the thin sand pack has half the thickness. A plot of the sand volume fraction, calculated using the C.R.I.M. model, is shown in figure N.9. The fits using $y = ax + b$ and $y = cx$ yield squared correlation coefficients of 0.988 and 0.986 respectively.

Though the quality of these fits is still quite acceptable, a quick look at the sand packs revealed that they had expanded several centimeters in the water. This is detrimental to the reproducibility of the measurements. After this measurement series the sand packs were modified rigorously to make sure they would stay in shape.

Another noticeable observation was that the measured time difference was quite sensitive to the water level in the inner pipe: as the last measurement in the table reveals, the measured time difference is too low when the pipe is not full. The data can be found in appendix N.2.2.

6.3 Improved sand packs

For this measurement series, all sand packs were reconstructed. Due to the new construction, the packs retain their shape nicely. These sand packs have been calibrated and the results of this calibration have been incorporated into the density calculation (figure N.10) by means of the “sand pack equivalent”. This SPEQ simply represents the relative volume for each sand pack. See table 5.2 in section 5.5 for the numerical values. The fits using $y = ax + b$ and $y = cx$ yield squared correlation coefficients of 0.992 and 0.989 respectively, which is about the same as for the previous measurements.

However, the sand pack thicknesses of the old sand packs are un-calibrated values which limits the reliability of the previous measurements. Moreover, a visual inspection of the plot reveals that most deviations from the fits are within the range of the accuracy of the oscilloscope. In order to make more accurate measurements, a scope with a higher sampling rate will be needed. The data can be found in appendix N.2.3.

6.4 Goodwill oscilloscope

The measurements from section 6.3 were repeated with a new Goodwill GDS-840S oscilloscope which was temporarily on loan. The theoretical time base accuracy of this oscilloscope is 2.5 times better than the Fluke Combiscope. A plot of the sand volume fraction, calculated using the C.R.I.M. model, is shown in figure N.11. The increased accuracy results in smaller error bars. The accuracy of the oscilloscope is no longer the limiting factor. The squared correlation coefficients are 0.986 and 0.975 for $y = ax + b$ and $y = cx$ respectively. The data can be found in appendix N.2.4.

6.5 Painted pipe

The iron pipe exhibited some serious corrosion, see figure 6.2(a). Because the presence of ions in the outer pipe might affect the measurements, the decision was made to remove the rust and coat the pipe and shields, see figure 6.2(b). The heavy strip on which the shields are bolted with three bolts per strip, is made of stainless steel. At all three bolting places, the coating of the shields is removed. This will lead to some oxidation, but electrical contact is more important. To ensure electrical contact between the stainless steel strip and the iron pipe, three pointed bolts (per strip) are driven through the coating, see figure 6.2(c).

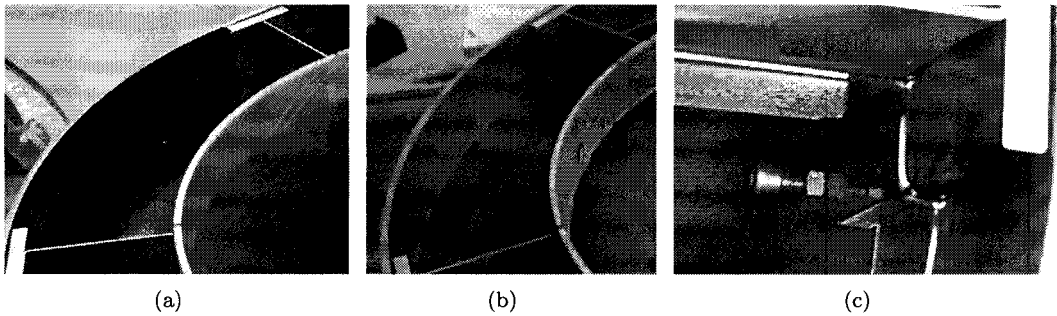


Figure 6.2: Section of the iron pipe before coating (a), showing a lot of corrosion, and after coating (b). To ensure electrical contact between the shields and the pipe, sharpened bolts are driven through the coating at three places per strip (c).

After the iron pipe had been sand blasted, primed with red lead and coated the density measurements were repeated to check for any changes. The results of these measurements are shown in figure N.12. The squared correlation coefficients are 0.969 and 0.957 for $y = ax + b$ and $y = cx$ respectively. This is quite a lot worse compared to the previous measurements. A visual inspection reveals quite some deviations from the fits. Also the slope of the fit is much higher than for the previous measurements. Only part (if any) of this can be attributed to the coating: a subsequent measurement yields much better results than this and does agree with previous measurements. This is shown in section 6.7.

The most likely cause of these deviations is the different frequency setting (60.2 MHz) and the higher VSWR that resulted from this. For this measurement, the frequency was chosen which gave the lowest VSWR (1:1.05) in an empty (just water) pipe. As it turns out, this can lead to much higher VSWR values (1:1.5) when the pipe is loaded with sand packs than usual. Therefore, measurements will be more accurate when the frequency is optimized (i.e. the VSWR is minimized) with a loaded pipe, in the density range that is most interesting. A final VSWR measurement with 4 sand packs at a frequency of 62 MHz instead of 60 MHz gives a VSWR of 1.10 instead of 1.38, which confirms that a frequency of about 62 MHz is more suitable for these measurements (in this exact configuration). The data can be found in appendix N.2.5

6.6 Third antenna

A third antenna was made and placed in the pipe at 60° from antenna #2 and 120° from antenna #1, see figure 6.3.

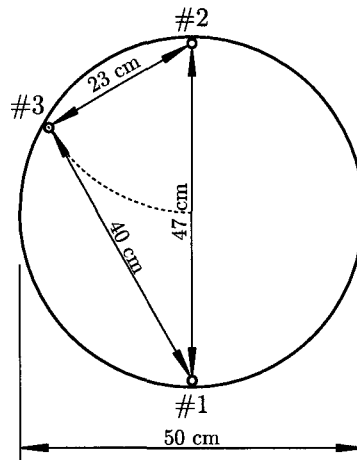


Figure 6.3: Configuration of the three antennas in the pipe, with approximate distances

Pure water

To compare the performance of all the new possible antenna configurations, the first measurements of this series were performed without sand packs. The same coaxial cables were used for all measurements and the frequency is kept constant, so the delay in the cables t_{wire} should be the same for all measurements. Using the same approach as used in appendix J, the propagation time t_{wave} and the propagation speed in pure water v can be calculated. These two values are related to the electromagnetic path by $d_{\text{wave}} = v(t_{\text{meas}} - t_{\text{wire}})$.

The electromagnetic paths are calculated and compared to the approximate geometrical distances between the antennas in table 6.2. It is assumed that the distance between antennas #1 and #2 equals the actual electromagnetic path so that the other paths can be calculated. As it turns out, the calculated electromagnetic paths do not correspond to the antenna separations.

Table 6.2: Calculated electromagnetic paths compared to the geometrical distance between the antennas.

Antenna config	t_{meas}	t_{wire}	t_{wave}	d_{wave}	d_{geom}
1 → 2	5.519	-8.416	13.934	0.47	0.47
1 → 3	5.119	-8.416	13.534	0.46	0.40
3 → 2	2.119	-8.416	10.534	0.36	0.23
3 → 1	5.219	-8.416	13.634	0.46	0.40
2 → 1	5.519	-8.416	13.934	0.47	0.47
2 → 3	3.219	-8.416	11.634	0.39	0.23

Sand packs

After the measurements without sand packs, an interesting measurement was performed where the sand packs were placed *not between* the antennas, but *parallel to* the two antennas as shown in figure 6.4.

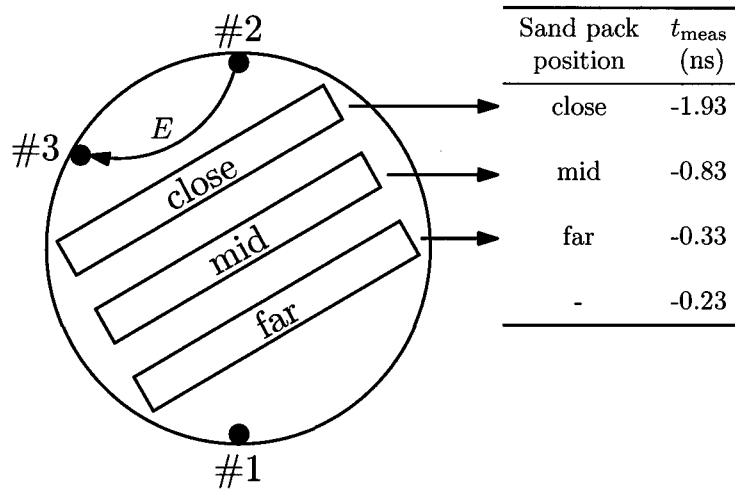


Figure 6.4: The presence of a sand pack near the antennas influences the propagation time of the electromagnetic wave E from antenna #2 to antenna #3, despite the fact that the sand pack is *not* placed *between* the antennas.

This shows that then density measurement is not really based on a point-to-point transmission, but has characteristics of a cavity which is ‘fed’ and ‘probed’. As a result, the measured density represents a much larger volume and can be seen as the *average* density in the pipe. This is an advantage over a point-to-point measurement. The data can be found in appendix N.2.6.

6.7 Agilent oscilloscope

These density measurements were performed with an Agilent 54832D oscilloscope, which has immensely better specifications than the Fluke or the Goodwill oscilloscopes. Especially the accuracy of the time difference measurements is much better, because these measurements are performed automatically by the scope’s built-in delta-time function. Furthermore, the oscilloscope records statistics: for all measured values the average, minimum, maximum and range (= max – min) is shown. The oscilloscope averaging was set to 64 measurements and each measurement was given some time (typically half a minute) until the average value reached a reasonably stable last digit.

While the margins of the previous measurements were estimated by the smallest time-step on the display, for these measurements both margins (upper and lower) are defined as half the range ($(\text{max} - \text{min})/2$). This gives a much better picture of the overall accuracy of the measurement setup and not just of the oscilloscope, see the plot of the density measurement in figure N.13. The squared correlation coefficients are 0.984 and 0.984 for $y = ax + b$ and $y = cx$ respectively.

At each density setting, measurements were also performed from antenna #1 to #3 and from antenna #2 to #3: instead of at opposite sites of the pipe, the antennas are located at 120° and 60° from each other respectively. As can be seen from the plots in figure N.14 and N.15, the measurements from antenna #1 to antenna #3 are still useful. The squared correlation coefficients are 0.974 and 0.954 respectively. The density measured using these antennas is a little higher than measured using antennas #1,#2. A plausible explanation is that the sand packs are not normal to the propagation path #1 \rightarrow #3 but normal to #1 \rightarrow #2. More about the effect of sand pack rotation can be found in section 7.5. The measurements from antenna #2 to antenna #3 show very little correlation: the squared correlation coefficients are 0.74 and 0.63. This is quite understandable as the sand packs are not even *between* the antennas.

6.8 Probe measurements

In order to obtain a better understanding of the discrepancies between the electromagnetic wave paths and the geometrical distances between the antennas, the phase and voltage was measured using a coaxial probe, at several positions in the pipe, all at the same horizontal plane at the center of the antennas. The positions are chosen at intervals of 5.0 cm, or even 2.5 cm at steep gradients, along the dashed lines from figure 6.5.

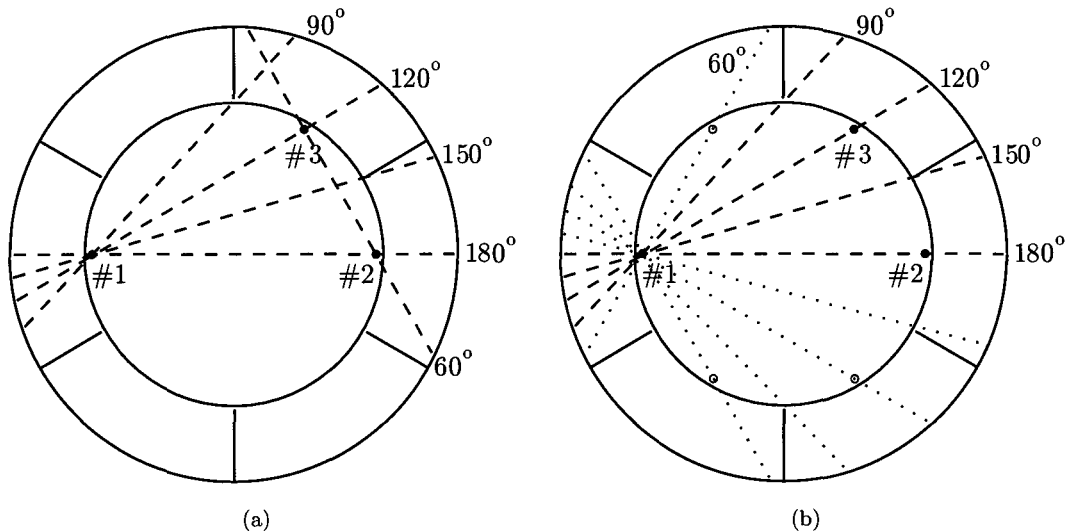


Figure 6.5: Phases and voltages were measured at several points along the dashed lines (a). The antenna positions are indicated by three solid circles. To obtain a complete cross-section of the pipe, the measurement at 60° was mirrored in a vertical axis and the other measurements were mirrored in a horizontal axis as indicated by the dotted lines (b). Note that because of the mirroring, this picture actually represents a pipe with six antennas instead of three, as indicated by the white circles.

These probe measurements do not take into account the interaction of the probe antenna with the near field, which actually alters the near field itself. It is assumed that the measurement probe is small enough not to disturb the field too much. Correction of near field measurement for the influence of the probe on the field is possible, but it requires knowledge of the far field distribution of the probe and some quite laborious calculations.

The results of these measurements were interpolated using Delaunay triangulation and isolines were determined, as shown in figures 6.6(a) and 6.6(b). The isophase lines show that the apparent propagation speed in the pipe is not constant. The isovoltage lines show that the shields have a serious impact on the electric field in the pipe: there is a significant voltage rise in the surroundings of each shield.

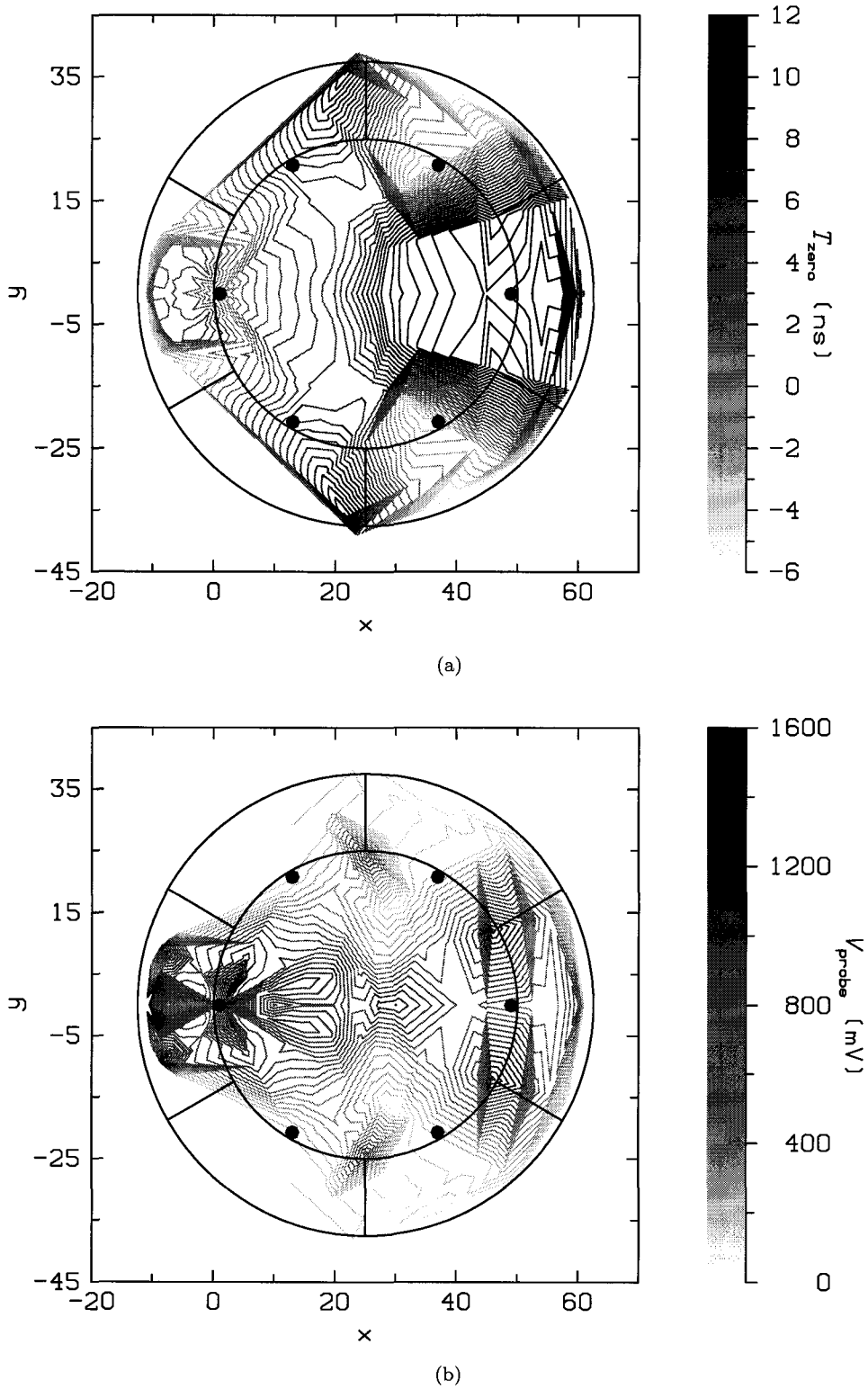


Figure 6.6: Isophase (a) and Isovoltage (b) lines, interpolated from the measured points.

6.9 Conclusions

The primary objective of the measurements in ‘pure’ water was to get an understanding of the characteristics of the antennas, the impedance matching, the measurement pipe, the signal generation and measurement system and the effects of sand in the pipe - without complicating the systems behaviour too much.

Antennas

The measurements have revealed that the driving point impedance is in reasonable agreement with the calculated values. The performance of the antennas, which were designed for application in river water, and the impedance matching system is excellent in pure water. A VSWR below 1 : 1.1 is achieved with the Q-match and in the frequency range 60 – 63 MHz. It is expected that the antenna performance will be more than sufficient for application in river water.

Measurement pipe

The measurement pipe exhibits unwanted reflections. It is suspected that these reflections will only appear in non-saline water, where there is only minimal signal attenuation. The slightest conductivity will probably attenuate the electromagnetic waves to such a degree that the reflected signal no longer noticeably interferes with the source signal.

A side effect of the absence of conductivity, is that the performance of the antennas varies with varying sand content in the pipe. In other words, the antennas ‘feel’ the presence of the sand packs. The VSWR of an antenna, tuned to a VSWR of 1 : 1.05 without sand, has been seen to increase to 1 : 1.5 with 3–4 sand packs in the pipe. Presumably this effect will also be less severe in more saline water.

Density measurements

Electromagnetic density measurements appear to be possible. The measured density represents a large volume of the pipe and can be seen as the *average* density in the pipe, in contrast with the radioactive density meter which probes only a small cross-section.

The changes in the measured time difference with and without one sand pack are in the order of 0.5 ns, so an accuracy of 0.01 – 0.05 ns is desirable to achieve a reasonable resolution. This demands quite a lot of the measurement circuit. However, this accuracy does not have to be obtained in a single shot, but may very well be the average of several hundreds of measurements. One density measurement every few seconds is sufficient, considering the performance of the radioactive density meter.

Measurements using antennas which are placed at a mutual angle of 120° instead of the usual 180°, show that this antenna configuration yields reproducible if electromagnetic transmission across the entire pipe is not possible (e.g. in highly saline water). Measurements using antennas at a mutual angle of 60° do not yield reliable data.

This page intentionally contains only this sentence.

Chapter 7

River water measurements

Contents

7.1	Introduction	72
7.2	Varying conductivity	72
7.3	Combined measurements	77
7.4	Probe Measurements	80
7.5	Pack rotation	81
7.6	Conclusions	86

7.1 Introduction

The typical conductivity of river water is assumed to be $0.65 \text{ S/m} = 6.5 \text{ mS/cm}$. Instead of using 'real' river water, a NaCl solution is created using ordinary salt, which is 99.9% NaCl and 0.1% KI. For 0.65 S/m , about 2.9 g/l of salt is needed. The salt was added while stirring and measuring the conductivity with a Henna conductivity probe.

The increased conductivity has a direct influence on the received signal. Whereas the typical voltage received by antenna #2 was 7.5 V in pure water, after adding the salt it was only 180 mV . The source voltage of the frequency generator is kept the same. Using these values the attenuation can be calculated:

$$\text{ATT} = 20 \cdot 10 \log \left(\frac{V_{\text{river}}}{V_{\text{pure}}} \right) = -32 \text{ dB.}$$

The slight rise in VSWR has been ignored. More importantly, the VSWR does not depend on the amount of sand in the pipe anymore, as it did in pure water. So the performance of the antennas has become more stable.

7.2 Varying conductivity

To get some insight in the effect of water conductivity, it was decided to perform the density measurements in 'river' water not only at the conductivity of 0.65 S/m , but also at a few lower and higher conductivities. The unprocessed measurement data can be found in appendix N.3. To calculate the sand volume fraction using the C.R.I.M. model, the propagation time and/or attenuation have to be determined.

Propagation time

A combined plot of the measured time differences for all river water measurements, combined with measurement #7 in pure water, is shown in figure 7.1. The computed linear fits are also shown.

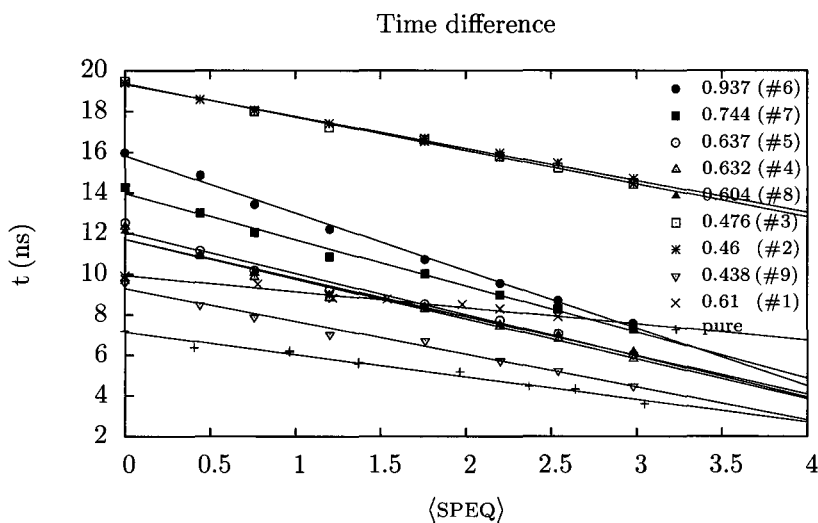


Figure 7.1: Measured time difference between the source and the received signal as a function of the sand volume in the pipe, for various conductivities. Fits using $y = ax + b$ are shown. The conductivity of the water in the outer pipe was negligible for the measurement series 'pure' and $\sigma_e = 0.61 \text{ S/m}$. For all other measurements, the conductivity in the outer pipe was 2.1 S/m .

Except for measurements #1,#2,#3 the measurements show a fairly consistent behaviour. The time difference decreases as the sand fraction in the pipe increases, which supports the calculated behaviour from example 1 in chapter 4. The largest gradient is found for $\sigma_e = 0.937$ S/m, the smallest gradient for pure water. The largest spread in the measured time difference is found *without* sand in the pipe and is reduced as the sand fraction increases. This behaviour makes sense, as an increase of the sand fraction ϕ means a decrease of the average conductivity. In the limit $\phi \rightarrow 1$ the time differences should all coincide.

The two upper outliers are measurements #2 and #3. The measured time differences are distinctly higher than for the subsequent measurements, most likely due to different wiring. This can be verified by calculating and plotting the propagation time instead of the time difference, as given by equations (4.2,4.4). A combined plot of the propagation times is shown in figure 7.2.

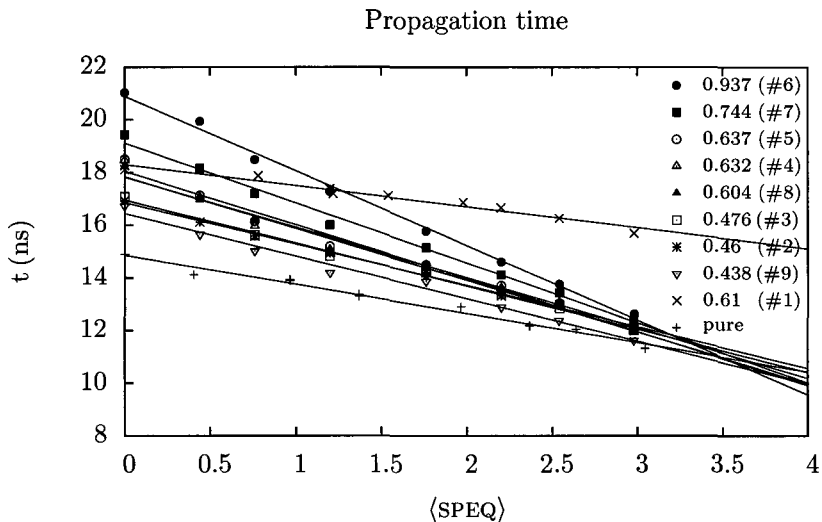


Figure 7.2: Propagation time, calculated using (4.2) and (4.4), as a function of the sand volume in the pipe, for water with conductivities $0.438 < \sigma_e$ (S/m) < 0.937 in the inner pipe. Fits using $y = ax + b$ are shown. The conductivity of the water in the outer pipe was negligible for the measurement series 'pure' and $\sigma_e = 0.61$ S/m. For all other measurements, the conductivity in the outer pipe was 2.1 S/m.

In this plot, measurements #2 and #3 do agree with the other measurements. So the higher times differences are a constant factor, most likely caused by accidentally using a longer coaxial cable in the receiver side of the circuit.

The lower outlier, measurement #1, still exists. This measurement at $\sigma_e = 0.61$ S/m was performed with non-saline water in the *outer* pipe. Because the water in the inner pipe is more conductive than the water in the outer pipe, it is quite plausible that a significant part of the measured signal travels through the pure water in the outer pipe and does not 'see' the sand packs.

To make certain that this would not happen for the subsequent measurements, salt was added to the water in the outer pipe to make it more conducting than the water in the inner pipe. The conductivity of the water in the outer pipe was set to 2.1 S/m, which is more than twice the maximum conductivity used in the inner pipe. Though the outer pipe conductivity was also zero for the pure water measurement, the water in the outer pipe did not present a *more favourable* path. This explains why the pure water measurement agrees with river water measurements #2-#9 and measurement #1 does not.

A questionable aspect of the calculated propagation times is that they more or less coincide between $\langle \text{SPEQ} \rangle = 3 - 3.5$. This should only just occur in pure sand, which has not been reached by far. This implies that the propagation times calculated using (4.2) and the inner pipe conductivity

are inaccurate, possibly because the electromagnetic wave not only travel through the inner pipe but also partly through the water in the outer pipe, which has a different conductivity.

To avoid this issue, an alternative determination of the propagation times has been performed by determining the *fixed* delay in the wiring t_{wire} and subtracting it from the measured time difference t_{meas} as indicated by equation (4.1). Using a fixed wiring delay is justified for measurements #4–#9 as the whole circuit has been exactly the same for these measurements. The propagation times, calculated using the fixed t_{wire} , are shown in figure 7.3 for the measurements #4–#9. The calculated propagation times display a reproducible behaviour.

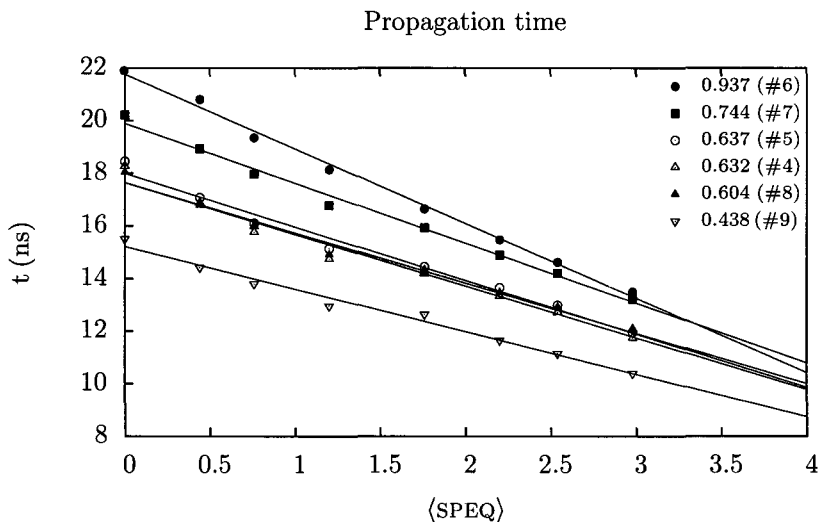


Figure 7.3: Propagation time, calculated using (4.1) and a fixed $t_{\text{wire}} = 5.924$ ns, as a function of the sand volume in the pipe, for water with conductivities $0.438 < \sigma_e$ (S/m) < 0.937 in the inner pipe. Fits using $y = ax + b$ are shown. The conductivity of the water in the outer pipe was negligible for the measurement series ‘pure’ and $\sigma_e = 0.61$ S/m. For all other measurements, the conductivity in the outer pipe was 2.1 S/m.

Attenuation

The voltages received on antenna #2 have been plotted for a few measurements in figure 7.4. Calculated exponential fits are shown.

The voltage measurement shows that the calculation of the attenuation constant is somewhat problematic at higher conductivities. Theoretically, if the sand volume fraction is decreased, the average conductivity increases and the received signal should decrease.

As figure 7.4 shows, the received voltage as a function of the sand fraction doesn’t follow the expected exponential behaviour at the lowest sand fractions for the measurements at ‘high’ conductivity ($\sigma_e \approx 1$). Instead, the received voltage increases as the sand fraction decreases to zero. For lower conductivities, this effect becomes less pronounced. Only for the measurements with $\sigma_e < 0.64$ decreases the voltage monotonously as the sand volume goes to zero. A plausible explanation for this behaviour is that here is an alternative signal path which is not hindered by the increase in conductivity.

Possible suspects, besides the shielding of the cables, include the shields in the outer pipe which may help the signal propagation, and the inner pipe. The inner pipe is made of a non-conducting dielectric material, on both sides surrounded by saline water which is a conducting material: effectively a *waveguide* has been created. The influence of the shields and the inner pipe is investigated as a function of the conductivity in chapter 8.

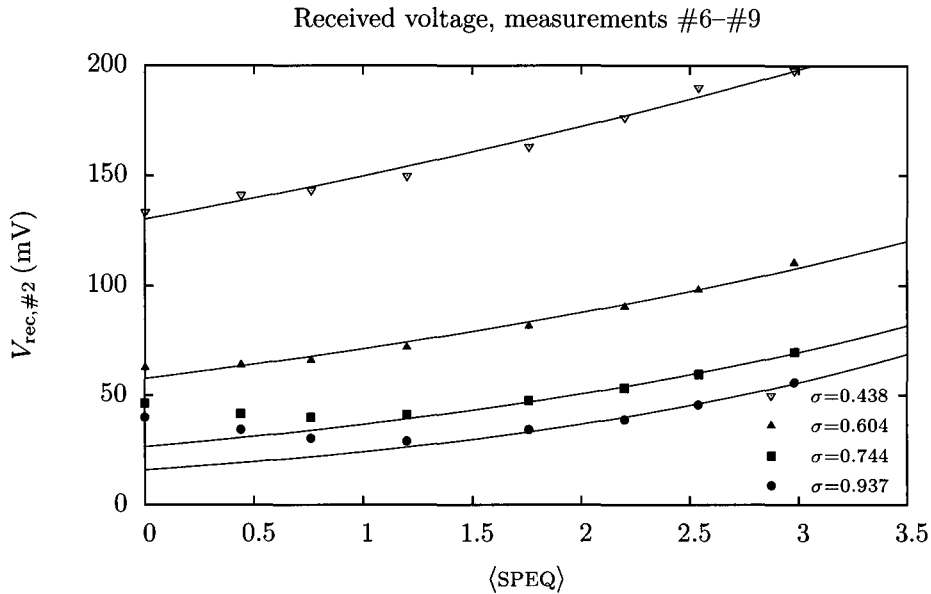


Figure 7.4: Plots of the voltage received by antenna #2 as a function of the sand volume fraction, for various water conductivities in the inner pipe. Fits using $y = a \exp(bx)$ are shown. The outer pipe conductivity is 2.1 (S/m). The fitted curves show the expected behaviour. The data points for $\sigma_e = 0.744$ S/m and $\sigma_e = 0.937$ S/m have been fitted using only the four measurement points for $\langle \text{SPEQ} \rangle > 1.5$, to show that the other four measured voltages are too high.

Apparent permittivity

Because the problems arising in the measurement of the attenuation (and thus the conductivity) do not seem to cause a noticeable disturbance of the time difference measurement, the C.R.I.M. method using the *apparent* permittivity (4.19) is preferred because it only needs a measurement of the propagation time. The propagation time is derived from the measured time difference using an average wiring delay of $t_{\text{wire}} = 5.924$ ns.

A characteristic density measurement (#5) is shown in figure 7.5 and a combined plot of the sand volume fractions calculated from measurements #4-#9 in river water using the C.R.I.M. model is shown in figure 7.6.

Two things stand out in these plots:

1. For higher $\langle \text{SPEQ} \rangle$ values the data points lie significantly below the fit .
2. The slope of the fits is not the same for the measurements at different conductivities.

The first aspect can be a systematic error in the calibration of the sand packs. It may also indicate a shortcoming of the C.R.I.M. model. The reason why the deviations occur mainly at *higher* $\langle \text{SPEQ} \rangle$ values is because the weighted fit puts more weight on the lower $\langle \text{SPEQ} \rangle$ values. The lower values have a smaller error because a higher sand $\langle \text{SPEQ} \rangle$ means that more sand packs have been used, each with its own uncertainty. In a practical density meter, a calibration using an *unweighted* fit is preferable, because it gives a constant density measurement error over the entire calibrated range.

The second aspect can be investigated more closely by searching a possible conductivity dependence in the slope. The fit parameters a and b of the linear fits $\phi = a \cdot \langle \text{SPEQ} \rangle + b$ in figure 7.6 are summarized in table N.17 in appendix N.3. A plot of the regression constant a , which corresponds to $\partial\phi/\partial\langle \text{SPEQ} \rangle$, is shown in figure 7.7. This plot does not show a significant conductivity dependence as the uncertainty in the slope is almost 100%.

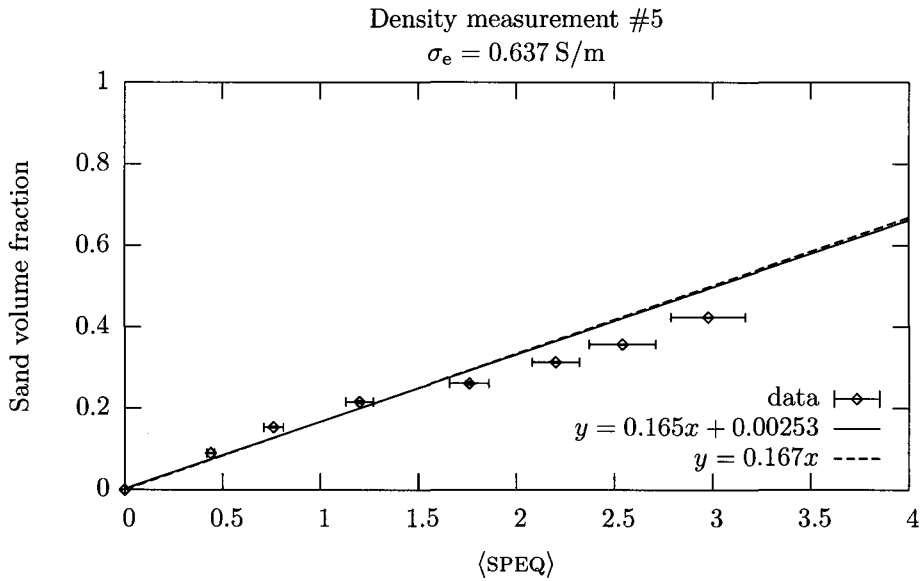


Figure 7.5: Measurement #5: Calculation of the sand volume fraction in the water using the C.R.I.M. model. Weighted fits using $y = ax + b$ and $y = cx$ yield $a = 0.165 \pm 0.011$, $b = 0.00253 \pm 0.00407$ and $c = 0.1673 \pm 0.0103$. The weighted sums of squared residuals are $\chi^2_\nu = 12.95$ and $\chi^2_\nu = 11.82$ respectively.

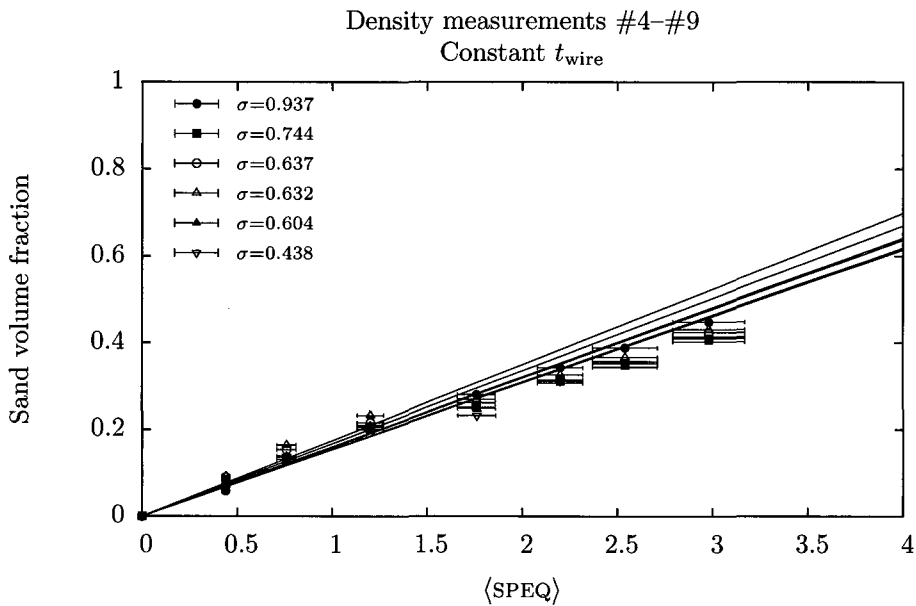


Figure 7.6: Calculated sand volume fractions in the water using the C.R.I.M. model. Weighted fits using $y = ax + b$ are shown.

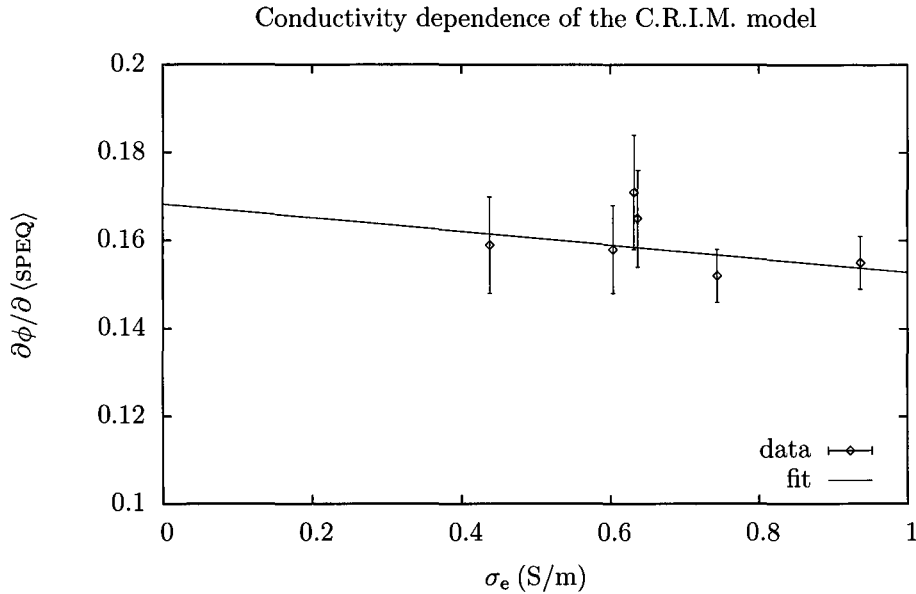


Figure 7.7: Conductivity dependence of the parameter a from the linear fit $y = ax + b$ which has been applied to the sand volume fractions calculated using the C.R.I.M.model. The found regression coefficients are $a = -0.0154 \pm 0.0152$ (98.6%) and $b = 0.168 \pm 0.012$ (6.9%).

7.3 Combined measurements

The difficulties arising in the use of the C.R.I.M. model can be resolved by using a semi-empirical model. As the propagation time measurements show the highest reproducibility, a model based on propagation time data looks favourable.

Again, only measurements #4–#9 have been used. Only data sets 4–9 are considered reliable enough to be used, because the measured time differences of measurements 2 and 3 were not in the same range (most likely due to different wiring) and measurement 1 was performed with non-saline water in the outer pipe.

Because the propagation time depends on both the permittivity and the conductivity of the propagation medium, one calibration measurement of the time difference between source and received signal, without sand in the pipe, is needed each time the conductivity of the water changes. This calibration time is t_0 and the corresponding density is 1 ton/m^3 . The time difference t_{meas} that is measured during normal operation of the density meter is compared to this calibration time, which gives rise to the introduction of the *relative* time difference:

$$t_r = t_{\text{meas}} - t_0. \quad (7.1)$$

In short, the parameter t_0 varies with varying conductivity and the parameter t_r varies (mainly) with varying density. To make a fit which results in the actual density instead of a sand volume fraction, the total density of the four used sand packs has been estimated from the change in water level in the pipe:

$$\phi = V_{\text{sand}}/V_{\text{total}} = \Delta h/h \quad (7.2)$$

$$\approx 0.43 \text{ m}/1.40 \text{ m} = 0.307. \quad (7.3)$$

Assuming $\rho_{\text{sand}} = 2.65 \text{ ton/m}^3$ the density can be calculated using (4.23):

$$\rho_{4\text{-packs}} = 1.51 \text{ ton/m}^3, \quad (7.4)$$

and the $\langle \text{SPEQ} \rangle$ -density relation is given by:

$$\frac{\rho}{1 \text{ ton/m}^3} = 1 + 0.1701 \cdot \langle \text{SPEQ} \rangle. \quad (7.5)$$

The determination of the fitting model relating the density ρ to the parameters $\{t_r, t_0\}$ can be found in appendix K. The result is the following model:

$$\rho(t_0, t_r) = 1 + a \cdot t_r + b \cdot t_r^2 + c \cdot t_0 \cdot t_r. \quad (7.6)$$

The results of the fit are shown in figure 7.8. The residuals are given by $\rho_{ij} - \hat{\rho}$ where ρ_{ij} represents the actual data points and $\hat{\rho} = \rho(t_0, t_r)$ represents the calculated values. A residual plot versus t_r , for all measurement series (and corresponding t_0) combined, is shown in figure 7.9.

The uncertainty in the residuals is composed of an uncertainty in ρ_{ij} due to the uncertainty in the measured values t_r and t_0 , which has been derived in appendix K, and an uncertainty in $\hat{\rho}$ due to the uncertainty in the regression constants a, b, c .

As the residual plot shows, the typical (RMS) uncertainty is $\pm 0.04 \text{ ton/m}^3$. Compared to the stated accuracy of the radioactive density meter of $\pm 1\%$ full scale, which corresponds to an RMS uncertainty of $\pm 0.018 \text{ ton/m}^3$ for $\rho \leq 1.8$, it can be concluded that this is an excellent performance!

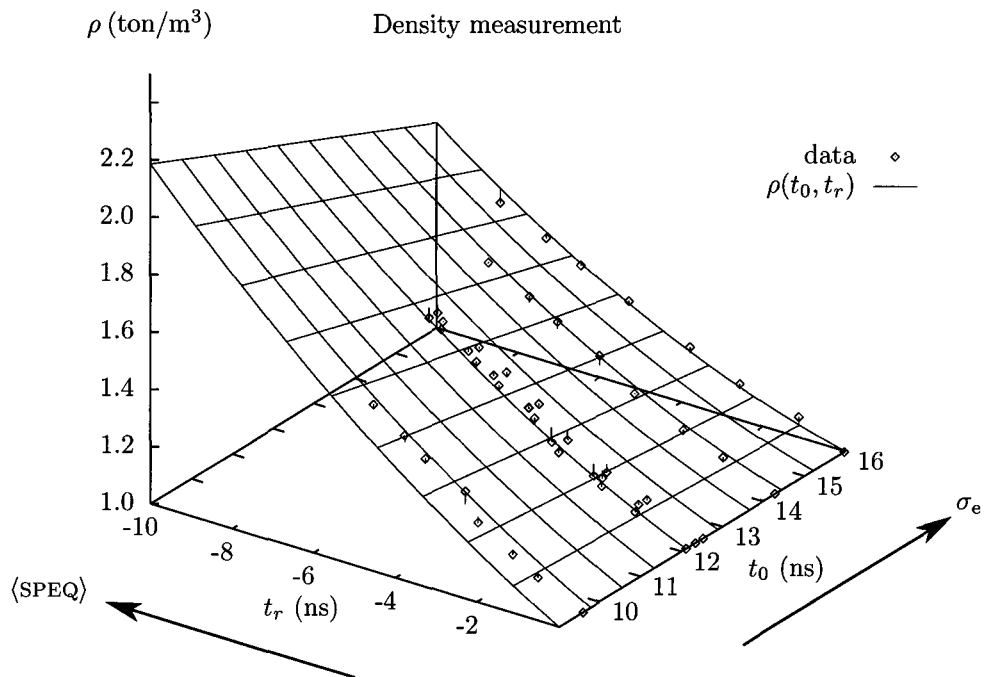


Figure 7.8: Combined measurements: plot of the calculated densities of all density measurements in ‘river’ water versus the time difference without sand t_0 (calibration point) and the change in the measured time difference $t_r = t_{\text{meas}} - t_0$. The typical $\langle \text{SPEQ} \rangle$ and σ_e dependencies of t_r and t_0 are indicated by arrows. A weighted fit has been made using $\rho(t_0, t_r) = 1 + a \cdot t_r + b \cdot t_r^2 + c \cdot t_0 \cdot t_r$. The result of the fit is $a = -0.1427 \pm 0.0052$, $b = 0.00363 \pm 0.00054$ and $c = 0.00673 \pm 0.00045$. The weighted sum of squared residuals is 38.9. The distance between the measurement points and the fitted surface is indicated by vertical lines.

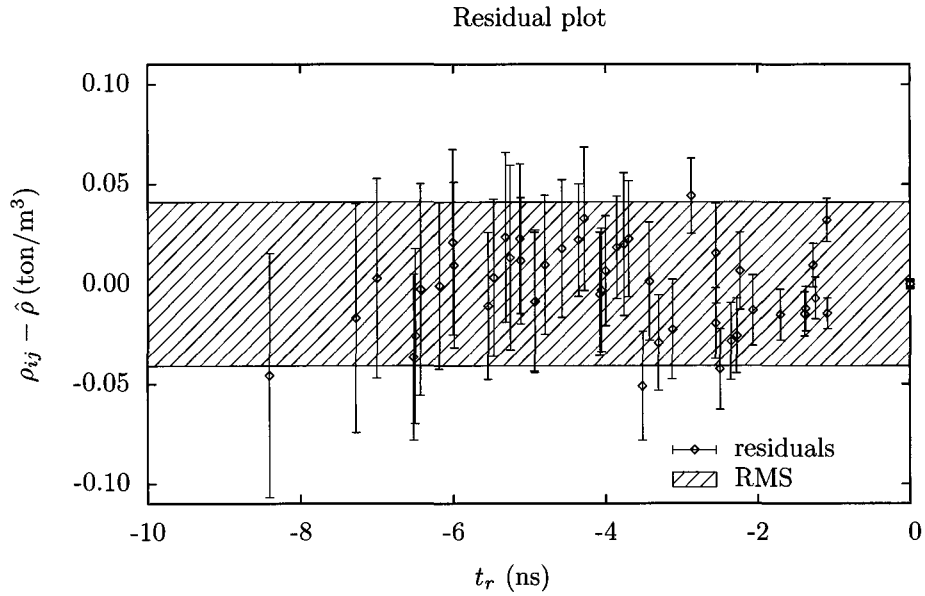


Figure 7.9: Residual plot of the combined measurements: plot of the residuals $\rho_{ij} - \hat{\rho}$ of all density measurements in ‘river’ water versus the change in the measured time difference $t_r = t_{\text{meas}} - t_0$. The parameter ρ_{ij} represents the actual data points, $\hat{\rho}$ represents the values calculated with model (7.6) The RMS of the total (measurement + regression) error is ± 0.04 as indicated by the hatched area.

7.4 Probe Measurements

To compare the pure water probe measurements with the river water measurements, the measurement along the line from antenna #1 to antenna #2 (180° in figure 6.5) was repeated with river water ($\sigma_e = 0.61$ S/m) in the inner pipe. The water in the outer pipe is non-saline. The plots are shown in figure 7.10.

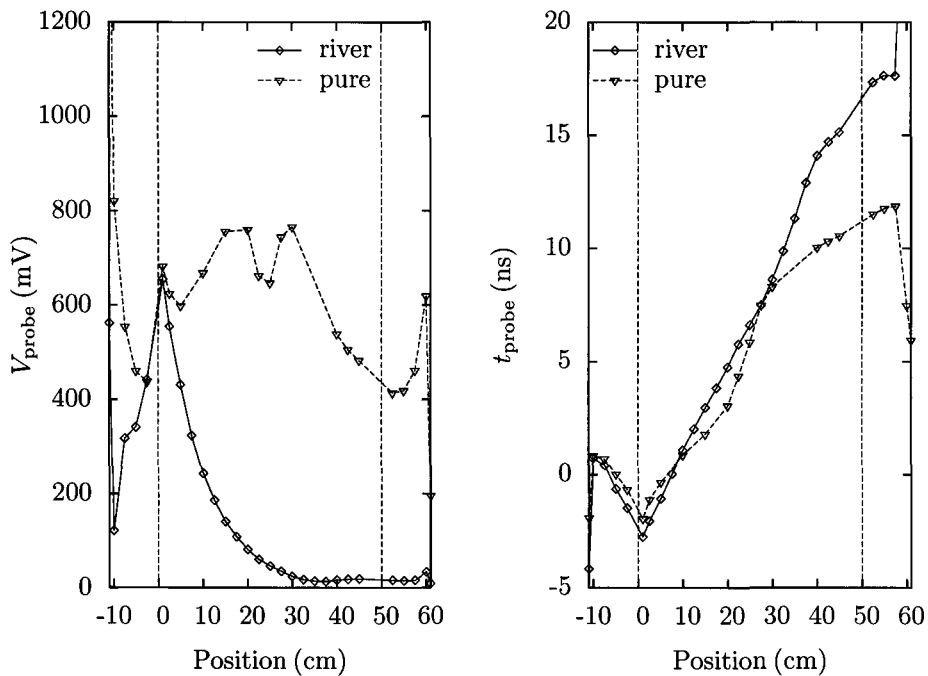


Figure 7.10: Probe voltages and time difference between the probe signal and the source signal (antenna #1) as a function of the probe position in the pipe, for river water and pure water in the inner pipe. The water in the outer pipe is non-saline in both cases. The probe is moved from behind antenna #1 to beyond antenna #2. The position of the inner pipe wall is indicated by the dashed lines. The antenna positions are approximately at 1 and 48 cm. The data points are connected with straight lines for visual reference only.

The plots show that the resonance effects, which are clearly present in the voltage measurement in pure water, are completely absent in the river water: the voltage decays exponentially, at least up to the position 35 cm. When the coaxial probe approaches the antenna #2, the exponential relation no longer holds. A possible explanation for this, is that the measured voltage is so low that other (e.g. reflected) signals become dominant.

Another possible explanation is the transition from reactive near field to radiating near or far field. The transverse electric field decays much faster in the reactive near field than in the radiating far field, as shown in section 3.4. A great part of this gradual transition takes place in the radiating near field zone, so a change in the electric field is very likely to appear there.

According to the guidelines, the transition to the radiating near field should occur at approximately 33 m from the antenna. However, this guideline should not be taken too strictly here as it is intended for bare antennas in free space and not for insulated antennas in water. A similar effect is shown in [36] and [1], where it is ascribed to a transition from the near to the ‘intermediate’ or far field. In the vicinity of the antenna, rapid attenuation is observed and at larger distances, the attenuation is vastly reduced.

Using the measurement points between 1 and 35 cm, the logarithm of probe voltage has been plotted against the probe position, see figure 7.11, which shows the excellent exponential decay

of the measured voltage. The found attenuation constant $\alpha = 11 \text{ m}^{-1}$ corresponds to an effective water conductivity of 0.71 S/m , as calculated using (3.8a).

The time measurement also shows an improvement: the apparent propagation speed (inverse of the slope) is much more constant in the river water than in the pure water, which means that the wave is much less affected by reflections in river water than in pure water.

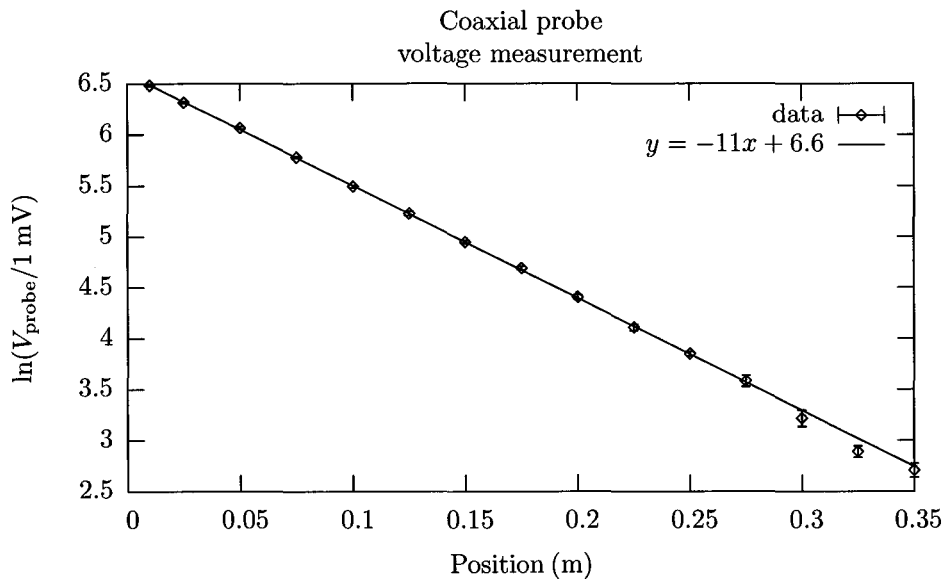


Figure 7.11: The logarithm of the probe voltages as a function of the probe position in the pipe. The linear fit $\ln(V) = ax + b$ shows that the probe voltage decreases exponentially. The squared correlation coefficient is $\chi^2_{\nu} = 0.87$.

7.5 Pack rotation

A general assumption which justifies the use of sand packs to represent slurry is that the sand packs do not reflect or refract the electromagnetic waves, but only change the propagation speed and attenuation. Thus a sand pack placed at a certain angle $\theta > 0$ with respect to the propagation vector will merely enlarge the electromagnetic path through the sand at the cost of the path through the water. To investigate this effect, the time difference and antenna voltage have been measured as a function of the sand pack orientation. The orientation θ of a sand pack with respect to the antenna configuration is defined as shown in figure 7.12. The results of the measurements are shown in figures 7.13 and 7.14.

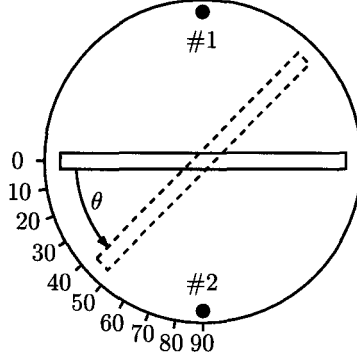


Figure 7.12: The orientation of the sand pack with respect to the antenna positions is given by the angle θ .

The electromagnetic path through a sand pack placed at angle θ with respect to the electromagnetic propagation vector is related to the pack thickness d_{pack} and the sand pack width w_{pack} by:

$$d_n(\theta) = \min \left\{ \frac{d_{\text{pack}}}{\cos \theta}, w_{\text{pack}} \right\}, \quad (7.7)$$

where the angle should be limited by $0 \leq \theta < 90^\circ$. For $\theta \approx 90^\circ$ the electromagnetic path through the sand pack reaches its maximum: the sand pack width w_{sand} .

Propagation time

The total propagation time of an electromagnetic wave in the pipe is given by:

$$\begin{aligned} t_{\text{wave}}(\theta) &= \frac{d_n(\theta)}{c_0} \sqrt{\varepsilon_{\text{ar}}^{\text{s}}} + \frac{d_{\text{wave}} - d_n(\theta)}{c_0} \sqrt{\varepsilon_{\text{ar}}^{\text{w}}} \\ &= \frac{1}{\cos \theta} \frac{d_{\text{pack}}}{c_0} (\sqrt{\varepsilon_{\text{ar}}^{\text{s}}} - \sqrt{\varepsilon_{\text{ar}}^{\text{w}}}) + \frac{d_{\text{pack}}}{c_0} \sqrt{\varepsilon_{\text{ar}}^{\text{w}}} \end{aligned} \quad (7.8)$$

where d_{wave} is the total electromagnetic path (antenna separation), $\varepsilon_{\text{ar}}^{\text{s}}$ the relative apparent permittivity of the saturated sand pack and $\varepsilon_{\text{ar}}^{\text{w}}$ the relative apparent permittivity of the water, which has a conductivity of 0.317 S/m during this experiment. Based on equation (7.8) the measured time differences are fitted using:

$$\frac{t_{\text{meas}}}{1 \text{ ns}} = \frac{1}{\cos \theta} \cdot a + b \quad (7.9)$$

where

$$\begin{aligned} a &= \frac{d_{\text{pack}}}{c_0} \cdot (\sqrt{\varepsilon_{\text{ar}}^{\text{s}}} - \sqrt{\varepsilon_{\text{ar}}^{\text{w}}}) / 1 \text{ ns} \\ b &= \left(\frac{d_{\text{pack}}}{c_0} \cdot \sqrt{\varepsilon_{\text{ar}}^{\text{w}}} + t_{\text{wire}} \right) / 1 \text{ ns}. \end{aligned}$$

Because the function $\cos^{-1} \theta$ goes to infinity when $\theta \rightarrow 90^\circ$, and because it is likely that for large angles the electromagnetic waves will ‘leak’ around the sand pack, the fit is limited to angles $0 \leq \theta \leq 45^\circ$. The plot of this fit is shown in figure 7.13. Using the following parameters:

$$d_{\text{pack}} = 0.06 \text{ m} \quad (7.10a)$$

$$d_{\text{wave}} = 0.47 \text{ m} \quad (7.10b)$$

$$\sqrt{\varepsilon_{\text{ar}}^{\text{w}}} = 9.99 \quad (7.10c)$$

and the found regression constant $a = -0.303 \pm 0.048$ the relative apparent permittivity of the sand pack can be calculated:

$$\epsilon_{\text{ar}}^{\text{s}} \approx 72 \quad (7.11)$$

which seems to be rather high. Literature values of saturated water indicate much lower relative apparent permittivities of soils. In [39] the measured relative apparent permittivities are below 40 for water content $(1 - \phi) < 0.5$. In other sources the stated relative apparent permittivities are still lower than that.

If the measured apparent permittivity had been $\epsilon_{\text{ar}}^{\text{s}} = 40$, the angular dependence would have been much more pronounced. The reduced angular dependence is an advantage for our purpose, because it makes a density meter less sensitive to the slurry density *distribution* in the pipe.

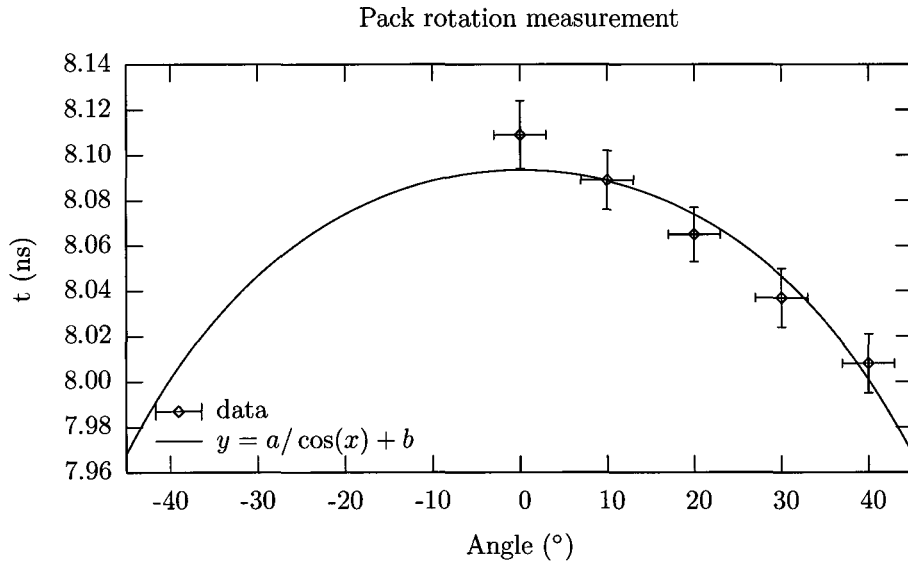


Figure 7.13: Measurement of the time difference between the source signal and the received signal as a function of the orientation of a sand pack. The orientation θ is as indicated in figure 7.12. Function (7.9) has been fitted through the data. The found regression constants are $a = -0.303 \pm 0.048$ and $b = 8.4 \pm 0.1$. The weighted sum of squared residuals is $\chi^2_{\nu} = 0.63$.

Voltage

The orientation dependence of the voltage of the received signal V is given by:

$$\begin{aligned} V(\theta)/V_0 &= \exp[-\alpha_w(d_{\text{wave}} - d_n(\theta))] \cdot \exp[-\alpha_s d_n(\theta)] \\ &= \exp[-\alpha_w d_{\text{wave}}] \cdot \exp[(\alpha_w - \alpha_s) d_{\text{pack}} \cos^{-1} \theta] \end{aligned} \quad (7.12)$$

which takes the form:

$$V(\theta)/V_0 = A \cdot B^{\cos^{-1} \theta} \quad (7.13)$$

where

$$\begin{aligned} A &= \exp[-\alpha_w d_{\text{wave}}] \\ B &= \exp[(\alpha_w - \alpha_s) d_{\text{pack}}]. \end{aligned}$$

This equation can be written as a Taylor expansion for $\theta \approx 0$ in radians:

$$V(\theta)/V_0 = AB \cdot [1 + 1/2 \ln(B) \theta^2 + \mathcal{O}(\theta^3)]. \quad (7.14)$$

Because the “zero conductivity” voltage V_0 is not available, the factor AB can only be determined by means of fitting to the measured data. For small angles, the Taylor expansion (7.14) can be reasonably approximated by a second order polynomial, which leads to the following fitting function:

$$\frac{V}{1 \text{ mV}} = a \cdot [1 + b \cdot \theta^2] \quad (7.15)$$

with θ in radians and

$$a = V_0 \cdot AB / 1 \text{ mV}$$

$$b = 1/2 \ln(2B) = 1/2 (\alpha_w - \alpha_s) d_{\text{pack}}.$$

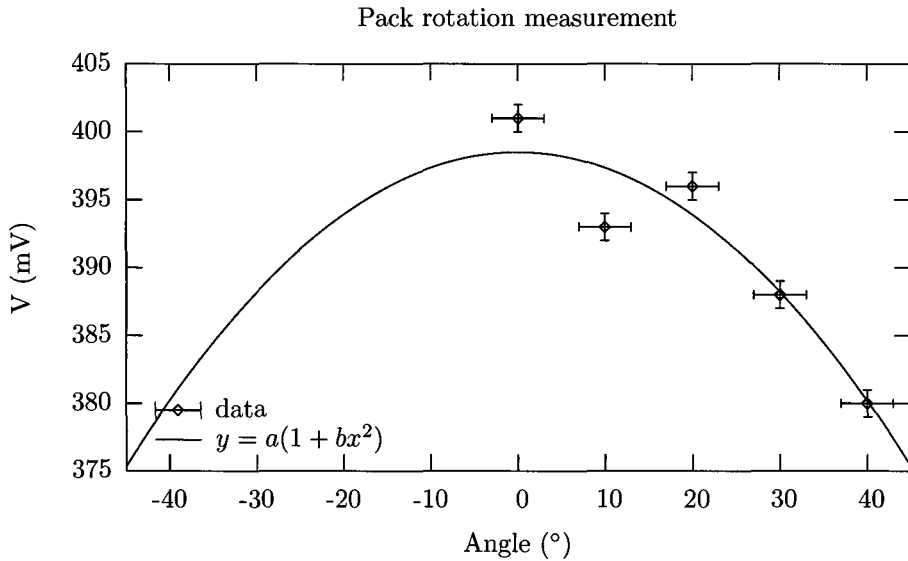


Figure 7.14: Measurement of the voltage received by antenna #2 as a function of the orientation of a sand pack. The orientation θ is as indicated in figure 7.12. Function (7.15) has been fitted through the data. The found regression constants are $a = 399 \pm 2.004$ and $b = -0.0942 \pm 0.0193$. The weighted sums of squared residuals is $\chi^2_\nu = 9.87$.

The attenuation constant of the water α_w can be calculated using (3.8a) with the measured conductivity of 0.317 S/m and an assumed relative effective permittivity $\epsilon_{\text{er}}^w = 79.0$:

$$\alpha_w \approx 5.98 \text{ m}^{-1}.$$

The attenuation constant of the saturated sand pack can be determined from the data fit, again limited for angles $\leq 45^\circ$ ($0 \leq \theta \leq \frac{\pi}{4}$) as shown in figure 7.14. Using the definition of regression constant b , the attenuation constant of the saturated sand pack can be determined:

$$\alpha_s \approx 9.12 \text{ m}^{-1}$$

which is actually higher than the attenuation constant in water. This is caused by the lower apparent permittivity of sand compared to water, as can be verified by looking at the permittivity dependence of the attenuation constant, which can be calculated by combining (E.5) and (E.7):

$$\alpha(\epsilon_{\text{ar}}) = \frac{\mu c_0}{2} \frac{\sigma_e}{\sqrt{\epsilon_{\text{ar}}}} \sim \frac{1}{\sqrt{\epsilon_{\text{ar}}}}. \quad (7.16)$$

The corresponding conductivity *in* the sand pack can be calculated using (7.16) and the measured relative permittivity of the sand pack (7.11):

$$\sigma_e^s = \frac{2}{\mu C_0} \alpha_s \sqrt{\epsilon_{\text{ar}}^s} = 0.41 \text{ S/m.} \quad (7.17)$$

Like the apparent permittivity, the measured conductivity is too high – higher than the conductivity of the water. However, for a lower and more realistic relative apparent permittivity $\epsilon_{\text{ar}}^s < 40$ the effective conductivity is also lower ($\sigma_e^s < 0.31 \text{ S/m}$) which is in better agreement with the conductivity of the water (0.317 S/m), though still a bit high.

With this single sand pack, the sand appears to have the same conductivity as the water. It seems that the sand pack is so *thin* and saturated to such a degree that the conductivity has not noticeably decreased.

This behaviour differs from the behaviour seen during the density measurements, which have been performed with *more* than one sand pack, as described in section 7.2. Those measurements demonstrate that at larger sand volume fractions the received voltage *increases*, as shown figure N.16 in appendix N.3.1. This can only mean that the attenuation constant is *lower* in the sand than in the water. Assuming that the apparent *permittivity* of the thicker sand pack, used for the density measurements, will be at most as high as the apparent permittivity of the single sand pack used here, this means that the effective conductivity in the thick sand pack is noticeably lower than the effective conductivity of the water, which seems reasonable.

From this point of view, the observed angular dependence of the received voltage appears to be exceptional, and attributable to the use of a single sand pack. This does not affect the density measurements, because the density calculation is only based on a time difference measurement.

Another cause for deviations is that in this model the electromagnetic propagation is treated as a straight point-to-point transmission without electromagnetic waves traveling around the sand pack, the sand pack as assumed to consist of only (saturated) sand, and it is assumed that the sand pack does not reflect and/or refract the electromagnetic waves, even at larger angles. This makes it plausible that this simplified model offers only a qualitative description and does not yield the exact numerical values.

7.6 Conclusions

Compared to the measurements in pure water, the measurements in river water have some advantages and some disadvantages:

- Advantages:
 - No more unpredictable reflection of waves: the waves show the expected wave decay.
 - The antenna performance is more constant, deduced from the much more constant VSWR.
- Disadvantages:
 - Signal loss is much higher due to the conductivity.
 - Waves may travel around the inner pipe, through the water in the inner pipe, so:
 - the water in the outer pipe must be made more conducting than in the inner pipe.

The density (or sand volume fraction) calculations using the C.R.I.M. model show a great deal of potential, though the observed deviations in the fit (figure 7.6) cannot be accounted for. Using a semi-empirical model, based only on the time-difference measurements, a model has been derived which results in a density calculation with an RMS uncertainty of $\pm 0.04 \text{ ton/m}^3$.

Chapter 8

High salinity measurements

Contents

8.1	Varying conductivity	88
8.2	Probe Measurement	91
8.3	Shields effect	92
8.4	Inner pipe effect	94
8.5	Crosstalk	96
8.6	Conclusions	96

8.1 Varying conductivity

To discover the operational limits of the experimental setup, measurements of the received voltage and propagation time were measured as a function of the conductivity of the water in the inner pipe σ_e^{in} , while keeping the water in the outer pipe non-saline. The results of these measurements are shown in figure 8.1 and the data can be found in appendix N.4.1.

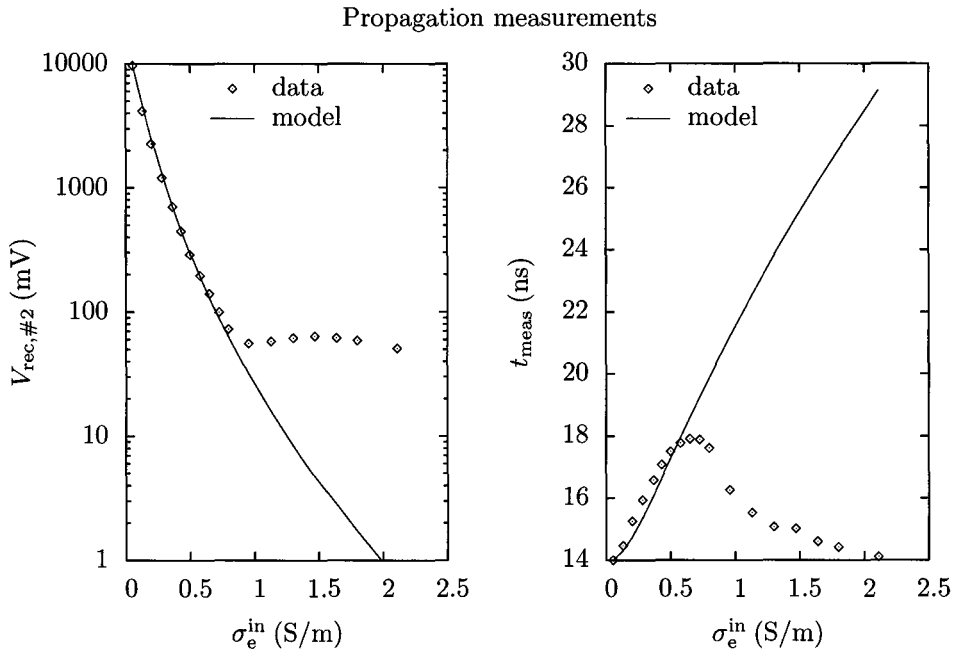


Figure 8.1: Plots of the voltage received by antenna #2 and the time difference between the source and receiver antenna #2 as a function of the effective conductivity of the water in the inner pipe σ_e^{in} . The exponentially decaying curve in the left plot is not a fit but calculated using (4.5) and matched to the point $\sigma_e^{\text{in}} \approx 0$. The square root curve in the right plot is calculated using (4.2) and also matched to the $\sigma_e^{\text{in}} \approx 0$ point.

The behaviour for conductivities above approximately 0.7 S/m diverges quite a lot from the model. The voltage measurements shows that the attenuation does not increase as the conductivity of the water in the inner pipe increases.

A plausible assumption is that a substantial part of the electromagnetic waves travels around the inner pipe, probably through the water in the outer pipe which is non-saline and causes less attenuation. The propagation time measurements support this assumption as the propagation time decreases where it should increase according to the model. The theoretical curve in the right plot of figure 8.1 shows that the measured time difference for $\sigma_e = 2.1$ S/m should be approximately one period longer. With the current measurement setup, this cannot be determined as all time differences are measured modulo T .

To verify this assumption, three measurement series were performed using saline water in the outer pipe. Additionally, a method was devised to send short sine wave packets instead of a continuous wave, and thus measure the *absolute* time difference between the start of the transmitted wave packet and the start of the received wave packet.

Theoretically, these short sine wave packets can be seen as a pulse-modulated sine wave. A screenshot of a signal obtained using 110 kHz square wave modulation is shown in figure 8.2. There is no retraceable wave packet start, only a subjective perception of a growing amplitude. In between the wave packets, the signal is still clearly present. At higher conductivities this subjective ‘start’ of the signal tends to disappear in the oscillations between the wave packets.

To obtain a retraceable wave packet start, the modulated signal must have a much faster rise time, preferably well below one period (16 ns), and have a negligible amplitude in between the wave packets. This practically excludes the use of amplitude modulation for this purpose.

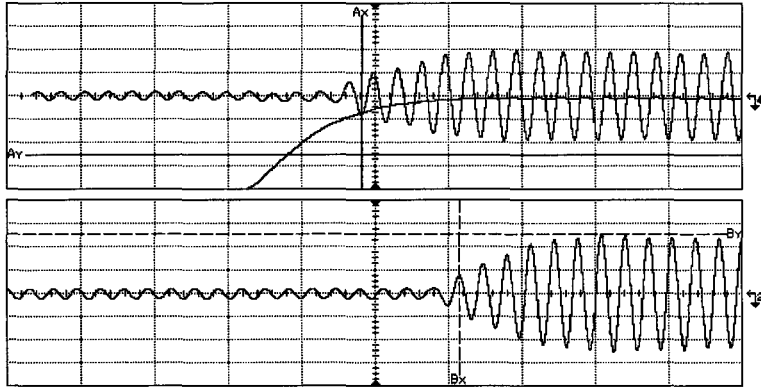


Figure 8.2: Oscilloscope screenshot showing the transmitted (upper) and received (lower) square wave modulated wave packet. The slowly rising step function is the 110 kHz square wave modulation signal. The time base is set to 50 ns/DIV, and the measured rise time of the square wave signal is clearly longer than one division.

A striking aspect in figure 8.2, is that the source signal is inverted in comparison to the received signal. A *direct* measurement of the waveform on the oscilloscope reveals that the polarity is reversed in the pickup coil. This has no influence on the measurements, because it only causes a change in the circuit delay t_{wire} .

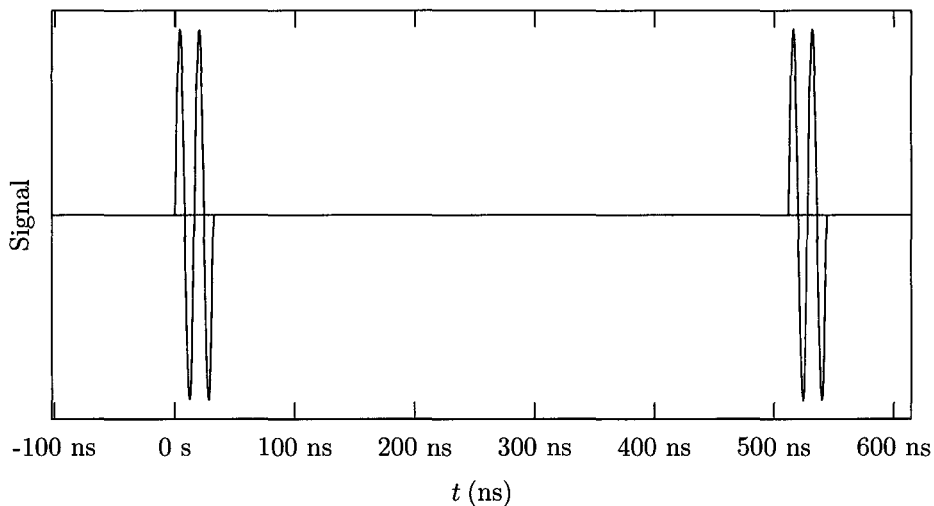


Figure 8.3: Synthesized sine wave packet for absolute time difference measurements.

The measurement series at $\sigma_e^{\text{out}} = 2.2 \text{ S/m}$ was performed with an Agilent 33250A arbitrary waveform generator, which was temporarily on loan. This device appears to be perfect for this task. The waveform that has been programmed is shown in figure 8.3. It is composed of 2 periods of the original 62.5 MHz sine wave, followed by 30 periods of silence.

This wave packet has been chosen because it is short enough for nearly complete signal damping in between the packets, yet still contains a significant frequency component near 62.5 MHz, so that the behaviour of the electromagnetic waves is not affected too much. This wave packet is only used to verify the time difference measurements performed with the continuous wave signal, which are performed automatically by the oscilloscope and are thus much more accurate.

The waveform generator is thus used in two modes: producing a normal continuous wave, for accurate automated time difference measurements, and producing the short sine wave packets, as a verification of the absolute time difference.

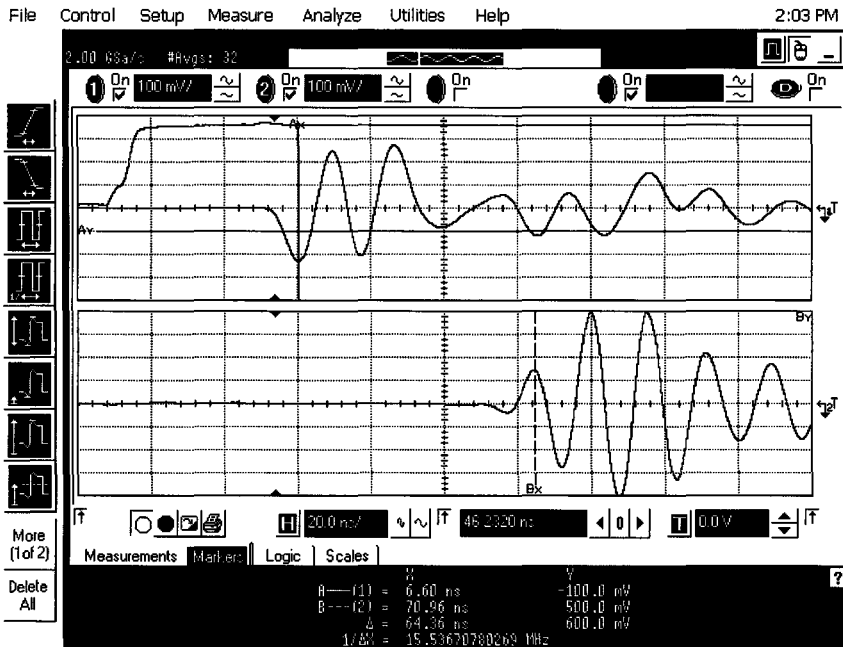


Figure 8.4: Transmitted (upper) and received (lower) sine wave packet in slightly saline water ($\sigma_e = 0.22$ S/m), revealing the absolute time difference. The step function in the left top of the screen is the TTL synchronization signal.

A screenshot of the oscilloscope, obtained during the measurement series at $\sigma_e^{\text{out}} = 2.2$ S/m and $\sigma_e^{\text{in}} = 0.22$ S/m is shown in figure 8.4. The upper sinusoidal waveform is the (inverted) source signal as obtained using the pickup coil, the lower waveform is the received signal.

The step function in the left top of the screen is the TTL synchronization signal from the waveform generator, used for triggering. The x-axis markers Ax and Bx are positioned at the points that were used as reference points for the absolute time difference measurement. The y-axis markers serve no particular purpose here.

The results of these measurements, and the measurement with pure water in the outer pipe, are shown in figure 8.5. The propagation time behaviour at higher conductivities has improved much and is monotonous up to $\sigma_e^{\text{in}} \approx 1.3$ S/m. The voltage plot has also improved, but still does not decay exponentially at higher conductivities. The data can be found in appendices N.4.2–N.4.4.

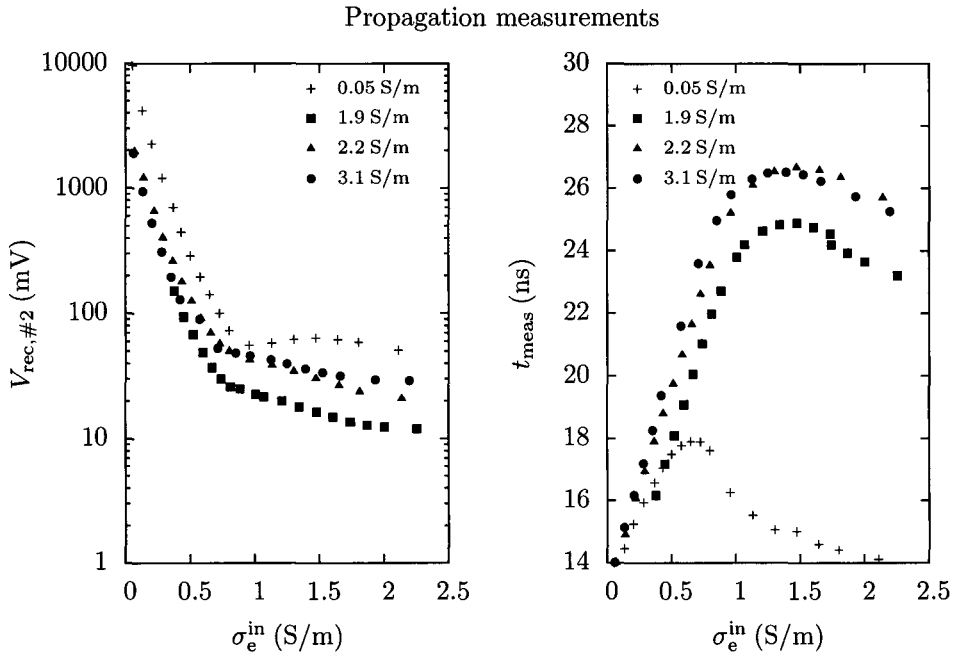


Figure 8.5: Plots of the voltage received by antenna #2 and the time difference between the source and receiver antenna #2 as a function of the effective conductivity of the water in the inner pipe σ_e^{in} at various outer pipe conductivities $\sigma_e^{out} = \{0.05, 1.9, 2.2, 3.1\}$ S/m.

8.2 Probe Measurement

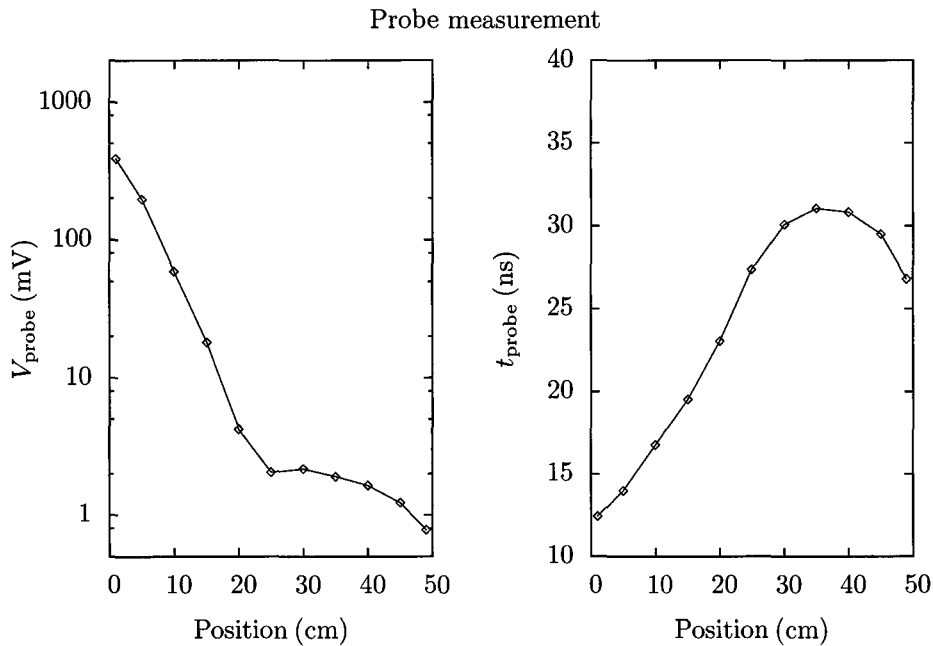


Figure 8.6: Plots of the probe voltage and time difference between the source and the coaxial probe as a function of the probe position, at $\sigma_e^{in} = 2.1$ S/m and $\sigma_e^{out} = 3.1$ S/m. The measurement points are connected with straight lines just for a visual reference.

To investigate the effects at higher conductivities further, measurements of the voltage and the time difference were performed using the coaxial probe, at several positions (approximately 5 cm apart) on a straight line from antenna #1 to antenna #2, all at the same horizontal plane at the center of the antennas. The time difference is determined relative to the source signal. The results of the probe measurement, performed at $\sigma_e^{\text{in}} = 2.1 \text{ S/m}$ and $\sigma_e^{\text{out}} = 3.2 \text{ S/m}$, is shown in figure 8.6.

The plot shows an exponentially decaying voltage and linearly increasing time difference up to approximately halfway the pipe. After that point, the signal decay rate has decreased significantly. A transition from a (reactive) near field to the radiating near or far field, which offers a plausible explanation for a similar effect in river water (see section 7.4), does not satisfactorily explain the observed behaviour here: the fact that the received signal does not decay *continuously* suggests that the received signal is distorted by reflected signals.

8.3 Shields effect

Because increasing the outer pipe conductivity does not enhance the electromagnetic wave propagation at higher conductivities, the cause is looked for elsewhere. As there is a possibility that the waves are ‘received’ and ‘re-transmitted’ by the long metal shields, as shown in figure 8.7, two series of measurements are performed.

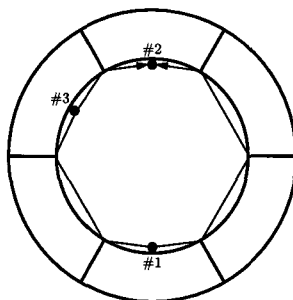


Figure 8.7: Possible propagation routes by receiving and re-transmitting metal shields. Antenna #3 may also have some influence in this process.

The first series is performed with the shields halfway antenna #1 and antenna #2 removed, thus leaving the four shields closest to the antennas. The second series is performed with all six shields removed.

Four shields

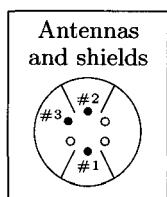


Figure 8.8: Configuration

The two of middle shields were removed, leaving only the four shields closest to antennas #1 and #2 and antennas, as shown in figure 8.8. The idea is, that the increased distance between the shields surrounding antenna #1 and the shields surrounding antenna #2 prevents the shields from ‘passing on’ the signal.

Voltage and time difference measurements were performed using the coaxial probe at several positions (approximately 5 cm apart) on a straight line from antenna #1 to antenna #2, at three different inner pipe water conductivities and a constant outer pipe water conductivity. The results are shown in figure 8.9. Comparison of the semi-log voltage plot with the corresponding plot in figure 8.6 shows that the largest improvement is obtained from increasing the conductivity of the water in the inner pipe and that removing the two shields does not improve the system much.

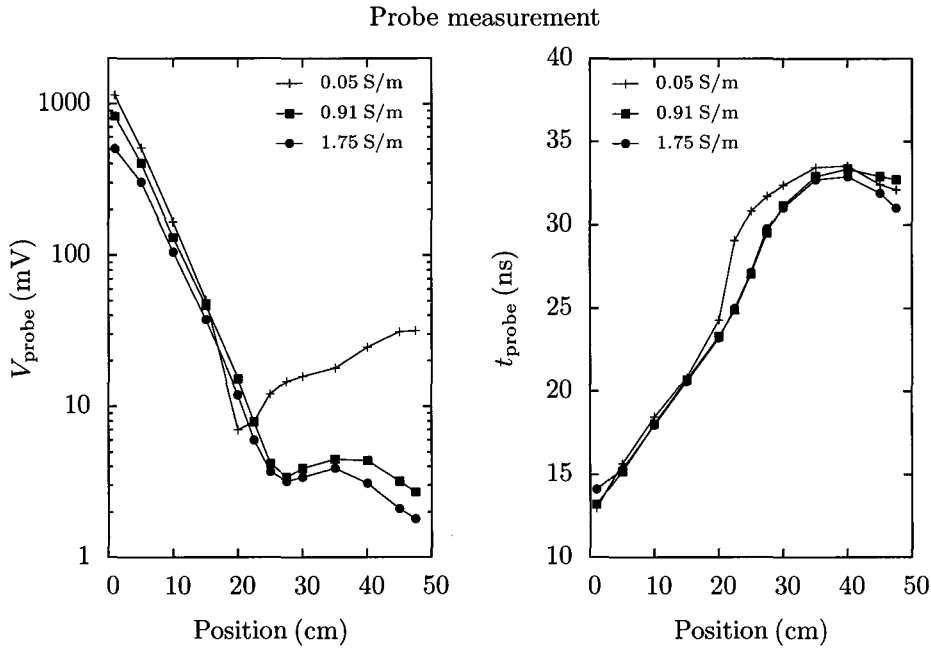


Figure 8.9: Plots of the probe voltage and time difference between the source and the coaxial probe as a function of the probe position, with four shields, at $\sigma_e^{\text{in}} = 2.1 \text{ S/m}$ and $\sigma_e^{\text{out}} = \{0.05, 0.91, 1.75\} \text{ S/m}$. The measurement points are connected with straight lines just for a visual reference.

No Shields

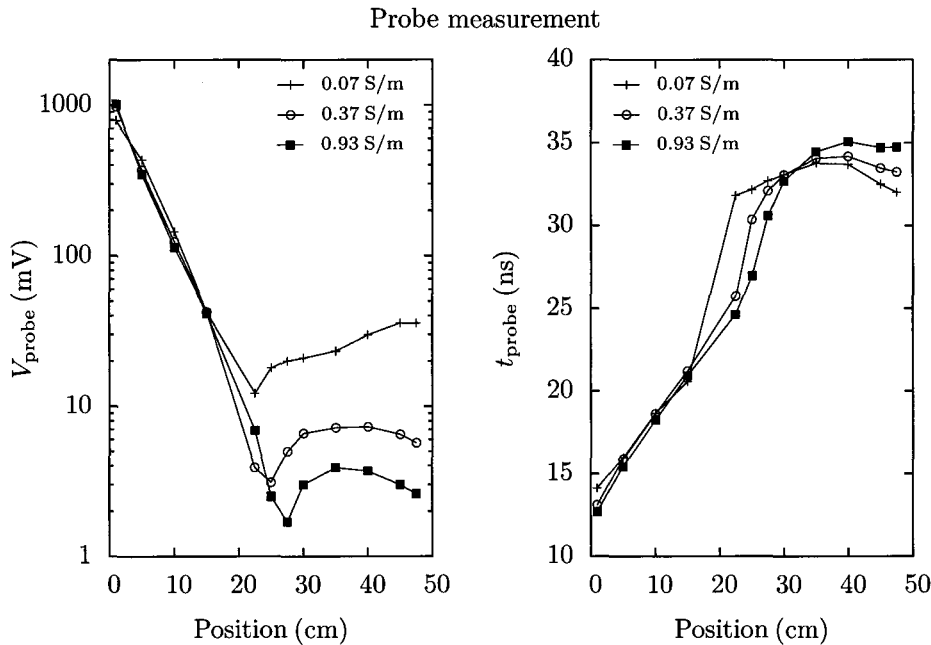


Figure 8.10: Plots of the probe voltage and time difference between the source and the coaxial probe as a function of the probe position, without shields in the outer pipe, at $\sigma_e^{\text{in}} = 2.1 \text{ S/m}$ and at various outer pipe conductivities $\sigma_e^{\text{out}} = \{0.07, 0.37, 0.93\} \text{ S/m}$. The measurement points are connected with straight lines just for a visual reference.

All six shields were removed, to rule them out as possible cause for the electromagnetic propagation around the inner pipe. The voltage and time difference is measured using the coaxial probe at several positions (approximately 5 cm apart) on a straight line from antenna #1 to antenna #2.

The results are shown in figure 8.10. The semi-log voltage plot shows that the performance has slightly degraded, because the signal at receiver antenna #2 is even higher than with the four shields. Without any shielding, the possibility of electromagnetic waves traveling around the inner pipe has increased. This is in agreement with the assumption that these waves around the inner pipe cause the increase in the voltage near the receiver antenna.

The probe voltage beyond 25 cm still shows a temporary increase instead of a gradual decrease, which is more pronounced with saline water in the outer pipe than with (almost) pure water. Even without shields, the electromagnetic signals still appear to be distorted.

8.4 Inner pipe effect

Because the removal of the shields did not resolve the problem of the apparent shortcut for the electromagnetic waves around the water in the inner pipe, it was devised that the shortcut could be the glass fibre pipe itself which, combined with the conducting water on both sides, constitutes a (lossy) waveguide.

After removing the inner pipe, the voltage at the receiver antenna and the time difference between the source and the receiver antenna were measured as a function of the conductivity of the water in the entire pipe. The shields were still left out, and to be certain that the antenna #3 would not spoil the results, it was removed as well. The results are shown in figure 8.11.

The voltage measurement shows a huge improvement. The measurement points follow the calculated curve, which is not a fit but only matched at the $\sigma_e \approx 0$ point, up to approximately $\sigma_e = 2.0$. At the highest measured conductivity, the agreement with the model is still very decent. The time difference measurement also reveals a reproducible behaviour, except for one or two outliers around $\sigma_e = 2.0$ which are probably caused by insufficiently dissolving the salt in the water.

After the measurement series at varying conductivity, voltage and time difference measurements as a function of the position in the pipe were performed with the coaxial probe. Because the inner pipe was removed, the coaxial probe is now moved over the entire outer pipe diameter. The results are shown in figure 8.12 and the data can be found in appendix N.4.5

This measurement shows a similar effect as measured with the coaxial probe in river water: the electromagnetic waves exhibit exponential decay and linearly increasing time difference up to 25 cm from the transmitter antenna. Beyond that point, the decay rate has decreased and does not show the strange behaviour as measured *with* the inner pipe (see figures 8.6,8.9,8.10). The most likely explanation of the decrease in the decay rate is a transition from a *reactive* near field to a *radiating* near or far field, as already described in section 7.4.

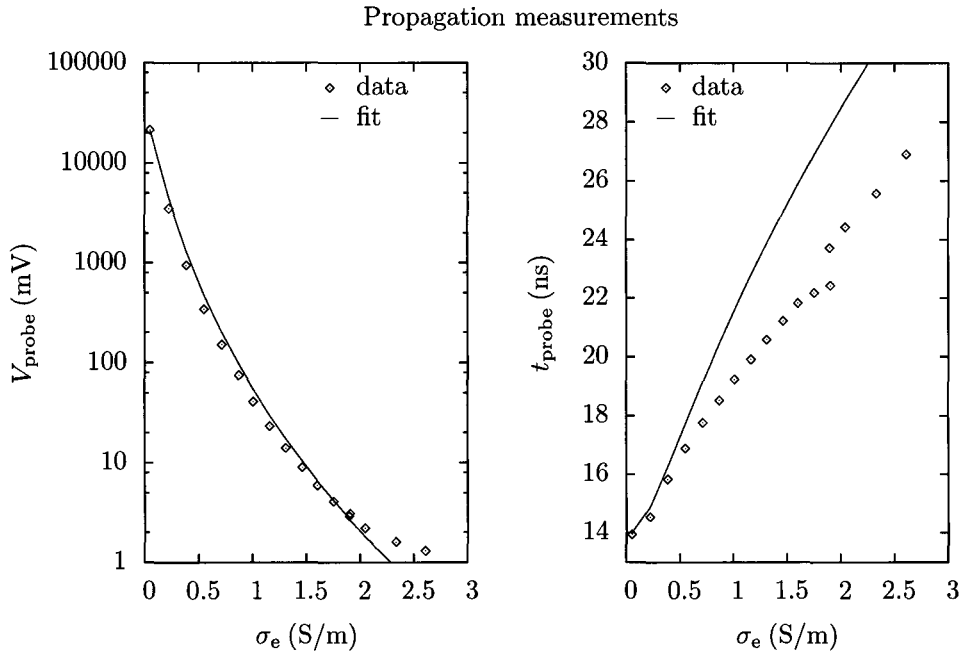


Figure 8.11: Plots of the voltage received by antenna #2 and the time difference between the source and receiver antenna #2, without inner pipe, as a function of the conductivity of the water in the entire pipe σ_e .

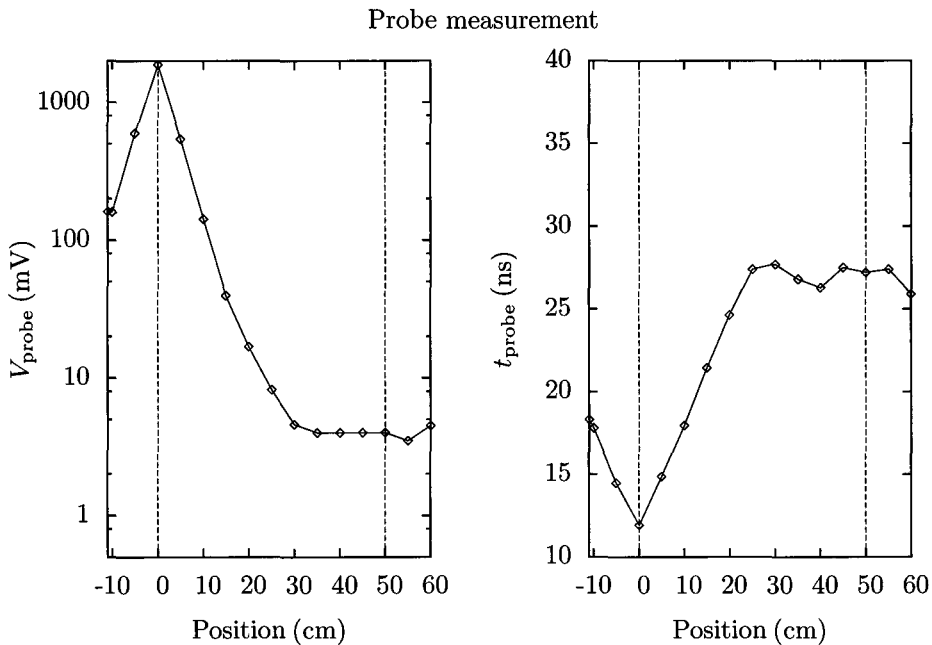


Figure 8.12: Plots of the probe voltage and time difference between the source and the coaxial probe as a function of the probe position, without inner pipe, at $\sigma_e = 2.61$ S/m. The position where the inner pipe wall used to be is indicated by the dashed lines. The measurement points are connected with straight lines just for a visual reference.

8.5 Crosstalk

The measurement circuit was checked for crosstalk by disconnecting the cable at the receiver antenna between the balun and the Q-match. Even after re-connecting the braid of the coaxial cable there is no measurable signal on the corresponding oscilloscope channel.

Because disconnecting the transmitter antenna between the balun and the Q-match causes an almost infinite VSWR, the coaxial cable is terminated using three $50\ \Omega$ resistors in parallel connection. Again, there is no measurable signal on the oscilloscope.

It is concluded that, at the used power levels of $0.5 - 1.0\ \text{W}$, crosstalk is of no measurable influence on the measurements.

8.6 Conclusions

The metal shields in the space between the outer and the inner pipe do not have a significant influence on the electromagnetic wave propagation, certainly when the conductivity of the water in the inner pipe is (slightly) conducting.

The theory that the seemingly conductivity independent signal propagation is caused by the inner pipe functioning as a waveguide is confirmed by measurements without the inner pipe. To avoid this issue, using a lossy material for the inner pipe will certainly help. However, a lossy material will also absorb part of the transmitted electromagnetic energy. This is unwanted, especially at higher conductivities where all amplifier power is needed to be able to transmit through the conducting water. So, the material should not be too lossy either.

Because of this waveguide effect, no density measurements could be performed in sea water. The operational range of an electromagnetic density meter is restricted to river water until this is resolved. According to [1], electromagnetic propagation in sea water *is* quite feasible, as long as the antennas are sufficiently insulated. Otherwise, the *conduction* losses in the vicinity of the antenna drain most of the power. It is not possible to make any well-founded predictions on the *accuracy* that can be expected in sea water yet.

Chapter 9

Concluding remarks

The project started not knowing if a density measurement using electromagnetic transmission would be technically feasible. The main problem was expected to occur in highly saline water such as sea water. According to calculations, measurements in sea water will require a high-gain amplifier. According to measurements performed up to a conductivity of 2.6 S/m, highly saline water causes the electromagnetic waves to search for an alternative, less conducting path. Such a shortcut has to be avoided.

Feasibility

Based on the performed measurements, it is expected that a density meter based on electromagnetic transmission is feasible with an RMS accuracy of $\pm 0.04 \text{ ton/m}^3$, at least under the following restraints:

- Restricted conductivity range, evidently at least up to 0.937 S/m. To verify the applicability of an electromagnetic density meter in water with higher conductivities, some modifications are needed with respect to the inner pipe material and the filling between the pipes, as described below.
- Limited diameter, at least for 0.50 m. The main limiting factor is the signal attenuation in a conductive medium, which increases exponentially with diameter size.
- Soil constituents should have no significant conductivity.

Sea water

Whether, and if so, with what accuracy, density measurements are possible in sea water can not be concluded based on these measurements. Based on measurements in [1], where electromagnetic transmission has been successfully performed in sea water ($\sigma_e = 4.0$) up to a distance of at least one meter and with approximately the same operating frequency, it is expected that density measurements in sea water may still be possible, with a carefully designed, high dynamic range setup and the issues which are described below resolved.

New issues

As a result of the experiments some new issues have emerged and some questions have risen. These subjects need to be addressed in the follow up phase:

- The space between the inner and the outer pipe should be filled with a lossy material instead of pure water, to prevent the electromagnetic waves from traveling through it. As far as the matching of the antennas to the wall is concerned, a high permittivity material is preferred because it reduces the physical dimensions of the device. Possible candidates are:

- saline water, possibly from the dredging area. By definition the conductivity of this water equals the highest conductivity of the slurry. The advantage is that the device can be transported in a light empty state.
 - a high permittivity liquid containing an electrolyte or other conducting particles like carbon.
 - a high permittivity solid, for example a — typically low permittivity — epoxy containing high permittivity ceramic particles and metal particles to provide conductivity. This way the permittivity can be chosen at will by changing the mixture. By making it higher than the permittivity of water the outer pipe diameter, and the total mass of the device, could be reduced.
- The inner pipe needs to be made of lossy material instead of the glass fibre reinforced epoxy. This should ideally match the conductivity of the medium to be measured, to prevent the electromagnetic waves from traveling through it. As long as the wall is thin, the permittivity is not very important. The conductivity should not be too high, as a highly conducting material near the antenna would consume all its power. A possible material would be carbon, which shares the strength of the glass fibre pipe and has a limited amount of conductivity.
 - The issue of the inner pipe material and the filling between the two pipes can be totally removed if a different antenna is used, which does not need a reflector behind it. In that case only a single metal pipe would be needed. An example of such an antenna is the horn antenna which radiates mainly in a forward direction. This horn should ideally be filled with a material with the same permittivity of water to make a correct impedance match to it.
 - An electronic circuit needs to be designed, capable of accurately measuring time differences in the order of 0.1 ns between two 10–100 MHz signals. The timing should be insensitive to temperature and moisture variations and vibrations. Using intermediate frequency (IF) modulation, the timing measurement could be performed on these IF signals, although the same accuracy would be needed.

Verification

At the project start, some assumptions were made. At that time these assumptions were necessary to limit the number of possible solutions and facilitate experiments. Now that the static experimental setup has shown that the principle of density measurements using electromagnetic transmission works, some of these assumptions deserve a reassessment:

- It has been assumed that the technical feasibility of density meter can be reliably tested using a static setup, because the time scale of the measurements is much shorter than the time scale of the slurry transport in the pipe. This has simplified the experimental setup considerably. However, a static setup does not take into account the possible effects of turbulence. It has been assumed so far that any turbulence will equally affect the radioactive density meter, but for the next phase a flowing setup, which enables verification of these two assumptions, would be desirable.
- Another assumption is that various slurry densities can be simulated by placing a stack of sand containing wooden frames in water. For a follow up, measurements with real slurry are preferred.

Suggestions

As a follow-up project the following options are suggested beforehand:

- Create a measurement device that can be connected in the 300 mm pipeline at MTI in Kinderdijk. For this purpose it may be necessary to reduce the pipe diameter to maintain a certain flow. However, to keep with reality, the pipe diameter should be as close to 500 mm as possible.

- Modify the construction in one out of two ways:
 - Design and build a dielectric-filled horn antenna and use a single metal pipe.
 - Embed the dipole antenna in an urethane layer in the inside of a carbon pipe and encapsulate the carbon pipe in a metal pipe with the smallest possible diameter, which is determined by the permittivity of the medium between the two pipes. A small pipe diameter requires a high permittivity solid or liquid mixture in the space between the two pipes.

This page intentionally contains only this sentence.

Appendices

to

“Electromagnetic Slurry
Density Measurement”

(AQT 05-03)

This page intentionally contains only this sentence.

Appendix A

Permittivity in detail

In literature, many different notations are used for the permittivity of materials, especially when conductivity is involved. An overview of these definition is given here. The permittivity is in general a complex constant. The real and imaginary parts of ε^* represent the refractive and absorptive properties of a dielectric material. For a *purely* dielectric (i.e. non-lossy) material, the complex permittivity is given by:

$$\varepsilon^* = \varepsilon' - j\varepsilon'' \quad (\text{A.1})$$

and for a *conducting* material, the complex conductivity σ^* can be written in a similar way:

$$\sigma^* = \sigma' - j\sigma'' \quad (\text{A.2})$$

In a material with *both* dielectric and conducting properties, i.e. a *lossy* dielectric material, the imaginary part of the permittivity (ε'') can be hard to distinguish from the real conductivity (σ') term, especially if ε'' has a $1/\omega$ dependence. This can be shown using (L.2a):

$$\nabla \times \mathbf{H} = \sigma \mathbf{E} + j\omega \varepsilon^* \mathbf{E} = j\omega \left[\varepsilon^* - j \frac{\sigma^*}{\omega} \right] \mathbf{E} = j\omega \tilde{\varepsilon} \mathbf{E}$$

where the permittivity and the conductivity have been combined in the complex permittivity $\tilde{\varepsilon}$ defined by:

$$\tilde{\varepsilon} = \varepsilon^* - j \frac{\sigma^*}{\omega}. \quad (\text{A.3})$$

An alternative notation of $\tilde{\varepsilon}$ can be obtained by substituting (A.1) and (A.2) and combining the real and imaginary parts,

$$\begin{aligned} \tilde{\varepsilon} &= \varepsilon' - j\varepsilon'' - \frac{j}{\omega} [\sigma' - j\sigma''] \\ &= \left[\varepsilon' - \frac{\sigma''}{\omega} \right] - j \frac{[\sigma' + \omega\varepsilon'']}{\omega}, \end{aligned}$$

which leads to the definitions of the (both real-valued) *effective* permittivity and conductivity:

$$\varepsilon_e = \varepsilon' - \frac{\sigma''}{\omega} \quad (\text{A.4a})$$

$$\sigma_e = \sigma' + \omega\varepsilon'' \quad (\text{A.4b})$$

The notation used in chapter 2 corresponds to these two equations, although with the assumption that the conductivity is real-valued, so $\sigma'' = 0$. The definition of the complex permittivity ε^* that is used there is based on definition (A.3) which, under the same assumption, can be written as:

$$\tilde{\varepsilon} = \varepsilon' - j \left(\varepsilon'' + \frac{\sigma'}{\omega} \right). \quad (\text{A.5})$$

For notational simplicity, the real part of the conductivity has been renamed to σ and the tilde has been replaced by an asterisk in the main text, see equation (2.2) in chapter 2.

Dielectric properties are sometimes described using the electric susceptibility instead of the electric permittivity. The complex susceptibility $\chi = \chi' - j\chi''$ is related to the complex permittivity by:

$$\chi'' = \varepsilon'' \tag{A.6a}$$

$$\chi' = \varepsilon' - 1 \tag{A.6b}$$

Appendix B

Temperature Density Salinity

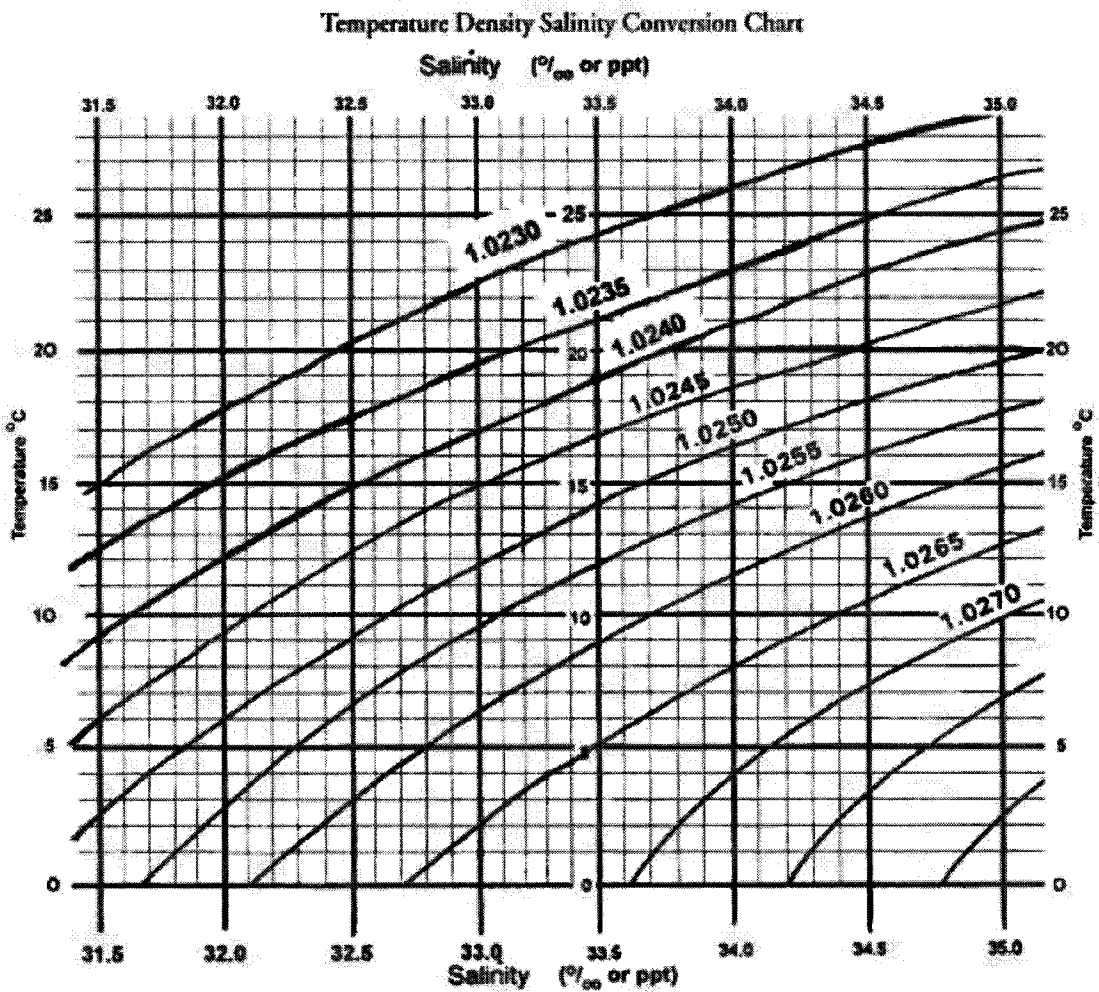


Figure B.1: Conversion chart defining the relationships between temperature, density and salinity of saline water, from the UCLA Marine Science Center.

This page intentionally contains only this sentence.

Appendix C

Water models

Permittivity

Permittivity of saline water as a function of salinity and temperature, according to [23], valid for $5 \leq T(^{\circ}\text{C}) \leq 30$ and $4 \leq S(\text{ppt}) \leq 35$:

$$\varepsilon_r^{\text{stat}}(T, S) = \varepsilon_r^{\text{stat}}(T) \cdot a(S, T) \quad (\text{C.1a})$$

$$\varepsilon_r^{\text{stat}}(T) = 87.134 - 1.949 \times 10^{-1}T - 1.276 \times 10^{-2}T^2 + 2.491 \times 10^{-4}T^3 \quad (\text{C.1b})$$

$$a(S, T) = 1.000 + 1.613 \times 10^{-5}ST - 3.656 \times 10^{-3}S + 3.210 \times 10^{-5}S^2 - 4.232 \times 10^{-7}S^3 \quad (\text{C.1c})$$

The relaxation time as a function of salinity and temperature, according to [23]:

$$\tau(T, S) = \tau(T, 0) \cdot b(S, T) \quad (\text{C.2a})$$

$$\tau(T, 0) = 1.768 \times 10^{-11} - 6.086 \times 10^{-13}T + 1.104 \times 10^{-14}T^2 - 8.111 \times 10^{-17}T^3 \quad (\text{C.2b})$$

$$b(S, T) = 1.000 + 2.282 \times 10^{-5}ST - 7.638 \times 10^{-4}S - 7.760 \times 10^{-6}S^2 + 1.105 \times 10^{-8}S^3 \quad (\text{C.2c})$$

Conductivity

Conductivity of sea water as a function of salinity and temperature, according to [38]:

$$\sigma_{\text{sea}}(T, S) = \sigma_{\text{sea}}(25, S) \cdot \exp(-\Delta \cdot \alpha(\Delta, S)) \quad (\text{C.3a})$$

$$\sigma_{\text{sea}}(25, S) = S [0.182521 - 1.46192 \times 10^{-3}S + 2.09324 \times 10^{-5}S^2 - 1.28205 \times 10^{-7}S^3] \quad (\text{C.3b})$$

$$\alpha(\Delta, S) = 2.033 \times 10^{-2} + 1.266 \times 10^{-4}\Delta + 2.464 \times 10^{-6}\Delta^2 - S [1.849 \times 10^{-5} -]. \quad (\text{C.3c})$$

where

$$\Delta = 25 - T \quad (\text{C.3d})$$

In [37], the conductivity of saline water is given as a function of *normality* and temperature. Normality is the number of mols of effective material per liter: a normal solution contains 1 mol of solute in 1 liter of solution. Though for acids and bases there is a difference between molarity and normality (normality = molarity \times number of available hydrogen/hydroxide ions), for a NaCl solution they are the same. The salinity is related to the normality as follows [23]:

$$N_{\text{sea}} = 0.9141 \cdot S \cdot [1.707 \times 10^{-2} + 1.205 \times 10^{-5}S + 4.058 \times 10^{-9}S^2]. \quad (\text{C.4})$$

For NaCl solutions, the factor 0.9141 is suppressed. The conductivity as a function of normality and temperature is then given by:

$$\sigma(T, N) = \sigma(25^{\circ}\text{C}, N) [1 + c(N)(T - 25)] \quad (\text{C.5a})$$

For $0 \leq N \leq 0.01$:

$$\sigma(25^\circ\text{C}, N) = N \cdot [12.653 - 8.974N^{1/2} + 4.682N \ln(N) + 18.234N] \quad (\text{C.5b})$$

$$c(N) = 0.0208 \quad (\text{C.5c})$$

For $0.01 \leq N \leq 0.1$:

$$\sigma(25^\circ\text{C}, N) = N \cdot [12.653 - 8.974N^{1/2} + 6.8046N + 33.567N^{3/2} - 1.4148 \times 10^2 N^2] + 1.6649 \times 10^2 N^{5/2} \quad (\text{C.5d})$$

$$c(N) = 0.0202 \quad (\text{C.5e})$$

For $0.1 \leq N \leq 1$:

$$\sigma(25^\circ\text{C}, N) = N \cdot [12.653 - 8.974N^{1/2} + 11.385N - 10.403N^{3/2} + 4.7224N^2 - 8.2288 \times 10^{-1} N^{5/2}] \quad (\text{C.5f})$$

$$c(N) = 0.0193 \quad (\text{C.5g})$$

$$(\text{C.5h})$$

Note the discrepancy in the use of the closing square-bracket in equations (C.5d) and (C.5b,C.5f), which could indicate a typesetting error.

Appendix D

Transmission line model

To model the behaviour of the insulated antenna in a conducting medium, it can be represented by a *coaxial transmission line*. In order to model the behaviour of the insulated antenna in a conducting medium, it can be represented by a *coaxial transmission line*, as shown in figure D.1.

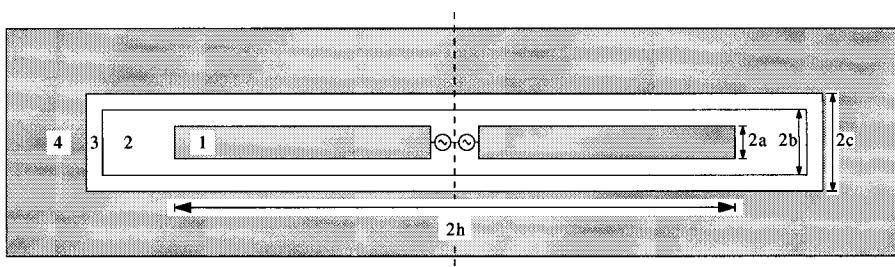


Figure D.1: Schematic representation of a dipole antenna (1) with two insulating layers (2) and (3) in medium (4).

Employing the same numbering convention as used by [17, 20, 21, 24, 42], the inner conductor (antenna) is assigned number 1, two insulating layers are numbered 2 and 3 and the ambient medium (water), which takes the role of outer conductor, is assigned number 4 - even in absence of insulating layer 3. An electronic representation of a coaxial transmission line is shown in figure D.2.

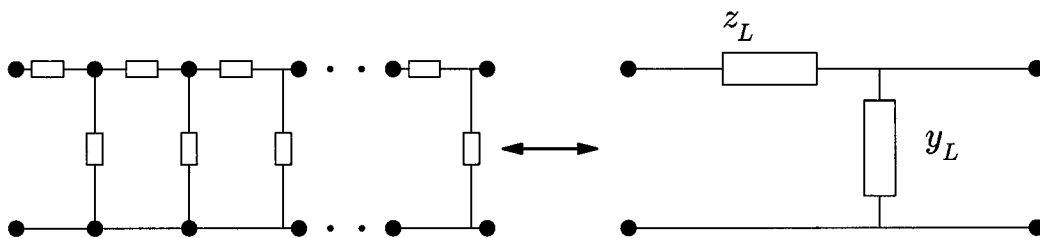


Figure D.2: Electronic representation of a coaxial transmission line. The series impedance z_L and shunt admittance y_L of a coaxial transmission line are distributed parameters.

In general, the series impedance (per unit length) consists of a resistance and an inductance ($z_L = R + j\omega L$) and the shunt admittance (per unit length) consists of a conductance and a capacitance ($y_L = G + j\omega C$). Both z_L and y_L are *distributed parameters*: impedance and admittance are spread out over the entire length of the transmission line and not confined to a single *lumped* element.

To be able to calculate the important antenna parameters *resonance frequency* and *driving point impedance* using the coaxial transmission line model, the derivation of the transmission line parameters *characteristic impedance* Z_0 (which is independent of the line length) and *complex wavenumber* k_L is needed.

The complex wavenumber k_L of the transmission line can be derived from the propagation constant:

$$k_L = -j\gamma = \sqrt{-1}\gamma \quad (\text{D.1})$$

and both the propagation constant γ and the characteristic impedance Z_0 can be derived from the distributed parameters z_L and y_L :

$$Z_0 = \sqrt{\frac{R + j\omega L}{G + j\omega C}} = \sqrt{\frac{z_L}{y_L}} \quad (\text{D.2})$$

$$\gamma = \sqrt{(R + j\omega L)(G + j\omega C)} = \sqrt{z_L y_L} \quad (\text{D.3})$$

Multiplying and dividing these equations leads to the following equations for the series impedance and the shunt admittance

$$z_L = j\omega L + R = \gamma Z_0 \quad (\text{D.4})$$

$$y_L = j\omega C + G = \gamma / Z_0 \quad (\text{D.5})$$

Because the shunt admittances and the series impedances are necessary for the calculation of all important parameters of the insulated antenna, they will be described in detail below.

Shunt admittances

In case of the insulated antenna of figure D.1, the effective shunt admittance per unit length y_L depends only on the properties of the two insulating dielectric layers:

$$y_L = \frac{y_2 y_3}{y_2 + y_3} \quad (\text{D.6})$$

where

$$y_2 = \frac{2\pi(\sigma_2 - j\omega\epsilon_2)}{\ln(b/a)} \quad (\text{D.7})$$

$$y_3 = \frac{2\pi(\sigma_3 - j\omega\epsilon_3)}{\ln(c/b)} \quad (\text{D.8})$$

This can be derived from the electric field in the dielectric between two conductors, as shown in figure D.3 (c), which is (for region 2) given by:

$$\int_V \nabla \cdot (\epsilon \mathbf{E}) d^3x = \epsilon \int_S \mathbf{E} \cdot \mathbf{n} d^2x = \epsilon \int_0^l \int_0^{2\pi r} \mathbf{E} \, ds dx = q \quad (\text{D.9})$$

$$\mathbf{E} = \frac{q}{2\pi r \epsilon l} \hat{\mathbf{r}} \quad (\text{D.10})$$

and the voltage difference between the conductors at $r = a$ and $r = b$

$$V = - \int_a^b \mathbf{E} \cdot d\mathbf{r} = \frac{q}{2\pi \epsilon l} \ln\left(\frac{b}{a}\right) \quad (\text{D.11})$$

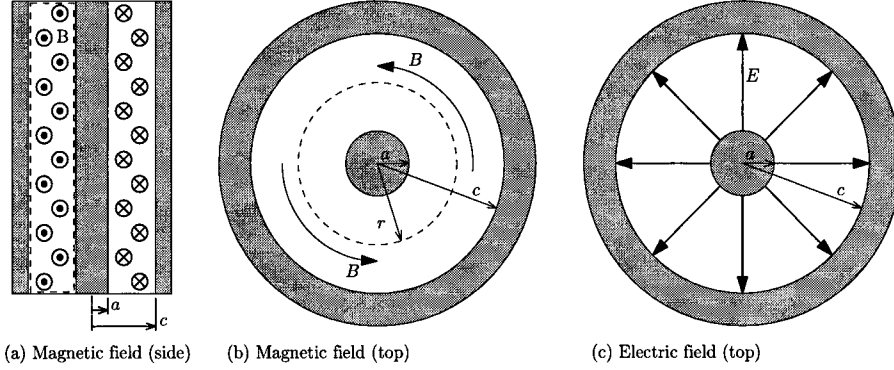


Figure D.3: Magnetic and electric field lines in a coaxial transmission line.

which leads to a capacity

$$C = \frac{q}{V} = \frac{2\pi\epsilon l}{\ln(b/a)} \quad (\text{D.12})$$

and a conductance, which can be approximated for low conductivities by [20]

$$G = \frac{\sigma}{\epsilon} C = \frac{2\pi\sigma l}{\ln(b/a)} \quad (\text{D.13})$$

leads to a shunt admittance $y_2 = Y/l$ of

$$y_2 = \frac{Y}{l} = \frac{G + j\omega C}{l} = \frac{2\pi(\sigma_2 + j\omega\epsilon_2)}{\ln(b/a)} \quad (\text{D.14})$$

which matches equation (D.7), apart from a minus.

In absence of dielectric layer 3, radius $b = c$ and

$$y_L = y_2 = \frac{2\pi(\sigma_2 - j\omega\epsilon_2)}{\ln(c/a)} = -j \frac{2\pi k_2^2}{\omega\mu \ln(c/a)}. \quad (\text{D.15})$$

where the general definition (3.3) has been used for k_2 .

Series impedances

The series impedance consists of three parts:

$$z_L = z_1^i + z_4^i + z^e \quad (\text{D.16})$$

where z_1^i and z_4^i are the impedances per unit length of the inner and outer conductors, and z^e is the impedance of the dielectric layers. The superscripts i and e stand for internal (inside the conductors) and external (outside the conductors). The impedance per unit length z_4^i includes the effects of both dissipation and radiation in the ambient medium [42]. This means that the radiated power is accounted for by a *distributed* parameter, which is quite unusual: radiation is generally a property of a *complete* circuit. According to [20], the internal series impedances are given by:

$$z_1^i = \frac{1}{\pi a^2 \sigma_1} \frac{k_1 a J_0(k_1 a)}{2 J_1(k_1 a)} \quad (\text{D.17})$$

$$z_4^i = \frac{1}{\pi c^2 \sigma_4} \frac{k_4 c J_0(k_4 c) H_1^{(1)}(k_4 d) - H_0^{(1)}(k_4 c) J_1(k_4 d)}{2 J_1(k_1 d) H_1^{(1)}(k_4 c) - H_1^{(1)}(k_4 d) J_1(k_4 c)} \quad (\text{D.18})$$

where k_1 and k_4 are the wavenumbers of medium 1 and 4 according to (3.3) and a, b, c the dimensions as indicated in figure D.1. The parameter d represents the outer dimension of the propagation medium 4.

These equations can both be simplified using small-argument approximations for the Hankel functions:

$$k_1 \in \mathbb{C} \setminus \mathbb{R}, |k_1 a| \gg 1 \Rightarrow \frac{J_0(k_1 a)}{J_1(k_1 a)} = -j$$

$$k_4 \in \mathbb{C} \setminus \mathbb{R}, |k_4 d| \gg 1 \Rightarrow \frac{H_1^{(1)}(k_4 d)}{J_1(k_4 d)} = 0$$

which are valid for a thin antenna and a large propagation medium and lead to the series impedance of a purely conducting antenna core ($k_1^2 = j\omega\mu\sigma_1$):

$$z_1^i \approx \frac{-jk_1}{2\pi a \sigma_1} = \frac{\omega\mu}{2\pi a k_1} \quad (\text{D.19})$$

and of the outer conductor

$$z_4^i = \frac{-1}{\pi c^2 \sigma_4} \frac{k_4 c H_0^{(1)}(k_4 c) - J_0(k_4 c) \frac{H_1^{(1)}(k_4 d)}{J_1(k_4 d)}}{2 H_1^{(1)}(k_4 c) - J_1(k_4 c) \frac{H_1^{(1)}(k_4 d)}{J_1(k_4 d)}}$$

$$\approx \frac{-k_4^2}{2\pi \sigma_4 k_4 c} \frac{H_0^{(1)}(k_4 c)}{H_1^{(1)}(k_4 c)} \quad (\text{D.20})$$

Finally the external impedance per unit length:

$$z^e = -j\omega\ell^e = -\frac{j\omega\mu}{2\pi} \ln\left(\frac{c}{a}\right) \quad (\text{D.21})$$

where ℓ^e is the inductance per unit length, so $\ell^e = L/l$. The inductance L of a of a conductor which encloses a flux Φ is given by:

$$L = \frac{\Phi}{I} \quad (\text{D.22})$$

with magnetic flux Φ through the dashed box in figure D.3 (a):

$$\Phi = \int_0^l \int_a^c \mathbf{B} \cdot \mathbf{n} \, dr dz = \mu l \int_a^c \mathbf{H} \cdot \mathbf{n} \, dr dz \quad (\text{D.23})$$

and Ampère's Law applied to a circle with radius r , see figure D.3 (b):

$$\oint_C \mathbf{B} \, ds = \oint_C \mu \mathbf{H} \, ds = \mu \mathbf{I}_{\text{enclosed}} \quad (\text{D.24})$$

$$\mathbf{H} = \frac{I}{2\pi r} \hat{\phi} \quad (\text{D.25})$$

which can be substituted in equation (D.23):

$$\Phi = \frac{\mu l I}{2\pi} \int_a^c \frac{1}{r} \, dr = \frac{\mu l I}{2\pi} \ln\left(\frac{c}{a}\right) \quad (\text{D.26})$$

$$\ell^e = \frac{\Phi}{lI} = \frac{\mu}{2\pi} \ln\left(\frac{c}{a}\right) \quad (\text{D.27})$$

Simplifications in water

An insulated antenna in water is effectively a coaxial transmission line with an extensive outer conductor (region 4). The applicability of the coaxial transmission line model depends of course on the conductivity of the outer conductor, which in turn depends on the salinity of the water. By definition, a good conductor fulfills the requirement

$$\frac{\sigma}{\omega\epsilon} \gg 1 \quad (\text{D.28})$$

whereas a good dielectric satisfies [16]

$$\left(\frac{\sigma}{\omega\epsilon}\right)^2 \ll 1 \quad (\text{D.29})$$

At first glance, this would mean that the following condition must be met:

$$\sigma_4 \gg \omega\epsilon_4 \quad (\text{D.30})$$

For sea-water ($\sigma \approx 4$ and $\epsilon \approx 80$) this poses the following limit on the frequency f [18]:

$$f \ll \frac{\sigma}{2\pi\epsilon} \leq \frac{4}{50\pi 80\epsilon_0} \approx 35 \text{ MHz.} \quad (\text{D.31})$$

However, this is *not* a necessary condition [20]. A sufficient condition is:

$$|k_4^2| = |\omega^2\mu(\epsilon_4 + j\sigma_4/\omega)| \gg |k_2^2| = |\omega^2\mu(\epsilon_2 + j\sigma_2/\omega)| \quad (\text{D.32})$$

For saline water and a single insulating layer of teflon ($\epsilon_2 \approx 2.1$) this poses the following restriction:

$$|\epsilon_4 + j\sigma_4/\omega| \gg \epsilon_2. \quad (\text{D.33})$$

The global frequency dependence changes around $\omega_c = \sigma_4/\epsilon_4$. For the intervals above and below ω_c the following conditions are found:

Saline water:

$$\omega \ll \sigma_4/\epsilon_2 \quad \text{for } \omega \ll \omega_c \quad (\text{D.34a})$$

$$\epsilon_4 \gg \epsilon_2 \quad \text{for } \omega \gg \omega_c \quad (\text{D.34b})$$

Pure water:

$$\epsilon_4 \gg \epsilon_2 \quad \text{for all freq.} \quad (\text{D.34c})$$

For water (saline or pure) conditions (D.34b) and (D.34c) are met easily, because the dielectric constant of most materials is well below 80. For $\omega \ll \omega_c = \sigma_4/\epsilon_4$ condition (D.34a) is always met if $\epsilon_4 > \epsilon_2$ which is generally true for water. In other words, there is no frequency restriction of the applicability of the coaxial transmission line model for an insulated antenna in water.

As mentioned above, the most interesting series impedance is z_4^i , because the real part r_4^i represents the radiation resistance [20]. Under the sufficient condition (D.32), the good-conductor approximation $k_4^2 = j\omega\mu\sigma_4$ can be inserted in the series impedance z_4^i (D.20):

$$\begin{aligned} z_4^i &= \frac{-k_4^2}{2\pi\sigma_4 k_4 c} \frac{H_0^{(1)}(k_4 c)}{H_1^{(1)}(k_4 c)} \\ &= \frac{-j\omega\mu}{2\pi k_4 c} \frac{H_0^{(1)}(k_4 c)}{H_1^{(1)}(k_4 c)} \end{aligned} \quad (\text{D.35})$$

Note that k_4 still appears in this equation, so it *does* depend on the conductivity of the water.

Water as a good conductor

In case the water (region 4) is a *good* conductor, as in sea water, the wavenumber k_4 , defined in (3.3), can be approximated by

$$k_4 \approx \sqrt{j\omega\mu\sigma_4} = (1+j)\sqrt{\frac{\omega\mu\sigma_4}{2}}.$$

Substitution of this approximation in the series impedance leads to:

$$z_4^i = \frac{-(1+j)}{2\pi c} \sqrt{\frac{\omega\mu}{2\sigma_4}} \frac{H_0^{(1)}(k_4 c)}{H_1^{(1)}(k_4 c)}. \quad (\text{D.36})$$

Using $z_4^i = r_4^i + jx_4^i$, the radiation series resistance is given by $r_4^i = \Re(z_4^i)$. The insulation layer is preferably thin. In the case of $|k_4 c| \ll 1$ the Hankel functions can be approximated by a truncated Taylor series:

$$\begin{aligned} H_0^{(1)}(k_4 c) &= 1 - \frac{2j}{\pi} \ln 2 + \frac{2j}{\pi} \ln(k_4 c) + \frac{2j}{\pi} \gamma + \mathcal{O}((k_4 c)^2) \\ &\approx 1 + \frac{2j}{\pi} \ln \frac{k_4 c \gamma'}{2} \end{aligned} \quad (\text{D.37a})$$

$$H_1^{(1)}(k_4 c) = \frac{-2j}{\pi} \frac{1}{k_4 c} + \mathcal{O}(k_4 c) \approx \frac{-2j}{\pi} \frac{1}{k_4 c} \quad (\text{D.37b})$$

where $\gamma' = \ln \gamma$ and γ is Euler's constant¹ (M.4). Using these approximations the series radiation resistance becomes:

$$r_4^i|_{\text{sea}} = \frac{\omega\mu}{8} \quad (\text{D.38})$$

water as a poor conductor

In case the water is a *poor* conductor, as in river water, the wavenumber k_4 can be approximated by

$$k_4 \approx \omega\sqrt{\mu\epsilon_4}.$$

Substitution of this approximation in the series impedance leads to:

$$z_4^i = \frac{-j\sqrt{\mu}}{2\pi\sqrt{\epsilon_4}c} \frac{H_0^{(1)}(k_4 c)}{H_1^{(1)}(k_4 c)}. \quad (\text{D.39})$$

Using the same approximations for the Hankel functions (D.37) yields

$$r_4^i|_{\text{river}} = \frac{\omega\mu}{4} \quad (\text{D.40})$$

The radiation resistance per unit length of an insulated antenna in river water is *twice* that in sea water!

The wavenumber

Returning to the wavenumber of the coaxial transmission line k_L , which was introduced in equation (3.13) and using the shunt admittance of a single dielectric layer from (D.15) and the series impedances from (D.19),(D.21) and (D.35) the following equations for the series impedance z_L and the shunt admittance y_L of the transmission line are obtained:

$$z_L = \frac{\omega\mu}{2\pi} \left[\frac{1}{k_1 a} - j \ln\left(\frac{c}{a}\right) - j \frac{1}{k_4 c} \frac{H_0^{(1)}(k_4 c)}{H_1^{(1)}(k_4 c)} \right] \quad (\text{D.41a})$$

$$y_L = -j \frac{2\pi k_2^2}{\omega\mu \ln(c/a)} \quad (\text{D.41b})$$

¹Not to be mistaken with the propagation constant γ used elsewhere.

Combining these equations using (D.1) yields the complex wavenumber of the transmission line:

$$k_L = k_2 \sqrt{1 + \frac{j}{k_1 a \ln(c/a)} + \frac{H_0^{(1)}(k_4 c)}{k_4 c H_1^{(1)}(k_4 c) \ln(c/a)}}.$$

Neglecting losses in the antenna ($k_1 \rightarrow \infty$) leads to the following simple equation:

$$k_L = k_2 \sqrt{1 + \frac{H_0^{(1)}(k_4 c)}{k_4 c H_1^{(1)}(k_4 c) \ln(c/a)}} \quad (\text{D.42})$$

Note that this equation is not valid in the limit $c \rightarrow a$. Physically, we expect that $k_L \rightarrow k_4$, but in this model $k_L \rightarrow \infty$. A modification of this model that does give the correct behaviour in the limit $c \rightarrow a$ can be found in [5]. However, this modification is not needed as the condition $|k_4^2 - k_L^2| \gg |k_L^2 - k_2^2|$ is met for both sea and river water.

According to [16] approximation (D.42) is excellent when the condition $|k_4^2/k_2^2| \approx \varepsilon_4/\varepsilon_2 \geq 16$ is satisfied, which means $\varepsilon_{2,r} \leq 5$ for insulated antennas in water. In sand water mixtures however, the permittivity $\varepsilon_{4,r}$ can become as low as 35, in which case the condition is no longer met and either an insulating material with a lower permittivity ($\varepsilon_{2,r} < 2.2$) or a more complex equation should be used. Using (D.2,D.41b,D.42) the characteristic impedance Z_0 can be derived:

$$Z_0 = \sqrt{\frac{z_L}{y_L}} = \frac{k_L}{j y_L} \quad (\text{D.43})$$

$$= \frac{\eta_2 k_L}{2\pi k_2} \ln(c/a) \quad (\text{D.44})$$

where $\eta_2 = \omega\mu/k_2$ is the complex characteristic impedance of medium 2.

Using (D.42) and (D.44) the driving point impedance Z_{ant} of an insulated dipole antenna of half-length h can be calculated:

$$Z_{\text{ant}} = 2j Z_0 \cot k_L h \quad (\text{D.45})$$

This page intentionally contains only this sentence.

Appendix E

Measurements to permittivity

As already shown in chapter 3, the relation between the complex wavenumber $k = \beta + j\alpha$ where β is the real wavenumber and α is the attenuation constant, and the effective permittivity and the effective conductivity of the propagation medium is given by:

$$\alpha = \beta_0 \sqrt{1/2} \sqrt{\sqrt{1 + \left(\frac{\sigma_e}{\epsilon_e \omega}\right)^2} - 1} \quad (\text{E.1a})$$

$$\beta = \beta_0 \sqrt{1/2} \sqrt{\sqrt{1 + \left(\frac{\sigma_e}{\epsilon_e \omega}\right)^2} + 1} \quad (\text{E.1b})$$

where β_0 is the real wavenumber at zero conductivity, given by:

$$\beta_0 = \frac{\omega}{c_0} \sqrt{\epsilon_{er}} = \omega \sqrt{\epsilon_0 \mu} \sqrt{\epsilon_{er}} \quad (\text{E.1c})$$

By combining these two equations, the effective permittivity and the conductivity can be derived from the complex wavenumber:

$$\alpha\beta = \frac{\omega\mu\sigma_e}{2} \quad (\text{E.2})$$

$$\beta^2 - \alpha^2 = \epsilon_0 \epsilon_{er} \mu \omega^2 \quad (\text{E.3})$$

Permittivity

The effective (relative) permittivity is easily derived from (E.3):

$$\epsilon_{er} = \frac{1}{\omega^2 \mu \epsilon_0} (\beta^2 - \alpha^2) \quad (\text{E.4})$$

where the real wavenumber β can be written similarly to (E.1c):

$$\beta = \frac{\omega}{c_0} \sqrt{\epsilon_{ar}} \quad (\text{E.5})$$

and ϵ_{ar} is the apparent permittivity as defined by (4.8). Combining (E.4) and (E.5) yields an equation very similar to (4.11). After substitution of (4.10) the following simple equation is obtained for the effective permittivity:

$$\epsilon_{er} = c_0^2 \left\{ \left(\frac{t_{\text{wave}}}{d} \right)^2 - \left(\frac{\alpha}{\omega} \right)^2 \right\} \quad (\text{E.6})$$

where both t_{wave} and α are to be measured at the same effective conductivity σ_e .

Conductivity

Similarly, the effective conductivity is easily derived from (E.2):

$$\sigma_e = \frac{2}{\omega\mu} \alpha\beta. \quad (\text{E.7})$$

After substitution of equations (E.5) and (4.10) the following simple equation is obtained for the effective conductivity:

$$\sigma_e = \frac{2}{\mu_0 d} \alpha t_{\text{wave}}. \quad (\text{E.8})$$

where, again, both t_{wave} and α are to be measured at the same effective conductivity σ_e .

Errors

An evaluation of the theoretical accuracy limitations on the determination the effective permittivity, the effective conductivity and the apparent permittivity is easiest performed using equations (E.4), (E.7) and the square of (E.5).

The relative error in the effective permittivity is given by:

$$\frac{\Delta\varepsilon_{\text{er}}}{\varepsilon_{\text{er}}} = \frac{2\beta\Delta\beta - 2\alpha\Delta\alpha}{\beta^2 - \alpha^2} \quad (\text{E.9})$$

which can be rewritten as

$$\frac{\Delta\varepsilon_{\text{er}}}{\varepsilon_{\text{er}}} = \frac{1}{1 - (\alpha/\beta)^2} \cdot \left[\frac{\Delta\beta}{\beta} - (\alpha/\beta)^2 \frac{\Delta\alpha}{\alpha} \right]. \quad (\text{E.10})$$

Because for higher salinities $\alpha/\beta \rightarrow 1$, as shown in figure 3.2, the error in the effective permittivity gets very large!

The relative error in the measured conductivity σ_e is given by:

$$\frac{\Delta\sigma_e}{\sigma_e} = \frac{\Delta\beta}{\beta} + \frac{\Delta\alpha}{\alpha}. \quad (\text{E.11})$$

The relative error in the calculated conductivity varies just linearly with the relative errors in α and β .

The relative error in the apparent permittivity is given by:

$$\frac{\Delta\varepsilon_{\text{ar}}}{\varepsilon_{\text{ar}}} = \frac{2\Delta\beta}{\beta} \quad (\text{E.12})$$

The *apparent* permittivity does not have the accuracy issue of the effective permittivity, because it only depends on β .

So it is expected that at higher conductivities, using the apparent permittivity or the conductivity will be more accurate than using the effective permittivity. At very low conductivities, the difference in conductivity at varying soil content is probably too small (compared to the noise) to notice.

Based on these error calculations the apparent permittivity is expected to be the most reliable parameter, as it can be determined with a limited error for both low and high conductivities.

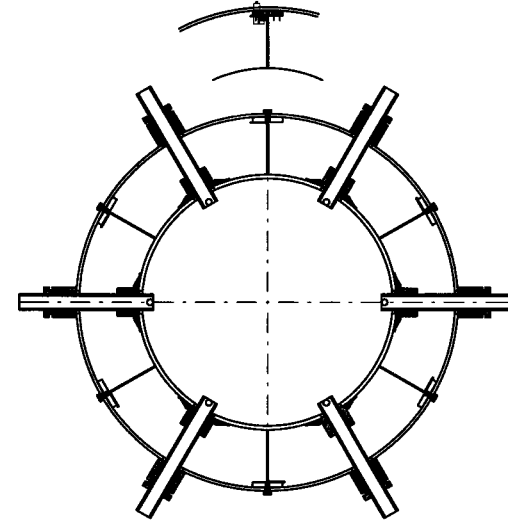
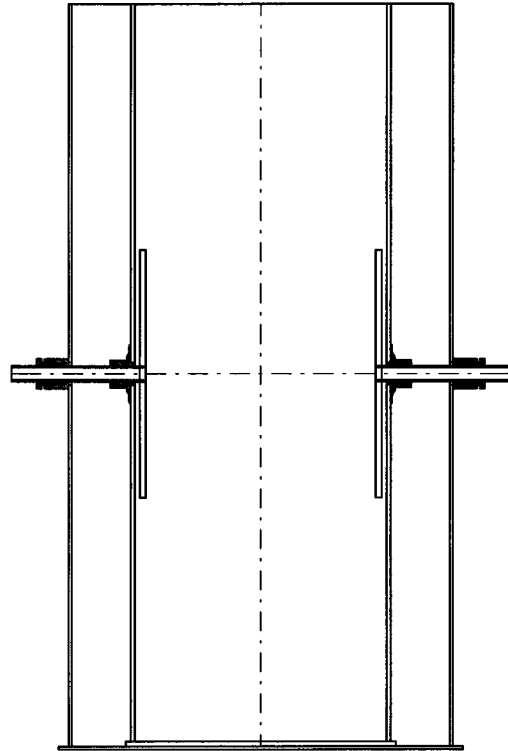
Appendix F

Construction drawings




For completeness, the AutoCAD drawings for the experimental setup are included here. The drawings are listed in table F.1

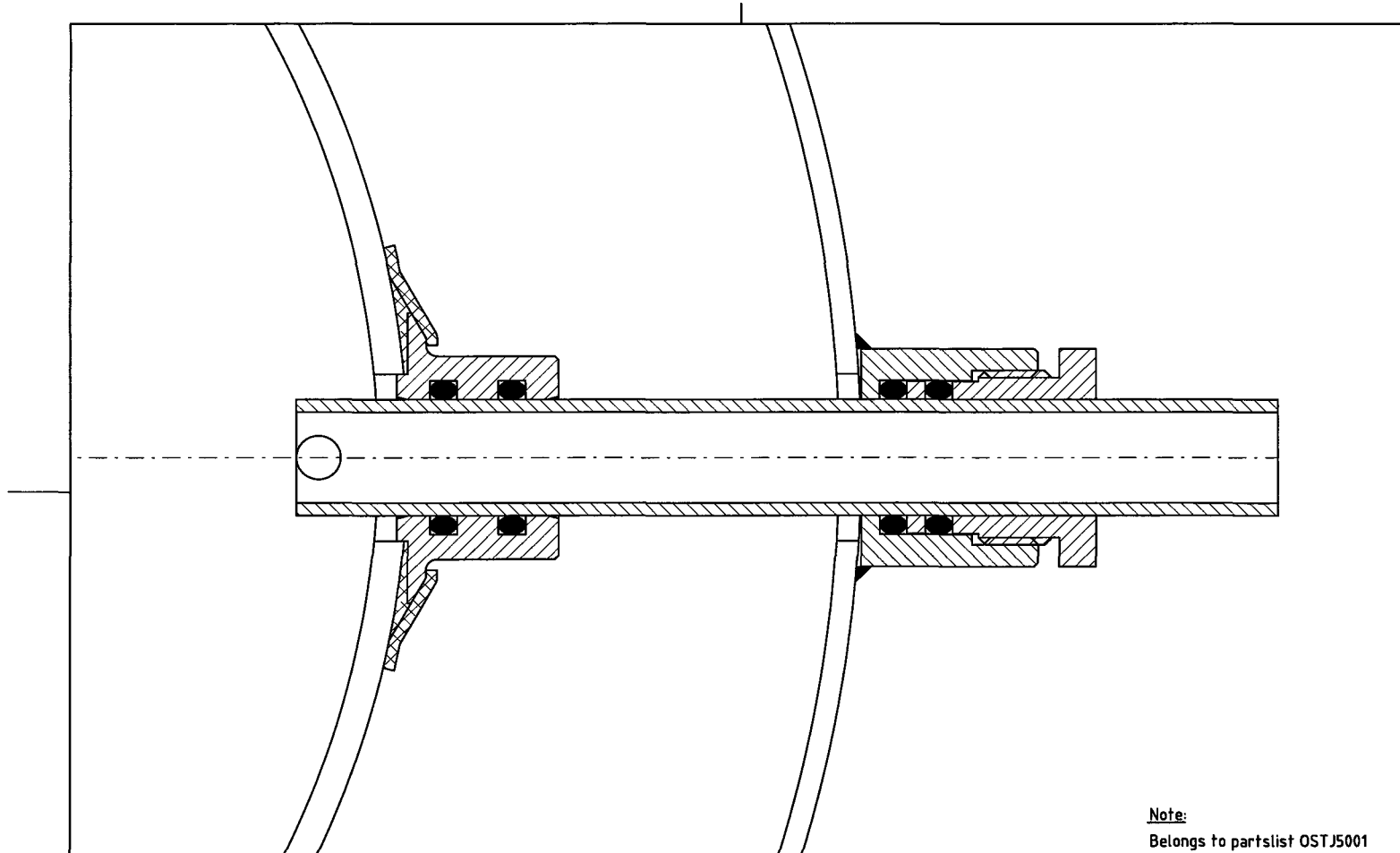
Table F.1: Description of the included AutoCAD drawings.

Doc. no.	Description
OSTJ1001	General description
OSTJ6001	PVC Flange
OSTJ6002	Steel Flange
OSTJ6003	Steel Ring
OSTJ6004	Steel Plug
OSTJ6005	Iron vessel
OSTJ6006	Steel strip
OSTJ6007	Iron shield
OSTJ6008	Iron handle




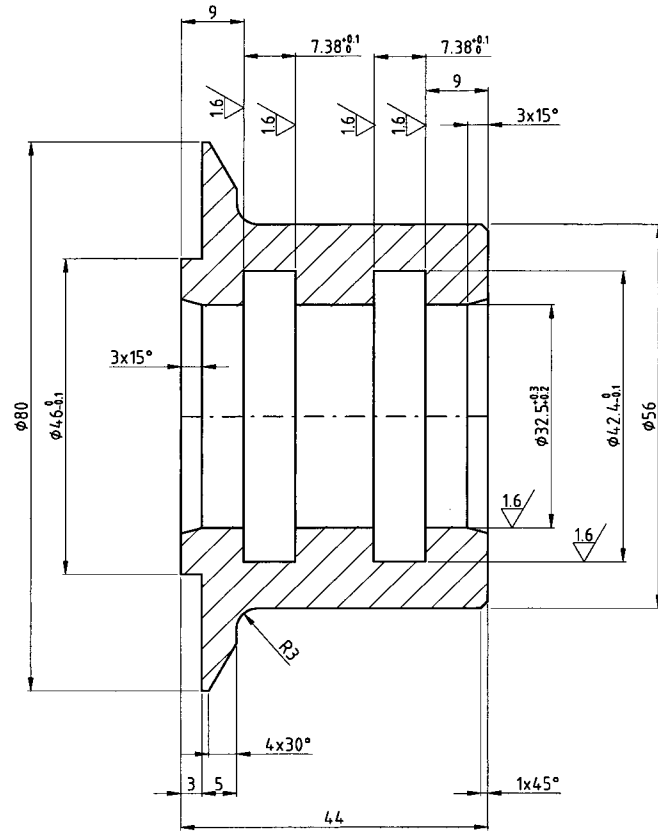
Note:
Belongs to partslist OSTJ5001

Customer : Ship name : Yard nr. : Order nr. : 970155	Drawn	C.H.	15-06-'04	IHC Systems B.V. P.O. Box 41 3360 AA Sliedrecht The Netherlands Phone : +31-184-43 19 22 Fax : +31-184-43 15 05	 IHC SYSTEMS B.V. © 2004	Product : Testopstelling Alternatieve Productiemeting		  Doc. no. OSTJ1001 - 9200 - 001	Sheet 1	Rev. 0
	Revised					Type nr. : Dwg. type : General description				
Revision description :	Print date :		09-07-'04							
	Scale : -/-		Paper size : A3							



Note:
Belongs to partlist OSTJ5001

Customer :	Drawn	C.H.	15-06-'04	IHC Systems B.V. P.O. Box 41 3360 AA Sliedrecht The Netherlands Phone : +31-184-43 19 22 Fax : +31-184-43 15 05	 IHC SYSTEMS B.V. © 2005	Product : Testopstelling Alternatieve Productiemeting	
	Ship name :	Revised				Type nr. :	
Yard nr. :	Checked		Par. :	Dwg. type : General description			
Order nr. : 970155	Print date :	14-09-'04		Doc. no.		Sheet	Rev.
Revision description :	Scale : -/-	Paper size : A3		OSTJ1001 - 9200 - 001		1	0



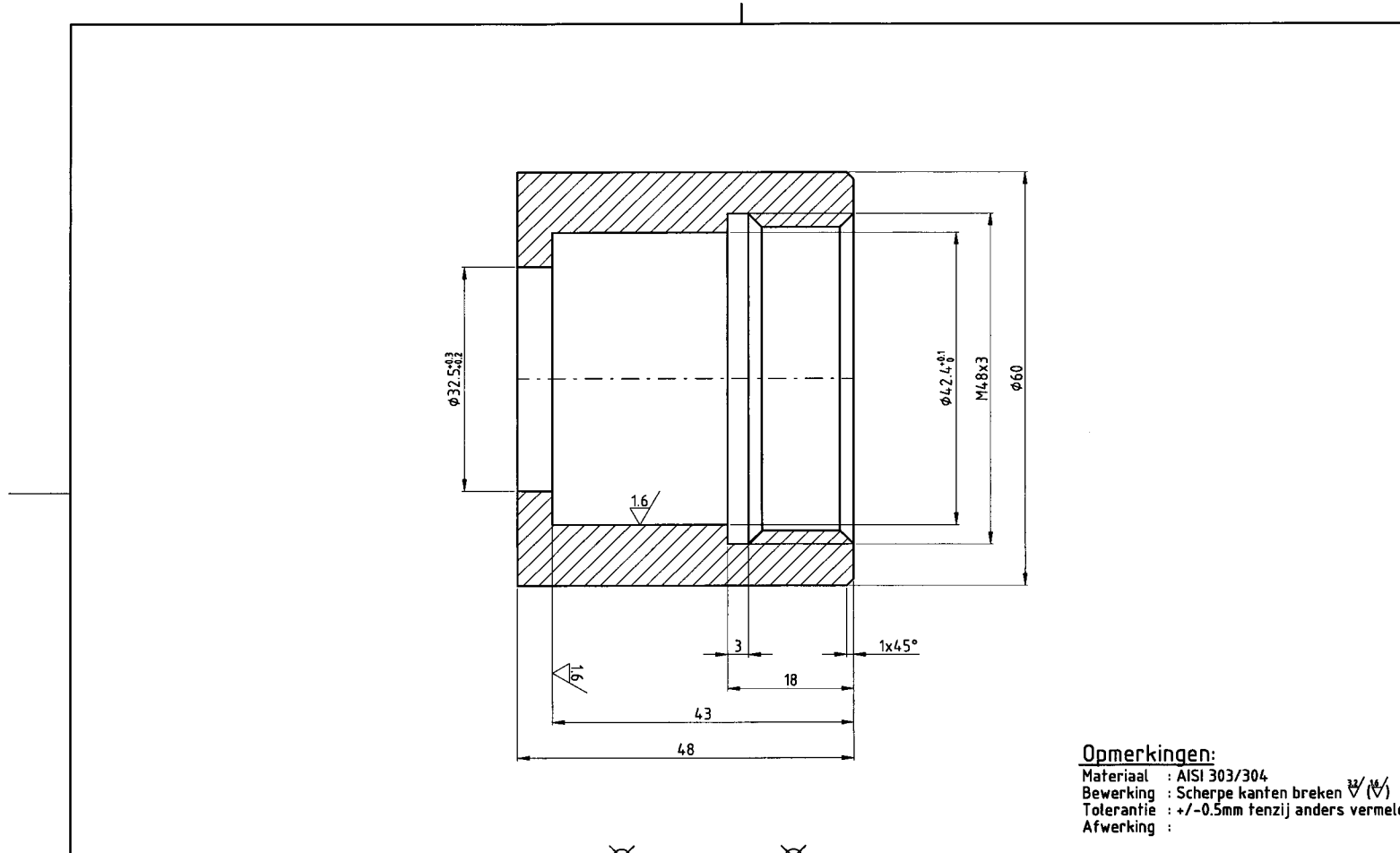
Opmerkingen:

Materiaal : PVC of PP
 Bewerking : Scherpe kanten breken $\sqrt{1.6}$
 Tolerantie : +/- 0.5mm tenzij anders vermeld
 Afwerking :

Customer :	Drawn	P.J.v.d.W.	02-07-'04
Ship name :	Revised	C.H.	13-08-'04
Yard nr. :	Checked	Par. :	
Order nr. : 970155	Print date :		13-08-'04
Revision description :	Scale :	-/-	Paper size : A3
Changed tolerance $\phi 32$			

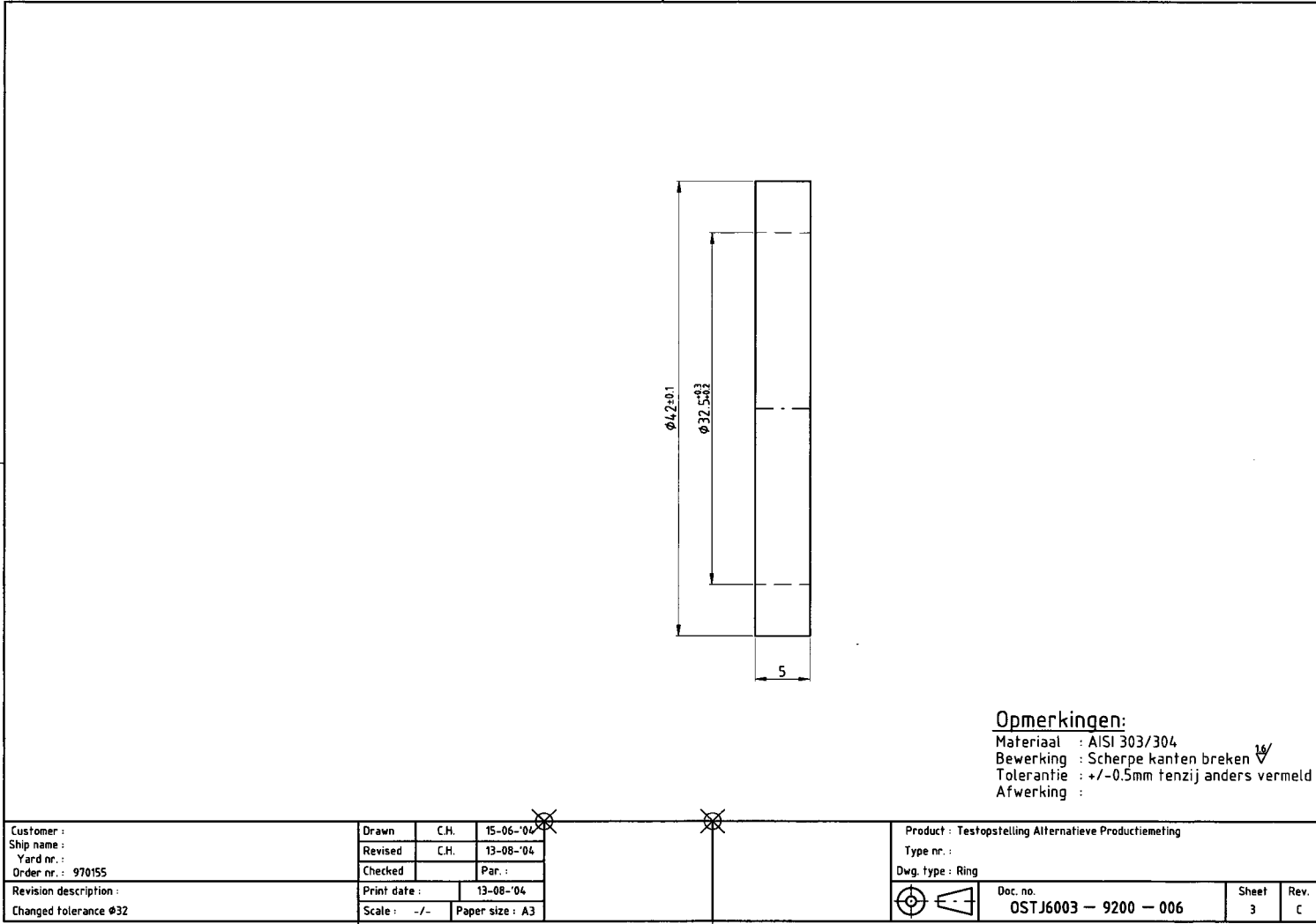
Product : Testopstelling Alternatieve Productiemeting
Type nr. :
Dwg. type : Doorvoer
Doc. no. : OSTJ6001 - 9200 - 006

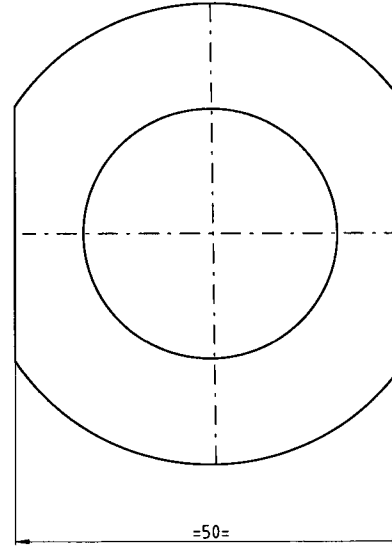
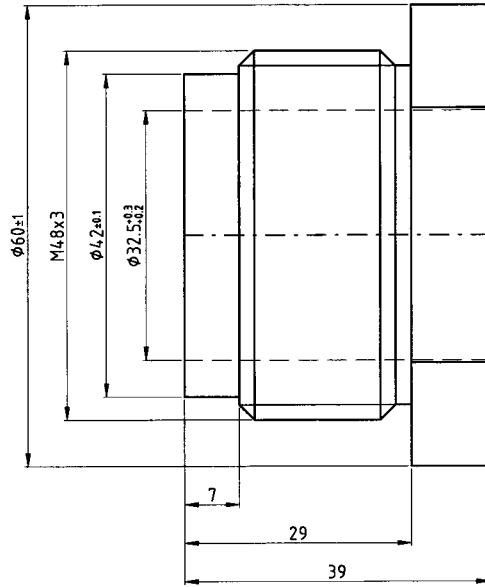
Sheet	Rev.
1	C



Opmerkingen:
 Materiaal : AISI 303/304
 Bewerking : Scherpe kanten breken ∇ (∇)
 Tolerantie : +/-0.5mm tenzij anders vermeld
 Afwerking :

Customer : Ship name : Yard nr. : Order nr. : 970155	Drawn	P.J.v.d.W.	15-06-'04	Product : Testopstelling Alternatieve Productiemeting Type nr. : Dwg. type : pijpdoorvoer	Doc. no. OSTJ6002 -- 9200 -- 006	Sheet 2	Rev. C
	Revised	C.H.	13-08-'04				
	Checked		Par. :				
	Print date :		13-08-'04				
Revision description : Changed tolerance Ø32	Scale : -/-		Paper size : A3				







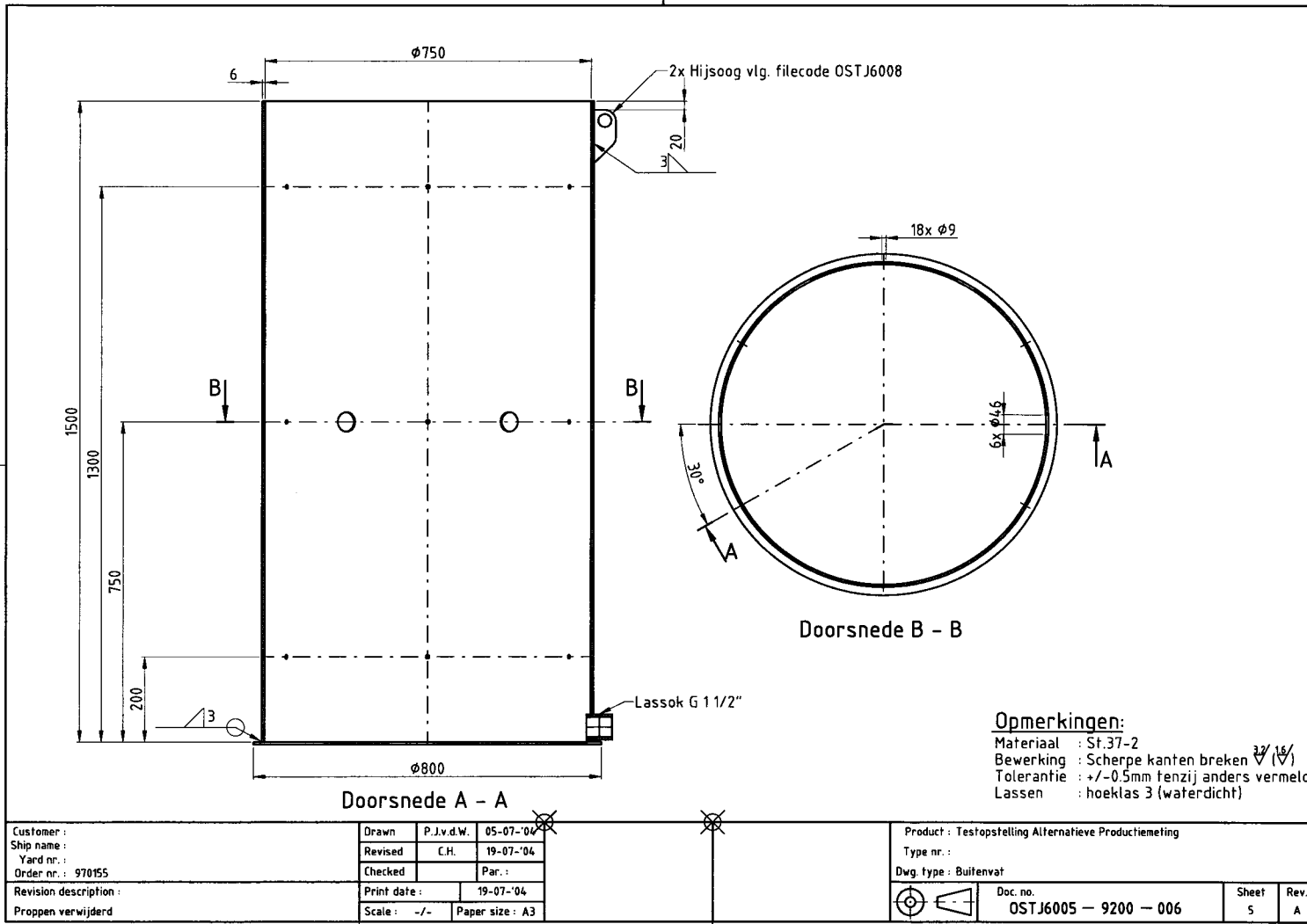
Opmerkingen:

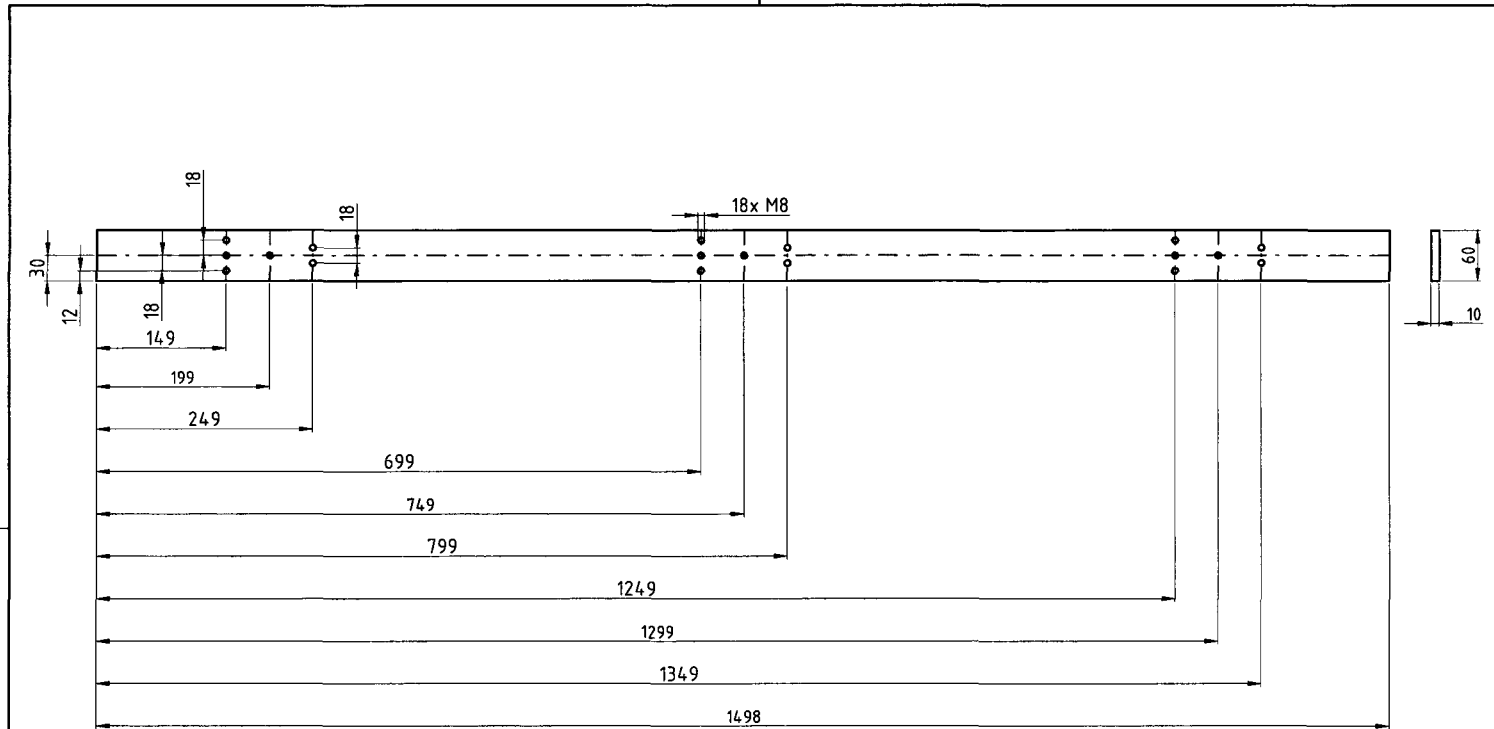
Materiaal : AISI 303/304

Bewerking : Scherpe kanten breken \checkmark

Tolerantie : +/-0.5mm tenzij anders vermeld

Customer : Ship name : Yard nr. : Order nr. : 970155	Drawn	C.H.	15-06-'04	IHC Systems B.V. P.O. Box 41 3360 AA Sliedrecht The Netherlands Phone : +31-184-43 19 22 Fax : +31-184-43 15 05	 IHC SYSTEMS B.V. © 2005	Product : Testopstelling Alternatieve Productiemeting		Sheet 4	Rev. C
	Revised	C.H.	12-08-'04			Type nr. :			
	Checked	Par. :				Dwg. type : pakking drukker			
Revision description : Changed tolerance $\phi 32$	Print date :	13-08-'04		 Doc. no. OSTJ6004 - 9200 - 006					
Scale : -/-	Par. :	Paper size : A3							





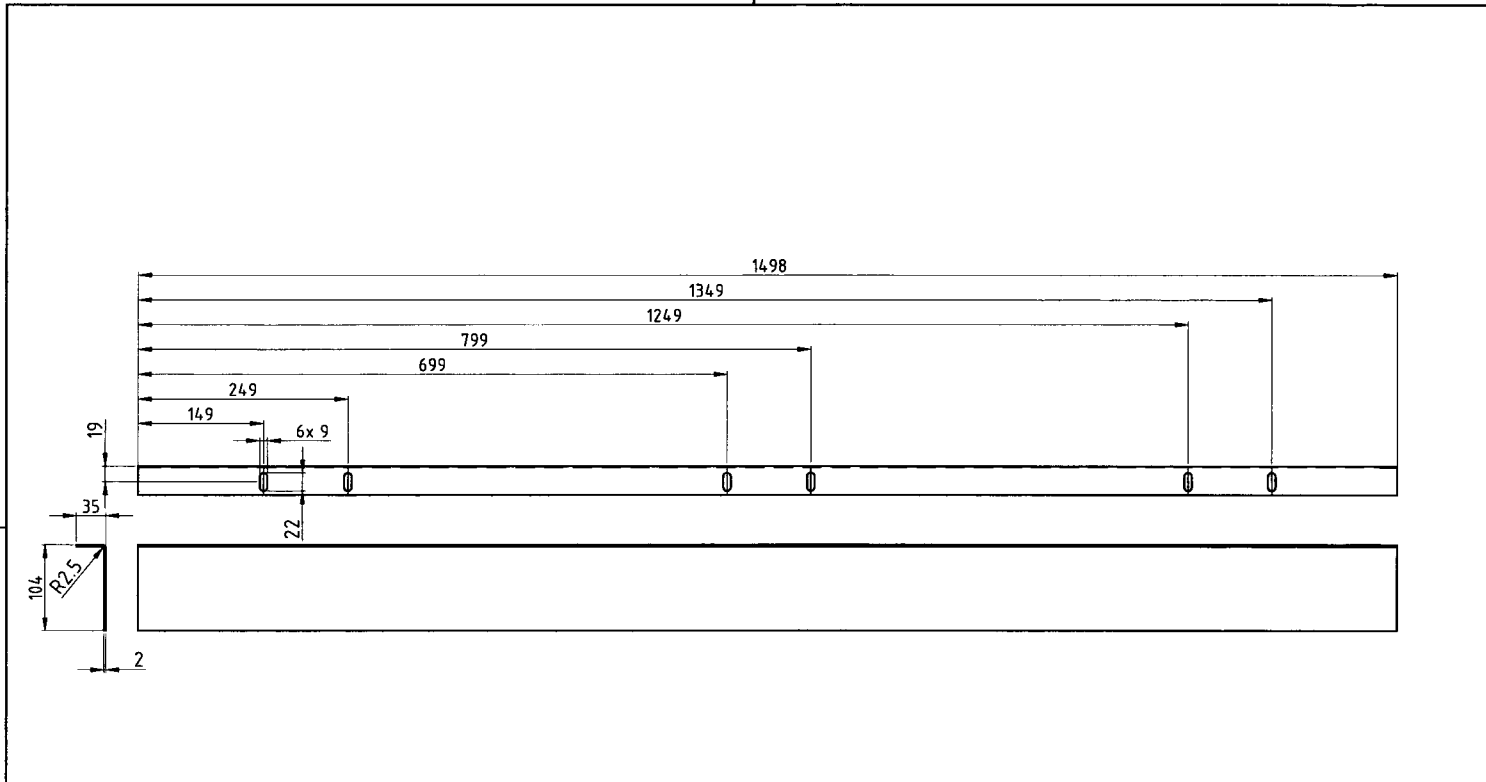
Opmerkingen:

Materiaal : AISI 304
 Bewerking : Scherpe kanten breken $\sqrt[3]{16}$ ($\sqrt[3]{16}$)
 Tolerantie : +/-0.5mm tenzij anders vermeld

Customer :	
Ship name :	
Yard nr. :	
Order nr. :	
Revision description :	

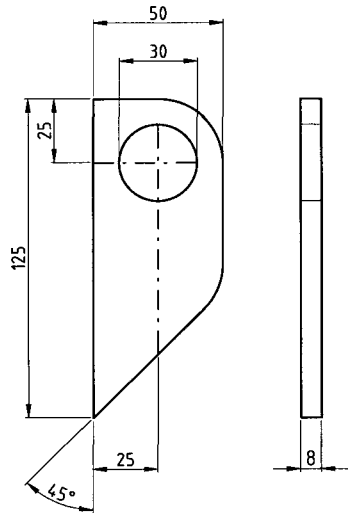
Drawn	P.J.v.d.W.	05-07-'04
Revised		
Checked		Par. :
Print date :		07-07-'04
Scale : -/-		Paper size : A3

Product : Test alternatieve productiemeting	
Type nr. :	
Dwg. type : Montage strip	
	Doc. no.
	OSTJ6006 - 9200 - 006
Sheet	Rev.
6	0



Opmerkingen:
 Materiaal : AISI 304
 Bewerking : Scherpe kanten breken $\sqrt[3]{16}$
 Tolerantie : +/-0.5mm tenzij anders vermeld

Customer :	Drawn	P.J.v.d.W.	05-07-'04	Product : Testopstelling alternatieve productiemeting	Type nr. :	Doc. no.	Sheet	Rev.
	Ship name :	Revised						
Yard nr. :	Checked		Par. :	Dwg. type : Schot		OSTJ6007 - 9200 - 006	7	0
Order nr. :	Print date :		07-07-'04					
Revision description :	Scale : -/-		Paper size : A3					



Opmerkingen:
 Materiaal : St.37-2
 Bewerking : Scherpe kanten breken \checkmark
 Tolerantie : +/-1mm tenzij anders vermeld

Customer :	Drawn	P.J.v.d.W.	05-07-'04	IHC Systems B.V. P.O. Box 41 3360 AA Sliedrecht The Netherlands	Product : Testopstelling alternatieve productiemeting	Type nr. :	Sheet	Rev.
	Ship name :	Revised						
Yard nr. :	Checked		Par. :	Phone : +31-184-43 19 22 Fax : +31-184-43 15 05	Doc. no. OSTJ6008 - 9200 - 006	OSTJ6008 - 9200 - 006	7	0
Order nr. :	Print date :		09-07-'04					
Revision description :	Scale :	-/-	Paper size :	A3				

This page intentionally contains only this sentence.

Appendix G

Transmission line transformer

A transmission-line transformer (TLT) can be used as an impedance matching device instead of a quarter wave match [32, 33, 35]. The main advantage of a TLT is that it's theoretically a broad-band device, whereas a quarter-wave match is tuned for a specific frequency. Two different approaches exist to transmission line transformers: the Guanella design and the Ruthroff design. The latter is used here. Its concept involves summing a direct voltage with a delayed voltage, as shown in figure G.1 for an unbalanced 1 : 2.25 TLT.

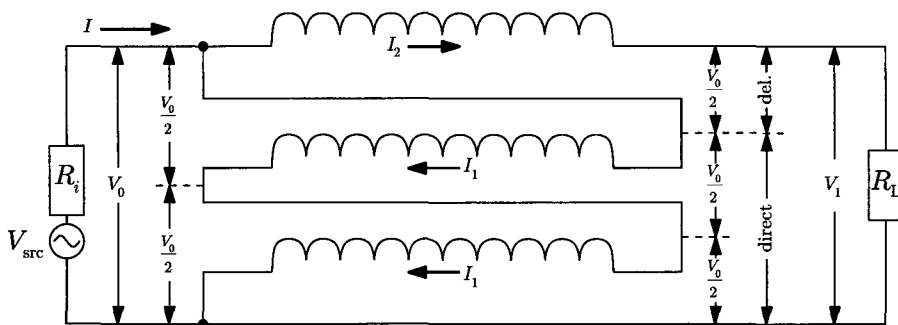


Figure G.1: Schematic circuit of a transmission line transformer which matches a source impedance R_i to a load impedance R_L . The indicated coiled wires are to be wound around a ferrite coil.

As indicated in the circuit, the TLT causes a voltage ratio $V_0 : V_1 = 2 : 3$. The impedance ratio is the square of the voltage ratio:

$$\frac{Z_i}{Z_L} = \left(\frac{V_0}{V_1}\right)^2 \approx \frac{1}{2.25}$$

Because a transmission line transformer can be made for specific impedance ratios only (like 1 : 4, 1 : 3, etc.) and because some impedance ratios have a wider bandwidth than others, a TLT for a 1 : 2.25 impedance ratio has been made, which matches a 50 Ω transmission line to a 22 Ω device (antenna). In order to maintain a high bandwidth, the wiring should be kept as short as possible. Because of this requirement, a 1 : 2.25 transmission line transformer has a much wider broadband than a 1 : 3 device which uses 5 instead of 3 parallel windings [35].

Using different types of wire and changing the sequence of the windings on the ferrite coil, a TLT can be tuned for various specific impedances. In the specific case of a 1 : 2.25, the windings that lead to 50 Ω : 112 Ω and 50 Ω : 22 Ω impedance ratios are shown in figure G.2.

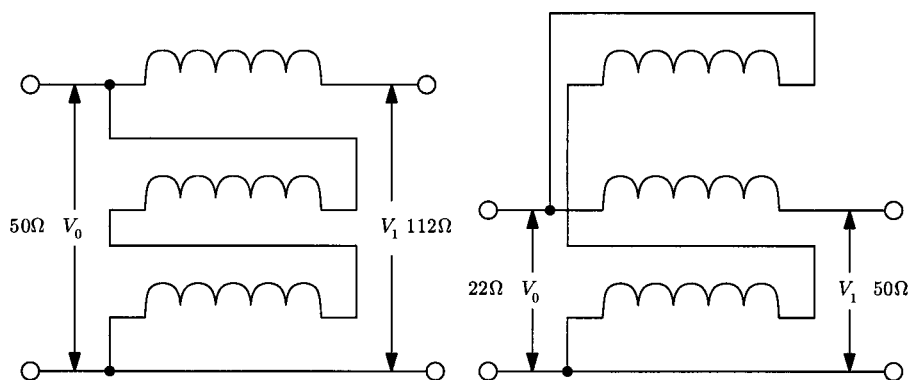


Figure G.2: A transmission line transformer which transforms $50\ \Omega$ to $112\ \Omega$ should be wound differently than a TLT which transforms $50\ \Omega$ to $22\ \Omega$.

A $1 : 2.25$ transmission line transformer has been made by winding 6 turns of 3 parallel wires of 0.85 mm enamel insulated copper wire (magnet wire) around a Ferroxcube 4C65 NiZn ferrite core (type TN14/9/5-4C65), see figure G.3. Its performance in the experimental setup has been measured, see appendix N.1.2.

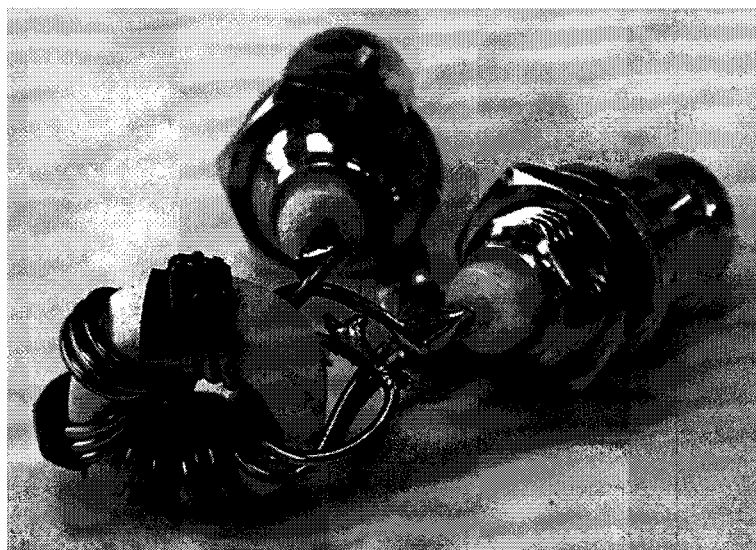


Figure G.3: The transmission line transformer built to transform a $50\ \Omega$ coaxial transmission line to $22\ \Omega$.

Appendix H

Pickup coil

To maintain galvanic separation between the transmitter and the receiver side, the source signal is fed to the scope by means of a pickup coil. The pickup coil works like a transformer, where the coaxial transmission line forms the single turn primary winding as shown in figure H.1(a). As in every transformer, the output voltage can be increased by using more windings on the secondary coil.

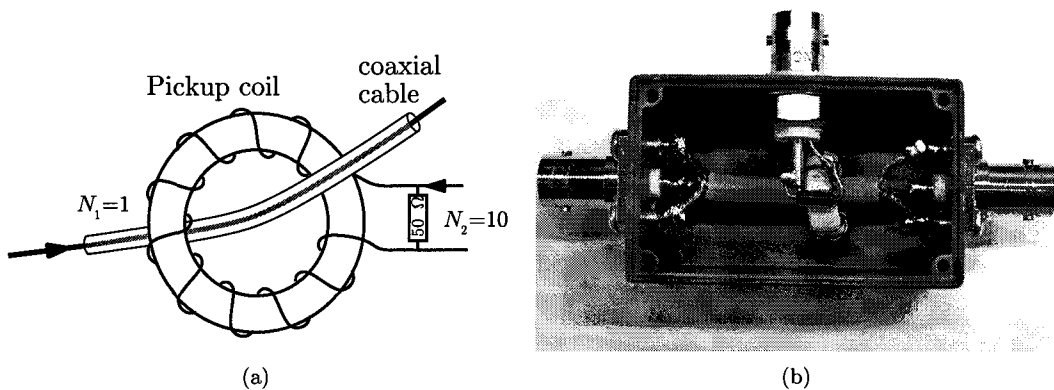


Figure H.1: Design (a) and photo (b) of the toroid pickup coil.

The pick-up coil does not respond to the current on the inner conductor of the coax cable, but only to currents on the outside of the braid, which should *ideally* be zero. In practice, there will always be a small current through the braid. Because any current on the outside of the coax braid will form standing waves, the picked up voltage depends on the position of the device on the cable. Thus the voltage of the pickup coil cannot be used as an absolute reference. In the experimental setup, it is used as the reference signal for the time difference measurements.

As indicated in the schematic drawing (figure H.1(a)), the secondary turns are distributed evenly over the entire ferrite coil to minimize capacitive coupling between the wires. The secondary winding is terminated with the characteristic impedance of the coax cable (50Ω) to avoid reflections caused by an impedance mismatch.

The core is a Ferroxcube 4C65 NiZn ferrite core (type TN14/9/5-4C65), the same as used for the transmission line transformer. Ferrite cores are generally made of NiZn or MnZn. A NiZn ferrite core has been chosen because it has a higher permeability in the 50–100 MHz range. Before resorting to the ferrite cores, some more easily obtainable iron powder cores have also been tested,

such as the TN-2 (colour code: red/clear) TN-6 (yellow/clear) and TN-12 (green/white) iron powder cores. These cores yielded significantly lower output voltages than the 4C65 ferrite core. This is quite understandable, as the permeability of iron cores is generally much lower than of ferrite cores.

Note: After the measurements it was devised that the pickup coil can be improved by isolating the mass of the side connector from the metal box.

Appendix I

Low pass filter

To attenuate possible higher harmonics from the frequency generator, a 5th order Chebyshev low pass filter with a corner frequency of 75 MHz was made, based on the circuit from figure I.1.

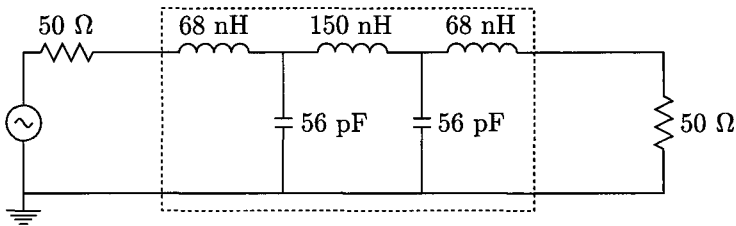


Figure I.1: Chebyshev 5th order low pass filter, shown in the dashed box, connected to a frequency generator with 50 Ω impedance on the left side and a 50 Ω load on the other side.

A frequency sweep was calculated using an evaluation version of pSpice 8.0, as shown in figure I.2.

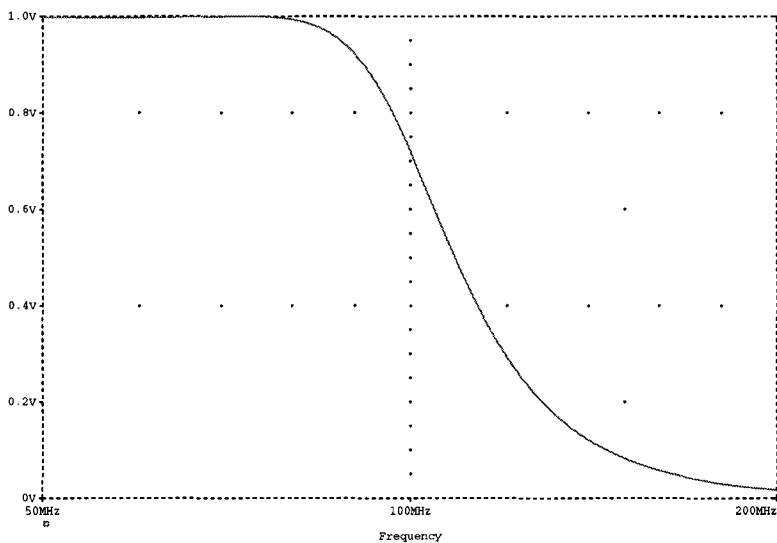


Figure I.2: Frequency sweep of the 5th order Chebyshev low pass filter with a corner frequency of 75 MHz.

This page intentionally contains only this sentence.

Appendix J

Measurement in detail

The first (pure water) density measurement in the pipe was performed when the first sand pack (#1) was ready. Measurements were performed with and without sand pack and when the pack was approximately 50% submerged. The measured time difference t_{meas} between the source signal and the received signal has two origins:

1. The electromagnetic wave in the tube: t_{wave}
2. A delay in the electric wiring: t_{wire}

Of course only the first part is of real interest, the second remains constant as long as the circuit remains the same. The propagation time depends on the propagation medium: the wavelength in sand is longer than in water, so the higher the density the shorter the propagation time. The relation between the apparent permittivity and the propagation time is given by equation (4.10). For non-saline water, the effective conductivity is assumed to be negligible ($\sigma_e \approx 0$), and the apparent permittivity becomes equal to the effective permittivity:

$$\epsilon_{\text{er}} = \left(\frac{c_0 t_{\text{wave}}}{d} \right)^2 \quad (\text{J.1})$$

where c_0 is the speed of light in vacuum (M.1). The propagation speed in pure water is given by

$$v = \frac{c_0}{\sqrt{\epsilon_e^{\text{w}}}} \approx 33729286.7 \text{ m/s}$$

which results in a propagation time $t_{\text{wave}} = d_{\text{wave}}/v$ after having traveled over a distance d_{wave} . Inserting the antenna distance $d_{\text{wave}} \approx 0.47 \text{ m}$ for d_{wave} gives the propagation time in pure water:

$$t_{\text{wave}} \approx 13.934 \text{ ns}$$

This calculated propagation time is to be compared to the measured time difference t_{meas} in pure water:

Density	$t_{\text{meas}} (+1T)$ (ns)	t_{meas} (ns)	t_{wave} (ns)
pure water	16.7	0.746	13.934
⋮	⋮	⋮	⋮

Thus the delay in the wiring (which includes the difference due to the modulo T determination of t_{meas}) can be calculated:

$$\begin{aligned} t_{\text{meas}} &= t_{\text{wave}} + t_{\text{wire}} \\ 0.746 &= 13.935 + t_{\text{wire}} \\ \Rightarrow t_{\text{wire}} &\approx -13.189 \text{ ns} \end{aligned}$$

Now the propagation times and the effective permittivities ε_{er} can be calculated for the other measurements.

Sand pack submerged (%)	$t_{\text{meas}} (+1T)$ (ns)	t_{meas} (ns)	t_{wave} (ns)	ε_{er}
0	16.7	0.746	13.934	79.0
50	16.2	0.246	5.291	73.4
100	15.5	-0.454	5.015	66.0

Using the C.R.I.M. model (4.15) and assuming $\varepsilon_{\text{er}}^{\text{s}} = 4.0$ and $\varepsilon_{\text{er}}^{\text{w}} = 79$ the sand volume fractions can be calculated:

Sand pack submerged (%)	ε_{er}	ϕ
0	79.0	0.00
50	73.4	0.05
100	66.0	0.11

Appendix K

Model selection

The difficulties arising in the use of the C.R.I.M. model gives problems at ‘higher’ conductivities call for a different method. As the propagation time measurement showed the least deviation, the semi-empirical model using only propagation time data looks favourable. The propagation times of density measurements 4–9 (in river water) have been plotted as a function of the sand volume and the conductivity, see figure K.1. Measurements 1,2,3 were not used because the measured time differences of measurements 2 and 3 were not in the same range and measurement 1 was performed with non-saline water in the outer pipe.

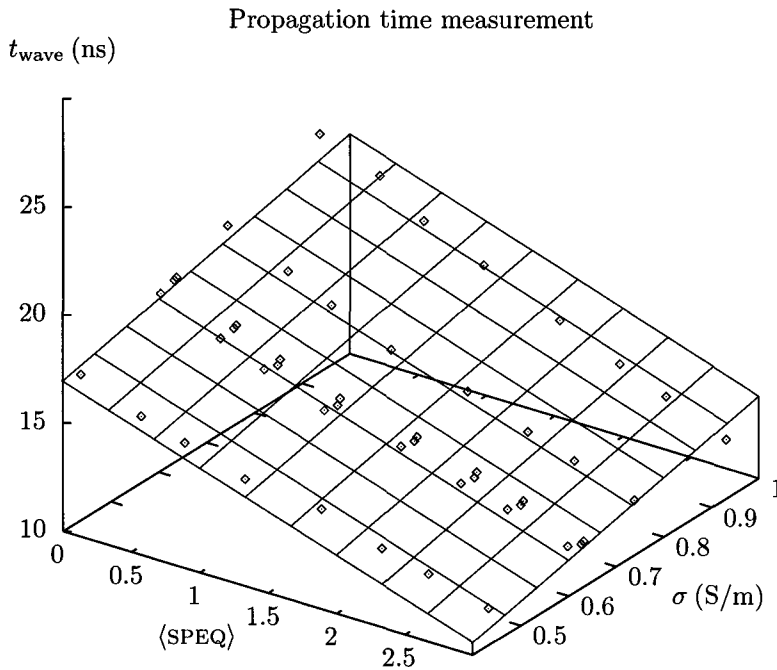


Figure K.1: Combined measurements: plot of the propagation times of all density measurements in ‘river’ water. A simple linear fit has been made using $T(x, y) = ax + by + c$, which yields $a = 5.46 \pm 0.53$, $b = -2.257 \pm 0.085$ and $c = 15.98 \pm 0.39$. The weighted sum of squared residuals has not been calculated.

This plot shows that for each value of the conductivity, there is a predictable relation between the propagation time and the sand volume, but also that there is a predictable relation between

the propagation time and the conductivity for each sand volume.

So it appears that the density can be calculated using only the propagation time t_{wave} , or even more practical: the time difference between the source signal and the received signal t_{meas} . Because the propagation time depends on both the permittivity and the conductivity of the propagation medium, one calibration measurement without sand is needed each time the conductivity of the water changes. This calibration time is t_0 and the corresponding density is 1 ton/m^3 . A plot of the measured calibration times of measurements #4–#9 is shown in figure K.2. The calibration time varies almost linearly with the conductivity of the water.

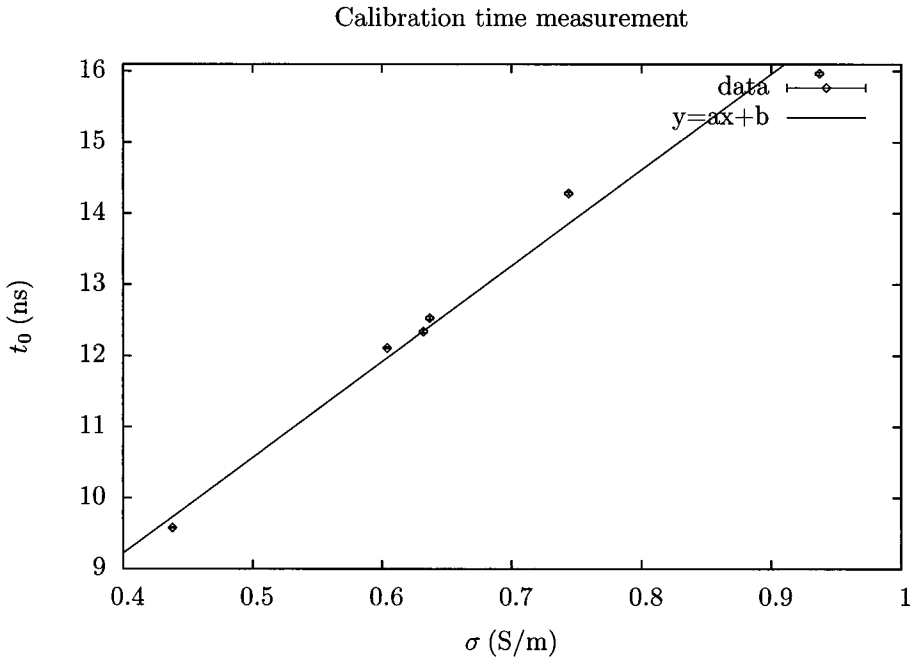


Figure K.2: The measured time difference between source signal and received signal without sand packs in the pipe is the calibration time t_0 .

The phase difference between the source signal and the received signal t_{meas} , measured during normal operation of the density meter is compared to this calibration time:

$$t_r = t_{\text{meas}} - t_0. \tag{K.1}$$

In short, a relation of the form $\rho \rightarrow \rho(t_r, t_0)$ is to be found. In order to get an idea which terms should be considered, the theory can be consulted. Using (4.12a, 4.15, 4.22, 4.23) the following approximate relations can be found:

$$\begin{aligned} \varepsilon &\sim t^2 \\ \phi &\sim \begin{cases} \sqrt{\varepsilon}, \text{ C.R.I.M.} \\ \varepsilon, \text{ Arith.} \end{cases} \\ \rho &\sim \phi. \end{aligned}$$

Considering $t_r \sim t$ these equations can be combined to:

$$\varepsilon \sim \begin{cases} t_r, \text{ C.R.I.M.} \\ t_r^2, \text{ Arith.} \end{cases}$$

which suggests using the terms t_r and t_r^2 . To be on the safe side, third and fourth order terms will also be considered.

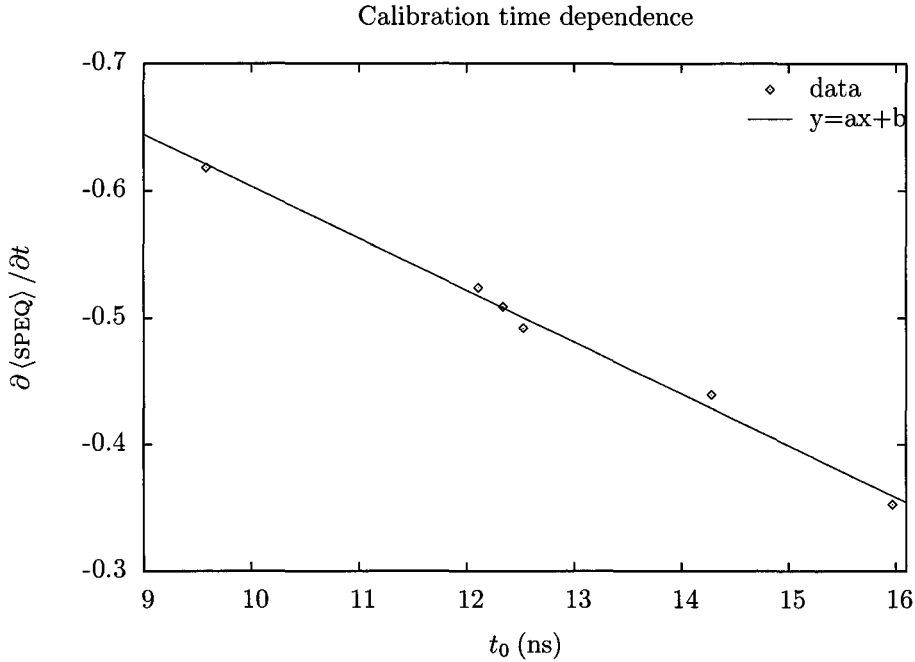


Figure K.3: The change of the gradient in figure as the conductivity changes 7.2 has been plotted versus the calibration time t_0 .

The plot in figure 7.2 shows that the conductivity causes a change of the gradient $\partial t / \partial \langle \text{SPEQ} \rangle$. A plot of the inverse of this gradient versus the calibration time t_0 is shown in figure K.3. This suggests the inclusion of the term $t_0 \cdot t_r$ in the density model. Because t_0 is defined as the propagation time at $\rho = 1$, there cannot be a direct t_0 dependence. This leads to the following set of candidates:

$$\rho \in (t_r, t_r^2, t_r^3, t_r^4, t_r \cdot t_0) \tag{K.2}$$

The objective is now to find the ‘best’ equation for the relation $\rho \rightarrow \rho(t_r, t_0)$, which is the *simplest* model that adequately fits the data. Such a regression equation can be found using forward stepwise multiple regression. This method starts with a constant (the intercept), and at each step the variable with the highest partial correlation coefficient is added to the model and the ‘Sum of Squared Errors’ (SSE) is calculated, until the addition of an extra term no longer improves the model. An objective parameter to assess the benefit of including an extra term is the ‘Proportional Reduction in Error’ (PRE), defined as:

$$\text{PRE} = 1 - \frac{\text{SSE}(A)}{\text{SSE}(C)}$$

where C stands for the Compact model and A the Augmented model. The PRE can be expressed as a fraction or a percentage and indicates by how much the error has been reduced by choosing the augmented model over the compact model. The frequently used coefficient of multiple determination R^2 is actually the PRE when the Compact model is the simple model $\rho = 1$. With the set of candidates (K.2) the following steps are found:

Table K.1: Stepwise multiple regression. The number of parameters p is increased and for each model the PRE and R^2 is calculated.

Model	p	SSE	PRE	R^2
$\rho = 1$	0	346282.6	-	-
$\rho = 1 + c_1 \cdot t_r$	1	10658.8	0.9692	0.9692
$\rho = 1 + c_1 \cdot t_r + c_2 \cdot t_0 \cdot t_r$	2	3665.55	0.6561	0.9894
$\rho = 1 + c_1 \cdot t_r + c_2 \cdot t_0 \cdot t_r + c_3 \cdot t_r^2$	3	1907.04	0.4797	0.9945
$\rho = 1 + c_1 \cdot t_r + c_2 \cdot t_0 \cdot t_r + c_3 \cdot t_r^2 + c_4 \cdot t_0 \cdot t_r^3$	4	1499.43	0.2137	0.9957

Though the PRE indicates that even the last step improves the model by about 21%, the absolute improvement is quite small, as indicated by R^2 . A plot of R^2 versus the number of parameters in the model is shown in figure K.4.

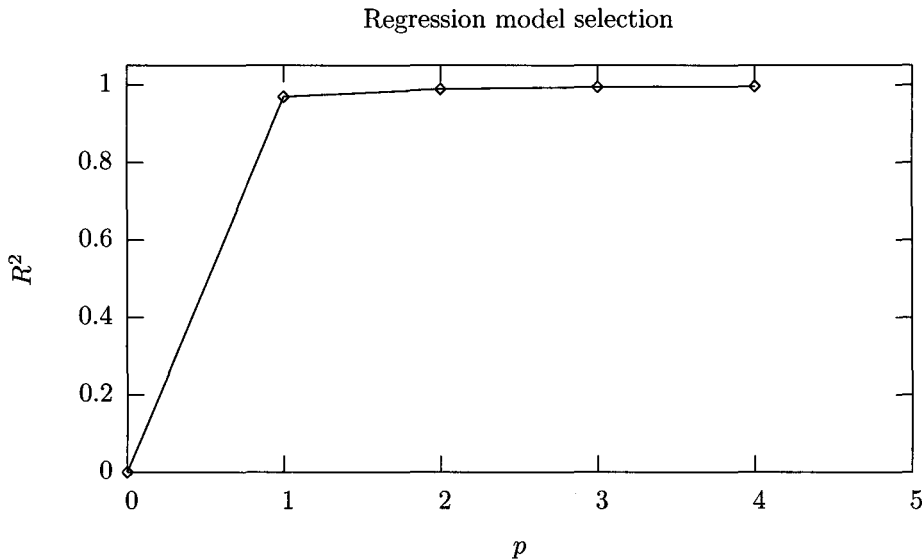


Figure K.4: The coefficient of multiple determination (R^2) as a function of the model complexity, indicated by the number of parameters p . A coefficient of 1 indicates a 100% correct model.

Considering:

- the small reduction in error in the last step;
- the lack of a physical basis for higher order terms;
- the term $t_0 \cdot t_r^3$ has the largest influence for large (positive or negative) values for t_r which occur less frequently in the data set;

the last step is discarded. So, the data is to be fitted using:

$$\rho(t_0, t_r) = 1 + a \cdot t_r + b \cdot t_r^2 + c \cdot t_0 \cdot t_r \quad (\text{K.3})$$

The error in the calculated density can be calculated from the errors in the measured propagation times using normal error propagation:

$$d\rho = \left| \frac{\partial f(t_0, t_r)}{\partial t_r} \right| dt_r + \left| \frac{\partial f(t_0, t_r)}{\partial t_0} \right| dt_0 \quad (\text{K.4})$$

$$d\rho = |a + 2b \cdot t_r + c \cdot t_0| dt_r + |c \cdot t_r| dt_0 \quad (\text{K.5})$$

where $dt_r = dt_{\text{meas}} + dt_0$ and $\{dt_{\text{meas}}, dt_0\}$ the average errors in the measured propagation times. The calculated error $d\rho$ depends on the regression parameters $\{a, b, c\}$ while the weighting factor for the fit is defined as $s = 1/d\rho^2$. This cyclic dependence is solved by estimating the parameters $\{a, b, c\}$ using a non-weighted fit first, calculating the error and then performing a couple of weighted fits while updating the error each time, until the values converge.

This page intentionally contains only this sentence.

Appendix L

The Maxwell equations

The (macroscopic) Maxwell equations are

$$\nabla \times \mathbf{H} = \mathbf{J} + \frac{\partial \mathbf{D}}{\partial t} \quad (\text{L.1a})$$

$$\nabla \times \mathbf{E} = -\frac{\partial \mathbf{B}}{\partial t} \quad (\text{L.1b})$$

$$\nabla \cdot \mathbf{D} = \rho \quad (\text{L.1c})$$

$$\nabla \cdot \mathbf{H} = 0 \quad (\text{L.1d})$$

where

$$\mathbf{D} = \varepsilon_0 \mathbf{E} + \mathbf{P} = \varepsilon_0 \varepsilon_r \mathbf{E} = \varepsilon \mathbf{E}$$

$$\mathbf{J} = \sigma \mathbf{E}$$

$$\mathbf{B} = \mu_0 \mu_r \mathbf{H} = \mu \mathbf{H}$$

$$\rho = \rho_{\text{true}} = \rho_{\text{total}} - \rho_{\text{pol}}$$

$$\rho_{\text{pol}} = -\nabla \cdot \mathbf{P}$$

Using the above definitions, these equations can be rewritten using only the \mathbf{E} and \mathbf{H} vectors

$$\nabla \times \mathbf{H} = \sigma \mathbf{E} + \varepsilon \frac{\partial \mathbf{E}}{\partial t} \quad (\text{L.2a})$$

$$\nabla \times \mathbf{E} = -\mu \frac{\partial \mathbf{H}}{\partial t} \quad (\text{L.2b})$$

$$\nabla \cdot \mathbf{E} = \frac{\rho}{\varepsilon} \quad (\text{L.2c})$$

$$\nabla \cdot \mathbf{H} = 0 \quad (\text{L.2d})$$

This page intentionally contains only this sentence.

Appendix M

Constants & Identities

Constants

$$c_0 = 299792458 \text{ ms}^{-1} \quad \text{speed of light in vacuum} \quad (\text{M.1})$$

$$\mu_0 = 4\pi \times 10^{-7} \text{ NA}^{-2} \quad \text{permeability in vacuum} \quad (\text{M.2})$$

$$\varepsilon_0 = 1/\mu_0 c^2 = 8.854187817 \times 10^{-12} \text{ Fm}^{-1} \quad \text{permittivity in vacuum} \quad (\text{M.3})$$

$$\gamma = 1 + 1/2 + 1/3 + \dots \approx 0.577215665 \quad \text{Euler's constant} \quad (\text{M.4})$$

Mathematical identities

$$\nabla \times \nabla \times A = \nabla(\nabla \cdot A) - \nabla^2 A \quad (\text{M.5})$$

$$\cot(z) = \frac{\sin(2x) - j \sinh(2y)}{\cos(2x) + \cosh(2y)}, \quad z = x + jy \quad (\text{M.6})$$

This page intentionally contains only this sentence.

Appendix N

Measurement data

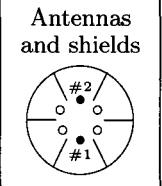
Contents

N.1 Preliminary	150
N.1.1 Quarter wave match	150
N.1.2 Transmission line transformer	152
N.1.3 Receiver antenna position	154
N.1.4 Calibration data	156
N.2 Pure water measurements	159
N.2.1 Measurement 1: First sand pack	159
N.2.2 Measurement 2: Three sand packs	161
N.2.3 Measurement 3: Improved sand packs	164
N.2.4 Measurement 4: Goodwill oscilloscope	166
N.2.5 Measurement 5: Painted pipe	168
N.2.6 Measurement 6: Third antenna	170
N.2.7 Measurement 7: Agilent oscilloscope	172
N.3 River water measurements	175
N.3.1 Measurement 1: 0.61 S/m	175
N.3.2 Measurement 2: 0.46 S/m	177
N.3.3 Measurement 3: 0.48 S/m	178
N.3.4 Measurement 4: 0.63 S/m	179
N.3.5 Measurement 5: 0.64 S/m	181
N.3.6 Measurement 6: 0.94 S/m	183
N.3.7 Measurement 7: 0.74 S/m	185
N.3.8 Measurement 8: 0.60 S/m	187
N.3.9 Measurement 9: 0.44 S/m	189
N.3.10 Measurement 10: Rotation	191
N.4 High salinity measurements	192
N.4.1 Measurement 1: 0 S/m	192
N.4.2 Measurement 2: 1.9 S/m	194
N.4.3 Measurement 3: 3.1 S/m	195
N.4.4 Measurement 4: 2.2 S/m	196
N.4.5 Measurement 5: no inner pipe	197

N.1 Preliminary

N.1.1 Quarter wave match

Measurement setup:

	Date: September 24, 2004		
	Experiment settings	Frequency: 62.6 MHz Antennas: Source: #1 Receive: #2 Shields: All 6 present Low pass filter: Yes Source signal: pickup before amplifier	
Equipment used	Frequency generator: Oscillator Power amplifier: - Pre amplifier: - VSWR meter: Diamond SX-1000 Oscilloscope: Fluke Combiscope PM3380B		
Oscilloscope settings	CH1:	Connection: Send Setting: 50 mV/DIV Termination: 50 Ω	
	CH2:	Connection: Receive Setting: 1 V/DIV Termination: 1 MΩ	
	Timing	Timebase: 5 ns/DIV Sampling rate: 10 GSa/s	
Remarks	Phase difference measured in degrees Send power: 0.5 W		

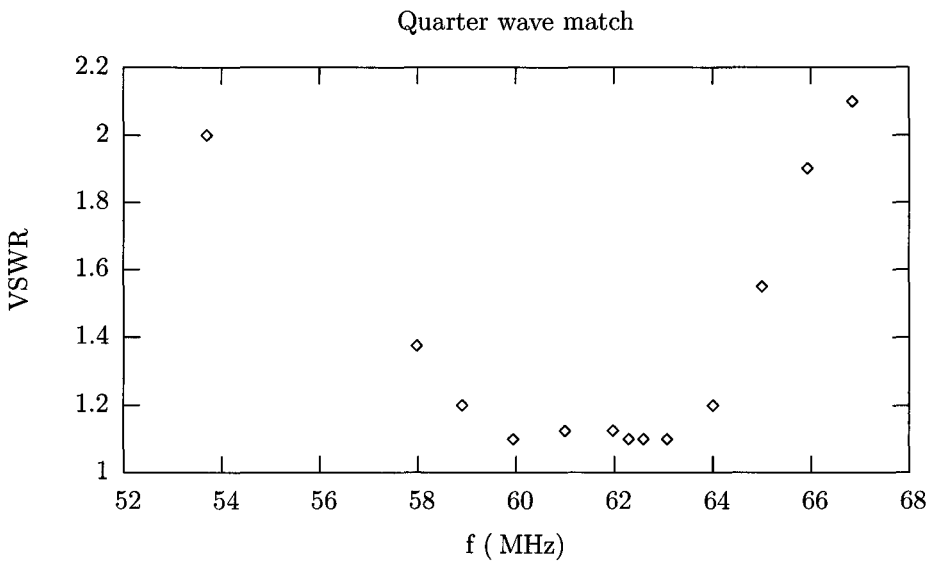


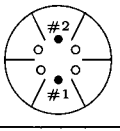
Figure N.1: VSWR vs. frequency for the quarter wave match.

Table N.1: Measurement data

d_{src} (cm)	f (MHz) ± 0.05	VSWR ± 0.03	V_{src} (mV) ± 1	V_{rec} (V) ± 0.04	$\Delta\phi$ ($^\circ$) ± 1	$V_{\text{rec}}/V_{\text{src}}$	Δt (ns)
0	53.69	2.00	189	3.71	24	19.6	1.22
	57.98	1.38	157	6.22	199	39.6	9.53
	58.91	1.20	149	6.54	232	43.9	10.94
	59.95	1.10	155	6.78	275	43.7	12.74
	61.00	1.13	150	7.13	318	47.5	14.48
	61.98	1.13	149	7.65	356	51.3	15.95
	62.30	1.10	149	7.52	360	50.5	16.05
	62.60	1.10	150	7.39	383	49.3	16.98
	63.08	1.10	153	7.40	392	48.4	17.26
	64.01	1.20	155	6.54	427	42.2	18.53
	65.00	1.55	147	6.07	460	41.3	19.66
	65.93	1.90	137	6.00	487	43.8	20.52
	66.85	2.10	109	5.21	518	47.8	21.52

N.1.2 Transmission line transformer

Measurement setup:

<div style="border: 1px solid black; padding: 5px; width: fit-content;"> <p>Antennas and shields</p>  </div>	Date: September 27, 2004			
	Experiment settings	Frequency:	63.0 MHz	
		Antennas:	Source:	#1
			Receive:	#2
		Shields:	All 6 present	
	Low pass filter:	Yes		
	Source signal:	pickup before amplifier		
Equipment used	Frequency generator:	Oscillator		
	Power amplifier:	-		
	Pre amplifier:	-		
	VSWR meter:	Diamond SX-1000		
	Oscilloscope:	Fluke Combiscope PM3380B		
Oscilloscope settings	CH1:	Connection:	Send	
		Setting:	50 mV/DIV	
		Termination:	50 Ω	
	CH2:	Connection:	Receive	
		Setting:	1 V/DIV	
		Termination:	1 MΩ	
	Timing	Timebase:	5 ns/DIV	
Sampling rate:		10 GSa/s		
Remarks	Phase difference measured in ns			

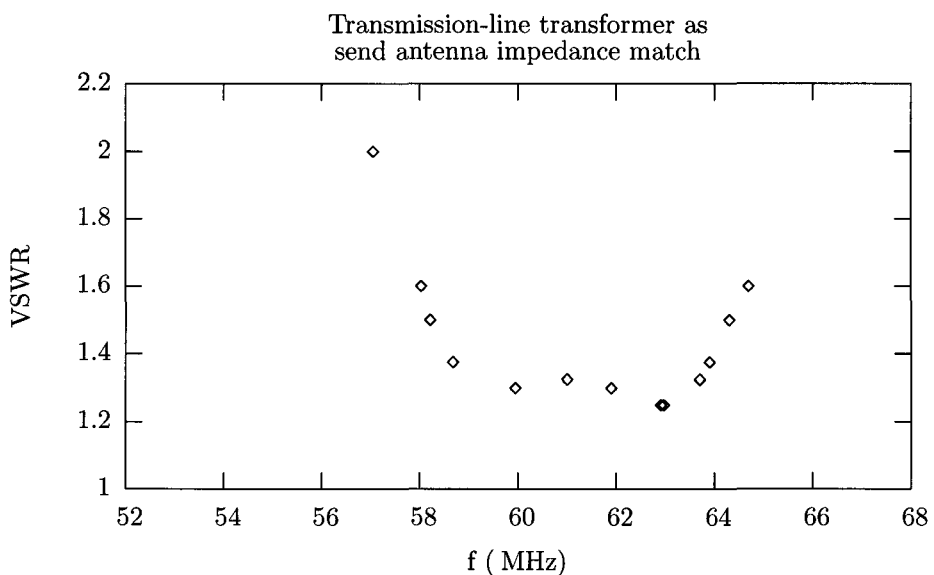


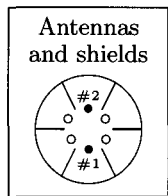
Figure N.2: VSWR vs. frequency for the transmission-line transformer.

Table N.2: Measurement data

d_{rec} (cm) ± 0.1	V_{src} (mV) ± 1	V_{rec} (V) ± 0.04	$V_{\text{rec}}/V_{\text{src}}$	$\Delta t(+1T)$ (ns) ± 0.1	Δt (ns) ± 0.1	$(\Delta t + 1T) - T$	VSWR ± 0.05
10.4	137	6.73	49.12	16.5	0.60	0.63	1.2
9.4	138	6.80	49.28	16.7	0.80	0.83	1.2
8.3	140	6.81	48.64	16.9	1.05	1.03	1.15
7.3	143	6.97	48.74	17.1	1.20	1.23	1.15
6.5	143	6.93	48.46	17.2	1.40	1.33	1.1
5.5	149	7.00	46.98	17.4	1.55	1.53	1.1
4.4	149	6.99	46.91	17.5	1.60	1.63	1.1
3.3	150	7.04	46.93	17.6	1.70	1.73	1.1
2.1	150	7.04	46.93	17.6	1.80	1.73	1.1
1.6	151	7.08	46.89	17.6	1.70	1.68	1.1
1.0	152	7.04	46.32	17.5	1.65	1.63	1.1
0.2	150	6.93	46.20	17.2	1.30	1.33	1.1

N.1.3 Receiver antenna position

Measurement setup:



Date: September 24, 2004	
Experiment settings	Frequency: 63.0 MHz
	Antennas: Source: #1 Receive: #2
	Shields: All 6 present
	Low pass filter: Yes
	Source signal: pickup before amplifier
Equipment used	Frequency generator: Oscillator
	Power amplifier: -
	Pre amplifier: -
	VSWR meter: Diamond SX-1000
	Oscilloscope: Fluke Combiscope PM3380B
Oscilloscope settings	CH1: Connection: Send
	Setting: 50 mV/DIV
	Termination: 50 Ω
	CH2: Connection: Receive
	Setting: 1 V/DIV
	Termination: 1 MΩ
Timing	Timebase: 5 ns/DIV
	Sampling rate: 10 GSa/s
Remarks	Send power: 0.5 W Send antenna placed along the inner pipe wall Source antenna position varied (0 cm = along the inner pipe wall)

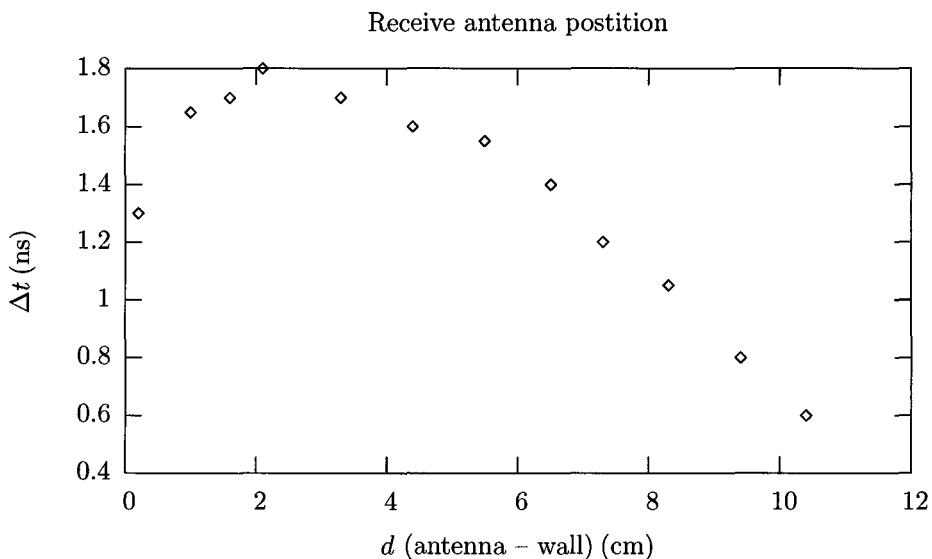


Figure N.3: Propagation time vs. the receiver antenna position.

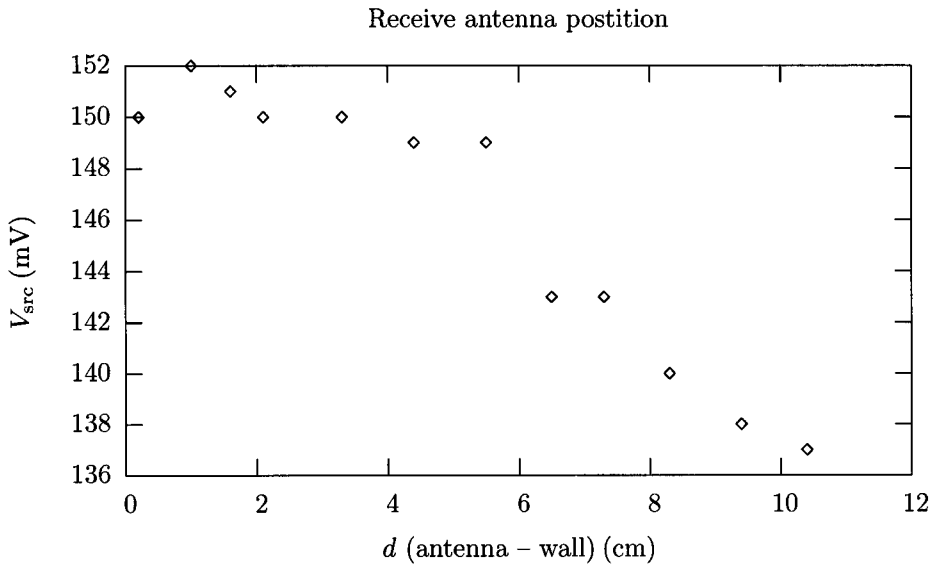


Figure N.4: Source antenna voltage vs. the receiver antenna position.

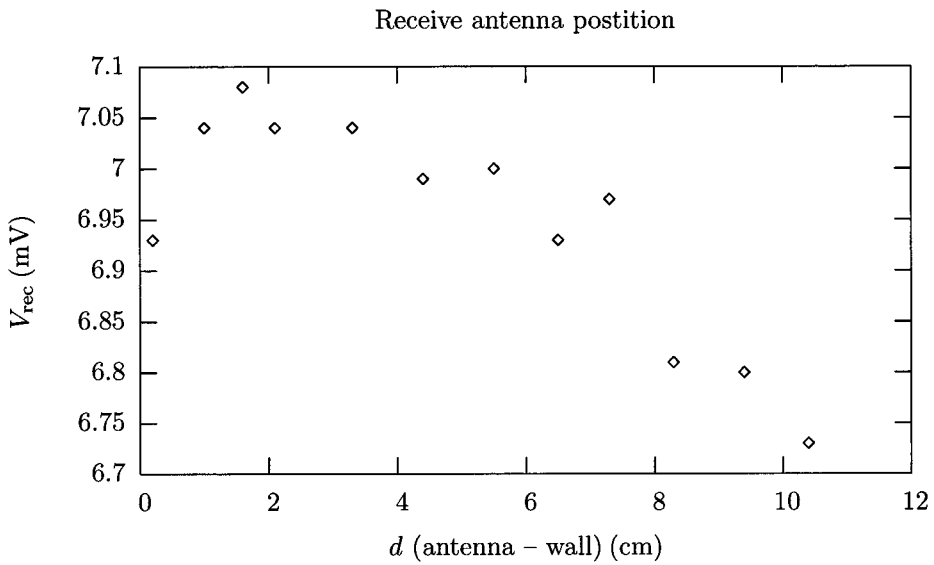


Figure N.5: Receiver antenna voltage vs. the receiver antenna position.

N.1.4 Calibration data

Radioactive

Table N.3: Data of the radioactive density meter calibration.

glass (mm)	ρ (ton/m ³)	Counts #1	Counts #2	Counts #3
(backgr.)		132	122	114
(water)	0	39934	40033	39901
170.8	1.2562	11319	11374	11259
288.9	1.43335	4885	4890	4882
459.7	1.68955	1518	1530	1557

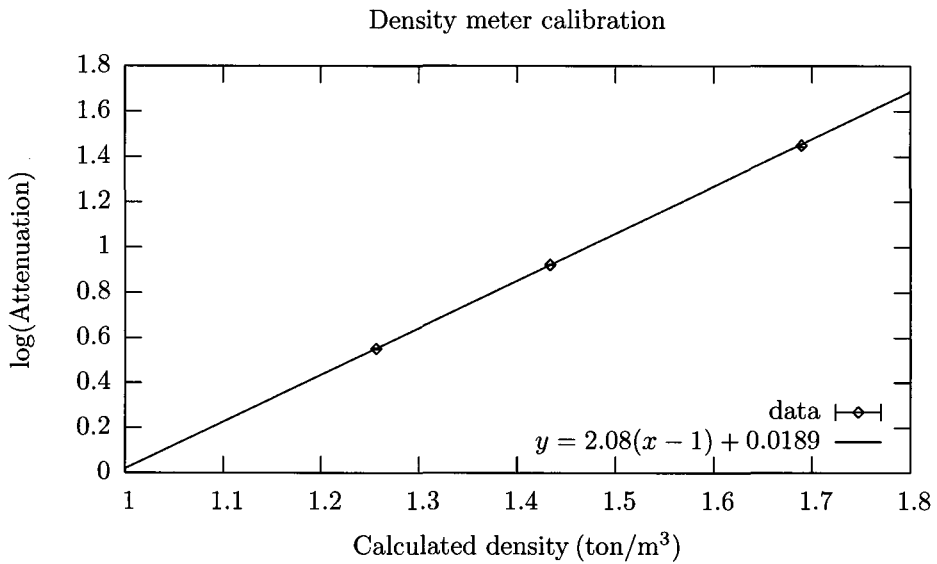


Figure N.6: Calibration of density meter 584-422A-1131 using the data from table N.3. A weighted fit using $y = a(x - 1) + b$ yields $a = 2.08 \pm 0.02$ and $b = 0.0189 \pm 0.0064$. The weighted sum of squared residuals is $\chi^2_\nu = 1.1$.

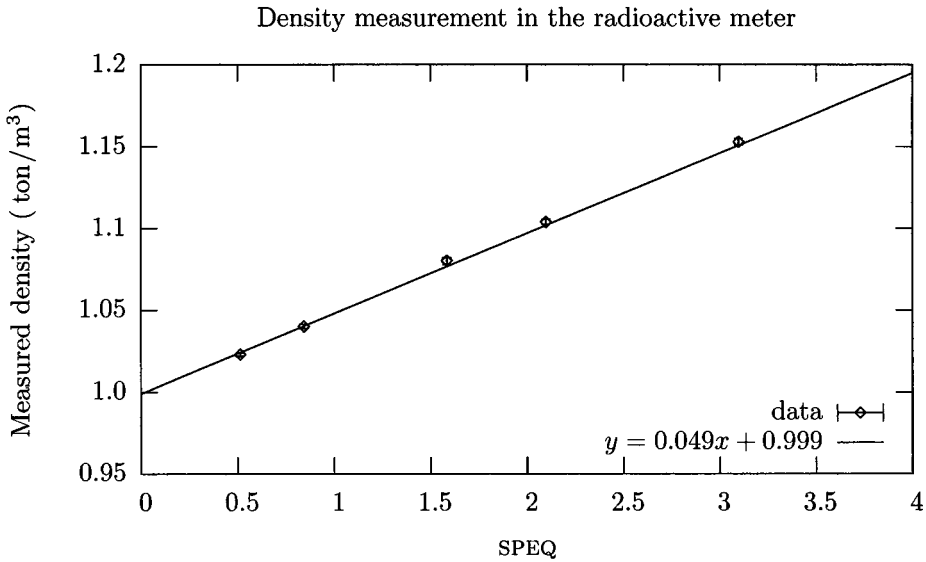


Figure N.7: Density measurement of the sand packs in the radioactive density meter. A weighted fit using $y = ax + b$ yields $a = 0.049 \pm 0.001$ and $b = 0.999 \pm 0.002$. The weighted sum of squared residuals is $\chi^2 = 2.77$.

Electromagnetic

Measurement setup:

	Date: Jan. 17&19, 2005	
	Experiment settings Frequency: 62.5 MHz Antennas: Source: #1 Receive: #2 Shields: All 6 present Low pass filter: No Source signal: pickup before amplifier	
Equipment used Frequency generator: HP 8647A Power amplifier: R.F.P.A. RF001220-25 Pre amplifier: - VSWR meter: Diamond SX-1000 Oscilloscope: Agilent Infiniium 54831D		
Oscilloscope settings	CH1: Connection: Send Setting: (variable) mV/DIV Termination: 50 Ω	
	CH2: Connection: Receive Setting: (variable) V/DIV Termination: 1 MΩ	
	Timing Timebase: 10 ns/DIV Sampling rate: 250 GSa/s (eq. time)	
Remarks	$\sigma_{\text{inner pipe}} = 0.470 \pm 0.05 \text{ S/m}, T = 16.6 \pm 0.2 \text{ }^\circ\text{C}$ $\sigma_{\text{outer pipe}} = 2.13 \pm 0.02 \text{ S/m}, T = 16.5 \pm 0.5 \text{ }^\circ\text{C}$	

Table N.4: Measurement series #1

pack #	V_{src} (mV) ± 2	V_{rec} (mV) ± 2	$V_r/V_s _0$	Δt (ns)	VSWR ± 0.025
-	311	192	1.00	19.40 \pm 0.02	1.60
3	309	185	0.97	18.71 \pm 0.02	1.60
5	310	178	0.93	18.19 \pm 0.02	1.60
4	310	178	0.93	18.30 \pm 0.02	1.60
2	310	174	0.91	17.90 \pm 0.02	1.60

Table N.5: Measurement series #2

pack #	V_{src} (mV) ± 1	V_{rec} (mV) ± 1	$V_r/V_s _0$	Δt (ns)
-	313	190	1.00	19.47 \pm 0.01
3	309	179	0.95	18.79 \pm 0.02
5	310	173	0.92	18.22 \pm 0.02
4	308	175	0.94	18.37 \pm 0.02
5	308	171	0.91	18.30 \pm 0.01
2	309	165	0.88	17.90 \pm 0.01
-	310	188	1.00	19.45 \pm 0.02

Water volume

Table N.6: Data of water volume calibration measurement

pack #	Δh (cm) ± 0.02	Relative volume
-	0	0
3	8.3	0.456
5	14.4	0.791
4	14.5	0.797
2	18.2	1.000

N.2 Pure water measurements

The first series of density measurements were performed in ‘pure’ water, i.e. tap water without the addition of salt. The primary objective of these measurements was to get an understanding of the characteristics of the antennas, the impedance matching, the measurement pipe, the signal generation and measurement system and the effects of sand in the pipe - without complicating the system’s behaviour too much.

The measurement data of all density measurements in pure water are contained in this section. The raw data from the coaxial probe measurements is not contained as these measurements are regarded to be of secondary importance.

N.2.1 Measurement 1: First sand pack

Measurement setup:

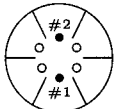
<div style="border: 1px solid black; padding: 5px; width: fit-content;"> <p>Antennas and shields</p>  </div>	Date: September 30, 2004	
	Experiment settings	Frequency: 62.7 MHz Antennas: Source: #1 Receive: #2 Shields: All 6 present Low pass filter: Yes Source signal: pickup before amplifier
Equipment used	Frequency generator: Oscillator Power amplifier: - Pre amplifier: - VSWR meter: Diamond SX-1000 Oscilloscope: Fluke Combiscope PM3380B	
Oscilloscope settings	CH1:	Connection: Send Setting: 50 mV/DIV Termination: 50 Ω
	CH2:	Connection: Receive Setting: 1 V/DIV Termination: 1 MΩ
	Timing	Timebase: 5 ns/DIV Sampling rate: 10 GSa/s
Remarks	Measurements were performed with sand pack #1. Phase difference was measured in interval $T < \Delta t < 2T$, hence the notation “ $\Delta t(+1T)$ ”	

Table N.7: Measurement data

Sand pack submerged (%)	V_{src} (mV) ± 1	V_{rec} (V) ± 0.04	$V_r/V_s _0$	$\Delta t(+1T)$ (ns) ± 0.1	Δt (ns)	VSWR ± 0.025
0	151	6.99	1.00	16.7	0.75	1.13
50	148	7.08	1.03	16.2	0.25	1.20
100	145	6.99	1.04	15.5	-0.45	1.30

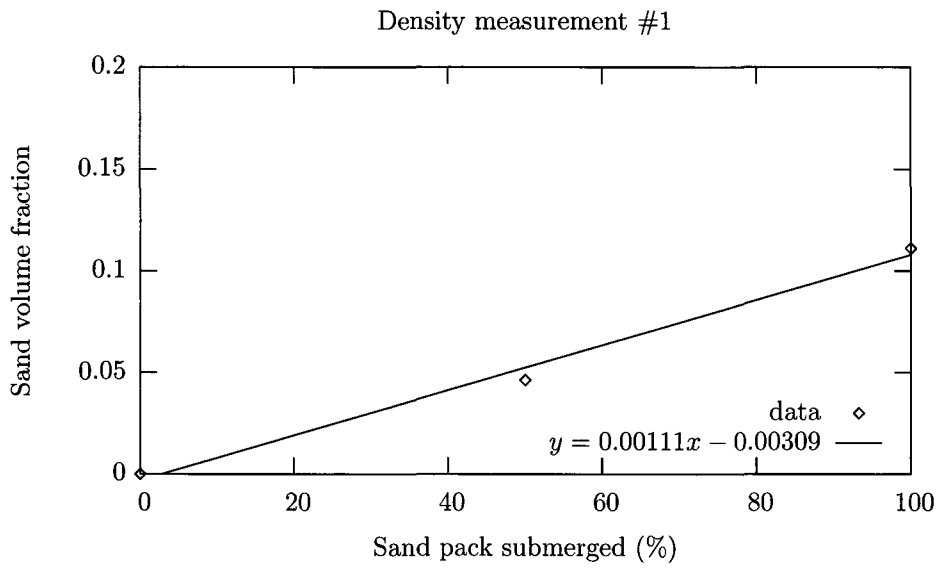
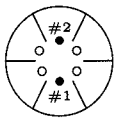


Figure N.8: Measurement 1: Calculation of the sand volume fraction in the water using the C.R.I.M. model. A non-weighted fit using $y = ax + b$ yields $a = 0.00111 \pm 0.00011$ and $b = -0.00309 \pm 0.0069$. The weighted sum of squared residuals was not determined.

N.2.2 Measurement 2: Three sand packs

Measurement setup:

<div style="border: 1px solid black; padding: 5px; display: inline-block;"> <p style="margin: 0;">Antennas and shields</p>  </div>	Date: October 4-6, 2004			
	Experiment settings	Frequency:	62.6 MHz	
		Antennas:	Source:	#1
			Receive:	#2
Shields:		All 6 present		
Low pass filter:	Yes			
Source signal:	pickup before amplifier			
Equipment used	Frequency generator:	Oscillator		
	Power amplifier:	-		
	Pre amplifier:	-		
	VSWR meter:	Diamond SX-1000		
	Oscilloscope:	Fluke Combiscope PM3380B		
Oscilloscope settings	CH1:	Connection:	Send	
		Setting:	50 mV/DIV	
		Termination:	50 Ω	
	CH2:	Connection:	Receive	
		Setting:	1 V/DIV	
		Termination:	1 MΩ	
	Timing	Timebase:	5 ns/DIV	
		Sampling rate:	10 GSa/s	
	Remarks	Phase difference was measured in interval $T < \Delta t < 2T$, hence the notation " $\Delta t(+1T)$ "		

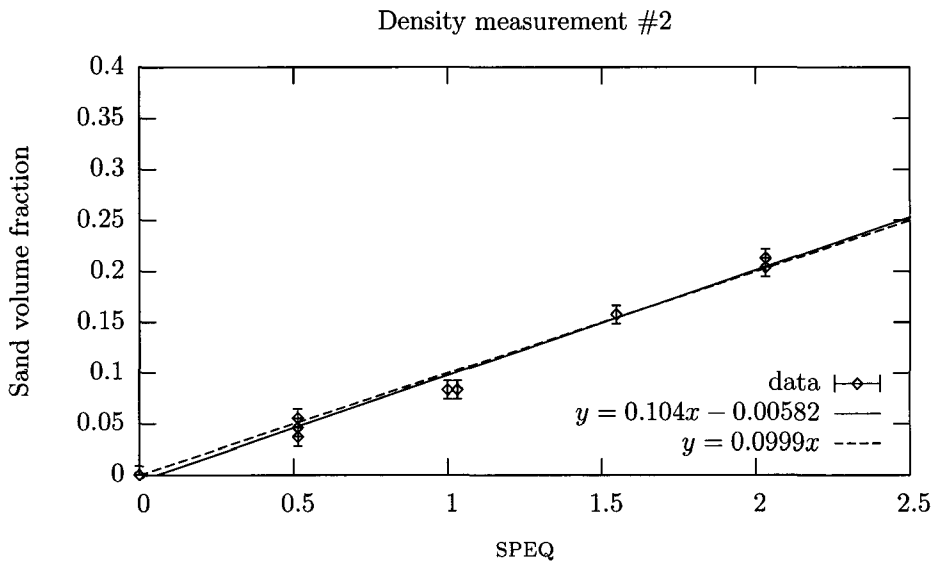


Figure N.9: Measurement 2: Calculation of the sand volume fraction in the water using the C.R.I.M. model. Weighted fits using $y = ax + b$ and $y = cx$ yield $a = 0.104 \pm 0.003$, $b = -0.00582 \pm 0.00346$ and $c = 0.09991 \pm 0.00208$. The weighted sums of squared residuals are $\chi^2_\nu = 1.14$ and $\chi^2_\nu = 1.27$ respectively.

Measurement data:

Table N.8: Measurement data

#packs	pack seq.	V_{src} (mV) ± 1	V_{rec} (V) ± 0.04	$V_r/V_s _0$	$\Delta t(+1T)$ (ns) ± 0.1	Δt (ns)	VSWR ± 0.025	Remarks
0		151	7.97	1.0	22.9	6.93	1.30	
1	1	141	7.25	0.97	22.0	6.03	1.20	sand level -20 cm
0		151	7.97	1.00	22.9	6.93	1.20	
0		151	7.84	0.98	22.9	6.93	1.20	
0		151	7.73	0.97	22.9	6.93	1.20	
1	2	148	7.92	1.01	22.0	6.03	1.30	
2	1,2	152	7.33	0.91	20.6	4.63	1.38	
2	1,2	148	7.13	0.91	20.7	4.73	1.35	
1	1	146	7.75	1.01	22.0	6.03	1.23	
0		149	7.57	0.96	22.9	6.93	1.20	
0.5	3	149	7.39	0.94	22.1	6.13	1.33	pack in mid pos.
0.5	3	156	7.22	0.88	21.9	5.93	1.30	pack near ant. #1
frame	3	150	7.65	0.97	22.9	6.93	1.20	empty frame
frame	2	151	7.91	0.99	22.7	6.73	1.20	empty frame
0		151	8.1	1.02	22.7	6.73	1.20	water level -30cm

Note: sand pack sequence from transmitter antenna to receiver antenna.

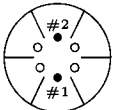
Table N.8: Measurement data (cont.)

#packs	pack seq.	V_{src} (mV) ± 1	V_{rec} (V) ± 0.04	$V_r/V_s _0$	$\Delta t(+1T)$ (ns) ± 0.1	Δt (ns)	VSWR ± 0.025	Remarks
0		146	7.48	1.00	22.9	6.93	1.20	
0.5	3	148	7.52	0.99	22.4	6.43	1.25	mid position
0.5	3	154	7.54	0.96	22.3	6.33	1.25	near transm. ant.
0.5	3	150	7.83	1.02	22.5	6.53	1.20	near receiver ant.
1.5	3,1	150	7.08	0.92	21.2	5.23	1.40	
2.5	3,1,2	152	7.22	0.93	20.0	4.03	1.33	
1.5	3,1	153			21.2	5.23	1.40	V_{rec} not measured
0.5	3	150	7.71	1.00	22.4	6.43	1.30	
1	1	141	7.25	0.97	22.0	6.03	1.2	
0	0	151	7.97	1.00	22.9	6.93	1.2	
0	0	151	7.84	0.98	22.9	6.93	1.2	
0	0	151	7.73	0.97	22.9	6.93	1.2	
1	2	148	7.92	1.01	22.0	6.03	1.3	
2	1,2	152	7.33	0.91	20.6	4.63	1.375	
2	1,2	148	7.13	0.91	20.7	4.73	1.35	
1	1	146	7.75	1.01	22.0	6.03	1.225	
0	0	149	7.57	0.96	22.9	6.93	1.2	

Note: sand pack sequence from transmitter antenna to receiver antenna.

N.2.3 Measurement 3: Improved sand packs

Measurement setup:

<div style="border: 1px solid black; padding: 5px; width: fit-content;"> <p>Antennas and shields</p>  </div>	Date: October 13, 2004		
	Experiment settings	Frequency:	62.6 MHz
		Antennas:	Source: #1 Receive: #2
		Shields:	All 6 present
		Low pass filter:	Yes
	Source signal:	pickup before amplifier	
Equipment used	Frequency generator:	Oscillator	
	Power amplifier:	-	
	Pre amplifier:	-	
	VSWR meter:	Diamond SX-1000	
	Oscilloscope:	Fluke Combiscope PM3380B	
Oscilloscope settings	CH1:	Connection:	Send
		Setting:	50 mV/DIV
		Termination:	50 Ω
	CH2:	Connection:	Receive
		Setting:	1 V/DIV
		Termination:	1 MΩ
Timing	Timebase:	5 ns/DIV	
	Sampling rate:	10 GSa/s	
Remarks	First measurements with the modified sand packs. Phase difference was measured in interval $T < \Delta t < 2T$, hence the notation " $\Delta t(+1T)$ "		

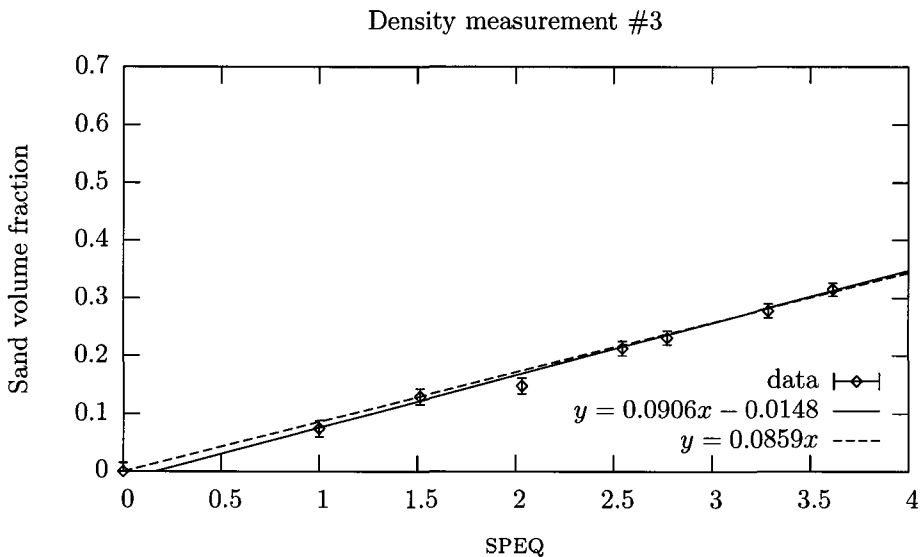


Figure N.10: Measurement 3: Calculation of the sand volume fraction in the water using the C.R.I.M. model. Weighted fits using $y = ax + b$ and $y = cx$ yield $a = 0.0906 \pm 0.003$, $b = -0.0148 \pm 0.0086$ and $c = 0.0859 \pm 0.0014$. The weighted sums of squared residuals are $\chi^2_\nu = 0.75$ and $\chi^2_\nu = 0.93$ respectively.

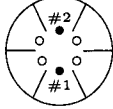
Table N.9: Measurement data

#packs	pack seq.	V_{src} (mV) ± 1	V_{rec} (V) ± 0.04	V_r/V_{s10}	$\Delta t(+1T)$ (ns) ± 0.1	Δt (ns)	VSWR ± 0.025
0		156	7.59	1.00	23.0	7.03	1.20
0.9638	2	153	7.45	1.00	22.2	6.23	1.28
1.3679	3,2	159	7.23	0.93	21.6	5.63	1.30
2.3679	3,2,1	160	7.01	0.90	20.7	4.73	1.33
1.9638	2,1	153	7.33	0.98	21.4	5.43	1.30
2.641	2,1,5	154	7.57	1.01	20.5	4.53	1.15
3.0451	3,2,1,5	157	7.64	1.00	20.0	4.03	1.18
3.8392	4,3,2,1,5	162	7.41	0.94	19.0	3.03	1.10
3.4351	4,2,1,5	161	7.71	0.98	19.6	3.63	1.13

Note: sand pack sequence from transmitter antenna to receiver antenna.

N.2.4 Measurement 4: Goodwill oscilloscope

Measurement setup:

<div style="border: 1px solid black; padding: 5px; display: inline-block;"> <p style="margin: 0;">Antennas and shields</p>  </div>	Date: October 14, 2004		
	Experiment settings	Frequency: 62.8 MHz Antennas: Source: #1 Receive: #2 Shields: All 6 present Low pass filter: Yes Source signal: pickup before amplifier	
Equipment used	Frequency generator: Oscillator Power amplifier: - Pre amplifier: - VSWR meter: Diamond SX-1000 Oscilloscope: Goodwill GDS-840S		
Oscilloscope settings	CH1:	Connection: Send Setting: 20 mV/DIV Termination: 50 Ω	
	CH2:	Connection: Receive Setting: 2 V/DIV Termination: 1 MΩ	
	Timing	Timebase: 1 ns/DIV Sampling rate: 25 GSa/s	
Remarks	Δt measured directly. VSWR measurements skipped.		

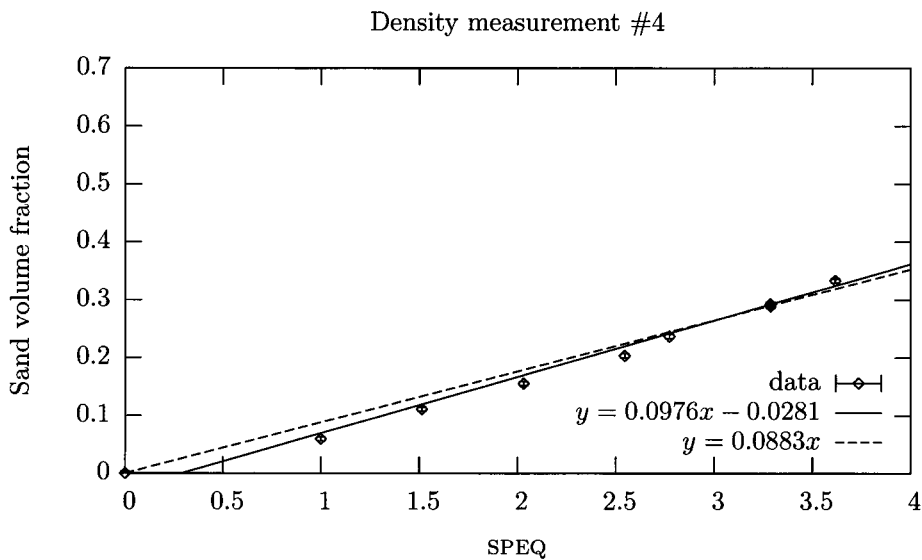


Figure N.11: Measurement 4: Calculation of the sand volume fraction in the water using the C.R.I.M. model. Weighted fits using $y = ax + b$ and $y = cx$ yield $a = 0.0976 \pm 0.0041$, $b = -0.0281 \pm 0.0112$ and $c = 0.08828 \pm 0.00235$. The weighted sums of squared residuals are $\chi^2_\nu = 18.5$ and $\chi^2_\nu = 29.41$ respectively.

Table N.10: Measurement data

#packs	pack seq.	V_{src} (mV) ± 1	V_{rec} (V) ± 0.04	$V_r/V_s _0$	Δt (ns) ± 0.04	VSWR ± 0.025
0		104	7.12	1.00	7.12	1.28
0.964	2	107	7.90	1.08	6.48	
1.368	3,2	105	8.08	1.12	5.92	
1.964	1,2	108	8.08	1.09	5.44	
2.368	3,2,1	111	7.68	1.01	4.92	
3.045	3,1,2,5	105	8.24	1.15	4.00	
2.641	1,2,5	105	8.20	1.14	4.56	
3.045	3,1,2,5	109	8.08	1.08	3.96	
3.839	4,3,1,2,5	108	8.00	1.08	2.84	
3.435	4,1,2,5	108	7.92	1.07	3.52	1.10

Note: sand pack sequence from transmitter antenna to receiver antenna.

N.2.5 Measurement 5: Painted pipe

Measurement setup:

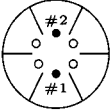
<div style="border: 1px solid black; padding: 5px; display: inline-block;"> <p style="margin: 0;">Antennas and shields</p>  </div>	Date: November 1, 2004		
	Experiment settings	Frequency:	60.2 MHz
	Antennas:	Source: #1	Receive: #2
	Shields:	All 6 present	
	Low pass filter:	Yes	
	Source signal:	pickup before amplifier	
Equipment used	Frequency generator:	Oscillator	
	Power amplifier:	-	
	Pre amplifier:	-	
	VSWR meter:	Diamond SX-1000	
	Oscilloscope:	Goodwill GDS-840S	
Oscilloscope settings	CH1:	Connection:	Send
		Setting:	20 mV/DIV
		Termination:	50 Ω
	CH2:	Connection:	Receive
		Setting:	2 V/DIV
		Termination:	1 MΩ
	Timing	Timebase:	1 ns/DIV
		Sampling rate:	25 GSa/s
Remarks	First measurement after the metal pipe has been sand blasted and coated. Two times the phase difference was measured including half a period, hence the column " $\Delta t(+1/2T)$ "		

Table N.11: Measurement data

#packs	pack seq.	V_{src} (mV) ± 1	V_{rec} (V) ± 0.04	$V_r/V_s _0$	$\Delta t(+1/2T)$ (ns) ± 0.04	Δt (ns) ± 0.04	VSWR ± 0.025
0		114	8.00	1.00		3.92	1.05
0.964	2	100	8.32	1.19		3.00	1.13
1.368	3,2	102	8.08	1.13		2.40	1.13
2.368	3,1,2	103	7.24	1.00		1.44	1.10
1.964	1,2	104	7.36	1.01		1.80	1.18
2.368	3,1,2	104	7.04	0.96		1.40	1.10
3.045	3,1,2,5	98.4	5.22	0.76	8.24	-0.07	1.50
2.641	1,2,5	102	4.64	0.65		0.40	1.50
3.045	3,1,2,5	102	5.04	0.70	8.28	-0.03	1.45
3.045	3,1,2,5	100	5.44	0.78		-0.28	1.50
3.435	4,1,2,5	104	5.92	0.81		-0.56	1.38
3.839	4,3,2,1,5	128	6.40	0.71		-1.48	1.20
3.435	4,1,2,5						1.10

Note: sand pack sequence from transmitter antenna to receiver antenna.

Note 2: Last measurement (VSWR only) performed at frequency of 61.97 MHz

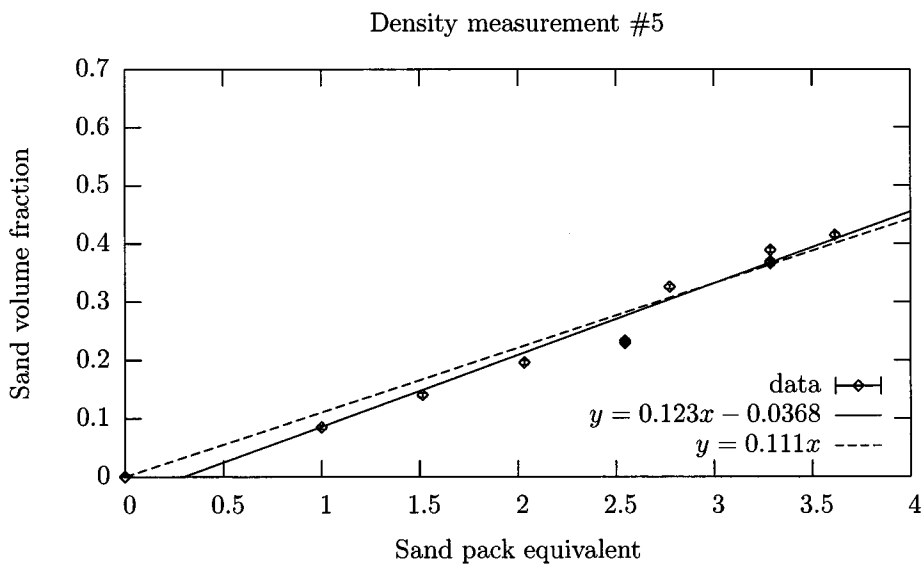


Figure N.12: Measurement 5: Calculation of the sand volume fraction in the water using the C.R.I.M. model. Weighted fits using $y = ax + b$ and $y = cx$ yield $a = 0.123 \pm 0.007$, $b = -0.0368 \pm 0.0192$ and $c = 0.1108 \pm 0.0032$. The weighted sums of squared residuals are $\chi^2_\nu = 55.03$ and $\chi^2_\nu = 68.46$ respectively.

N.2.6 Measurement 6: Third antenna

Measurement setup:

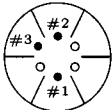
<div style="border: 1px solid black; padding: 5px; display: inline-block;"> <p style="margin: 0;">Antennas and shields</p>  </div>	Date: November 8, 2004		
	Experiment settings	Frequency:	61.8 MHz
		Antennas:	Source: varies
			Receive: varies
Shields:		All 6 present	
	Low pass filter:	Yes	
	Source signal:	pickup before amplifier	
Equipment used	Frequency generator:	Oscillator	
	Power amplifier:	-	
	Pre amplifier:	-	
	VSWR meter:	Diamond SX-1000	
	Oscilloscope:	Fluke Combiscope PM3380B	
Oscilloscope settings	CH1:	Connection:	Send
		Setting:	20 mV/DIV
		Termination:	50 Ω
	CH2:	Connection:	Receive
		Setting:	0.5 V/DIV
		Termination:	1 M Ω
	Timing	Timebase:	5 ns/DIV
Sampling rate:		10 GSa/s	
Remarks	Phase difference was measured in interval $T < \Delta t < 2T$, hence the notation " $\Delta t(+1T)$ "		

Table N.12: Measurements between all three antennas

Antenna config	d_{ant} (m)	#packs	V_{src} (mV) ± 1	V_{rec} (V) ± 0.04	$V_r/V_s _0$	$\Delta t(+1T)$ (ns) ± 0.1	Δt (ns) ± 0.1	VSWR ± 0.025
1 \rightarrow 2	0.47	0	151	7.36	1.00	21.7	5.52	1.05
1 \rightarrow 3	0.40	0	151	5.15	0.70	21.3	5.12	1.13
3 \rightarrow 2	0.23	0	170	3.23	0.39	18.3	2.12	1.13
3 \rightarrow 1	0.40	0	162	3.39	0.43	21.4	5.22	1.10
2 \rightarrow 1	0.47	0	163	7.03	0.89	21.7	5.52	1.18
2 \rightarrow 3	0.23	0	156	4.27	0.56	19.4	3.22	1.10

Table N.13: Measurements between antennas #1 and #2 (at 180 $^\circ$)

Antenna config	#packs	pack seq.	V_{src} (mV) ± 1	V_{rec} (V) ± 0.04	$V_r/V_s _0$	$\Delta t(+1T)$ (ns) ± 0.1	Δt (ns) ± 0.1	VSWR ± 0.025
1 \rightarrow 2	0		158	7.24	1.00	19.8	3.17	1.10
1 \rightarrow 2	0.720	5 \perp (#1, #2)	149	6.86	1.00	18.8	2.17	1.20
2 \rightarrow 1	0.720	5 \perp (#1, #2)	160	6.94	0.95	19.5	2.87	1.08

Note: sand pack sequence "5 \perp (#1, #2)" means that sand pack number 5 has been placed perpendicular to the line through antennas #1 and #2.

Table N.14: Measurements between antennas #1 and #3 (at 120°)

Antenna config	#packs	pack seq.	V_{src} (mV) ± 1	V_{rec} (V) ± 0.04	$V_r/V_s _0$	$\Delta t(+1T)$ (ns) ± 0.1	Δt (ns) ± 0.1	VSWR ± 0.025
3 → 1	0		177	3.74	1.00	19.7	3.07	1.20
1 → 3	0.720	5 \perp (#1, #2)	147	4.34	1.40	18.5	1.87	1.30
1 → 3	0.720	5 \perp (#1, #2)	150	4.38	1.38	18.7	2.07	1.30
1 → 3	0.720	5 \perp (#1, #2)	148	4.23	1.35	17.4	0.77	1.40

Note: sand pack sequence “5 \perp (#1, #2)” means that sand pack number 5 has been placed perpendicular to the line through antennas #1 and #2.

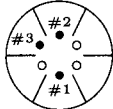
Table N.15: Measurements between antennas #2 and #3 (at 60°)

Antenna config	#packs	pack seq.	V_{src} (mV) ± 1	V_{rec} (V) ± 0.04	$V_r/V_s _0$	$\Delta t(+1T)$ (ns) ± 0.1	Δt (ns) ± 0.1	VSWR ± 0.025	Remarks
3 → 2	0		171	4.43	1.00	17.7	1.07	1.10	
2 → 3	0		136	4.82	1.37	16.4	-0.23	1.30	
2 → 3	0.720	5 \perp (#1, #2)	140	6.06	1.67	15.5	-1.13	1.40	
2 → 3	0.720	5 \parallel (#2, #3)	139	6.69	1.86	15.8	-0.83	1.30	mid position
2 → 3	0.720	5 \parallel (#2, #3)	137	5.35	1.51	16.3	-0.33	1.30	far from ant.
2 → 3	0.720	5 \parallel (#2, #3)	136	4.94	1.40	14.7	-1.93	1.30	close to ant.
2 → 3	0.720	5 \parallel (#2, #3)	137	5.31	1.50	16.3	-0.33	1.30	far from ant.
2 → 3	1.720	1,5 \parallel (#2, #3)	140	6.65	1.83	15.6	-1.03	1.30	1: mid, 5: far
2 → 3	0.720		137	6.52	1.84	15.6	-1.03	1.30	
2 → 3	0.720		132	4.62	1.35	16.2	-0.43	1.30	

Note: sand pack sequence “5 \parallel (#2, #3)” means that sand pack number 5 has been placed parallel to the line through antennas #2 and #3.

N.2.7 Measurement 7: Agilent oscilloscope

Measurement setup:

<div style="border: 1px solid black; padding: 5px; width: fit-content;"> <p style="margin: 0;">Antennas and shields</p>  </div>	Date: November 12, 2004			
	Experiment settings	Frequency:	62.518 MHz	
		Antennas:	Source:	#1
		Receive:	#2	
	Shields:	All 6 present		
	Low pass filter:	Yes		
	Source signal:	pickup before amplifier		
Equipment used	Frequency generator:	Oscillator		
	Power amplifier:	-		
	Pre amplifier:	-		
	VSWR meter:	Diamond SX-1000		
	Oscilloscope:	Agilent 54832D		
Oscilloscope settings	CH1:	Connection:	Send	
		Setting:	50 mV/DIV	
		Termination:	50 Ω	
	CH2:	Connection:	Receive	
		Setting:	2 V/DIV	
		Termination:	1 MΩ	
Timing	Timebase:	500 ps - 1 ns/DIV		
	Sampling rate:	250 GSa/s (eq. time)		
Remarks	Phase difference was measured in interval $T < \Delta t < 2T$, hence the notation " $\Delta t(+1T)$ "			

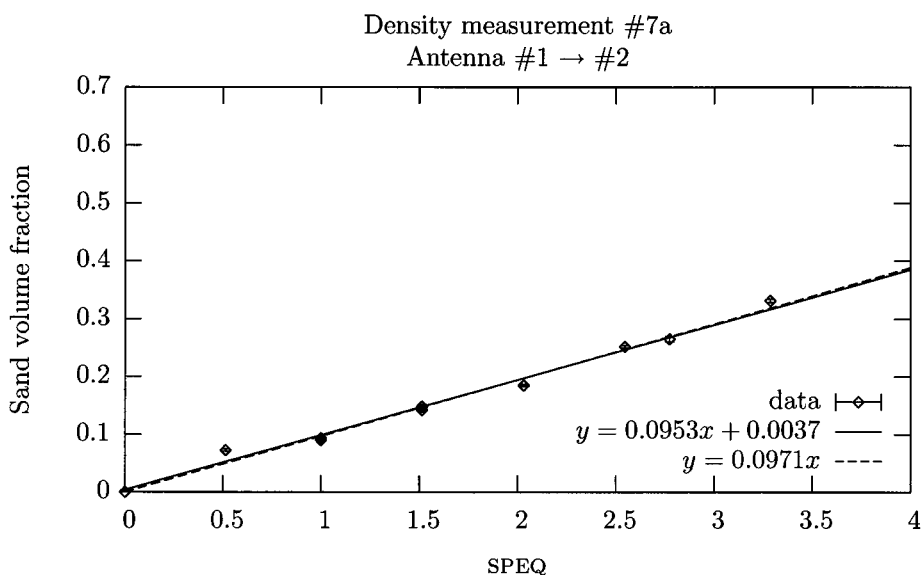


Figure N.13: Measurement 7a: Calculation of the sand volume fraction in the water using the C.R.I.M. model. Weighted fits using $y = ax + b$ and $y = cx$ yield $a = 0.0953 \pm 0.0043$, $b = 0.0037 \pm 0.0075$ and $c = 0.09706 \pm 0.00214$. The weighted sums of squared residuals are $\chi^2_\nu = 29.72$ and $\chi^2_\nu = 27.22$ respectively.

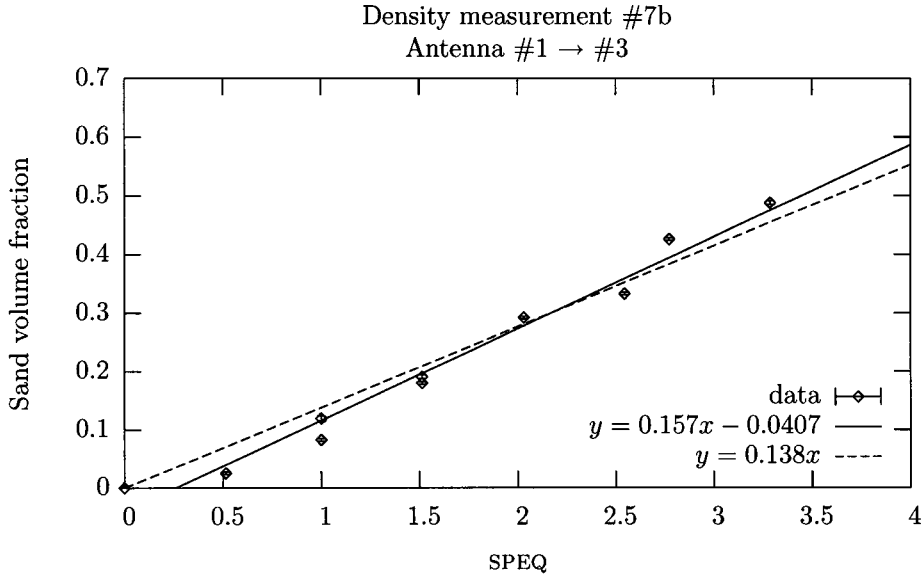


Figure N.14: Measurement 7b: Calculation of the sand volume fraction in the water using the C.R.I.M. model. Weighted fits using $y = ax + b$ and $y = cx$ yield $a = 0.157 \pm 0.009$, $b = -0.0407 \pm 0.0168$ and $c = 0.1382 \pm 0.006$. The weighted sums of squared residuals are $\chi^2_\nu = 137.16$ and $\chi^2_\nu = 211.74$ respectively.

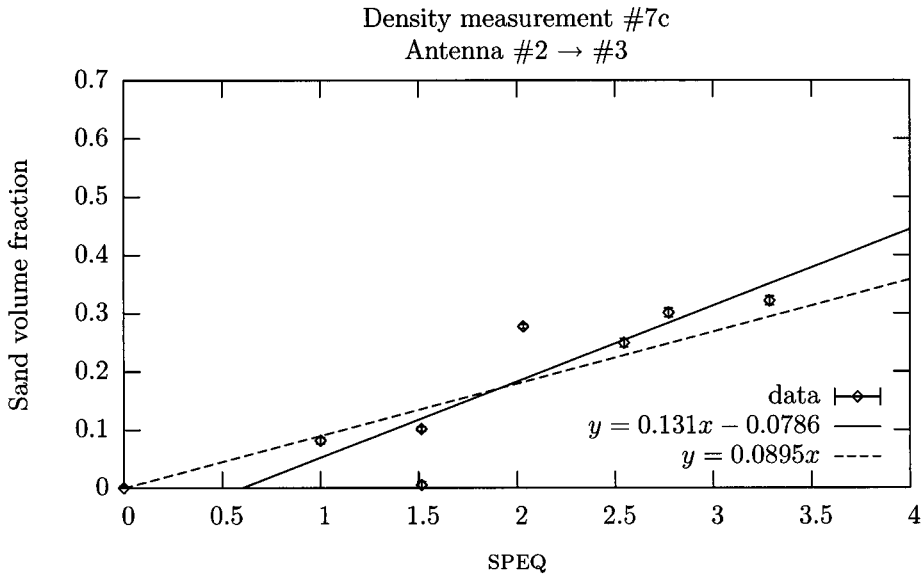


Figure N.15: Measurement 7c: Calculation of the sand volume fraction in the water using the C.R.I.M. model. Weighted fits using $y = ax + b$ and $y = cx$ yield $a = 0.131 \pm 0.028$, $b = -0.0786 \pm 0.043$ and $c = 0.08954 \pm 0.01778$. The weighted sums of squared residuals are $\chi^2_\nu = 259.81$ and $\chi^2_\nu = 327.36$ respectively.

Table N.16: Measurements with all three antennas

Antenna config	d_{ant} m	#packs	V_{src} (mV) ± 3	V_{rec} (V) ± 0.2	$V_r/V_s _0$	Δt (ns)	VSWR ± 0.025
1 → 2	0.47	0	159.5	9.35	1.00	7.18 ± 0.03	1.25
1 → 3	0.40	0	164.0	6.33	1.00	6.57 ± 0.02	1.10
2 → 3	0.23	0	164.0	4.31	1.00	3.83 ± 0.02	1.10
1 → 2	0.47	0.964	156.6	9.14	1.00	6.21 ± 0.02	1.20
1 → 3	0.40	0.964	153.1	7.56	1.28	5.47 ± 0.04	1.10
2 → 3	0.23	0.964	156.5	7.62	1.85	3.40 ± 0.03	1.10
1 → 2	0.47	1.368	158.1	8.78	0.95	5.65 ± 0.03	1.20
1 → 3	0.40	1.368	152.0	7.69	1.31	4.82 ± 0.03	1.10
2 → 3	0.23	1.368	148.6	8.97	2.30	3.29 ± 0.02	1.10
1 → 2	0.47	2.368	161.0	8.51	0.90	4.47 ± 0.02	1.20
1 → 3	0.40	2.368	155.3	7.43	1.24	3.51 ± 0.02	1.10
2 → 3	0.23	2.368	151.0	10.95	2.76	2.51 ± 0.04	1.10
1 → 2	0.47	2.368	162.9	8.35	0.87	4.45 ± 0.03	1.20
1 → 2	0.47	3.045	162.5	7.06	0.74	3.60 ± 0.03	1.20
1 → 3	0.40	3.045	161.2	6.29	1.01	2.09 ± 0.03	1.10
2 → 3	0.23	3.045	147.8	9.58	2.47	2.13 ± 0.04	1.10
1 → 2	0.47	2.641	165.6	7.99	0.82	4.32 ± 0.05	1.20
1 → 3	0.40	2.641	163.0	6.97	1.11	2.66 ± 0.02	1.10
2 → 3	0.23	2.641	147.5	9.77	2.52	2.24 ± 0.04	1.10
1 → 2	0.47	1.964	151.8	8.63	0.97	5.19 ± 0.02	1.20
1 → 3	0.40	1.964	149.6	7.50	1.30	3.89 ± 0.02	1.10
2 → 3	0.23	1.964	154.2	9.77	2.41	2.36 ± 0.02	1.10
1 → 2	0.47	0.964	161.6	9.34	0.99	6.18 ± 0.02	1.20
1 → 3	0.40	0.964	157.4	8.05	1.33	5.81 ± 0.02	1.10
2 → 3	0.23	0.964	161.5	8.00	1.89	4.08 ± 0.03	1.10
1 → 2	0.47	1.368	162.2	8.78	0.92	5.59 ± 0.04	1.20
1 → 3	0.40	1.368	156.5	8.18	1.35	4.92 ± 0.02	1.10
2 → 3	0.23	1.368	155.5	9.39	2.30	3.80 ± 0.03	1.10
1 → 2	0.47	0.404	162.2	9.11	0.96	6.40 ± 0.02	1.20
1 → 3	0.40	0.404	161.7	7.26	1.16	6.34 ± 0.02	1.10
2 → 3	0.23	0.404	161.8	6.01	1.41	4.23 ± 0.02	1.10

N.3 River water measurements

Measurements in “river” water were not performed in real river water, but ordinary salt was added to tap water. This way, the salinity of the water could be controlled more easily and varied more accurately. The density measurements were fitted to the C.R.I.M. model. The regression parameters of the linear fit $y = ax + b$ are summarized in table N.17 below for measurements #4–#9.

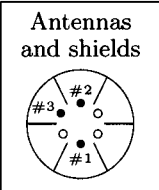
The measurement data of all density measurements in pure water are contained in this section. The raw data from the coaxial probe measurements is not contained as these measurements are regarded to be of secondary importance.

Table N.17: Summary of density measurements in river water. The fit ($y = ax + b$) corresponds to the C.R.I.M. model, where $y = \rho$ and $x = \langle \text{SPEQ} \rangle$.

Meas.#	σ_{inner} (S/m)	σ_{outer} (S/m)	$y = ax + b$	
			$a/10^{-3}$	$b/10^{-3}$
4	0.632	2.1	171 ± 13	3.2 ± 4.9
5	0.637	2.1	165 ± 11	2.5 ± 4.1
6	0.937	2.1	155 ± 6	-0.4 ± 1.7
7	0.744	2.1	152 ± 6	1.7 ± 2.6
8	0.604	2.1	158 ± 10	1.6 ± 3.0
9	0.438	2.1	159 ± 11	1.6 ± 3.1

N.3.1 Measurement 1: 0.61 S/m

Measurement setup:

	Date: December 17, 2004	
	Experiment settings	Frequency: 62.5 MHz Antennas: Source: #1 Receive: #2 Shields: All 6 present Low pass filter: Yes Source signal: pickup before amplifier
Equipment used	Frequency generator: HP 8647A Power amplifier: R.F.P.A. RF001220-25 Pre amplifier: - VSWR meter: Diamond SX-1000 Oscilloscope: Agilent Infiniium 54831D	
Oscilloscope settings	CH1:	Connection: Send Setting: (variable) mV/DIV Termination: 50 Ω
	CH2:	Connection: Receive Setting: (variable) V/DIV Termination: 1 M Ω
	Timing	Timebase: 10 ns/DIV Sampling rate: 250 GSa/s (eq. time)
Remarks	$\sigma_{\text{inner pipe}} = 0.61 \pm 0.01 \text{ S/m}, T = 15.5 \pm 0.5 \text{ }^\circ\text{C}$	

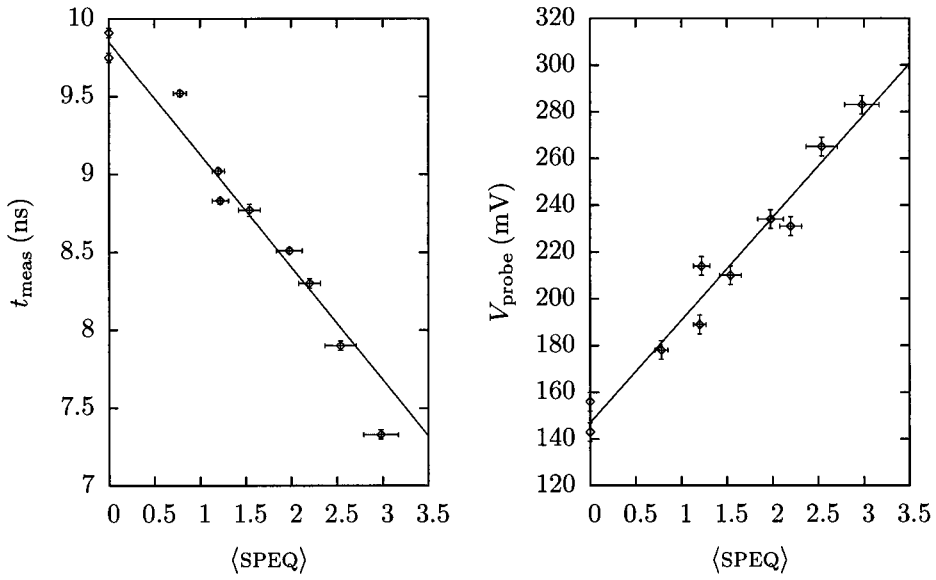


Figure N.16: Measurement 1: plots of the measured propagation times and voltages received by antenna #2.

Table N.18: Measurement data

pack seq.	SPEQ	V_{src} (mV) ± 4	V_{rec} (mV) ± 4	$V_r/V_s _0$	Δt (ns)	VSWR ± 0.03
-	0	188	143	1.00	9.91 \pm 0.03	1.35
4	0.794	187	178	1.25	9.52 \pm 0.02	1.35
4,3	1.198	187	214	1.50	8.83 \pm 0.02	1.35
4,3,5	1.875	187	234	1.65	8.51 \pm 0.02	1.35
4,5	1.471	187	210	1.48	8.77 \pm 0.04	1.35
4,2,5	2.435	186	265	1.87	7.90 \pm 0.03	1.35
4,2,3,5	2.839	186	283	2.00	7.33 \pm 0.03	1.35
2,3,5	2.045	186	231	1.63	8.30 \pm 0.03	1.35
3,5	1.081	186	189	1.34	9.02 \pm 0.02	1.35
-	0	187	156	1.10	9.75 \pm 0.03	1.35

N.3.2 Measurement 2: 0.46 S/m

Measurement setup:

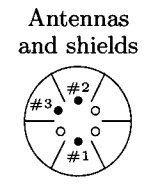
 <p>Antennas and shields</p>	Date: January 17, 2005		
	Experiment settings	Frequency:	62.5 MHz
		Antennas:	Source: #1 Receive: #2
		Shields:	All 6 present
		Low pass filter:	No
	Source signal:	pickup before amplifier	
Equipment used	Frequency generator:	HP 8647A	
	Power amplifier:	R.F.P.A. RF001220-25	
	Pre amplifier:	-	
	VSWR meter:	Diamond SX-1000	
	Oscilloscope:	Agilent Infiniium 54831D	
Oscilloscope settings	CH1:	Connection:	Send
		Setting:	(variable) mV/DIV
		Termination:	50 Ω
	CH2:	Connection:	Receive
		Setting:	(variable) V/DIV
		Termination:	1 MΩ
	Timing	Timebase:	10 ns/DIV
		Sampling rate:	250 GSa/s (eq. time)
Remarks	$\sigma_{\text{inner pipe}} = 0.46 \pm 0.01 \text{ S/m}, T = 16.0 \pm 0.5 \text{ }^\circ\text{C}$ $\sigma_{\text{outer pipe}} = 2.13 \pm 0.02 \text{ S/m}, T = 16.5 \pm 0.5 \text{ }^\circ\text{C}$		

Table N.19: Measurement data

pack seq.	SPEQ	V_{src} (mV) ±2	V_{rec} (mV) ±2	$V_r/V_s _0$	Δt (ns)	VSWR ±0.03
5,2,3,4	2.839	317	192	0.98	14.71 ± 0.02	1.65
5,2,4	2.435	314	183	0.94	15.46 ± 0.03	1.65
5,2,3	2.045	312	175	0.91	15.96 ± 0.01	1.60
5,2	1.641	312	167	0.87	16.68 ± 0.04	1.60
5,3	1.081	310	166	0.87	17.41 ± 0.04	1.60
5	0.677	310	167	0.87	18.06 ± 0.02	1.60
3	0.404	311	183	0.95	18.59 ± 0.02	1.60
-	0	311	192	1.00	19.40 ± 0.02	1.60
5,2	1.641	310	165	0.86	16.52 ± 0.01	1.60
5,2,3	2.045	310	169	0.88	15.79 ± 0.01	1.60
5,2,3,4	2.839	310	177	0.92	14.46 ± 0.01	1.65

N.3.3 Measurement 3: 0.48 S/m

Measurement setup:

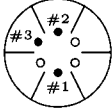
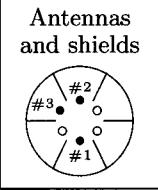
<div style="border: 1px solid black; padding: 5px; display: inline-block;"> <p style="text-align: center; margin: 0;">Antennas and shields</p>  </div>	Date: January 18, 2005			
	Experiment settings	Frequency:	62.5 MHz	
		Antennas:	Source:	#1
			Receive:	#2
Shields:		All 6 present		
	Low pass filter:	No		
	Source signal:	pickup before amplifier		
Equipment used	Frequency generator:	HP 8647A		
	Power amplifier:	R.F.P.A. RF001220-25		
	Pre amplifier:	-		
	VSWR meter:	Diamond SX-1000		
	Oscilloscope:	Agilent Infiniium 54831D		
Oscilloscope settings	CH1:	Connection:	Send	
		Setting:	(variable) mV/DIV	
		Termination:	50 Ω	
	CH2:	Connection:	Receive	
		Setting:	(variable) V/DIV	
		Termination:	1 M Ω	
Timing	Timebase:	10 ns/DIV		
	Sampling rate:	250 GSa/s (eq. time)		
Remarks	$\sigma_{\text{inner pipe}} = 0.476 \pm 0.002 \text{ S/m}, T = 16.7 \pm 0.2 \text{ }^\circ\text{C}$			
	$\sigma_{\text{outer pipe}} = 2.13 \pm 0.02 \text{ S/m}, T = 16.5 \pm 0.5 \text{ }^\circ\text{C}$			

Table N.20: Measurement data

pack seq.	SPEQ	V_{src} (mV) ± 1	V_{rec} (mV) ± 1	$V_r/V_s _0$	Δt (ns)	VSWR ± 0.03
5,2,3,4	2.839	308	172	0.92	14.44 \pm 0.01	1.65
5,2,4	2.435	309	168	0.90	15.24 \pm 0.01	1.65
5,2,3	2.045	309	166	0.89	15.80 \pm 0.02	1.65
5,2	1.641	307	161	0.87	16.61 \pm 0.02	1.65
5,3	1.081	308	162	0.87	17.23 \pm 0.02	1.65
5	0.677	307	162	0.87	18.01 \pm 0.02	1.65
-	0	308	186	1.00	19.48 \pm 0.02	1.65

N.3.4 Measurement 4: 0.63 S/m

Measurement setup:

	Date: January 24, 2005	
	Experiment settings	Frequency: 62.5 MHz Antennas: Source: #1 Receive: #2 Shields: All 6 present Low pass filter: No Source signal: pickup before amplifier
Equipment used	Frequency generator: HP 8647A Power amplifier: R.F.P.A. RF001220-25 Pre amplifier: - VSWR meter: Diamond SX-1000 Oscilloscope: Agilent Infiniium 54831D	
Oscilloscope settings	CH1:	Connection: Send Setting: (variable) mV/DIV Termination: 50 Ω
	CH2:	Connection: Receive Setting: (variable) V/DIV Termination: 1 MΩ
	Timing	Timebase: 10 ns/DIV Sampling rate: 250 GSa/s (eq. time)
Remarks	$\sigma_{\text{inner pipe}} = 0.632 \pm 0.07 \text{ S/m}, T = 15.2 \pm 0.2 \text{ }^\circ\text{C}$ $\sigma_{\text{outer pipe}} = 2.13 \pm 0.02 \text{ S/m}, T = 16.5 \pm 0.5 \text{ }^\circ\text{C}$	

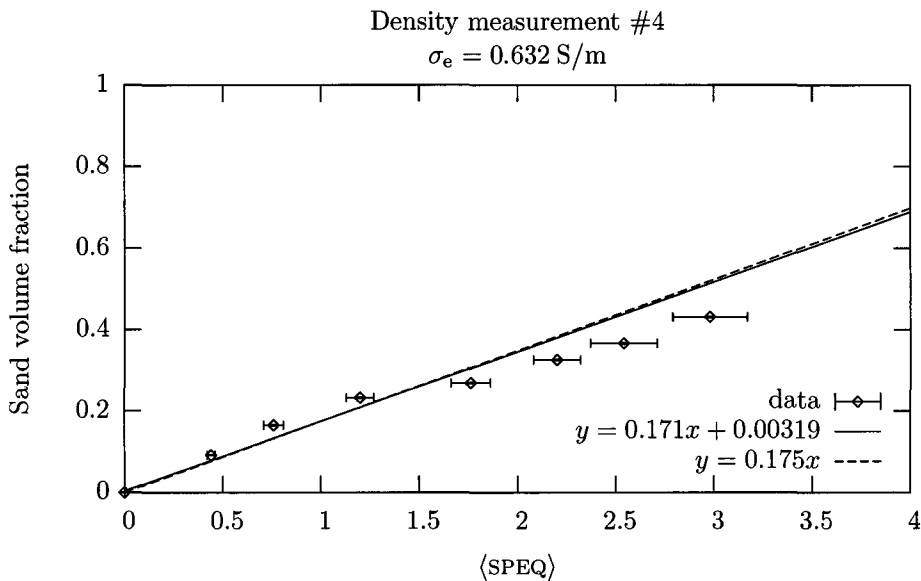


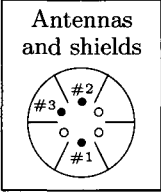
Figure N.17: Measurement 4: Calculation of the sand volume fraction in the water using the C.R.I.M. model. Weighted fits using $y = ax + b$ and $y = cx$ yield $a = 0.171 \pm 0.013$, $b = 0.00319 \pm 0.00493$ and $c = 0.1745 \pm 0.0112$. The weighted sums of squared residuals are $\chi^2_\nu = 15.28$ and $\chi^2_\nu = 14.01$ respectively.

Table N.21: Measurement data

pack seq.	SPEQ	V_{src} (mV) ± 1	V_{rec} (mV) ± 1	$V_r/V_s _0$	Δt (ns)	VSWR ± 0.03
5,2,3,4	2.839	266	121	2.09	5.82 \pm 0.02	1.90
5,2,4	2.435	266	108	1.86	6.79 \pm 0.04	1.90
5,2,3	2.045	266	98	1.69	7.41 \pm 0.03	1.90
5,2	1.641	266	87	1.50	8.26 \pm 0.02	1.90
5,3	1.081	266	76	1.31	8.82 \pm 0.02	1.90
5	0.677	267	68	1.17	9.84 \pm 0.02	1.90
3	0.404	266	61	1.05	10.95 \pm 0.02	1.90
-	0	266	58	1.00	12.34 \pm 0.02	1.90
5	0.677	266	64	1.10	10.06 \pm 0.01	1.90
5,2	1.641	266	80	1.38	8.28 \pm 0.02	1.90
5,2,3	2.045	266	90	1.55	7.41 \pm 0.02	1.90
5,2,3,4	2.839	265	109	1.89	6.16 \pm 0.01	1.90

N.3.5 Measurement 5: 0.64 S/m

Measurement setup:

	Date: January 25, 2005	
	Experiment settings	Frequency: 62.5 MHz Antennas: Source: #1 Receive: #2 Shields: All 6 present Low pass filter: No Source signal: pickup before amplifier
Equipment used	Frequency generator: HP 8647A Power amplifier: R.F.P.A. RF001220-25 Pre amplifier: - VSWR meter: Diamond SX-1000 Oscilloscope: Agilent Infiniium 54831D	
Oscilloscope settings	CH1:	Connection: Send Setting: (variable) mV/DIV Termination: 50 Ω
	CH2:	Connection: Receive Setting: (variable) V/DIV Termination: 1 MΩ
	Timing	Timebase: 10 ns/DIV Sampling rate: 250 GSa/s (eq. time)
Remarks	$\sigma_{\text{inner pipe}} = 0.637 \pm 0.002 \text{ S/m}, T = 15.4 \pm 0.2 \text{ }^\circ\text{C}$ $\sigma_{\text{outer pipe}} = 2.13 \pm 0.02 \text{ S/m}, T = 16.5 \pm 0.5 \text{ }^\circ\text{C}$	

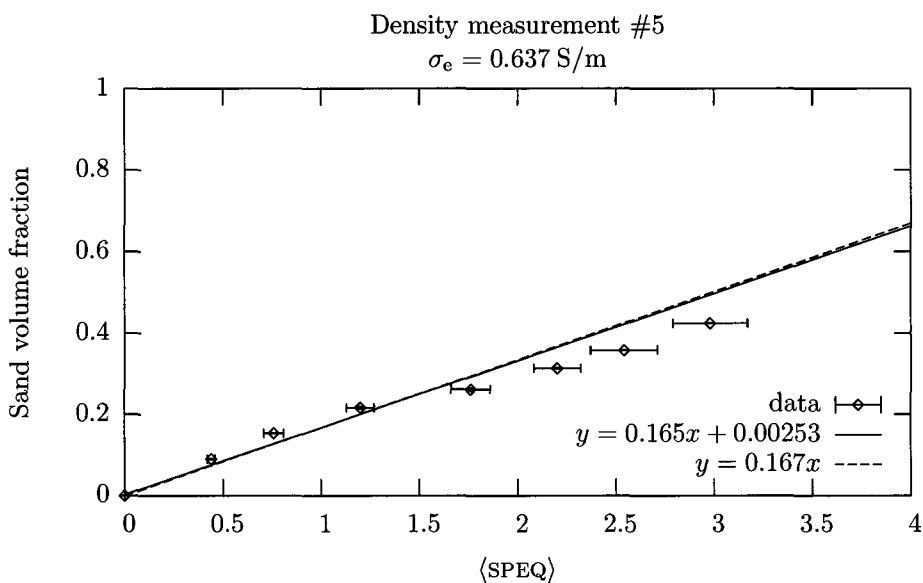


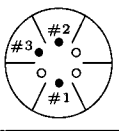
Figure N.18: Measurement 5: Calculation of the sand volume fraction in the water using the C.R.I.M. model. Weighted fits using $y = ax + b$ and $y = cx$ yield $a = 0.165 \pm 0.011$, $b = 0.00253 \pm 0.00407$ and $c = 0.1673 \pm 0.0103$. The weighted sums of squared residuals are $\chi^2_\nu = 12.95$ and $\chi^2_\nu = 11.82$ respectively.

Table N.22: Measurement data

pack seq.	SPEQ	V_{src} (mV) ± 1	V_{rec} (mV) ± 1	$V_r/V_s _0$	Δt (ns)	VSWR ± 0.03
5,2,3,4	2.839	266	109	1.98	6.03 \pm 0.01	1.90
5,2,4	2.435	266	94	1.71	7.05 \pm 0.02	1.90
5,2,3	2.045	266	87	1.58	7.72 \pm 0.03	1.90
5,2	1.641	266	77	1.40	8.52 \pm 0.06	1.90
5,3	1.081	265	65	1.19	9.22 \pm 0.05	1.90
5	0.677	265	61	1.11	10.17 \pm 0.02	1.90
3	0.404	265	56	1.02	11.15 \pm 0.02	1.90
-	0	266	55	1.00	12.53 \pm 0.02	1.90

N.3.6 Measurement 6: 0.94 S/m

Measurement setup:

<div style="border: 1px solid black; padding: 5px; width: fit-content;"> <p>Antennas and shields</p>  </div>	Date: January 28, 2005		
	Experiment settings	Frequency: 62.5 MHz Antennas: Source: #1 Receive: #2 Shields: All 6 present Low pass filter: No Source signal: pickup before amplifier	
Equipment used	Frequency generator: HP 8647A Power amplifier: R.F.P.A. RF001220-25 Pre amplifier: - VSWR meter: Diamond SX-1000 Oscilloscope: Agilent Infinium 54831D		
Oscilloscope settings	CH1:	Connection: Send Setting: (variable) mV/DIV Termination: 50 Ω	
	CH2:	Connection: Receive Setting: (variable) V/DIV Termination: 1 MΩ	
	Timing	Timebase: 10 ns/DIV Sampling rate: 250 GSa/s (eq. time)	
Remarks	$\sigma_{\text{inner pipe}} = 0.937 \pm 0.007 \text{ S/m}, T = 16.0 \pm 0.2 \text{ }^\circ\text{C}$ $\sigma_{\text{outer pipe}} = 2.13 \pm 0.02 \text{ S/m}, T = 16.5 \pm 0.5 \text{ }^\circ\text{C}$		

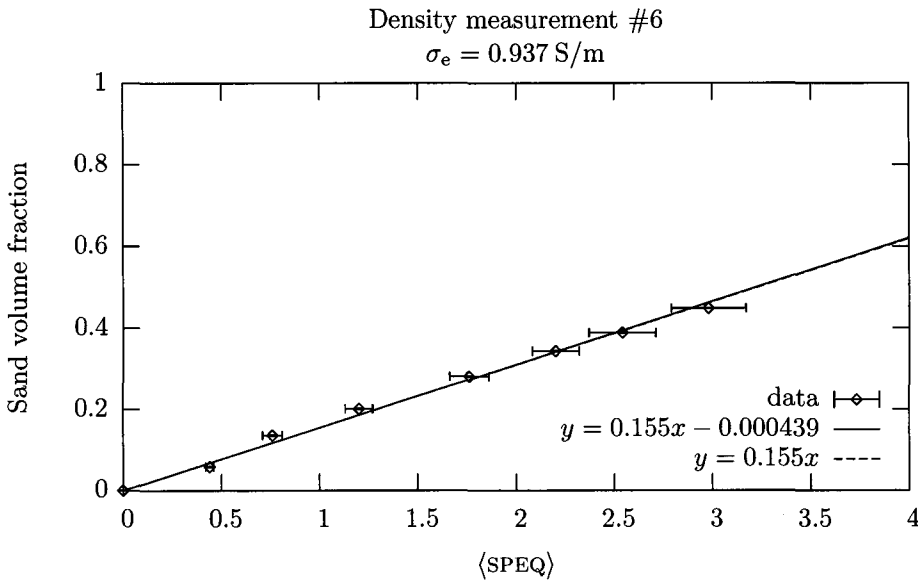


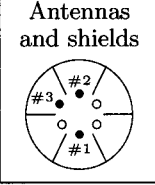
Figure N.19: Measurement 6: Calculation of the sand volume fraction in the water using the C.R.I.M. model. Weighted fits using $y = ax + b$ and $y = cx$ yield $a = 0.155 \pm 0.006$, $b = -0.000439 \pm 0.001653$ and $c = 0.1547 \pm 0.0052$. The weighted sums of squared residuals are $\chi^2_v = 2.79$ and $\chi^2_v = 2.42$ respectively.

Table N.23: Measurement data

pack seq.	SPEQ	V_{src} (mV) ± 1	V_{rec} (mV) ± 0.2	$V_r/V_s _0$	Δt (ns)
5,2,3,4	2.839	258	55.8	1.36	7.57 \pm 0.02
5,2,4	2.435	255	45.5	1.12	8.69 \pm 0.02
5,2,3	2.045	253	38.8	0.97	9.54 \pm 0.03
5,2	1.641	253	34.4	0.86	10.71 \pm 0.03
5,3	1.081	252	29.1	0.73	12.21 \pm 0.03
5	0.677	251	30.5	0.77	13.42 \pm 0.03
3	0.404	251	34.4	0.86	14.88 \pm 0.03
-	0	252	40.0	1.00	15.97 \pm 0.02

N.3.7 Measurement 7: 0.74 S/m

Measurement setup:

	Date: January 28, 2005	
	Experiment settings	Frequency: 62.5 MHz Antennas: Source: #1 Receive: #2 Shields: All 6 present Low pass filter: No Source signal: pickup before amplifier
Equipment used	Frequency generator: HP 8647A Power amplifier: R.F.P.A. RF001220-25 Pre amplifier: - VSWR meter: Diamond SX-1000 Oscilloscope: Agilent Infiniium 54831D	
Oscilloscope settings	CH1:	Connection: Send Setting: (variable) mV/DIV Termination: 50 Ω
	CH2:	Connection: Receive Setting: (variable) V/DIV Termination: 1 MΩ
Timing		Timebase: 10 ns/DIV
		Sampling rate: 250 GSa/s (eq. time)
Remarks	$\sigma_{\text{inner pipe}} = 0.744 \pm 0.005 \text{ S/m}, T = 16.6 \pm 0.5 \text{ }^\circ\text{C}$ $\sigma_{\text{outer pipe}} = 2.13 \pm 0.02 \text{ S/m}, T = 16.5 \pm 0.5 \text{ }^\circ\text{C}$	

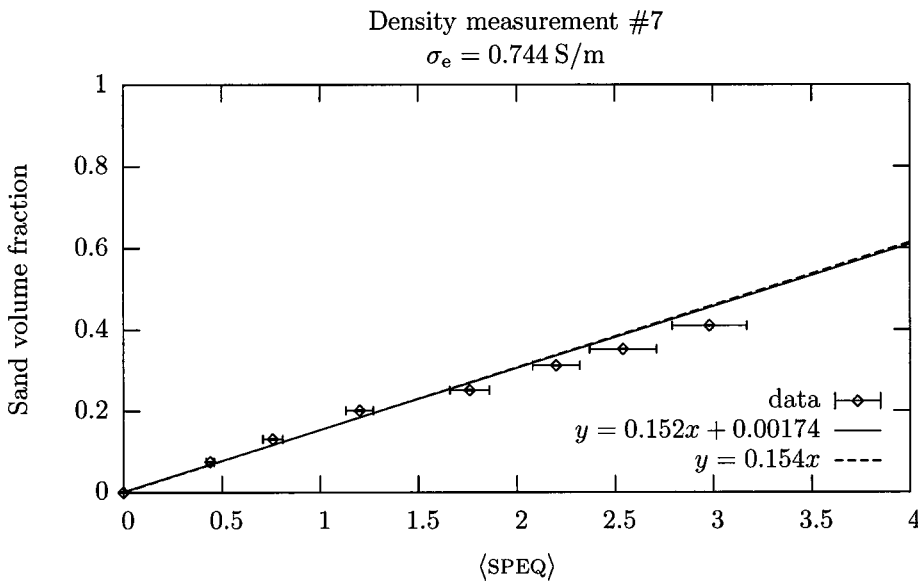


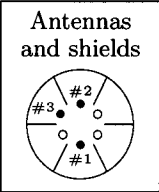
Figure N.20: Measurement 7: Calculation of the sand volume fraction in the water using the C.R.I.M. model. Weighted fits using $y = ax + b$ and $y = cx$ yield $a = 0.152 \pm 0.006$, $b = 0.00174 \pm 0.00261$ and $c = 0.1536 \pm 0.0056$. The weighted sums of squared residuals are $\chi^2_\nu = 3.84$ and $\chi^2_\nu = 3.54$ respectively.

Table N.24: Measurement data

pack seq.	#packs	V_{src} (mV) ± 1	V_{rec} (mV) ± 0.3	$V_r/V_s _0$	Δt (ns)
-	0	253	46.3	1.00	14.28 \pm 0.02
3	0.404	254	41.5	0.89	13.01 \pm 0.02
5	0.677	252	39.9	0.87	12.05 \pm 0.03
5,3	1.081	253	41.0	0.89	10.86 \pm 0.03
5,2	1.641	252	47.6	1.03	10.00 \pm 0.02
5,2,3	2.045	252	53.1	1.15	8.97 \pm 0.02
5,2,4	2.435	252	59.4	1.29	8.28 \pm 0.02
5,2,3,4	2.839	252	69.6	1.51	7.29 \pm 0.02

N.3.8 Measurement 8: 0.60 S/m

Measurement setup:

	Date: January 31, 2005			
	Experiment settings	Frequency:	62.5 MHz	
		Antennas:	Source:	#1
			Receive:	#2
		Shields:	All 6 present	
	Low pass filter:	No		
	Source signal:	pickup before amplifier		
Equipment used	Frequency generator:	HP 8647A		
	Power amplifier:	R.F.P.A. RF001220-25		
	Pre amplifier:	-		
	VSWR meter:	Diamond SX-1000		
	Oscilloscope:	Agilent Infiniium 54831D		
Oscilloscope settings	CH1:	Connection:	Send	
		Setting:	(variable) mV/DIV	
		Termination:	50 Ω	
	CH2:	Connection:	Receive	
		Setting:	(variable) V/DIV	
		Termination:	1 MΩ	
Timing	Timebase:	10 ns/DIV		
	Sampling rate:	250 GSa/s (eq. time)		
Remarks	$\sigma_{\text{inner pipe}} = 0.604 \pm 0.003 \text{ S/m}, T = 15.9 \pm 0.5 \text{ }^\circ\text{C}$ $\sigma_{\text{outer pipe}} = 2.13 \pm 0.02 \text{ S/m}, T = 16.5 \pm 0.5 \text{ }^\circ\text{C}$			

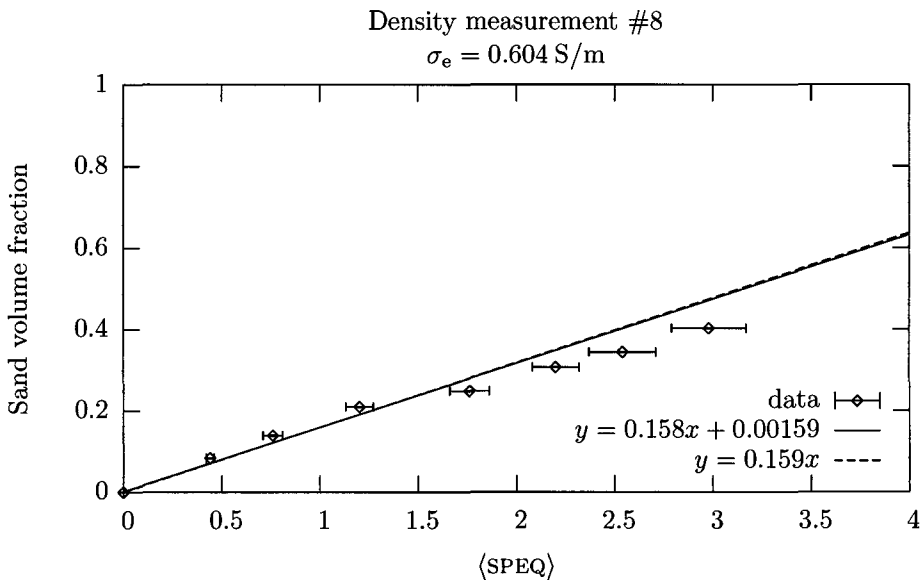


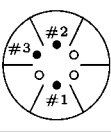
Figure N.21: Measurement 8: Calculation of the sand volume fraction in the water using the C.R.I.M. model. Weighted fits using $y = ax + b$ and $y = cx$ yield $a = 0.158 \pm 0.01$, $b = 0.00159 \pm 0.003$ and $c = 0.1592 \pm 0.0088$. The weighted sums of squared residuals are $\chi^2 = 10.77$ and $\chi^2 = 9.66$ respectively.

Table N.25: Measurement data

pack seq.	#packs	V_{src} (mV) ± 1	V_{rec} (mV) ± 0.3	$V_r/V_s _0$	Δt (ns)
-	0	254	62.4	1.00	12.11 \pm 0.01
5,2,3,4	2.839	255	110.3	1.76	6.12 \pm 0.01
5,2,4	2.435	255	98.0	1.56	6.99 \pm 0.02
5,2,3	2.045	255	90.2	1.44	7.54 \pm 0.01
5,2	1.641	255	81.3	1.30	8.41 \pm 0.02
5,3	1.081	255	71.6	1.14	8.99 \pm 0.01
5	0.677	255	65.8	1.05	10.05 \pm 0.02
3	0.404	254	63.6	1.02	10.87 \pm 0.01
-	0	254	62.4	1.00	12.11 \pm 0.01

N.3.9 Measurement 9: 0.44 S/m

Measurement setup:

<div style="border: 1px solid black; padding: 5px; display: inline-block;"> <p style="text-align: center; margin: 0;">Antennas and shields</p>  </div>	Date: February 1, 2005	
	Experiment settings	Frequency: 62.5 MHz Antennas: Source: #1 Receive: #2 Shields: All 6 present Low pass filter: No Source signal: pickup before amplifier
	Equipment used	Frequency generator: HP 8647A Power amplifier: R.F.P.A. RF001220-25 Pre amplifier: - VSWR meter: Diamond SX-1000 Oscilloscope: Agilent Infinium 54831D
	Oscilloscope settings	CH1: Connection: Send Setting: (variable) mV/DIV Termination: 50 Ω <hr/> CH2: Connection: Receive Setting: (variable) V/DIV Termination: 1 MΩ <hr/> Timing Timebase: 10 ns/DIV Sampling rate: 250 GSa/s (eq. time)
Remarks	$\sigma_{\text{inner pipe}} = 0.438 \pm 0.003 \text{ S/m}, T = 15.3 \pm 0.5 \text{ }^\circ\text{C}$ $\sigma_{\text{outer pipe}} = 2.13 \pm 0.02 \text{ S/m}, T = 16.5 \pm 0.5 \text{ }^\circ\text{C}$	

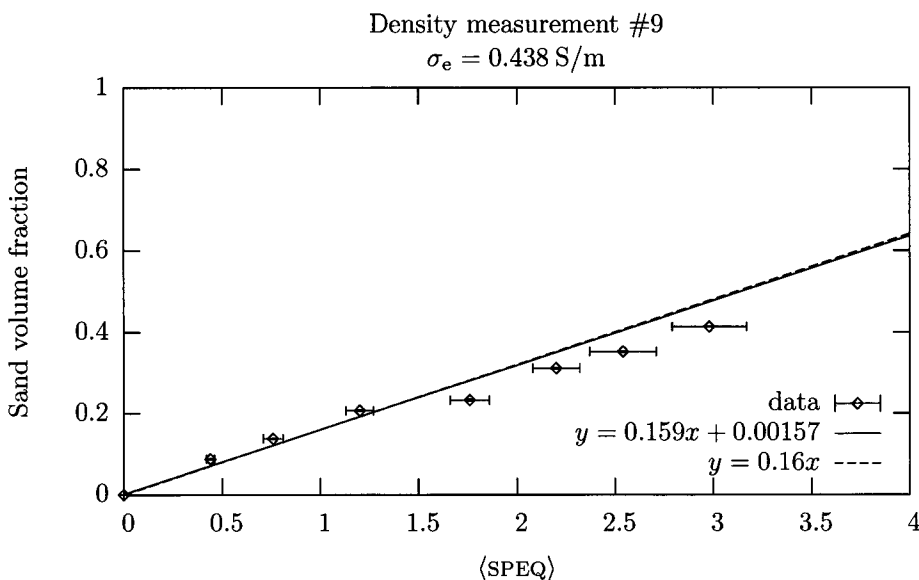


Figure N.22: Measurement 9: Calculation of the sand volume fraction in the water using the C.R.I.M. model. Weighted fits using $y = ax + b$ and $y = cx$ yield $a = 0.159 \pm 0.011$, $b = 0.00157 \pm 0.00312$ and $c = 0.1603 \pm 0.0098$. The weighted sums of squared residuals are $\chi^2_\nu = 12.87$ and $\chi^2_\nu = 11.5$ respectively.

Table N.26: Measurement data

pack seq.	#packs	V_{src} (mV) ± 1	V_{rec} (mV) ± 0.5	$V_r/V_s _0$	Δt (ns)
-	0	261	133.3	1.00	9.58 \pm 0.01
5,2,3,4	2.839	261	197.9	1.48	4.47 \pm 0.01
5,2,4	2.435	262	190.1	1.42	5.22 \pm 0.01
5,2,3	2.045	262	176.4	1.32	5.73 \pm 0.02
5,2	1.641	261	163.0	1.22	6.71 \pm 0.03
5,3	1.081	261	149.7	1.12	7.03 \pm 0.02
5	0.677	261	143.2	1.07	7.87 \pm 0.01
3	0.404	261	141.0	1.06	8.49 \pm 0.01
-	0	261	133.3	1.00	9.58 \pm 0.01

N.3.10 Measurement 10: Rotation

Measurement setup:

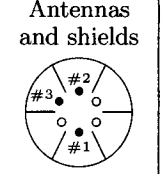
	Date: February 7, 2005		
	Experiment settings	Frequency: 62.5 MHz Antennas: Source: #1 Receive: #2 Shields: All 6 present Low pass filter: No Source signal: pickup before amplifier	
Equipment used	Frequency generator: HP 8647A Power amplifier: R.F.P.A. RF001220-25 Pre amplifier: - VSWR meter: Diamond SX-1000 Oscilloscope: Agilent Infiniium 54831D		
Oscilloscope settings	CH1:	Connection: Send Setting: (variable) mV/DIV Termination: 50 Ω	
	CH2:	Connection: Receive Setting: (variable) V/DIV Termination: 1 M Ω	
	Timing	Timebase: 10 ns/DIV Sampling rate: 250 GSa/s (eq. time)	
Remarks	$\sigma_{\text{inner pipe}} = 0.317 \pm 0.003 \text{ S/m}, T = 15.8 \pm 0.5 \text{ }^\circ\text{C}$ $\sigma_{\text{outer pipe}} = 2.13 \pm 0.02 \text{ S/m}, T = 15.7 \pm 0.5 \text{ }^\circ\text{C}$ Sand pack #5 is rotated around the centerline of then pipe.		

Table N.27: Measurement data

Angle	V_{src} (mV)	V_{rec} (mV)	Δt (ns)
0	282 \pm 1	401 \pm 1	8.109 \pm 0.015
10	283 \pm 1	393 \pm 1	8.089 \pm 0.013
20	283 \pm 1	396 \pm 1	8.065 \pm 0.012
30	283 \pm 1	388 \pm 1	8.037 \pm 0.013
40	283 \pm 1	380 \pm 1	8.008 \pm 0.013
50	284 \pm 1	366 \pm 1	7.958 \pm 0.012
60	286 \pm 1	354 \pm 2	7.911 \pm 0.016
70	287 \pm 1	342 \pm 1	7.801 \pm 0.014
80	287 \pm 1	326 \pm 1	7.640 \pm 0.015
90	286 \pm 1	322 \pm 1	7.536 \pm 0.014

N.4 High salinity measurements

The purpose of the high salinity measurements, is to observe what happens to the electromagnetic propagation from antenna #1 to antenna #2 as the conductivity of the water in the inner pipe increases. These measurements have been repeated for water with various conductivities in the outer pipe.

The time difference and received voltage data of the measurements is contained in this section. The raw data from the coaxial probe measurements is not contained as these measurements are regarded to be of secondary importance.

N.4.1 Measurement 1: 0 S/m

Measurement setup:

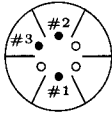
<div style="border: 1px solid black; padding: 5px; display: inline-block;"> Antennas and shields  </div>	Date: December 24, 2004			
	Experiment settings	Frequency:	62.5 MHz	
		Antennas:	Source:	#1
			Receive:	#2
Shields:		All 6 present		
Low pass filter:	Yes			
Source signal:	pickup before amplifier			
Equipment used	Frequency generator:	HP 8647A		
	Power amplifier:	R.F.P.A. RF001220-25		
	Pre amplifier:	-		
	VSWR meter:	Diamond SX-1000		
	Oscilloscope:	Agilent Infiniium 54831D		
Oscilloscope settings	CH1:	Connection:	Send	
		Setting:	(variable) mV/DIV	
		Termination:	50 Ω	
	CH2:	Connection:	Receive	
		Setting:	(variable) V/DIV	
		Termination:	1 MΩ	
Timing	Timebase:	10 ns/DIV		
	Sampling rate:	250 GSa/s (eq. time)		
Remarks	$\sigma_{\text{inner pipe}} = (\text{variable}), T = 12.2 \pm 0.8 \text{ } ^\circ\text{C}$ $\sigma_{\text{outer pipe}} \approx 0$			

Table N.28: Measurement data

Salt (g)	σ (S/m)	V_{src} (mV)	V_{rec} (mV)	Δt (ns)
0	0.054 ± 0.002	179 ± 4	9670 ± 122	5.928 ± 0.021
100	0.13 ± 0.02	176 ± 3	4161 ± 45	6.393 ± 0.044
200	0.20 ± 0.05	179 ± 4	2264 ± 44	7.181 ± 0.050
300	0.28 ± 0.05	182 ± 4	1205 ± 11	7.865 ± 0.017
400	0.37 ± 0.05	183 ± 4	702 ± 8	8.512 ± 0.026
500	0.43 ± 0.05	184 ± 4	447 ± 6	9.002 ± 0.034
600	0.50 ± 0.02	185 ± 4	289 ± 4	9.428 ± 0.024
700	0.58 ± 0.02	185 ± 4	196 ± 3	9.704 ± 0.030
800	0.65 ± 0.02	185 ± 4	141 ± 2	9.833 ± 0.013
900	0.73 ± 0.02	185 ± 4	100 ± 2	9.819 ± 0.038
1000	0.80 ± 0.02	184 ± 4	73 ± 2	9.543 ± 0.017
1250	0.96 ± 0.03	183 ± 4	56 ± 2	8.190 ± 0.017
1500	1.13 ± 0.02	182 ± 3	58 ± 2	7.462 ± 0.021
1750	1.30 ± 0.02	180 ± 4	62 ± 2	7.000 ± 0.020
2000	1.47 ± 0.03	180 ± 4	64 ± 2	6.942 ± 0.031
2250	1.64 ± 0.05	179 ± 4	62 ± 1	6.532 ± 0.016
2500	1.80 ± 0.05	178 ± 4	59 ± 2	6.347 ± 0.034
3000	2.11 ± 0.05	176 ± 4	51 ± 1	6.037 ± 0.064

N.4.2 Measurement 2: 1.9 S/m

Measurement setup:

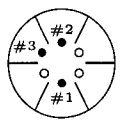
<div style="border: 1px solid black; padding: 5px; display: inline-block;"> <p style="text-align: center; margin: 0;">Antennas and shields</p>  </div>	Date: January 10, 2005			
	Experiment settings	Frequency:	62.5 MHz	
	Antennas:	Source:	#1	
		Receive:	#2	
	Shields:	All 6 present		
	Low pass filter:	No		
	Source signal:	pickup before amplifier		
Equipment used	Frequency generator:	HP 8647A		
	Power amplifier:	R.F.P.A. RF001220-25		
	Pre amplifier:	-		
	VSWR meter:	Diamond SX-1000		
	Oscilloscope:	Agilent Infiniium 54831D		
Oscilloscope settings	CH1:	Connection:	Send	
		Setting:	(variable) mV/DIV	
		Termination:	50 Ω	
	CH2:	Connection:	Receive	
		Setting:	(variable) V/DIV	
		Termination:	1 M Ω	
	Timing	Timebase:	10 ns/DIV	
		Sampling rate:	250 GSa/s (eq. time)	
Remarks	$\sigma_{\text{inner pipe}} = (\text{variable}), T = 14.8 \pm 1.0 \text{ }^\circ\text{C}$ $\sigma_{\text{outer pipe}} = 1.87 \pm 0.01 \text{ S/m}, T = 16 \pm 0.5 \text{ }^\circ\text{C}$			

Table N.29: Measurement data

Salt (g)	σ (S/m)	V_{src} (mV)	V_{rec} (mV)	Δt (ns)
0	0.38 ± 0.01	170 ± 2	152 ± 2	8.52 ± 0.04
100	0.45 ± 0.02	169 ± 2	94 ± 1	9.54 ± 0.03
200	0.52 ± 0.02	166 ± 1	68 ± 1	10.44 ± 0.06
300	0.60 ± 0.02	165 ± 2	49 ± 2	11.44 ± 0.03
400	0.66 ± 0.01	163 ± 2	37 ± 1	12.41 ± 0.07
500	0.74 ± 0.02	162 ± 2	30 ± 2	13.39 ± 0.05
600	0.81 ± 0.02	161 ± 2	26 ± 1	14.33 ± 0.08
700	0.88 ± 0.02	161 ± 1	25 ± 1	15.06 ± 0.07
800	1.01 ± 0.02	159 ± 1	22.6 ± 1	16.15 ± 0.11
900	1.07 ± 0.02	159 ± 1	21.6 ± 1	16.55 ± 0.05
1000	1.21 ± 0.03	158 ± 1	20.0 ± 1	16.98 ± 0.08
1250	1.34 ± 0.02	157 ± 1	18.1 ± 1	17.18 ± 0.07
1500	1.48 ± 0.02	157 ± 1	16.4 ± 1	17.24 ± 0.06
1750	1.60 ± 0.02	156 ± 2	14.9 ± 1	17.10 ± 0.10
2000	1.73 ± 0.03	156 ± 2	13.6 ± 1	16.89 ± 0.15
2000	1.74 ± 0.03	158 ± 2	13.6 ± 1	16.55 ± 0.06
2200	1.87 ± 0.02	157 ± 1	12.8 ± 1	16.29 ± 0.06
2400	2.00 ± 0.02	158 ± 2	12.4 ± 1	16.00 ± 0.10
2800	2.25 ± 0.02	157 ± 1	12.0 ± 1	15.56 ± 0.05

N.4.3 Measurement 3: 3.1 S/m

Measurement setup:

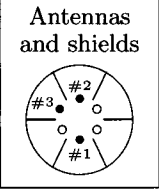
	Date: January 11, 2005	
	Experiment settings	Frequency: 62.5 MHz Antennas: Source: #1 Receive: #2 Shields: All 6 present Low pass filter: No Source signal: pickup before amplifier
	Equipment used	Frequency generator: HP 8647A Power amplifier: R.F.P.A. RF001220-25 Pre amplifier: - VSWR meter: Diamond SX-1000 Oscilloscope: Agilent Infiniium 54831D
	Oscilloscope settings	CH1: Connection: Send Setting: (variable) mV/DIV Termination: 50 Ω CH2: Connection: Receive Setting: (variable) V/DIV Termination: 1 M Ω Timing: Timebase: 10 ns/DIV Sampling rate: 250 GSa/s (eq. time)
	Remarks	$\sigma_{\text{inner pipe}} = (\text{variable}), T = 12.5 \pm 0.8 \text{ }^\circ\text{C}$ $\sigma_{\text{outer pipe}} = 3.10 \pm 0.05 \text{ S/m}, T = 12.0 \pm 0.5 \text{ }^\circ\text{C}$ Source power is 1.1 W instead of 0.5 W.

Table N.30: Measurement data

Salt (g)	σ (S/m)	V_{src} (mV)	V_{rec} (mV)	Δt (ns)
0	0.06 ± 0.01	276 ± 2	1901 ± 11	3.77 ± 0.02
100	0.13 ± 0.01	271 ± 2	942 ± 5	4.91 ± 0.02
200	0.21 ± 0.02	267 ± 2	527 ± 3	5.93 ± 0.02
300	0.28 ± 0.01	262 ± 2	311 ± 3	6.96 ± 0.03
400	0.35 ± 0.01	258 ± 2	196 ± 2	8.02 ± 0.02
500	0.42 ± 0.02	256 ± 2	129 ± 1	9.14 ± 0.02
700	0.57 ± 0.02	251 ± 1	89.8 ± 1	11.35 ± 0.04
900	0.71 ± 0.02	246 ± 2	52.7 ± 1	13.35 ± 0.03
1100	0.85 ± 0.02	242 ± 3	48.4 ± 1	14.72 ± 0.03
1300	0.96 ± 0.02	241 ± 3	46.0 ± 1	15.55 ± 0.03
1500	1.12 ± 0.02	237 ± 2	42.7 ± 1	16.05 ± 0.02
1700	1.25 ± 0.02	236 ± 2	39.6 ± 1	16.24 ± 0.03
1900	1.39 ± 0.02	235 ± 2	36.2 ± 0.5	16.26 ± 0.02
2100	1.52 ± 0.02	234 ± 1	33.8 ± 0.4	16.20 ± 0.03
2300	1.66 ± 0.02	233 ± 2	31.7 ± 0.4	15.99 ± 0.05
2700	1.93 ± 0.02	233 ± 1	29.5 ± 0.2	15.49 ± 0.04
3100	2.19 ± 0.02	232 ± 1	29.0 ± 0.1	15.01 ± 0.06

N.4.4 Measurement 4: 2.2 S/m

Measurement setup:

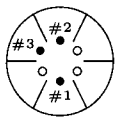
<div style="border: 1px solid black; padding: 5px; display: inline-block;"> <p style="text-align: center; margin: 0;">Antennas and shields</p>  </div>	Date: January 26, 2005			
	Experiment settings	Frequency:	62.5 MHz	
		Antennas:	Source:	#1
			Receive:	#2
		Shields:	All 6 present	
	Low pass filter:	No		
	Source signal:	pickup before amplifier		
Equipment used	Frequency generator:	HP 8647A		
	Power amplifier:	R.F.P.A. RF001220-25		
	Pre amplifier:	-		
	VSWR meter:	Diamond SX-1000		
	Oscilloscope:	Agilent Infiniium 54831D		
Oscilloscope settings	CH1:	Connection:	Send	
		Setting:	(variable) mV/DIV	
		Termination:	50 Ω	
	CH2:	Connection:	Receive	
		Setting:	(variable) V/DIV	
		Termination:	1 M Ω	
	Timing	Timebase:	10 ns/DIV	
		Sampling rate:	250 GSa/s (eq. time)	
Remarks	$\sigma_{\text{inner pipe}} = (\text{variable}), T = 11.7 \pm 0.7 \text{ }^\circ\text{C}$ $\sigma_{\text{outer pipe}} = 2.20 \pm 0.05 \text{ S/m}, T = 12.0 \pm 0.5 \text{ }^\circ\text{C}$ Source power is 1.1 W instead of 0.5 W.			

Table N.31: Measurement data

Salt (g)	σ (S/m)	V_{src} (mV)	V_{rec} (mV)	Δt (ns)
0	0.068 ± 0.01	263 ± 1	1969 ± 6	4.295 ± 0.017
100	0.137 ± 0.02	268 ± 1	1211 ± 4	5.196 ± 0.026
200	0.218 ± 0.02	270 ± 1	654 ± 2	6.347 ± 0.016
300	0.289 ± 0.01	272 ± 1	404 ± 1	7.225 ± 0.013
400	0.364 ± 0.02	273 ± 1	261 ± 1	8.181 ± 0.014
500	0.434 ± 0.02	273 ± 1	179 ± 1	9.085 ± 0.018
600	0.509 ± 0.01	273 ± 1	125 ± 1	10.032 ± 0.030
700	0.58 ± 0.02	272 ± 1	91.4 ± 0.2	10.964 ± 0.017
800	0.656 ± 0.02	271 ± 1	69.9 ± 0.3	11.932 ± 0.022
900	0.726 ± 0.02	271 ± 1	57.3 ± 0.2	12.895 ± 0.024
1000	0.799 ± 0.02	270 ± 1	50.1 ± 0.2	13.812 ± 0.035
1250	0.958 ± 0.02	268 ± 1	42.6 ± 0.3	15.483 ± 0.030
1500	1.13 ± 0.02	266 ± 1	38.6 ± 0.3	16.370 ± 0.030
1750	1.298 ± 0.02	263 ± 1	34.4 ± 0.3	16.808 ± 0.036
2000	1.469 ± 0.02	262 ± 1	30.3 ± 0.3	16.948 ± 0.038
2250	1.647 ± 0.02	260 ± 1	26.6 ± 0.3	16.854 ± 0.055
2500	1.812 ± 0.02	257 ± 1	23.7 ± 0.3	16.630 ± 0.060
3000	2.138 ± 0.02	254 ± 1	20.9 ± 0.2	15.975 ± 0.050

N.4.5 Measurement 5: no inner pipe

Measurement setup:

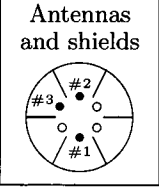
	Date: February 9, 2005			
	Experiment settings	Frequency:	62.5 MHz	
	Antennas:	Source:	#1	
		Receive:	#2	
	Shields:	All 6 present		
	Low pass filter:	No		
	Source signal:	pickup before amplifier		
Equipment used	Frequency generator:	HP 8647A		
	Power amplifier:	R.F.P.A. RF001220-25		
	Pre amplifier:	-		
	VSWR meter:	Diamond SX-1000		
	Oscilloscope:	Agilent Infiniium 54831D		
Oscilloscope settings	CH1:	Connection:	Send	
		Setting:	(variable) mV/DIV	
		Termination:	50 Ω	
	CH2:	Connection:	Receive	
		Setting:	(variable) V/DIV	
		Termination:	1 M Ω	
	Timing	Timebase:	10 ns/DIV	
		Sampling rate:	250 GSa/s (eq. time)	
Remarks	$\sigma = (\text{variable}), T = \pm 0.5^\circ\text{C}$ The inner pipe has been removed.			

Table N.32: Measurement data

Salt (g)	σ (S/m)	V_{src} (mV)	V_{rec} (mV)	Δt (ns)
0	0.05 ± 0.01	282 ± 2	21459 ± 137	9.24 ± 0.02
500	0.22 ± 0.01	288 ± 1	3544 ± 8	9.85 ± 0.01
1000	0.39 ± 0.01	286 ± 1	948 ± 2	11.13 ± 0.01
1500	0.55 ± 0.01	282 ± 2	344 ± 1	12.19 ± 0.01
2000	0.71 ± 0.01	277 ± 2	152 ± 1	13.06 ± 0.02
2500	0.87 ± 0.01	272 ± 2	75.2 ± 0.3	13.82 ± 0.02
3000	1.01 ± 0.01	267 ± 2	40.8 ± 0.4	14.53 ± 0.02
3500	1.16 ± 0.01	263 ± 2	23.3 ± 0.2	15.21 ± 0.03
4000	1.31 ± 0.01	260 ± 1	14.1 ± 0.1	15.88 ± 0.05
4500	1.46 ± 0.01	256 ± 1	9 ± 0.2	16.52 ± 0.08
5000	1.60 ± 0.01	254 ± 1	5.9 ± 0.2	17.13 ± 0.10
5500	1.75 ± 0.01	252 ± 1	4.1 ± 0.3	17.49 ± 0.23
6000	1.90 ± 0.01	252 ± 1	3.1 ± 0.2	17.73 ± 0.29
6000	1.90 ± 0.01	237 ± 1	2.9 ± 0.2	19.02 ± 0.33
6500	2.04 ± 0.01	235 ± 1	2.2 ± 0.3	19.74 ± 0.29
7500	2.33 ± 0.01	232 ± 2	1.6 ± 0.2	20.87 ± 0.50
8500	2.61 ± 0.01	231 ± 1	1.3 ± 0.2	22.20 ± 0.70

This page intentionally contains only this sentence.

Bibliography

- [1] A. Al-Shamma'a, A. Shaw, and S. Saman. Propagation of electromagnetic waves at mhz frequencies through seawater. *IEEE Trans. Antennas Propagat.*, 52:2843–2849, 2004.
- [2] C. Balanis. *Antenna Theory: analysis and design*. Wiley, 2nd edition, 1997.
- [3] J. Barros. New concepts for density meter in dredging. Technical report, IHC Systems, Dec. 2003.
- [4] A. Chelkowski. *Dielectric Physics*. Elsevier Scientific Publishing Company, 1980.
- [5] K. Chen and L. Warne. A uniformly valid loaded antenna theory. *IEEE Trans. Antennas Propagat.*, 40(11):1313–1323, Nov. 1992.
- [6] D. Daniels. Surface-penetrating radar. *Electron. Commun. Eng.*, 8(4):165–182, Aug. 1996.
- [7] M. Dobson, F. Ulaby, M. Hallikainen, and M. El-Rayes. Microwave dielectric behavior of wet soil, part ii: Dielectric mixing models. *IEEE Trans. Geosci. Remote Sensing*, 23(1):35–46, Jan. 1985.
- [8] P. Ferré and G. Topp. Time-domain reflectometry techniques for soil water content and electrical conductivity measurements. *Sensors Update*, 7(1):227–300, Apr. 2001.
- [9] J. Galejs. Driving point impedance of linear antennas in the presence of a stratified dielectric. *IEEE Trans. Antennas Propagat.*, 13(5):725–737, Sep. 1965.
- [10] J. Galejs. Mutual impedance of linear antennas in the presence of a stratified dielectric. *IEEE Trans. Antennas Propagat.*, 14(2):195–202, Mar. 1966.
- [11] M. Hilhorst, C. Dirksen, F. Kampers, and R. Feddes. New dielectric mixture equation for porous materials based on depolarization factors. *Soil Sci. Soc. Am.*, 64:1581–1587, 2000.
- [12] J. Hilland. Simple sensor system for measuring the dielectric properties of saline solutions. *Meas. Sci. Technol.*, 8(8):901–910, Aug. 1997.
- [13] K. Iizuka. An experimental study of the insulated dipole antenna immersed in a conducting medium. *IEEE Trans. Antennas Propagat.*, 11(5):518–532, Sep. 1963.
- [14] K. Kärkkäinen, A. Sihvola, and K. Nikoskinen. Effective permittivity of mixtures: Numerical validation by the fdtd method. *IEEE Trans. Geosci. Remote Sensing*, 38(3):1303–1308, May 2000.
- [15] A. Kaya. Evaluation of soil porosity using low mhz range dielectric constant. *Turkish J. Eng. Env. Sci.*, 26(4):301–307, 2002.
- [16] R. King and C. Harrison. *Antennas and Waves: a modern approach*. M.I.T. Press, 1970.
- [17] R. King, K.-M. Lee, S. Mishra, and G. Smith. Insulated linear antenna: Theory and experiment. *J. Appl. Phys.*, 45(4):1688–1697, Apr. 1974.

- [18] R. King, K.-M. Lee, G. Smith, and S. Mishra. Insulated linear antenna: Theory and experiment. ii. *J. Appl. Phys.*, 46(3):1091–1098, mar. 1975.
- [19] R. King and L. Shen. Two-element array of insulated antennas in a relatively dense medium. *J. Appl. Phys.*, 47(12):5226–5235, Dec. 1976.
- [20] R. King, G. Smith, M. Owens, and T. Wu. *Antennas in Matter*. M.I.T. Press, 1981.
- [21] R. King, B. Trembly, and J. Strohbehn. The electromagnetic field of an insulated antenna in a conducting or dielectric medium. *IEEE Trans. Microwave Theory Tech.*, 83(7):574–583, Jul. 1983.
- [22] R. King and T. Wu. Coupled insulated antennas in a relatively dense medium: Currents and admittances. *Radio Sci.*, 11(8,9):661–669, Aug.–Sep. 1976.
- [23] L. Klein and C. Swift. An improved model for the dielectric constant of sea water at microwave frequencies. *IEEE Trans. Antennas Propagat.*, 25(1):104–111, Jan. 1977.
- [24] K.-M. Lee, T. Wu, and R. King. Theory of an insulated linear antenna in a dissipative medium. *Radio Sci.*, 12(2):195–203, Mar.–Apr. 1977.
- [25] A. Martinez and A. Byrnes. Modeling dielectric-constant values of geologic materials: An aid to ground-penetrating radar data collection and interpretation. Technical report, Kansas Geological Survey, Dec. 2001. URL <http://www.kgs.ukans.edu/Current/2001/martinez/martinez.pdf>. Dec. 3, 2001.
- [26] P. Meaney and K. Paulsen. Two-dimensional microwave imaging apparatus and methods. US Patent 5,841,288, Nov. 1998. Assignee: Microwave Imaging System Technologies, Inc., Hanover, N.H.
- [27] G. Milton. Bounds on the complex dielectric constant of a composite material. *Applied Physics Letters*, 37(3):300–302, Aug. 1980.
- [28] M. Mojid, G. Wyseure, and D. Rose. Electrical conductivity problems associated with time-domain reflectometry (tdr) measurement in geotechnical engineering. *Geotechnical and Geological Engineering*, 21(3):243–258, 2003.
- [29] N. Peplinski, F. Ulaby, and M. Dobson. Corrections to "dielectric properties of soils in the 0.3-1.3-ghz range". *IEEE Trans. Geosci. Remote Sensing*, 33(6):1340, Nov. 1995.
- [30] N. Peplinski, F. Ulaby, and M. Dobson. Dielectric properties of soils in the 0.2-1.3-ghz range. *IEEE Trans. Geosci. Remote Sensing*, 33(3):803–807, May 1995.
- [31] D. Robinson, S. Jones, J. Wraith, D. Or, and S. Friedman. A review of advances in dielectric and electrical conductivity measurement in soils using time domain reflectometry. *Vadose Zone Journal*, 2(-):444–475, Nov. 2003.
- [32] E. Rotholz. Transmission-line transformers. *IEEE Trans. Microwave Theory Tech.*, 29:4, Apr. 1981.
- [33] C. Ruthroff. Some broad-band transformers. *Proc. IRE*, 47(-):1337–1342, Aug. 1959.
- [34] J. Sevick. Design and realization of broadband transmission line matching transformers. *IEEE Emerging Practices in Technology*, pages 1–12, Mar. 1994. URL <http://standards.ieee.org/reading/ieee/ept/trans.pdf>. accessed sep. 16, 2004.
- [35] J. Sevick. *Transmission Line Transformers*. Noble Publishing, 3 edition, 1996.
- [36] M. Siegel and R. King. Electromagnetic propagation between antennas submerged in the ocean. *IEEE Trans. Antennas Propagat.*, 21(4):507–513, 1973.

- [37] G. Smith and J. W.R. Scott. The use of emulsions to represent dielectric materials in electromagnetic scale models. *IEEE Trans. Antennas Propagat.*, 38(3):323–334, Mar. 1990.
- [38] A. Stogryn. Equations for calculating the dielectric constant of saline water. *IEEE Trans. Microwave Theory Tech.*, 19(8):733–736, Aug. 1971.
- [39] M. Tomer, B. Clothier, I. Vogeler, and S. Green. A dielectric–water content relationship for sandy volcanic soils in new zealand. *Soil Sci. Soc. Am.*, 63:777–781, 1999.
- [40] G. Topp, J. Davis, and A. Annan. Electromagnetic determination of soil water content: Measurements in coaxial transmission lines. *Water Resources Research*, 16:574–582, 1980.
- [41] I. White, S. Zegelin, G. Topp, and A. Fish. Effect of bulk electrical conductivity on tdr measurement of water content in porous media. In *Symposium and Workshop on Time Domain Reflectometry in Enviromental, Infrastructure, and Mining Applications*. Washington, D.C.: U.S. Bureau of Mines, Sep. 1994. URL http://www.iti.northwestern.edu/publications/tdr/1994_papers/inw.html. accessed Mar. 7, 2005.
- [42] T. Wu. The insulated dipole antenna in a relatively dense medium. *Radio Sci.*, 8(7):699–709, Jul. 1973.
- [43] M. Yasumoto, Y.Iwai, and I. S. andT. Nozu. Measuring method and apparatus for measuring size of solid in mixture fluid of solid and liquid. Japan Patent Office, Publication 09-159623, jun. 1997. Assignee: Toda Constr Co. Ltd, Kodan Electron. Co. Ltd.
- [44] M. Yasumoto, Y.Iwai, and I. S. andT. Nozu. Measuring method and device for solid density or the like in solid-liquid mixture fluid. Japan Patent Office, Publication 09-159595, jun. 1997. Assignee: Toda Constr Co. Ltd, Kodan Electron. Co. Ltd.
- [45] T. Zakri, J.-P. Laurent, and M. Vauclin. Theoretical evidence for ‘lichtenecker’s mixture formulae’ based on the effective medium theory. *J. Phys. D Appl. Phys.*, 31(13):1589–1594, Jul. 1998.

This page intentionally contains only this sentence.